CALCULATION OF RESPONSE
IN NUCLEAR MAGNETIC RESONANCE

A Thesis Submitted to

The Faculty of Graduate Studies and Research

at the University of Manitoba

In Partial Fulfillment

of the Requirements for the Degree of

Doctor of Philosophy

by

Bruce W. Goodwin

April, 1973

THE UNIVERSITY OF MANITOBA LIBRARIES

CALCULATION OF RESPONSE IN NUCLEAR MAGNETIC RESONANCE

By: Bruce W. Goodwin

A dissertation submitted to the Faculty of Graduate Studies of the University of Manitoba in partial fulfillment of the requirements of the degree of

DOCTOR OF PHILOSOPHY

© 1973

Permission has been granted to the LIBRARY OF THE UNIVERSITY OF MANITOBA to lend or sell copies of this dissertation, to the NATIONAL LIBRARY OF CANADA to microfilm this dissertation and to lend or sell copies of the film, and UNIVERSITY MICROFILMS to publish an abstract of this dissertation.

The author reserves other publication rights, and neither the dissertation nor extensive extracts from it may be printed or otherwise reproduced without the author's written permission.

To my dog

Who was always willing to take me out for a walk.

ACKNOWLEDGEMENTS

It is a pleasure to acknowledge the advice and direction given me by Dr. R. Wallace. His discussions, often inspired by M. B. Labatt, invariably helped in easing the proctalgia associated with programming.

I am also obliged to Dr. E. Bock for his discussions, and to Dr. T. Schaefer, who led me into the field of NMR and who was instrumental in the assembly of this dissertation. The patience of Dr. E. Wells is also noted, in particular for his elucidations on the density matrix theory.

Many of my colleagues also helped in the development of this dissertation, notably R. Wasylishen and J. Peeling, who were only too willing to point out the advantages of experimental work as opposed to the inadequacies of theoretical. I must also thank B. Kuppers for his programming advice, and especially A. Penner, whose proofreading left very little to be faulted and whose advice, albeit often irrelevant, was always diverting.

Finally, I am indebted to the National Research Council of Canada for their financial support during the time this research was carried out.

ABSTRACT

A new technique is developed by means of which the dynamic response of multispin systems may be evaluated, as a function of the high-resolution nuclear magnetic resonance parameters and variables. The technique involves the description of a spin system in terms of the spin density matrix formalism, and the interpretation of the resultant equations as an initial value problem. The numerical solutions thereby obtained are dynamic in the sense that the steady-state approximation is not required. In addition, a number of other assumptions, often invoked by other methods for the calculation of response, are not required so that the present method is not subject to many of the limitations and restrictions normally imposed on other methods.

The density matrix formalism is described briefly, with its application to the high-resolution NMR problem being of special interest. Variations of the NMR experiments are described by characterizing their corresponding perturbation Hamiltonians, and effects of inhomogeneity of the static magnetic field are included in the models employed. The resultant equations are then solved entirely by numerical methods, with the main problem involving the procedure whereby the equation of motion of the spin density matrix is solved.

This problem is dealt with by the Runge-Kutta-Gill algorithm, which is outlined in some detail. The solution then consists of a series of (numerical) spin density matrices as a function of the time

(and experimental conditions), from which is calculated the signal as a function of time. Other effects, such as those due to inhomogeneity or the presence of filters (in double resonance), are then taken into consideration, and a final net signal is obtained.

Computer programmes have been written for the simulation of the response of systems of two spin-1/2 nuclei. Some spectra and plots are reproduced for a variety of experimental conditions, including single resonance, double resonance, some nonselective pulse sequences and a selective pulse sequence. In general these results are in good agreement with observed features and with other calculations. For some cases, however, this dynamic technique is unique in its ability to reproduce experimental features, and it should find application for the simulation of those experiments.

TABLE OF CONTENTS

CHAPTER PAGE

Acknowledgements iii

Abstract iv

Table of Contents vi

List of Tables x

List of Figures xi

I. INTRODUCTION

A. General Discussion 1

B. Other Methods for the Calculation of Response 4

1. The Bloch Equations 4

a. Continuous Wave Experiments 6

b. Pulsed Experiments 8

2. Quantum Mechanical Treatments 11

a. Indirect Methods 12

b. Direct Methods 14

C. Scope of this Dissertation 16

II. THE DENSITY MATRIX FORMALISM

A. Definition and Properties of the Density Matrix 18

B. The Concept of the Spin Density Matrix 23

1. The Phenomenological Model 23

2. The Theoretical Model 25

3. The Relaxation Mechanisms 29

4. Summary 35

CHAPTER PAGE

II. (continued)

C. The NMR Observable 37

1. Derivation of the Observable 37

2. The Effect of a Finite Sweep Rate 39

3. Interpretation of the Observable 41

4. The Effects of Relaxation 45

III. FORMULATION OF THE PROBLEM

A. Introduction 50

B. The High-Resolution NMR Hamiltonian 52

C. The Single Resonance Experiment 57

D. The Double Resonance Experiment 62

E. The Pulse Experiments 68

1. The Free Induction Decay Experiment 70

2. Pulse Experiments for the Measurement of T_1 .. 71

3. Spin-Echo Experiments 72

4. Selective Pulse Experiments 74

F. Other High-Resolution NMR Experiments 76

G. Other Considerations 77

IV. A DYNAMIC METHOD FOR THE CALCULATION OF RESPONSE

A. Introduction 84

B. Solution of the Equation of Motion 87

1. The Runge-Kutta-Gill Algorithm 88

CHAPTER PAGE

IV. (continued)

2. Convergence of the Algorithm 91

C. Solution of the Inhomogeneity Integrals 100

1. Introduction 100

2. The Pulsed NMR Integrals 102

3. The Continuous Wave NMR Integrals 106

4. Fourier Transform Integrals 109

D. Filtering of the Double Resonance Signal 112

E. Evaluation of the Fourier Transforms 117

V. SOME SIMULATED HIGH-RESOLUTION NMR SPECTRA

A. Introduction 120

B. Simulations of the Single Resonance Experiment 125

1. The Initial Transients 125

2. Simulations of A_2 Systems 128

3. Simulations of AB Systems 135

C. Simulations of the Double Resonance Experiment 164

1. Simulation of an A_2 system 164

2. Simulations of AX systems 166

3. Simulations of AB systems 176

D. Simulations of Some Nonselective Pulse Experiments . 192

1. Introduction 192

2. Simulations of the FID Experiment 194

3. Simulations of Some Spin-Echo Experiments 200

CHAPTER PAGE

V. (continued)

4. Simulation of a Partially-Relaxed Fourier Transform Experiment .. 209

E. Simulation of a Selective Pulse Experiment 214

VI. CONCLUSIONS

1. Introduction 221

2. Extensions of the Simulations 222

APPENDIX

A. The Spin Angular Momentum Vector Operators 227

B. Methods of Solution Using the Steady-State Approximation .. 232

1. Single Resonance 232

2. Double Resonance 238

3. The First Echo of the Carr-Purcell Pulse Sequence 241

C. Selective Pulse Experiments 246

1. Definition 246

2. The Pulse Parameters 249

D. Listings of the Computer Programmes 252

BIBLIOGRAPHY..... 289

LIST OF TABLES

TABLE PAGE

I. Elements of the Relaxation Matrix 32

II. Half-height Line Widths for an AB system of Nuclei 47

III. Eigenenergies, Eigenvectors and Transition Frequencies and Amplitudes for an AB System ... 55

LIST OF FIGURES

FIGURE		PAGE
1.	Vector model diagram for a π-τ-$\pi/2$ pulse sequence	9
2.	Energy level diagram and spectrum for a system of two spin-1/2 nuclei	42
3.	Energy level diagram and spectrum for a system of two spin-1/2 nuclei with a second perturbing field ..	42
4.	Energy level diagram for a system of 3 spin-1/2 nuclei ..	44
5.	Stability region for a Runge-Kutta algorithm	94
6.	Convergence of the inhomogeneity integrals for a pulse experiment applied to an A_2 system ..	104
7.	Convergence of the inhomogeneity integrals for a pulse experiment applied to an AB system ..	105
8.	Convergence of the cw inhomogeneity integrals	108
9.	The Fourier transform of a FID experiment and the corresponding cw single resonance spectrum	111
10.	Convergence of the filtering routine	115
11.	Convergence of the Fourier transform routine	119
12.	A_2 spectra as a function of the rf amplitude	127
13.	A_2 spectra as a function of the sweep rate	129
14.	A_2 spectra as a function of the relaxation times	130
15.	Experimental spectra of simple spin systems	132
16.	The wiggle-beat effect	134
17.	AB spectra as a function of sweep rate	136
18.	AB spectra as a function of the rf amplitude	138/9

FIGURE		PAGE
19.	Experimental spectra of an AB system of nuclei	140
20.	AB spectra as a function of chemical exchange rate	142/3
21.	A comparison of models A and B	145
22.	A_2 spectra as a function of inhomogeneity widths	148
23.	AB spectra as a function of inhomogeneity widths	149
24.	AB spectra using the phenomenological relaxation times .	151
25.	AB spectra using the RFUC relaxation mechanism	152
26.	AB spectra using the RFC relaxation mechanism	153
27.	AB spectra using the DD relaxation mechanism	154
28.	AB spectra using intermediate relaxation mechanisms	156
29.	AB spectra for different inhomogeneity distributions ...	159
30.	Experimental AB spectra for the study of relaxation	160
31.	Simulations of spectra for the study of relaxation	161/2
32.	Double resonance simulations of an A_2 system	165
33.	Experimental double resonance spectra	167
34.	Simulations of the spin-decoupling of an AX system	168
35.	Simulations of the spin-decoupling of an AX system	169
36.	Experimental spin-decoupled AX spectra	170
37.	Double resonance AX spectra for various positions of the perturbation frequency	172
38.	Simulations of the spin-tickling of an AX system	174
39.	Simulations of the spin-decoupling of an AB system	177/8
40.	Experimental double resonance AB spectra	179
41.	Simulations of the spin-tickling of an AB system	180

FIGURE PAGE

42. Simulations of the spin-tickling of an AB system 181

43. Simulations showing the asymmetry in regressive and progressive doublets .. 184

44. Simulations of the double resonance of an AB system with perturbation of the double quantum transition 186

45. Double resonance AB spectra for various positions of the perturbation frequency .. 188

46. Simulations of a double resonance experiment 189

47. Experimental double resonance spectra 190

48. FID signals and Fourier transform of an A_2 system 195

49. FID signals and Fourier transform of an AB system 196

50. Simulations of the CP experiment for an A_2 system 198

51. Simulations of the CP experiment for an AB system 199

52. Experimental spectra of a CP experiment 202

53. Modulation of the CP echo envelopes for an AB system 204

54. Experimental echo envelopes for an AB system 205

55. Echo envelope for a CPMG pulse sequence 208

56. Calculated partially-relaxed Fourier transform spectra of an AB system of nuclei . 211

57. The effect of inhomogeneity on a selective pulse sequence 215

58. Simulation of a selective pulse sequence 217

59. Experimental spectra for a selective pulse sequence 219

CHAPTER I. INTRODUCTION

A. General Discussion

One of the most widely applied areas of spectroscopy is that dealing with the nuclear magnetic resonance (NMR) phenomenon. Nuclei possessing spin angular momentum show substantial sensitivity to their electronic (chemical) environment, and as a result NMR is of unquestionable value as an analytical tool for the study of many fundamental molecular properties. Applications of the discipline, ranging from determinations of molecular structure to studies of molecular motion and relaxation times, may be found in a number of standard texts (1-8).

In common with other branches of spectroscopy, the application of NMR involves a preliminary step whereby observed spectra are interpreted in terms of a set of useful parameters. For many problems of interest, it is often sufficient to evaluate a number of empirical parameters, such as chemical shifts, coupling constants, spin-spin relaxation times, etc., which contain the information necessary to characterize a given spectrum. Other problems, however, may require a further interpretation of these parameters as functions of some molecular properties such as electron densities, internuclear separations, and so forth. These tasks are beyond the scope of this dissertation, which is directed at the inverse problem, namely the problem of the calculation of an observed spectrum from an assumed list of empirical parameters and experimental variables.

Aside from its interest in the theory of response of physical

systems, the calculation of the NMR signal is of practical significance to the experimentalist for two distinct reasons. Consider first of all the case of continuous wave (cw) experiments. The calculated spectra may be employed to predict and reproduce the observed features, thereby providing greater insight into the processes causing, for example, ringing (9), wiggle-beats(10), the asymmetric broadening of connected transitions in double resonance (11), etc. In addition, calculated spectra are useful in the inverse problem, that of the analysis of spectra to extract the required empirical parameters. This last procedure is basic to some computer programmes, such as LACOON3 (12,13), for the evaluation of chemical shifts and coupling constants. There are also some cw experiments for which the only method of analysis involves the comparison of experimental spectra with the calculated spectra; one might mention, for example, those experiments designed for the study of chemical exchange (14-16) or for the study of the nature of the interactions responsible for relaxation processes (17,18).

Calculation of the signal is also important in the case of pulsed NMR, and for much the same reasons. One might, for example, calculate the response of a spin system to a Carr-Purcell pulse sequence (19,20) in order to explain the complicated effects caused by the inhomogeneity of the static magnetic field and by relaxation. On the other hand, the analysis of some experiments is often strongly dependent on comparisons made between calculated and observed spectra, a typical example being the Carr-Purcell experiment applied to the study of chemical exchange (21,22) or to the study of the effect of

a coupling constant on the echo envelope (23,24).

It becomes apparent, then, that there is a definite need for methods enabling the calculation of response in NMR. In the following section, some methods are reviewed which have been developed with this objective in mind, and their various limitations and restrictions are discussed in anticipation of an alternate technique whose description constitutes the bulk of this dissertation. Although the technique developed here may be applied to the general NMR experiment, the ensuing discussion and the actual calculations performed have been confined to high-resolution NMR, ie. the NMR of liquids and gases, for experimental conditions corresponding to both cw and pulsed NMR.

B. Other Methods for the Calculation of Response

In his original formulation of the NMR phenomenon, Bloch (25) introduced a set of phenomenological equations which describe the behaviour of a macroscopic magnetization vector. These equations have been widely employed in the calculation of response for both cw and pulsed NMR (see references (26-42) for example). Modifications to include the effects of chemical exchange have also been described (1,4,5,21,43-60). Although the Bloch equations are limited to systems of uncoupled nuclei, they are otherwise sufficiently accurate for the description of many NMR experiments (30,31), and in fact the method by which the effects of the interaction of a nuclear magnetic moment with its surroundings are introduced into the formalism is intimately related to other methods for the calculation of response in multi-spin systems. Consequently a brief discussion below is devoted to a consideration of the Bloch equations; their application to cw and pulsed NMR are treated separately. More detailed discussions may be found in a number of texts (1-8) or in the references cited above.

1. The Bloch Equations.

Using vector notation, the Bloch equations for the time rate of change of the bulk magnetization $\underline{M}$ may be put in the form

$$\frac{d\underline{M}}{dt} = \underline{M} \times \gamma \underline{H}(t) - \frac{1}{T_2}(M_x \underline{i} + M_y \underline{j}) - \frac{1}{T_1}(M_z - M_o)\underline{k} \qquad [1.1]$$

where the nuclei with gyromagnetic ratio γ have an equilibrium magnetization M_o along the z-axis in the presence of a static magnetic field $H_o \underline{k}$ (the unit vectors $\underline{i}$, $\underline{j}$ and $\underline{k}$ are directed along the Cartesian x-y- and z-axes, respectively). For the usual experimental situation

described by [1.1], the magnetic field consists of a large static contribution $H_o\underline{k}$ which causes the nuclear magnetic moments to precess about the z-axis at the Larmor frequency $\omega_o = \gamma H_o$, and a much smaller rotating magnetic field $\underline{H}_p(t) = H_p\ (\underline{i}\ \mathrm{Cos}\ \omega t - \underline{j}\ \mathrm{Sin}\ \omega t)$ which results in a nutation motion in the precession. These effects are more conveniently considered in a frame rotating at an angular velocity $-\omega\underline{k}$ (60), for which the time rate of change of $\underline{M}'$ is

$$\frac{d\underline{M}'}{dt} = \underline{M}' \times [(\omega_o - \omega)\underline{k}' + \omega_p \underline{i}'\ ] - \frac{1}{T_2}(M'_x\underline{i}' + M'_y\underline{j}') - \frac{1}{T_1}(M'_z - M_o)\underline{k}' \quad . \qquad [1.2]$$

The new coordinate system is represented by the primes (but $\underline{k}'=\underline{k}$) and the explicit time-dependence of the magnetic field $\underline{H}(t)$ has been removed, with the effect that the perturbing field now appears as a static field of magnitude $H_p = \omega_p/\gamma$ aligned along the x'-axis. When the Larmor frequency ω_o and the angular frequency ω approach sufficiently close so that the term $\omega_p\underline{i}'$ dominates in [1.2] , an initial magnetization of $\underline{M}'=M_o\underline{k}'$ will be tipped through the y'z' plane; the resultant absorption of energy from the rotating field $\underline{H}_p(t)$ constitutes the resonance phenomenon (1-8,25).

The last two terms on the rhs of [1.1] and [1.2] represent first order decay processes with characteristic times T_1 and T_2. These terms were included by Bloch in an explicit manner since spontaneous emission is negligible in NMR (4), and a mechanism is required by means of which the nuclear moments can establish an equilibrium configuration. The spin-lattice or longitudinal relaxation time T_1 governs the rate at which the z-component of the magnetization approaches its

equilibrium value of M_o through the transfer of energy between the nuclear moments and the other degrees of freedom of the system, denoted as the "lattice". By way of contrast, the spin-spin or transverse relaxation time T_2, governing the rate at which the x- and y-components of $\underline{M}$ vanish, does not involve energy changes of the spin system, although the processes responsible for T_2 may derive from the same source as for T_1 (1-8,25,27).

a. Continuous wave experiments.

In order to apply the Bloch equations to the NMR experiment, it remains to specify the actual nature of the perturbing field $\underline{H}_p(t)$. Consider first of all the cw experiment, for which the rotating magnetic field is of constant amplitude while its frequency is swept near the resonance position at $\omega = \omega_o$. The differential equation [1.2] is often simplified by assuming a steady-state condition, synonymous with a slow passage sweep rate, so that $d\underline{M}'/dt = 0$; the resultant linear inhomogeneous equations are readily solved and the expressions may be found in most texts dealing with magnetic resonance (1-8). Transformation back to the lab frame then yields (analytical) solutions for the components M_x, M_y and M_z of the bulk magnetization vector; ie. equation [1.1] has also been solved.

It remains now to calculate the actual response of the system to the perturbation field. The detector usually employed is a receiver coil aligned along the y-axis, and the detected response is a voltage induced in this coil by changes in the magnetization along that axis. An expression for the observed signal S follows

from an application of Faraday's Law (1,25):

$$S(\omega) \quad \propto \quad dM_y/dt \ .$$

The signal consists of two components, one in-phase and one out-of-phase with the field $\underline{H}_p(t)$, with the interesting part being their amplitudes. A more convenient expression for S is

$$S(\omega) \quad \propto \quad dM_+/dt \qquad [1.3]$$

where the substitution $M_+ = M_x + iM_y$ (i is the imaginary number) facilitates the inclusion of the two common modes of observation, the dispersion mode (in-phase with $\underline{H}_p(t)$) and the absorption mode (out-of-phase), as the real and imaginary parts of S, respectively. The absorption mode response, for example, is a Lorentzian curve (in the slow passage limit) centered at the Larmor frequency and possessing a width at the half-height of $2/T_2$ radians/second:

$$S_{abs}(\omega) \quad \propto \quad \frac{T_2}{1 + (\omega-\omega_o)^2 T_2^{\ 2} + \gamma^2 H_p^{\ 2} T_1 T_2} \ . \qquad [1.4]$$

The last term in the denominator of [1.4] is a component of the so-called "saturation factor", and it indicates that for strong perturbing magnetic fields the response is saturated in the sense that the signal tends to vanish.

The essential assumption leading to analytical solutions such as [1.4] is the steady-state approximation. For the more general case, analytical solutions of the differential equations [1.1] or [1.2] are not known, although numerical approaches have been described (9,35-37). Jacobsohn and Wangsness (9), for example, have presented

calculated line shapes as a function of the (linear) sweep rate of the frequency ω.

b. Pulsed experiments.

The experimental arrangement for pulsed NMR involves a sequence of times for which the amplitude of the rotating magnetic field is alternately zero or nonzero, while its frequency is (usually) fixed. During a pulse, the magnitude H_p and the pulse duration time τ_p are adjusted so that[+] (8)

$$\gamma H_p \tau_p = \theta \text{ (radians)}. \qquad [1.5]$$

Once again there are usually introduced assumptions which simplify the analytical solutions of [1.2]. The most common approximations are that the angle θ is some integral multiple of $\pi/2$ and that, during a pulse,

$$\omega_p = \gamma H_p >> |\omega - \omega_o| \qquad [1.6]$$

and $$\tau_p << T_1, T_2 .$$

The problem is now partitioned into two parts; one considers equation [1.2] separately for the two cases when the pulse is on or when it is off. Using [1.6], it may be readily deduced that the effect of a pulse is to rotate the magnetization vector $\underline{M}$ by an angle of θ radians through a plane perpendicular to the x'-axis. Shown in figure 1, for example, is the effect of a π and a $\pi/2$ pulse when the magnetization

---

[+]the following discussion assumes that nonselective pulses are employed. The distinction between selective and nonselective pulses is discussed in Appendix C.

Figure 1.

Vector model diagram of a π-τ-$\pi/2$ sequence of pulses, often employed for the determination of the spin-lattice relaxation time (see text). At time t=0, a π pulse is applied to a system of nuclear moments which is in a state of thermal equilibrium in a static magnetic field $H_o\underline{k}$. The magnetization vector $\underline{M}'$, initially aligned along the z'-axis, is rotated 180 degrees through the y'-axis to the negative z-axis, as displayed in (a). At time $t = \tau + \tau_p$, as shown in (b), a second $\pi/2$ pulse rotates the partially-decayed magnetization into the negative y'-axis, where subsequent spin-spin relaxation occurs. The corresponding signal for a diode detector is represented schematically in (c). The first "peak" is the expected response as $\underline{M}'$ is rotated through the y'-axis, and the other near-vertical line is the expected response to the $\pi/2$ pulse. The signal then decays as the magnetization dephases due to spin-spin relaxation and inhomogeneity effects. At time $t = \tau + \tau_p \simeq \tau$, the signal amplitude is proportional to $[1 - 2 \exp(-\tau/T_1)]$.

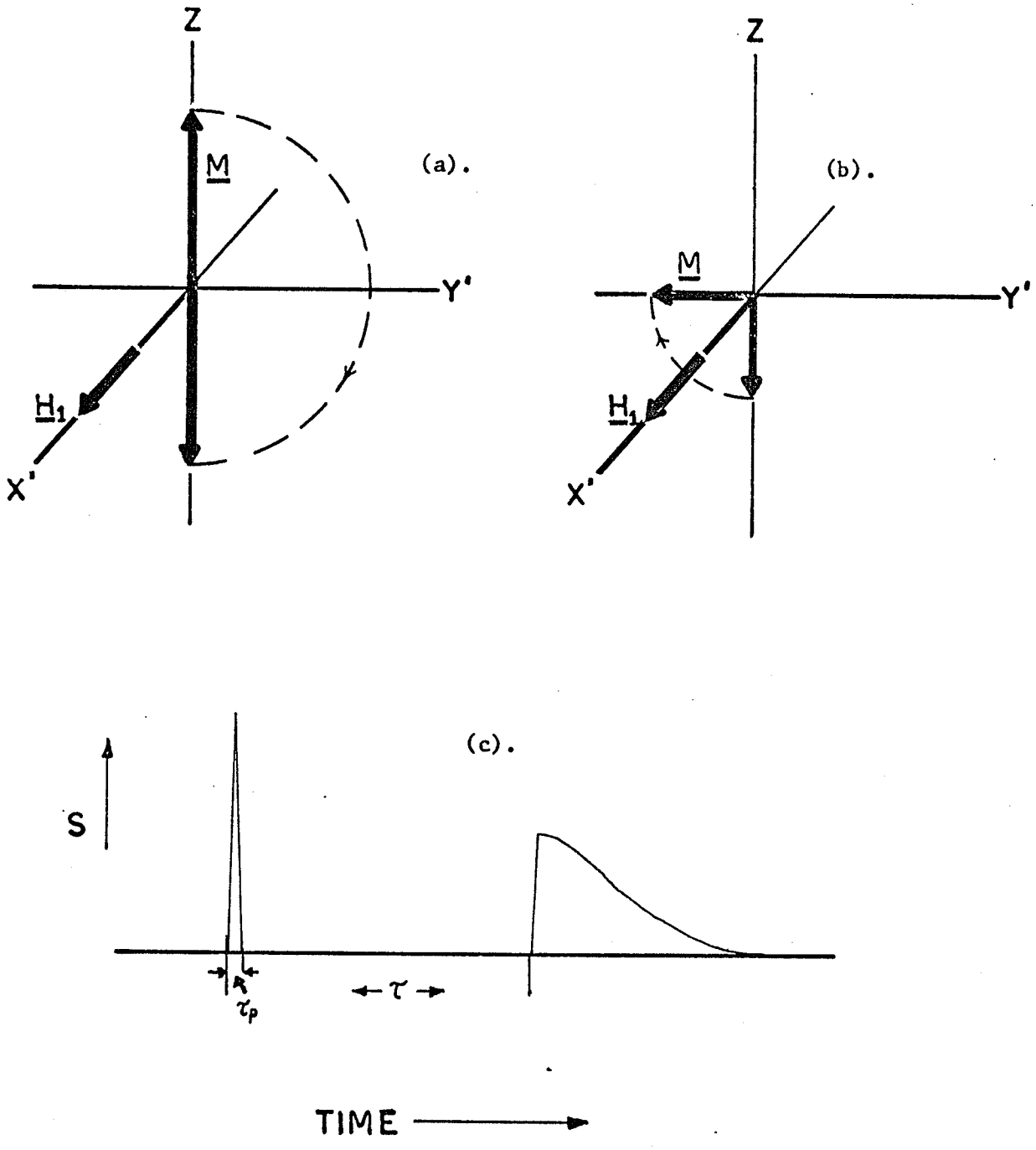
Z
M
(a).
Y'
H1
X'
Z
(b).
M
Y'
H1
X'
(c).
S
τp
τ
TIME

is initially aligned along the z'-axis; in both cases the rotation occurs through the y'z' plane.

In order to solve [1.2] when the pulse is off, one assumes that the pulse duration times are negligibly small so that, effectively, no relaxation takes place during the pulse. The differential equation may be simplified further by assuming $\omega=\omega_o$; one then obtains a simple equation whose solution is of the nature of an exponential decay. If, for example, either of M_x and M_y or M_z is initially zero at the start of the sequence of time with $H_p=0$, then the solution for the other component(s) is just a simple exponential decay with a characteristic time constant T_1 or T_2. Both of these situations are encountered in figure 1: immediately following the π pulse, M_z decays according to $\exp(-t/T_1)$, while following the $\pi/2$ pulse M_x and M_y both decay according to $\exp(-t/T_2)$ (ignoring inhomogeneity effects). The response detected is obtained either from a phase-sensitive detector, with the corresponding expression being [1.3], or from a diode detector, whose corresponding expression is the modulus of equation [1.3]. Shown schematically in figure 1c is the signal for the $\pi - \tau - \pi/2$ pulse sequence (the notation $\pi/2$ etc. denotes some combination of H_p and τ_p yielding an angle $\theta = \pi/2$) using a diode detector. During a pulse the signal is experimentally unobservable because of receiver saturation due to the presence of $\underline{H}_p(t)$, and the signal shown is the predicted pattern. Note that the $\pi/2$ pulse in effect renders the magnetization M_z observable at time $t\simeq\tau$ (assuming $\tau_p<<\tau$), and, according to the solution of [1.2] , that

$$S(\tau) = [1 - 2 \exp(-\tau/T_1)] \quad . \qquad [1.7]$$

This pulse sequence has been applied for the measurement of T_1 through plots of $S(\tau)$ for different values of τ. The signal for times $t \geq \tau$, according to a solution of [1.2], should follow an exponential decay with a rate constant $1/T_2$. The pattern displayed is not exponential since inhomogeneity of the static magnetic field produces some distortions (the curve for $t \geq \tau$ resembles a Gaussian curve (8)). This effect will be discussed in more detail at a later stage.

Similar vector models and corresponding solutions from the Bloch equations have also been used to explain other pulse experiments as applied to simple spin systems (8). Some recent applications, for example, include the study of systems of uncoupled magnetically inequivalent nuclei (proton-decoupled C^{13} NMR (61,62)). In general, however, it is not possible to obtain analytical solutions for a general sequence of pulses, although numerical methods of solution have been discussed for some experiments (54,57,59,63).

2. Quantum Mechanical Treatments.

The Bloch equations have not been successfully applied to the description of multispin systems, principally because quantum mechanical effects may appear which are not readily handled by these equations. One must then resort to more sophisticated descriptions, most of which may be assigned to one of two classes of methods, the "direct" class and the "indirect" class[+](13,16,64-71). A brief review of these methods is presented below; more detailed discussions

[+]the distinction is usually made only for methods of calculation in cw NMR, although a similar dichotomy may be found for pulsed NMR.

may be found in the references cited and in Appendices B and C (for the direct class of methods). It is instructive to recognize here the important distinction between the two classes of methods. The direct method is direct in the sense that spectra are computed directly from an expression for the response of the spin system. In opposition to this procedure, the indirect methods usually require intermediate solutions to a Hamiltonian eigenvalue problem, followed by applications of perturbation theory in order to obtain transition frequencies and probabilities, before the observable is finally evaluated.

a. Indirect Methods.

This last case may be rendered more lucid by a brief outline of the sequence of steps involved for the calculation of a cw single resonance spectum. The basic formulation begins with a stationary eigenvalue problem

$$H\ |\Psi_i\rangle \quad = \quad E_i\ |\Psi_i\rangle \qquad [1.8]$$

where H is the well-known high-resolution NMR Hamiltonian in the rotating frame (1-7), including a nuclear Zeeman term and a term for the spin-spin coupling constants. It is implicitly assumed that the spin ensemble consists of non-interacting spin systems which are the moving molecules containing the coupled nuclear spins. A spin system is described by a spin wave function $|\Psi_i\rangle$ whose eigenenergy is E_i, and an eigenvalue problem is constructed by expanding $|\Psi_i\rangle$ into an orthonormal set of basis product vectors $\{\ |n\rangle\ \}$ which are eigenvectors of the Zeeman term. After some manipulation, one obtains the secular determinant:

$$| H_{mn} - F_k \delta_{mn} | = 0 . \qquad [1.9]$$

Here F_k is the eigenenergy of the eigenvector $|\psi_k\rangle$ (some linear combination of the product vectors $|n\rangle$) and δ_{mn} is the Kronecker delta function. The usual solution procedure (12,13) involves a numerical solution of [1.9] for the eigenvectors and eigenenergies; transitions induced by a weak perturbing rf field are then computed using the selection rule

$$I_{kl} \propto | \lambda_{kl} |^2 = | \langle \psi_k | I_+ | \psi_l \rangle |^2 \qquad [1.10]$$

deriving from first order perturbation theory (1-7). The unsaturated cw spectrum therefore consists of a number of transitions between eigenstates $|\psi_k\rangle$ and $|\psi_l\rangle$ at the frequencies $\omega_{kl} = (E_l - E_k)/\hbar$ and with intensities I_{kl} ($\hbar$ is Planck's modified constant). The symbol I_+ in [1.10] represents the familiar raising or ladder operator ((1-7); Appendix A). Although the result is a "stick" spectrum, it can be made to resemble more closely an experimental spectrum by fitting suitable line shapes and relaxation times (for example the Lorentzian curve in [1.4] or other variations (72)) to each transition possessing a nonzero transition probability.

Extensions of the indirect method for cw NMR include similar procedures for the calculation of multiple resonance (73-78) and for multiple-quantum transitions (2.79). In general, however, it becomes clear that the indirect method is inadequate for the accurate reproduction of the observed line shape, and in particular the method must fail in the description of a variety of experiments, such as those for which saturation, chemical exchange or transient responses (for example, ringing) are important features.

Much the same procedure as summarized above is employed for the calculation of response of a multispin system in pulsed NMR. Only a few of the pulse experiments, such as the Carr-Purcell (19) or the Hahn (29) spin echo experiments, have been described using the indirect method (2,23,47,80-84) and, as before, the calculated results are made to resemble the observed results only after a rather empirical inclusion of the effects due to relaxation (and inhomogeneity of the static magnetic field): - generally through a process of "extrapolation" of the predictions of the Bloch equations for simple spin systems. In addition, there are required some qualifying restrictions on some of the parameters (principally the pulse parameters), and the method cannot describe the complicating effects of chemical exchange.

b. Direct Methods.

These limitations led to the development of the direct class of methods, which yield more accurate solutions for the entire response of multispin systems, and which have a wider range of application. The original description is due to Bloch and others (30,85-87), with later reformulations for cw NMR including applications to single resonance (13,16,64-66), double resonance (67-71,77,78,88-95), multiple-quantum transitions (95,96) and the NMR of systems which are undergoing chemical exchange (14,16,97-100). The method of interest here is that based on the density matrix formalism, and a more detailed description of the usual procedures involved is deferred to the discussion in Appendix B. It should be noted, however, that these methods of solution of the relevant density matrix equations place some restr-

ictions on their regions of applicability, and that many of these restrictions are effectively lifted by the solution procedure to be discussed in this thesis. One such assumption, for example, is the steady-state approximation, which limits the calculated spectra to the slow passage limit as well as prohibiting the calculation for experiments such as the periodically pulsed cw experiment (101) or the Torrey experiment (28) (although generally classified as a pulse experiment, the Torrey experiment is closely related to a cw experiment). There is also a variety of additional assumptions and approximations which are often invoked for the other methods; for example Binsch (16,65,66) requires the assumption of a weak rf field which precludes the possibility of calculation for cases where saturation and/or multiple-quantum transitions are of interest. On the other hand, methods of solution for the double resonance experiment commonly allow for a variable strength of the perturbing rf field, but not for the observing rf field (67-71), or else the calculations may fail for those cases involving degeneracies or near-degeneracies of the eigenenergies (the "Bloch" approximation (88)).

More recently, there have appeared a number of reports dealing with the feasibility of studying the explicit nature of relaxation processes, using both single resonance (17,102,103) and double resonance (18,104-107) techniques. For these studies, one desires that the observed spectral features are accurately reproduced by the calculated line shape, and as such the steady-state approximation often imposes undesirable restrictions on the calculations (see, for example, the discussion by Hoffman (17), pages 172-174). The procedure to be discussed herein is unique in its ability to lift this approximation.

The density matrix formulation has also been applied to the calculation of response in pulsed NMR, with most of the literature devoted to studies of the effect of chemical exchange on pulse sequences of the Carr-Purcell variety (24,108-112). Once again, however, the usual methods of solution involve a number of restrictions which limit their range of application; in fact the restrictions are much the same as for the indirect method with the exception that chemical exchange effects may now be described. Thus, for example, relaxation effects are described in a phenomenological manner, the pulse parameters must define only nonselective pulses, and inhomogeneity is not accounted for so that the entire signal is not calculable (for the spin echo experiments (19,20,29), only part of the signal, at defined points in time, is independent of inhomogeneity). These restrictions also preclude the possibility of calculation for selective pulse experiments (63). Recently, one type of selective pulse experiment has been described for the elucidation of relaxation interactions in some spin systems (113), although no attempt was made to calculate the actual signal. This situation is indicative of the general situation for pulsed NMR, in that techniques may exist for the calculation or the interpretation of the response (or parts of the response), but no single method has been developed to calculate the entire signal for an arbitrary pulse sequence applied to a multispin system. Since the technique to be discussed below does not suffer from any of the above limitations, it should find considerable application for the calculation of response in pulsed NMR.

C. Scope of this Dissertation.

In the ensuing discussion, an alternate method is discussed which enables the calculation of the exact response in high-resolution NMR for both cw and pulse experiments (114-116). This new technique is not subject to many of the limitations of other methods, and it possesses a unity of approach in that solutions for most types of experiments are found in much the same manner. The technique belongs to the "direct" class of methods, involving a dynamic numerical solution of the equation of motion of the spin density matrix, and it is more general than any one of the methods mentioned above since many of the restrictions and limitations are not required. As a consequence it should find application where the other methods fail or are insufficiently accurate; for example, in cw NMR where transients due a finite sweep rate become important, or in pulsed NMR where the pulses are selective or where the entire response is desired.

The density matrix formalism is outlined briefly in the next chapter, along with a number of different models which may be used to describe the effects of relaxation and inhomogeneity. Details of the numerical techniques are also discussed, and examples of some computed spectra are presented in Chapter V. All calculations have been confined to systems of two spin-1/2 nuclei for simplicity, although extensions to the computer programmes written should be readily realized.

CHAPTER II. THE DENSITY MATRIX FORMALISM

A. Definition and Properties of the Density Matrix.

The indirect method for the calculation of response in cw NMR accurately predicts transition frequencies because the magnetic interactions between different molecular spin systems are very weak, and consequently a macroscopic sample of spins may be considered as an ensemble of isolated identical molecular spin systems to a good approximation. The advent of the high-resolution spectrometer and more sophisticated pulse sequences, however, makes it feasible to observe these interactions more clearly since the obscuring effects of inhomogeneity can be largely overcome. This development establishes the need for more exact methods for the calculation of the response of an ensemble of spins, and such calculations are afforded by the density matrix formulation.

The density matrix theory begins by considering an isolated spin system which is described by the spin wave function $|\Psi_j(t)\rangle$. Expanding $|\Psi_j(t)\rangle$ into a complete set of orthonormal basis functions $\{|n\rangle\}$, one obtains the expression

$$|\Psi_j(t)\rangle = \sum_n c_n^j(t) \, |n\rangle \qquad [2.1]$$

with the time-dependence conveniently carried in the coefficients $c_n^j(t)$. The expectation value of an observable with corresponding operator O is then given by the simple expression

$$\begin{aligned} \langle O^j \rangle &= \langle \Psi_j(t)|O|\Psi_j(t)\rangle \\ &= \sum_n \sum_{n'} c_{n'}^j(t)^* \, c_n^j(t) \, \langle n'|O|n\rangle \\ &= \mathrm{tr}\,(PO) = \mathrm{tr}\,(OP) \end{aligned} \qquad [2.2]$$

where tr indicates a trace of the matrix product in the brackets, and where the matrix elements $P^j_{nn'}$ are defined by

$$P^j_{nn'} = [c^j_{n'}(t)]^* \, c^j_n(t) \qquad [2.3]$$

Thus far the development has not deviated other than in notation from the indirect method outlined previously; one could calculate transition probability amplitudes from [2.2] using the appropriate operator and the selection rule [1.10]. In this sense the indirect method assumes that a system is in a "pure" state (99,117,118) characterized by the existence of an experiment which yields a result with certainty; in cw NMR this experiment could involve the location of Dirac delta functions corresponding to transition frequencies. For an ensemble of similar molecules which are not isolated, this concept becomes inadequate since there is no longer one pure state but rather an unspecified superposition of spin states (a "nonpure" state (117)). The same experiment applied to such an ensemble would then yield only a localized range of frequencies corresponding to that transition instead of a Dirac function.

To describe this interacting ensemble, one introduces the idea of a statistical distribution, with weights p_j, that a given molecule is described by the wave function $|\Psi_j(t)>$. The expectation value of an operator for the entire ensemble, denoted by $<\bar{O}>$, is then

$$<\bar{O}> = \sum_j p_j <O^j> = \sum_{j,n,n'} p_j \, P^j_{nn'} \, O_{n'n}$$

$$= \mathrm{tr}\,(\rho O) = \mathrm{tr}\,(O\rho) \, . \qquad [2.4]$$

Here the symbol ρ denotes a density matrix, defined by (117,118)

$$\rho_{nn'} = \sum_j p_j \, p^j_{nn'} = \sum_j p_j \, [c^j_{n'}(t)]^* \, c^j_n(t) \qquad [2.5]$$

or equivalently by (4,7,99)

$$\rho_{nn'} = \overline{c_{n'}(t)^* \, c_n(t)}$$

where the bar indicates an ensemble average. In either case the salient feature of the density matrix formalism displayed by [2.4] is a double average: one average is a quantum-mechanical average given by [2.2] and the other average is a statistical average over the ensemble. Equations [2.4] and [2.5] also express the result that the expectation values of different observables for the same system vary only as the matrix elements of their corresponding operators, whereas the expectation value of an operator for two different ensembles will vary according to the density matrix describing those ensembles.

The steps leading to the definition [2.5] do not, however, immediately offer an explicit interpretation of the actual form of the density matrix. To this end it is instructive to consider the expectation value of the Kronecker delta function δ_{mn}

$$\langle \delta_{mn} \rangle = \mathrm{tr} \, (\delta_{mn} \, \rho) = \rho_{nn} \qquad [2.6]$$

(the bar above the operator on the lhs has been dropped for convenience). Now δ_{mn} represents the probability of finding the entire ensemble described by the basis function $|n\rangle$; consequently the diagonal element ρ_{nn} represents the population of the basis function $|n\rangle$. In particular, for a system which is in thermal equilibrium, these populations are just the Boltzmann distributions if the basis functions $|n\rangle$ are eigenfunctions of the Hamiltonian. Thus the thermal equilibrium

density matrix ρ^o may be defined by its elements, with

$$\rho^o = (1/Z) \exp(-E_m/kT) \qquad [2.7a]$$

where k is the Boltzmann constant, T is the temperature, E_m is the eigenenergy of the eigenvector $|m\rangle$, and where

$$Z = \sum_m \exp(-E_m/kT). \qquad [2.7b]$$

A more convenient expression is possible since ρ^o is diagonal in this basis (see below)

$$\rho^o = (1/Z) \exp(-\hbar H/kT) \qquad [2.7c]$$

where it is assumed that the Hamiltonian H (in frequency units) is identical for each member of the ensemble.

The interpretation of the off-diagonal elements of the density matrix is facilitated by assuming that some operator O has only one nonzero matrix element O_{lm}; it then follows from [2.4] that the expectation value $\langle O \rangle$ is proportional to ρ_{ml}. It will be shown below, for example, that the signal intensity of a transition in cw NMR may often be related to a specific density matrix element at a first approximation. Hence the off-diagonal element ρ_{ml} corresponds to the transition probability between the states $|l\rangle$ and $|m\rangle$. Of course for a system in thermal equilibrium such transition probabilities must be zero, and therefore ρ^o is necessarily diagonal in the appropriate basis consisting of eigenvectors of the Hamiltonian (7).

The definition [2.5] may be used to derive a number of properties which serve to characterize the density matrix concept more fully. Some of the more useful properties are listed below.

(a). Since the expectation value of the identity matrix $\mathbb{I}$ is unity, it follows that

$$\langle \mathbb{I} \rangle = \mathrm{tr}\,(\rho I) = \mathrm{tr}\,(\rho) = 1. \qquad [2.8]$$

That is, the trace of the density matrix is unity, reflecting the orthonormality of the basis set $\{|n\rangle\}$.

(b). Since the expectation values are real and correspond to Hermitian operators, the density matrix is also Hermitian:

$$\rho_{nn'} = (\rho_{n'n})^* \qquad [2.9]$$

(c). The equation of motion of the density matrix is given by

$$d\rho/dt = i\,[\rho, H] \qquad [2.10]$$

where the square braces indicate a commutator, and where the Hamiltonian, in units of $\hbar$, is assumed to be constant over the ensemble. This vital equation follows from the definition [2.5] and from the Schrödinger equation for $|\Psi_j(t)\rangle$ (4,7,99,117,118). Note that the equation of motion conserves the normalization property since (17)

$$\mathrm{tr}\,(d\rho/dt) = \mathrm{tr}\,(\,i\,[\rho, H]) = 0$$

and the hermiticity since

$$d\rho_{nn'}/dt = i \sum_k (\rho_{nk} H_{kn'} - H_{nk} \rho_{kn'})$$

$$= (d\rho_{n'n}/dt)^* .$$

The preceding definitions and properties contain sufficient information to describe a density matrix, and the next problem will be to relate this formalism to the description of the nuclear magnetic resonance phenomenon.

B. The Concept of the Spin Density Matrix.

The density matrix formalism may be applied to the description of NMR by following two distinct approaches, both of which yield somewhat similar models for the characterization of a system of spinning nuclei. Both approaches are described briefly below, although it should be emphasized that the actual solution technique does not depend on the details for a given model.

1. The Phenomenological Model.

Perhaps the most intuitive approach is the phenomenological method originally presented by Alexander (98)[+] for the study of the effects of chemical exchange on single resonance spectra. His model has also been applied to calculations for single resonance spectra without exchange (65,66) and to calculations for some spin echo experiments (22,24,50,51,55,112). In this phenomenological approach, Alexander accepts equations [2.7] - [2.10] as results which are applicable to a spin density matrix describing an ensemble of spins isolated from one another and from the lattice. In particular, the equation of motion of the spin density matrix is, as before, $d\rho/dt = i[\rho,\mathcal{H}_S]$, where $\mathcal{H}_S$ is the usual NMR Hamiltonian and ρ the spin density matrix.

By analogy with the Bloch equations, relaxation effects deriving from interactions between the spins and their surroundings are accounted for by adding to the equation of motion an extra relaxation term (the effects of chemical exchange are accommodated by adding yet another term). The equation of motion for ρ of a "real" ensemble then becomes

---

[+]actually a simplified version of the other, chronologically prior model.

$$d\rho/dt = i\,[\rho, H_s] + (\partial\rho/\partial t)_{relax} . \qquad [2.11]$$

With the further assumption that relaxation processes are first order decay processes acting on deviations from thermal equilibrium, as for the Bloch equations, one has that (98)

$$(\partial\rho/\partial t)_{relax} = (\rho^o - \rho)/T_{1_{diag}} + (-\rho/T_2)_{odiag} \qquad [2.12]$$

where ρ^o is the spin density matrix in thermal equilibrium with its surroundings, as defined by [2.7] with H the spin Hamiltonian. As before, T_1 and T_2 are the spin-lattice and spin-spin relaxation times[+], and the terms diag and odiag refer to the diagonal and off-diagonal elements respectively. The analogy with the Bloch equations is exact for a system consisting of a single nucleus possessing spin: equations [2.11] and [2.12] are just a reformulation of equation [1.1]. It is easy to show, for example, that both M_z and the diagonal elements of ρ relax at the same rate $1/T_1$ (compare also with the decay of the surplus populations in equation [11] of Bloembergen et. al. (27)). This statement follows from [2.4] with the expectation value of M_z being associated with the spin vector operator I_z (ignoring constants of proportionality):

$$\langle M_z \rangle \propto tr\,(\rho I_z).$$

Now since I_z is diagonal and time-independent in a basis product representation (1-7),

---

[+]assumed hereafter to be identical for each nucleus. Although it is possible to construct a relaxation term involving different relaxation times for each different nucleus, the inherent complications of the resultant equations do not justify their use as an alternative to the more theoretical approach to spin relaxation discussed below.

$$\text{tr}\ (\rho I_z) \quad = \quad \sum_n \rho_{nn}\ (I_z)_{nn}$$

and

$$d\langle M_z\rangle/dt \quad = \quad \sum_n (d\rho_{nn}/dt)\ (I_z)_{nn}$$

A similar argument relates the relaxation rates for M_x and M_y with the relaxation rates for the off-diagonal elements of the spin density matrix (7), and it becomes clear that [2.11] and [2.12] are identical with [1.1] since the extra terms, the cross product in [1.1] and the commutator in [2.11] , are equivalent terms describing the interactions of the (single) spin with the external magnetic fields.

Since the Bloch equations yield accurate line shapes for single spin systems, apart from some inhomogeneity effects, Alexander reasoned that the phenomenological description of relaxation could be extended to multispin systems. In the calculated spectra presented below, this conclusion is shown to be partly true; the spectra deviate from the observed patterns, for example, in cw NMR when saturation effects are important or in pulsed NMR when a selective pulse sequence is employed to extract explicit information about relaxation processes[+]. The versatility of these equations is in fact surprising when they are compared with the relatively complicated equations deriving from the more theoretical approach to the application of the density matrix formalism to NMR.

2. The Theoretical Model.

This latter approach was originally proposed by Wangsness and

---

[+] the calculations described in references (22,24,50,51,65,66,112) and elsewhere use [2.11] and [2.12], but they do not fall into these categories.

Bloch (30) and Bloch (85,86), although applications generally follow the later reformulation due to Redfield (87). The following discussion is a brief recapitulation of some of the more important features of their theory; more complete discourses may be found elsewhere (4,7,16-18,99).

The starting point is once again equation [2.10] which is now interpreted as the equation of motion of a particular molecule in an ensemble. Now, however, the Hamiltonian consists of the two parts

$$H = H_s(t) + H_r(t) \qquad [2.13]$$

where $H_s(t)$ is the spin Hamiltonian (including rf field(s)), and $H_r(t)$ is presumed to be a stationary random function describing the interactions of the molecule with its surroundings. It is this interaction which is responsible for the relaxation of the spins.

In an interaction representation given by the unitary operator U, where

$$dU/dt = i\, U\, H_s(t) \qquad [2.14]$$

the equation of motion of the transformed spin density matrix becomes

$$d\rho^i/dt = i\,[\rho^i, H_r{}^i] \qquad [2.15]$$

where $\rho^i = U\rho U^{-1}$ and $H_r{}^i = U\, H_r(t)\, U^{-1}$. Now, since the relaxation effects are due to very weak interactions, equation [2.15] may be expanded to second order to a good approximation, yielding

$$d\rho^i/dt = i\,[\rho(0)^i, H_r^i] - \int_0^t [[\rho(0)^i, H_r^i(t+\tau)], H_r^i(t)]\, d\tau \,. \qquad [2.16]$$

This last equation represents the (approximate) equation of motion for one molecule. For an ensemble of molecules, each with an

identical Hamiltonian $H_s(t)$, [2.16] must be replaced by an ensemble average. The new averaged density matrix, represented by the symbol $\bar{\rho}^i$, has the equation of motion of [2.16] but with bars over the commutators indicating an averaging process. If $\rho^i(0)$ and $H_r(t)$ are not appreciably correlated, then they may be averaged separately, and, since $H_r(t)$ is a stationary random function, its ensemble average is zero so that the first term vanishes, and one obtains

$$d\bar{\rho}^i/dt = -\int_0^t \overline{[[\rho(t)^i, \overline{H_r^i(t+\tau)}], H_r^i(t)]}\, d\tau \quad . \qquad [2.17]$$

In this equation, $\rho(t)^i$ has been substituted for $\rho(t=0)^i$ since a previous assumption allowed that relaxation interactions are weak and therefore the time rate of change of ρ^i is not rapid.

The integral appearing on the rhs of [2.17] may be made more tractable by invoking the extreme narrowing approximation (4,7,16-18, 85-87,99)[+]

$$| H_s(t)\ \tau_c | \ll 1 \qquad [2.18]$$

where τ_c is the molecular correlation time, an average time between the collisions of the molecules which give rise to the random interactions. With the additional assumption that the time t in the integral is long compared with the correlation time, the limits may be extended to $\pm \infty$ by premultiplying by 1/2 (4,7,16-18,99). Finally, if it is assumed that the molecular correlation function may be simplified as follows,

---

[+] a good approximation for most high-resolution NMR experiments. A less stringent approximation is the nonviscous liquid approximation (4,17,18).

$$\overline{H_r^i(t+\tau)\, H_r^i(t)} \simeq 2\,\tau_c\, \overline{H_r^i(t)\, H_r^i(t)}\, \delta(\tau) \qquad [2.19]$$

where $\delta(\tau)$ is a Dirac delta function, then the integral in [2.17] is readily evaluated and the resultant expression, in the Schrödinger representation (the original, laboratory, representation) is

$$d\rho/dt = i\,[\rho, H_s(t)] - [[\rho(t), \overline{H_r(t)}], H_r(t)]\,\tau_c \qquad [2.20]$$

dropping the bars on ρ for convenience of notation. A last point to be noted is that if the lattice is explicitly introduced into [2.13] and the subsequent derivations, then the effect is to replace $\rho(t)$ in [2.20] by the term $\rho(t)-\rho^o$ (see for example Abragam (4)):

$$d\rho/dt = i\,[\rho, H_s(t)] - [[\rho(t)-\rho^o, \overline{H_r(t)}], H_r(t)]\,\tau_c. \qquad [2.21]$$

This last equation often appears in the compact notation due to Redfield (87):

$$d\rho/dt = i\,[\rho, H_s(t)] - \Gamma\,(\rho-\rho^o) \qquad [2.22a]$$

where the Redfield relaxation matrix R is defined by the following equations:

$$\Gamma_{\alpha\alpha'}(\rho-\rho^o) = \sum_{\beta}\sum_{\beta'} R_{\alpha\alpha'\beta\beta'}\,(\rho-\rho^o)_{\beta\beta'} \qquad [2.22b]$$

and

$$R_{\alpha\alpha'\beta\beta'} = J_{\alpha\beta\alpha'\beta'} - \tfrac{1}{2}\delta_{\alpha'\beta'}\sum_{\nu} J_{\alpha\nu\beta\nu} - \tfrac{1}{2}\,\delta_{\alpha\beta}\sum_{\nu} J_{\nu\alpha'\nu\beta'}$$

with

$$J_{\alpha\beta\alpha'\beta'} = 2\,\tau_c\, \overline{\langle\alpha|H_r(t)|\beta\rangle\,\langle\alpha'|H_r(t)|\beta'\rangle^*}. \qquad [2.22c,d]$$

The spectral densities J also obey the relations $J_{\alpha\beta\alpha'\beta'}=J_{\alpha'\beta'\alpha\beta}=J_{\beta\alpha\beta'\alpha'}=J_{\beta'\alpha'\beta\alpha}$. Although the notation in [2.22a] is more compact than in [2.21], the problem is not simplified since the double commutator has simply evolved into a double set of indices for the Redfield

matrix and for the spectral densities. It has been found that, at least for the spin systems encountered here, equation [2.21] is more convenient to work with.

It is interesting to note that the equation of motion of the spin density matrix given by the Bloch-Wangsness-Redfield approach may be put into the simple form of [2.11] with

$$(\partial\rho/\partial t)_{relax} = - [[\rho-\rho^{o}, \overline{H_r(t)}], H_r(t)] \tau_c \qquad [2.23]$$

Thus the two approaches to the spin density matrix concept both arrive at similar expressions, but with the relaxation interactions described by different models. The phenomenological relaxation model [2.12] is already in an explicit form, although it cannot yield specific information about the type of mechanisms responsible for the interactions since a simple exponential decay of undefined origin has been assumed. For the relaxation term [2.23], however, it remains to find a more useful form (or forms) which will depend explicitly on the mechanism responsible for the relaxation of the spins.

3. The Relaxation Mechanisms.

A number of different mechanisms have been discussed by Nageswara Rao (18) and by Farrar and Becker (8); however the discussion here will be restricted to those mechanisms prevalent in proton NMR, namely the isotropic random field mechanism and the intramolecular dipole-dipole mechanism. The actual origin of the former mechanism is not well-defined, and Kumar and Rao (119) have discussed some cases for which various interactions might be approximated by that mechanism.

A general expression may be written for the Hamiltonian $\mathcal{H}_r(t)$ describing the interaction of the spins with their surroundings (4, 17,18)

$$\mathcal{H}_r(t) = \sum_q F_q(t)\, A_q \qquad [2.24]$$

where the $F_q(t)$ are stationary random functions of the lattice and the A_q are functions of the spin angular momentum vector operators, with $F_q = (F_{-q})^*$ and $A_q = (A_{-q})^\dagger$ (following the definition of Abragam (4); the asterisk denotes a complex conjugate and the dagger denotes a Hermitian conjugate). The spin system of interest here involves two spin-1/2 nuclei, denoted by the subscripts A and B, and the Hamiltonian $\mathcal{H}_r(t)$ may be written in the form (4,17,18,103-107,113)

$$\mathcal{H}_r(t)^{RF} = \sum_i \gamma_i \left(H_{ix} I_{ix} + H_{iy} I_{iy} + H_{iz} I_{iz}\right) \qquad [2.25a]$$

with $\overline{|H_{ix}|^2} = \overline{|H_{iy}|^2} = \overline{|H_{iz}|^2} = \overline{|H_i|^2}/3$ and i=A,B; [2.25b]

and

$$\mathcal{H}_r(t)^{DD} = \{I_{Az}I_{Bz} - \tfrac{1}{4}(I_{A+}I_{B-} + I_{A-}I_{B+})\} F_o + (I_{Az}I_{B+} + I_{A+}I_{Bz}) F_1 + (I_{Az}I_{B-} + I_{A-}I_{Bz}) F_{-1} + (I_{A+}I_{B+}) F_2 + (I_{A-}I_{B-}) F_{-2} \qquad [2.26a]$$

with $\overline{|F_o|^2} = 4/5k^2$; $\overline{|F_1|^2} = \overline{|F_2|^2} = 3/10k^2$ and $k = \hbar\gamma_A\gamma_B(r_{AB})^{-6}$. [2.26b]

Here the superscript RF denotes the isotropic random field mechanism with components of the field H_{AX} etc. at nucleus A, and the superscript DD denotes the intramolecular dipole-dipole mechanism with

components F_i which are dependent on the internuclear separation r_{AB}. The isotropism of the RF mechanism is contained in [2.25b], while equation [2.26b] displays the expected r^{-6} of a dipolar interaction. It should also be pointed out that these equations are derived with the assumption that any interactions occur independently of one another.

Using the expressions in [2.25] and [2.26] in equation [2.23],+ the relaxation matrix $(\partial\rho/\partial t)_{relax}$ may be evaluated in a straight-forward manner. The resultant matrix is real and symmetric, and its elements in the upper triangle have been listed in Table I, relative to the basis set of product vectors (see Appendix A), for the two mechanisms. Note that the matrix (for either mechanism and for the phenomenological model) is also symmetric about the secondary diagonal, reflecting a spin-inversion symmetry (17). Another very useful result, which follows from the extreme narrowing approximation (18, 104), is that the expressions for a given term are valid not only in the Schrödinger representation, but also in an interaction representation (see Chapter III) provided that the spin density matrix elements ρ_{ij} are replaced by their corresponding interaction repres-

---

+the Redfield notation in equation [2.22] may also be employed; for example the element $\Gamma_{1111}(\rho-\rho^o)$ is given by

$$\Gamma_{1111}(\rho-\rho^o) = \sum_{\beta,\beta'} \sum R_{11\beta\beta'} (\rho-\rho^o)_{\beta\beta'} .$$

For the DD mechanism, it follows that the only nonzero terms $R_{11\beta\beta'}$ are $R_{1111}=-3/5(T_D)^{-1}$ and $R_{1122}=R_{1133}=R_{1123}=R_{1132}=R_{1144}/4 = (T_D)^{-1}/10$, which yields a result identical with the expression in Table I for the element $(\partial\rho_{11}/\partial t)_{relax}$.

Table I.

Elements of the symmetric relaxation matrix $(\partial\rho/\partial t)_{relax}$ for a system of two spin-1/2 nuclei, relative to the basis set of spin product vectors $|1\rangle = |\alpha\alpha\rangle$, $|2\rangle = |\alpha\beta\rangle$, $|3\rangle = |\beta\alpha\rangle$ and $|4\rangle = |\beta\beta\rangle$. The relaxation mechanisms are external isotropic random fields (RF) and intramolecular dipole-dipole (DD). The diagonal elements ρ_{ii} are abbreviations, and should be written as $(\rho_{ii}-\rho^{o}_{ii})$. The parameters ω_s, η, r and T_D are defined in equations [2.27] and [2.28].

Element	RF[a]	DD[b]
(1,1)	$-2\rho_{11} + (1-\eta)\rho_{22} + (1+\eta)\rho_{33} + r(\rho_{23}+\rho_{32})$	$-3/5\rho_{11} + 1/10(\rho_{22} + \rho_{23} + \rho_{32} + \rho_{33} + 4\rho_{44})$
(1,2)	$-(3-\eta)\rho_{12} - r(\rho_{13}-\rho_{24}) + (1+\eta)\rho_{34}$	$-17/30\rho_{12} + 1/10(\rho_{24} + \rho_{34}) - 7/30\rho_{13}$
(1,3)	$-(3+\eta)\rho_{13} - r(\rho_{12}-\rho_{34}) + (1-\eta)\rho_{24}$	$-17/30\rho_{13} + 1/10(\rho_{24}+\rho_{34}) - 7/30\rho_{12}$
(1,4)	$-(4+2r)\rho_{14}$	$-3/5\rho_{14}$
(2,2)	$-2\rho_{22} + (1-\eta)\rho_{11} + (1+\eta)\rho_{44} + r(\rho_{23}+\rho_{32})$	$-4/15\rho_{22} + 1/10(\rho_{11} - \rho_{23} - \rho_{32} + \rho_{44}) + 1/15\rho_{33}$
(2,3)	$r(\rho_{11} - \rho_{22} - \rho_{33} + \rho_{44}) - (4-2r)\rho_{23}$	$-4/15\rho_{23} + 1/10(\rho_{11} - \rho_{22} - \rho_{33} + \rho_{44}) + 1/15\rho_{32}$
(2,4)	$-(3+\eta)\rho_{24} + r(\rho_{12}-\rho_{34}) + (1-\eta)\rho_{13}$	$-17/30\rho_{24} + 1/10(\rho_{13}+\rho_{12}) - 7/30\rho_{34}$

Table I (continued)

Element	RF[a]	DD[b]
(3,3)	$-2\rho_{33} + (1+\eta)\rho_{11} + (1-\eta)\rho_{44} - r(\rho_{23}+\rho_{32})$	$-4/15\rho_{33} + 1/10(\rho_{11} - \rho_{23} - \rho_{32} + \rho_{44}) + 1/15\rho_{22}$
(3,4)	$-(3-\eta)\rho_{34} + r(\rho_{13}-\rho_{24}) + (1+\eta)\rho_{13}$	$-17/30\rho_{34} + 1/10(\rho_{12}+\rho_{13}) -7/30\rho_{24}$
(4,4)	$-2\rho_{44} + (1-\eta)\rho_{11} + (1+\eta)\rho_{22} + r(\rho_{23}+\rho_{32})$	$-3/5\rho_{44} + 1/10(\rho_{22} + \rho_{23} + \rho_{32} + \rho_{33} + 4\rho_{11})$

[a] to be premultiplied by $\omega_s/3$.

[b] to be premultiplied by $(T_D)^{-1}$.

entation elements $\rho_{ij}{}^{i}$.

The elements for the RF mechanism have been expressed in terms of the following definitions (cf. Hoffman (17))

$$\omega_s = \tfrac{1}{2} \{\gamma_A{}^2 \overline{|H_A{}^2|} + \gamma_B{}^2 \overline{|H_B{}^2|} \} \tau_c \qquad [2.27a]$$

$$\eta = \{\overline{|H_B{}^2|} - \overline{|H_A{}^2|} \} / \{ \overline{|H_A{}^2|} + \overline{|H_B{}^2|} \} \qquad [2.27b]$$

and $$r = 2 \overline{|H_{Ax} H_{Bx}|} / \{\overline{|H_A{}^2|} + \overline{|H_B{}^2|} \} \qquad [2.27c]$$

with $\gamma_A = \gamma_B$. These parameters are, respectively, a measure of the strength of the interaction of the spins with their surroundings, the asymmetry of the interaction at the two nuclei (η=0 corresponds to the case where both nuclei interact equally), and the extent of correlation of the random fields at the two nuclei. With respect to the correlation parameter r, two extreme cases are often reported in the literature: - the completely correlated random field (r=1), which will be denoted as RFC, and the uncorrelated (r=0) random field, RFUC.

The elements of the dipole-dipole mechanism are expressed in terms of the parameter T_D (after Freeman et. al. (113)), where

$$T_D = (3/2\ k^2\ \tau_c)^{-1} \qquad [2.28]$$

and which is inversely related to the strength of the dipolar interaction.

It is also possible to have both of the above mechanisms competing independently to relax the spin system, in which case the relaxation matrix is given by a matrix sum for the two mechanisms. This case has been studied by Freeman et. al. (113), although most of the research in this area assumes that one or other of the mechanisms dominate in

the relaxation of protons (17,18,101-107).

Compared with the phenomenological model, where the diagonal elements are of the simple form $(\rho-\rho^{o})_{ii}/T_1$ and the off-diagonals of the form $-\rho_{ij}/T_2$, it is clear that the more theoretical models yield considerably more complex expressions for the relaxation matrix. It appears, for example, that it is no longer possible to define simple parameters like the spin-spin and spin-lattice relaxation times[+]. A further interpretation and comparison of these results must be deferred until the latter half of the next section.

4. Summary.

To summarize the discussion of the spin density matrix to this point, the following features might be restated:

(a). the equation of motion of the spin density matrix is

$$d\rho/dt = i\,[\rho, H_s(t)] + (\partial\rho/\partial t)_{relax}$$

where the term $(\partial\rho/\partial t)_{relax}$ is given either by [2.12] or by [2.23] (and the required expressions in Table I for a particular mechanism).

(b). The Hamiltonian $H_s(t)$ in the above expression is the usual NMR Hamiltonian; its explicit form is presented in some detail in Chapter III for the variations of the NMR experiment.

(c). The equilibrium spin density matrix required by [2.12] or [2.23] obeys equation [2.7] with H being the static part of $H_s(t)$ (see Chapter III).

[+]for a single spin-1/2 system and using the above mechanisms, one can define parameters T_1 and T_2 describing the relaxation of the diagonal and off-diagonal elements.

(d). The properties [2.8] and [2.9] and equation [2.4] are obeyed by the spin density matrix; in particular it may be shown that the equation of motion conserves the normalization and Hermiticity properties (cf. Hoffman (17)) for either of the relaxation models described. The equation [2.4] is concerned with the observable in NMR, which is the subject of the next section.

C. The NMR Observable.

1. Derivation of the Observable.

In order to complete the density matrix description of the NMR phenomenon, it remains to specify an operator corresponding to the NMR observable. As mentioned for the Bloch equations, the common method of detection involves a receiver coil mounted along the y-axis, and the signal S is an induced voltage which depends on the time rate of change of the magnetization along that axis. It follows that

$$S \propto d\langle M_y \rangle / dt \quad . \qquad [2.29]$$

Associating the magnetization M_y with the operator I_y and using [2.4], a general expression for the signal is

$$S \propto \frac{d}{dt} \; tr\,(\rho I_y), \qquad [2.30]$$

ignoring constants of proportionality.

In the solution of the equation of motion of the spin density matrix, it is convenient to work in an interaction representation defined by some unitary operator U. Since the trace of a matrix is invariant under a unitary transformation, [2.30] may be rewritten as

$$S \propto \frac{d}{dt} \; tr\,(\rho^i I_y^{\,i}) = tr\,\{\frac{d\rho^i}{dt} I_y^{\,i} + \rho^i \frac{dI_y^{\,i}}{dt}\} \qquad [2.31]$$

where $\rho^i = U\,\rho\,U^{-1}$ and $I_y^{\,i} = U\,I_y\,U^{-1}$. The choice of a suitable representation is invariably made so that $d\rho^i/dt$ is small[+], and consequently it may be shown that the first term on the rhs of [2.31] becomes negligible. An example of such a transformation is given by

[+] the steady-state approximation (cf. Appendix B) allows that $d\rho^i/dt \simeq 0$.

$$U = \exp(i\omega_1' t\, I_z) \qquad [2.32]$$

and which gives the familar frame rotating at the frequency ω_1' of the perturbing rf field. This rf field is of the form $H_p(\text{Cos } \omega_1' t\, \underline{i} - \text{Sin } \omega_1' t\, \underline{j})$ for single resonance cw NMR (Chapter III), and ω_1' is of the order of the Larmor frequencies. Using [2.11], [2.31] and [2.32],

$$d\rho^r/dt = i[\rho^r, H_s^r] + (\partial\rho^r/\partial t)_{relax} \qquad [2.33a]$$

$$d(I_y{}^r)/dt = \omega_1' (I_x \text{ Cos } \omega_1' t + I_y \text{ Sin } \omega_1' t) \qquad [2.33b]$$

where the superscript "r" denotes the rotating frame. Now it may be easily shown that it is the commutator which dominates in [2.23a], and that the magnitude of the expression for $d\rho^r/dt$ is of the order of the Larmor frequency difference $\Delta\omega_i$ in this representation. It follows, therefore, that the first term in [2.31] is negligibly small since Larmor frequency differences are much less than Larmor frequencies (ie. $\Delta\omega_i << \omega_1'$; cf. Bloch (85)).

It is useful to pursue these equations further, using [2.33b] and [2.31] to obtain the expression

$$S = \omega_1' \text{ tr } (\rho^r I_x) \text{ Cos } \omega_1' t + \omega_1' \text{ tr } (\rho^r I_y) \text{ Sin } \omega_1' t \qquad [2.34]$$

where ρ^r is in the rotating frame while I_x and I_y are in the stationary (lab) frame. It was mentioned in section 1.2 that the detection system employed may be phase-sensitive, and it is the voltage <u>amplitude</u> which is of interest. With respect to the observing field of frequency ω_1', the in-phase or dispersion mode is given by the cosine term and the out-of-phase or absorption mode is given by the sine term (1). It is

convenient to incorporate these effects by rewriting [2.34] as

$$S = \omega_1' \ tr\ (\rho^r I_+) \qquad [2.35]$$

where the substitution $I_+ = I_x + iI_y$ is introduced, as for the Bloch equations, so that the real and imaginary parts of S correspond to the dispersion and absorption modes, respectively. Note that although the expectation values of an observable in quantum mechanics should be real quantities, the disparity implied by [2.35] is artificial. This last equation is the form of the signal appearing most often in the literature (see for example references (17) and (18)); in the lab frame its form is (cf. Bloch (85), equations [7.75] and [7.76])

$$S = \omega_1' \ tr\ (\rho I_+) \exp(-i\omega_1' t) \qquad [2.36]$$

where t is the time at which the signal is sampled[+]. The effect of the term $\exp(-i\omega_1' t)$ is to remove the cosine and sine oscillations, as in [2.31], and as such this term simulates the demodulator present in a high-resolution NMR spectrometer.

2. The Effect of a Finite Sweep Rate.

For the detection system used in cw NMR, a further alteration to equation [2.36] may be required since the observing frequency ω_1' is often a variable quantity. Consequently the term $\exp(-i\omega_1' t)$ must

---

[+] note that the equation

$$S \propto \frac{d}{dt} \{ tr\ (\rho I_+) \} \exp(-i\omega_1' t)$$

appearing in reference (114) is consistent with [2.35] and [2.36] since the above argument allows that, in the rotating frame, $d\rho^r/dt = 0$, and therefore that $S \propto tr(\rho^r I_+)$ as required.

be replaced by the term (cf. Bloch (85), equation [3.13])

$$\exp\left(-i \int_0^t \omega_1'(\tau)\, d\tau \right) \qquad [2.37]$$

where $\omega_1'(\tau)$ describes the functional dependence of the frequency ω_1' on time. The common experimental arrangement is a linear sweep[+]

$$\omega_1' = \omega_o' + a\tau \qquad [2.38]$$

where $\omega_1'=\omega_o'$ at time t=0 (by definition) and where "a" is the rate of frequency scan in units of radians/second/second. The presence of a variable frequency also complicates the development leading from [2.31] to [2.34]; however for a linear sweep rate obeying the inequality $|a|<<\omega_1'$, a similar argument yields [2.34] (the case for $|a|\simeq \omega_1'$ is not commonly encountered in high-resolution NMR; however the problem could arise, for example, in experiments using the earth's magnetic field as the static magnetic field).

Finally, another complication should be mentioned for the case of double or multiple resonance experiments. For more than one rf field, the signal defined above contains a number of components, each oscillating at different frequencies, whereas the desired response is (usually) that component oscillating at the frequency ω_1' of the

---

[+]the ensuing discussion and equations assume a linear frequency scan. An alternate arrangement allows that the static field is swept linearly in its magnitude H_o, and suitable modifications must then be made to the nuclear Zeeman terms of the static NMR Hamiltonian. For single resonance, the two types of sweep yield very similar results, while for double resonance a frequency sweep is usually more desirable so that any analyses are simplified (77).

observing rf field. This component is extracted by means of a Fourier analysis for other methods of calculation (see, for example, references (18,67-69,77,85,86,88-95,104-107)), corresponding to the use of frequency filters in the spectrometer. The Fourier analysis method becomes very complex for a time-dependent frequency, and an alternate method, to be discussed in Chapter IV for double resonance experiments, must be devised for the method of calculation discussed herein.

3. Interpretation of the Observable.

It is now possible to use the above results to interpret the various off-diagonal elements of the spin density matrix as transition probabilities. Suppose, for example, that the basis product vectors are eigenvectors of the Hamiltonian for a two spin-1/2 system (the "AX" limit (1-3); cf. page 124). The matrix for the raising operator I_+, relative to this basis, is simply

$$I_+ = \begin{bmatrix} 0 & 1 & 1 & 0 \\ 0 & 0 & 0 & 1 \\ 0 & 0 & 0 & 1 \\ 0 & 0 & 0 & 0 \end{bmatrix} \qquad [2.39]$$

and, upon taking the trace called for by equation [2.35], it follows that

$$S \propto \rho^r_{21} + \rho^r_{31} + \rho^r_{42} + \rho^r_{43} \qquad [2.40]$$

These elements are now calculated from the expression [2.11], and in the steady-state non-saturated limit (and in the rotating frame), it may be shown (cf. Appendix B) that ρ^r_{21} corresponds to the transition $|\alpha\beta\rangle \rightarrow |\alpha\alpha\rangle$, ρ^r_{31} to the transition $|\beta\alpha\rangle \rightarrow |\alpha\alpha\rangle$, etc. These results are shown diagrammatically in figure 2. The double quantum transition (forbidden in the AX limit) is associated with the element ρ^r_{41},

Figure 2.

Schematic energy level diagram and corresponding single resonance spectrum of a system of two coupled spin-1/2 nuclei. The basis product vectors $|1\rangle = |\alpha\alpha\rangle$, $|2\rangle = |\alpha\beta\rangle$, $|3\rangle = |\beta\alpha\rangle$ and $|4\rangle = |\beta\beta\rangle$ are eigenvectors of the nuclear Zeeman part of the high-resolution NMR Hamiltonian. DQ denotes the double quantum transition.

Figure 3.

Schematic energy level diagram of a system of two coupled spin-1/2 nuclei, subjected to a strong rf field centered at transition 1 (of figure 2) and which tends to mix the two vectors $|1\rangle$ and $|3\rangle$. The spectrum on the right is a schematic representation of the expected frequency-swept signal, showing intensity changes due to population transfers and the appearance of new frequencies due to the strong mixing of the perturbed energy levels.

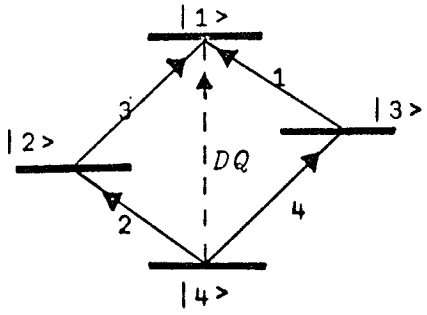
|1>
|2>
|3>
|4>
DQ
1
2
3
4

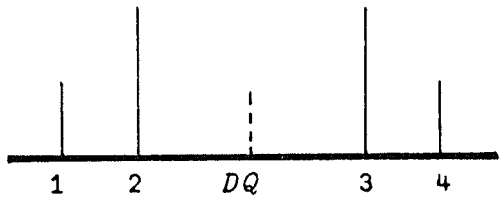
1
2
DQ
3
4

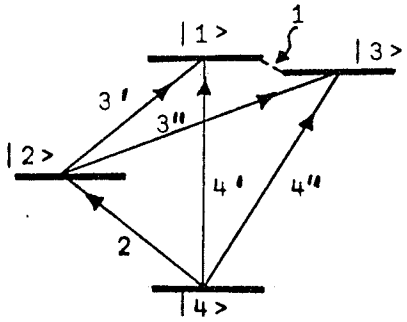
|1>
|2>
|3>
|4>
1
3'
3"
4'
4"
2

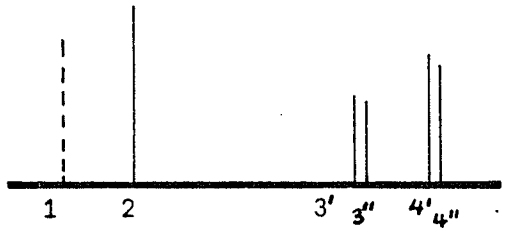
1
2
3'
3"
4'
4"

while the transition corresponding to the off-diagonal ρ^r_{32} is not allowed (17).

Consider now the double resonance experiment in which the transition 1 of figure 2 is perturbed by the second rf field. The resultant energy level diagram is shown schematically in figure 3, where it is assumed that the perturbation mixes the connected energy levels so strongly that they become near-degenerate. The "extra" transitions 3" and 4" correspond to the matrix elements ρ^r_{41} and ρ^r_{32} which do not appear explicitly in [2.40], but which are coupled into the expressions for ρ^r_{21}, ρ^r_{31}, etc., by virtue of the second rf field (cf. Appendix B).

As a final example, consider the case of three spin-1/2 nuclei. Using the basis product set of vectors, one has that

$$S \propto \rho^r_{21} + \rho^r_{31} + \rho^r_{41} + \rho^r_{52} + \rho^r_{62} + \rho^r_{53} + \rho^r_{73} + \rho^r_{64} + \rho^r_{74} + \rho^r_{85} + \rho^r_{86} + \rho^r_{87} \qquad [2.41]$$

with each element corresponding to one of the twelve possible transitions of an AMX system (1-3) as shown in figure 4. It is well-known that an ABC may have up to fifteen transitions; the extra "combination" lines may be shown to correspond to the elements ρ^r_{54}, ρ^r_{63} and ρ^r_{72} which are coupled into the relevant expressions for the elements in [2.41] due to spin-spin coupling. These results display the general case of the observable in the density matrix description for a system of spins. Each element of the spin density matrix appearing in [2.35] corresponds to one of the first-order transitions of that system, and any extra lines may be assigned to various other off-diagonal elements which appear implicitly in equation [2.35].

Figure 4.

Schematic energy level diagram for a system of three spin-1/2 nuclei. The basis product set $|1\rangle=|\alpha\alpha\alpha\rangle$, $|2\rangle=|\alpha\alpha\beta\rangle$, $|3\rangle=|\alpha\beta\alpha\rangle$, $|4\rangle=|\beta\alpha\alpha\rangle$, $|5\rangle=|\alpha\beta\beta\rangle$, $|6\rangle=|\beta\alpha\beta\rangle$, $|7\rangle=|\beta\beta\alpha\rangle$ and $|8\rangle=|\beta\beta\beta\rangle$ are eigenvectors of the nuclear Zeeman part of the high-resolution NMR Hamiltonian. The first-order transitions and their corresponding off-diagonal elements are shown by the solid lines between energy levels, while the combination lines and their corresponding elements are given by the broken lines.

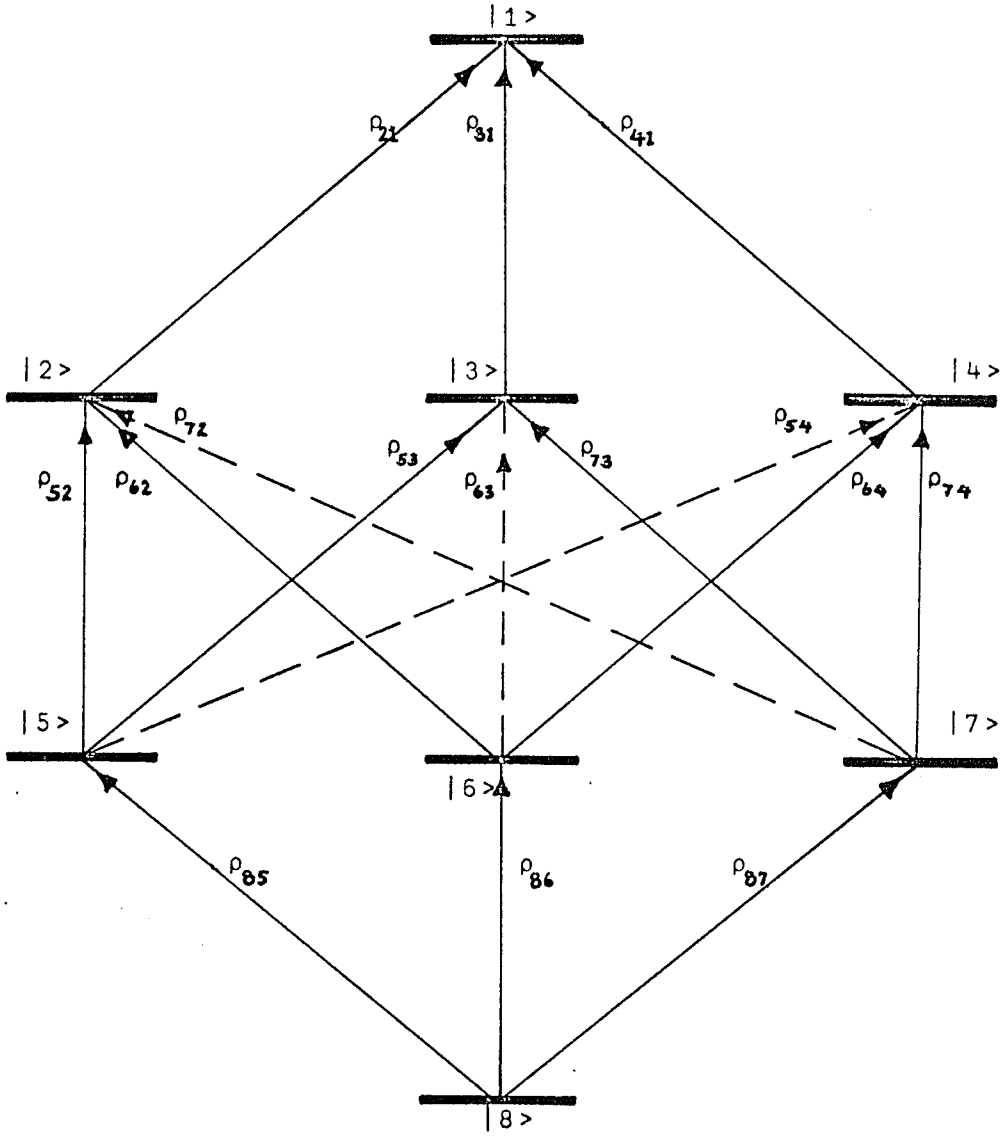
|1>
|2>
|3>
|4>
|5>
|6>
|7>
|8>
ρ21
ρ31
ρ41
ρ72
ρ53
ρ73
ρ54
ρ52
ρ62
ρ63
ρ64
ρ74
ρ85
ρ86
ρ87

4. The Effects of Relaxation.

It is also instructive to consider here the different models available to describe relaxation interactions. First of all, the commutator in [2.11] largely determines the transition frequencies, while it is the relaxation matrix $(\partial\rho/\partial t)_{relax}$ which largely determines the shape of the transition. Consider, for the moment, an AX system of spin-1/2 nuclei so that the basis product vectors are eigenvectors of the high-resolution Hamiltonian, and suppose further that the transitions are well-separated in frequency (ie. there is no overlap). It can then be shown (cf. Appendix B) that the unsaturated absorption mode signal is of the form

$$S \propto \sum_{k=1}^{4} \frac{T_{2k}}{1 + T_{2k}^{2} (\omega_k - \omega_1')^2} \qquad [2.42]$$

where ω_k is the transition frequency, and where T_{2k} denotes that term premultiplying the matrix element ρ_{ij}^r in $(\partial\rho_{ij}^r/\partial t)_{relax}$. The element ρ_{ij}^r is that matrix element, from the list in [2.40], which corresponds to the transition at frequency ω_k.

Each term in the summation [2.42] resembles equation [1.4] - the solution of a Bloch equation for a single transition, and one therefore associates the parameter T_{2k} with the spin-spin relaxation time of the transition at ω_k. For the phenomenological relaxation model, one finds the not unexpected result that $T_{2k}=T_2$, so that the half-height line width of each transition described by this model should be $2/T_2$ seconds^{-1}.

For the case of an AB system of spin-1/2 nuclei, similar results

may be obtained if the transitions are well-separated, and using the Hamiltonian eigenvector basis (see Chapter III, section 2). The half-height line widths for an AB system and for the two models (including the DD and RF mechanisms for the Bloch-Wangsness-Redfield model) have been tabulated in Table II; the results for an AX system may be obtained by setting $2\phi=0$. Some of the more striking observations are listed below.

(a). Only the more theoretical model allows that different transitions may have different half-height line widths (but recall the footnote on page 23), and in every case the DD mechanism always has that the inner transitions are broader than the outer transitions.

(b). As $2\phi \to 0$, the transitions all possess the same line width for the DD mechanism, whereas for the RF mechanism the "A" transitions (1 and 2) and the "B" transitions (3 and 4) have different line widths provided that $\eta \neq 0$.

(c). The double quantum transitions are (usually) narrower than the single quantum transitions[+], and it appears that the phenomenological model underestimates this width if this model is to be representative of either the RFUC, RFC or DD mechanisms.

(d). It appears that the RF mechanism may be used to approximate a number of interactions, as reported by Kumar and Rao (119), since there

---

[+] the term premultiplying ρ^r_{41} is the line-width, whereas the term pre-multiplying, for example, ρ^r_{21} is one-half the line-width. In general, for a transition involving n quanta, a factor of 1/n must be introduced into the required term for the line width; this point is discussed in some detail in references (17) and (96).

Table II.

The full line width at half-height for the transitions of an AB system of spin-1/2 nuclei, assuming well-separated transitions and no effects due to saturation. Relaxation effects are described by the phenomenological model (phen.) and by the more theoretical Bloch-Wangsness-Redfield model; for this last model the mechanisms are the external isotropic random field (RF) and the intramolecular dipole-dipole mechanisms. Refer to figure 2 for the labelling of the transitions, and to Chapter III (Table III) for the definition of the angle ϕ.

Transition	Model		
	phen.	RF[a]	DD[b]
1	$2/T_2$	$3+\eta\text{Cos}2\phi-r\text{Sin}2\phi$	$17/30-7/30\text{Sin}2\phi$
2	$2/T_2$	$3+\eta\text{Cos}2\phi+r\text{Sin}2\phi$	$17/30+7/30\text{Sin}2\phi$
3	$2/T_2$	$3-\eta\text{Cos}2\phi+r\text{Sin}2\phi$	$17/30+7/30\text{Sin}2\phi$
4	$2/T_2$	$3-\eta\text{Cos}2\phi-r\text{Sin}2\phi$	$17/30-7/30\text{Sin}2\phi$
DQ	$1/T_2$	$2+r$	$-9/30$

[a] in units of $2\omega_s/3$.

[b] in units of $2/T_D$.

are a number of adjustable parameters which allow a wide variation in the resultant line shapes.

A last point which might be mentioned is that the phenomenological model oversimplifies the description of the rate of relaxation of the diagonal elements of ρ if that model is to represent a given relaxation mechanism. For the more theoretical models, one may define "generalized longitudinal relaxation times" T_{1k} for the spin state $|k\rangle$ with population ρ_{kk} (4,17,84), but in general each population is coupled to every other population in a complex manner (cf. Table I and Abragam (4), page 523), and it becomes a difficult task to interpret the resultant expressions.

A more straight-forward approach is to scrutinize closely the equations in Table I, in order to gain some insight into spin-lattice type relaxation. Now since strong rf fields (or some pulse sequences; see Appendix C) tend to equalize population distributions, one can make, for example, the following predictions:

(a). for the single resonance of an AB system, if that system is relaxed by a DD mechanism as opposed to an RF mechanism, then (all other things being equal) the DQ transition should saturate less quickly. This follows since the DQ transition connects the spin states $|1\rangle$ and $|4\rangle$, tending to equalize ρ^r_{11} and ρ^r_{44}, and only the DD mechanism allows a <u>direct</u> path whereby the two states can relax with one another (ie. ρ^r_{11} and ρ^r_{44} are coupled directly).

(b). The nuclear Overhauser effect (77,120) occurs when one strong rf field disturbs the population distribution of two spin states, with the effects monitored by a second rf field. One can therefore explain

the "inverted" intensities in figure 3 in terms of a population redistribution, with $|1\rangle$ gaining population at the expense of $|3\rangle$. Since the intensity of a transition depends on the population difference between the spin states it connects, one predicts that the transitions 3' and 3" are attenuated while the transitions 4' and 4" are enhanced as the rf field centered at transition 1 grows in intensity. Furthermore, one predicts that there will appear differential effects in intensities if the system is relaxed by the DD or the RF mechanisms or if the system is described by the phenomenological model.

These last two observations serve as a basis for the determination of the explicit nature of the relaxation mechanisms using high-resolution NMR (cf. Worvill and Harris (102) and Nageswara Rao (18)). The required premise is simply that different relaxation mechanisms may relax a given system in different ways, and when one employs an rf field which is either strong enough to compete effectively with the relaxation or which inverts a population distribution, differential effects may become observable. An interpretation of the observed results is usually achieved by comparison of experimental spectra with calculated spectra (in cw NMR).

CHAPTER III. FORMULATION OF THE PROBLEM

A. Introduction.

The relevant equations for the spin density matrix have been discussed in the previous chapter, with the two important expressions being that for the signal and that for the equation of motion of the spin density matrix. It was shown that the expression for the signal:

$$S \propto \mathrm{tr}\,(\rho\, I_+)\, \exp(-i\omega_1' t) \qquad [3.1]$$

involves a number of off-diagonal elements of ρ, and it remains now to calculate these elements using

$$d\rho/dt = i[\rho, H_s(t)] + (\partial\rho/\partial t)_{\mathrm{relax}} . \qquad [3.2]$$

In the special case that the system is in a state of thermal equilibrium, the spin density matrix is given by ρ^o where

$$\rho^o = 1/Z \exp(-\hbar H/kT) \qquad [3.3]$$

with H being the high-resolution NMR Hamiltonian.

Equation [3.2] is considerably simplified by invoking the steady-state approximation; this approximation (or related approximations) are often used in other methods for the calculation of response in NMR (cf. Appendix B). To achieve this end, the Hamiltonian is partitioned

$$H_s(t) = H + H_p(t) \qquad [3.4]$$

where H is the usual high-resolution NMR Hamiltonian and $H_p(t)$ represents a time-dependent perturbation characterizing the type of experiment being performed. Both Hamiltonians are discussed in some detail below; here it suffices to note that the dominant term in [3.4] and also in [3.2] is that involving H. It was shown previously that

a suitably-chosen unitary transformation to an interaction representation largely eliminates the effect of H, so that the transformed equation of motion is very small. That is, for the equation

$$d\rho^i/dt = i[\rho^i, H_s^i(t)] + (\partial\rho/\partial t)_{relax} \qquad [3.5]$$

it follows that $|d\rho^i/dt| << |d\rho/dt|$. This result then allows the introduction of the steady-state approximation, with $d\rho^i/dt \equiv 0$, and [3.5] therefore reduces to a system of coupled linear equations in the matrix elements of ρ^i. These equations may be solved numerically (or in favorable cases, analytically) for the required off-diagonal elements ρ^i_{mn} appearing in the expression

$$S \propto tr\ (\rho^i\ I_+^i)\ \exp(-i\omega_1't) \qquad [3.6]$$

for the signal. These solutions are, however, restricted to the calculation of those experiments which allow a steady-state (or related) approximation; for a general solution one must solve the system of coupled linear differential equations [3.2] or [3.5]. The development of such a technique represents the primary goal of this thesis; however it is anticipated here that the transformation to an interaction representation represents a desirable simplification of the set of differential equations. The steady-state approximation will <u>not</u> be invoked however (nor will a number of other assumptions), and consequently the signal eventually calculated represents the actual dynamic response of the spin system to a given perturbation. The details of the technique are deferred to Chapter IV; the remainder of this chapter is concerned with the Hamiltonian and other features required to describe the high-resolution NMR experiments.

B. The High-Resolution NMR Hamiltonian.

The Hamiltonian required in equation [3.2] is partitioned according to [3.4] into two parts. The term $H_p(t)$ characterizes the type of experiment being performed, and it is discussed below; on the other hand H is common to all the high-resolution NMR experiments and it characterizes the actual spin system under study.

The nature of H has been well-established, and it may be written in the general form (cf. references (1-7))

$$H = H_o + H_c \qquad [3.7]$$

in units of $\hbar$. The first term on the rhs of this equations is the nuclear Zeeman interaction, representing the energy of interaction between the nuclei in a molecule possessing a nuclear magnetic moment $\underline{\mu}$, and the static magnetic field $\underline{H}_o$. Classically, this energy of interaction is given by the vector dot product $-\underline{\mu} \cdot \underline{H}_o$ and the quantum mechanical expression is found by associating a spin angular momentum vector operator $\underline{I}$ with $\underline{\mu}$: $\underline{\mu} = \sum_n \gamma_n \underline{I}_n$. Here γ_n is the gyromagnetic ratio of nuclear species n and the summation is over all those nuclei possessing spin. For a static magnetic field $\underline{H}_o = -H_o \underline{k}$ defining the negative z-axis[+], the nuclear Zeeman term becomes

$$H_o = \sum_n \gamma_n H_o I_{nz} \qquad [3.8]$$

where I_{nz} is the z-component of $\underline{I}$. For high-resolution NMR, it is

---

[+] often $\underline{H}_o$ is taken to define the positive z-axis so that the resultant energies are negative. This also inverts the order of the eigenstates and the sense of the transitions, although the differences are really just semantic in origin.

well-known that the Zeeman energy of a nucleus depends on its chemical environment (1-8), and the energy differences have been attributed to a partial "screening" of the nuclei from the field $\underline{H}_o$ due to an induced magnetic field set up by the precession of the electrons about $\underline{H}_o$. This induced field is antiparallel and proportional to the field so that [3.8] is modified to

$$H_o = \sum_n \gamma_n (1-\sigma_n) H_o I_{nz} = \sum_n \omega_n I_{nz} \qquad [3.9]$$

with $\omega_n = \gamma_n(1-\sigma_n)$ and where σ_n, the nuclear screening (shielding) constant, is a function of the chemical environment or electronic distribution at nuclear species n. It is the screening constant, and through it the Larmor frequency ω_n, which reflects the sensitivity of a nucleus to its environment. In a typical proton system, for example, with $H_o=10^4$ gauss and $\gamma_p=2.67519\times10^4$ radians/second/gauss, the Larmor frequencies may vary by hundreds of radians/second from the bare proton resonance at $\gamma_p H_o=2.67519\times10^8$ radians/second.

The second term on the rhs of [3.7] is the Hamiltonian describing the interactions between two or more magnetic moments in the molecule. These interactions result in the appearance of multiplets in the place of a single transition, and the nature of these multiplets led to the expression (1-8):

$$H_c = \sum_{m<n} \sum J_{mn} \underline{I}_m \cdot \underline{I}_n \qquad [3.10]$$

where J_{mn}, the spin-spin coupling constant, is a scalar[+] describing the magnitude of the interaction between spin species m and n. The double

[+] in fact both J and σ are tensor quantities which may be approximated by scalars due to the rapid isotropic motion of liquids and gases (1-8).

summation in this equation merely indicates a sum over all pairs of spin-spin interactions.

An example of the matrix representation of H is presented below for two spin-1/2 nuclei, using the basis product vectors. Proceeding as in equation [1.9] for the indirect method, one finds the corresponding eigenvalues and eigenvectors listed in Table III; the eigenvalue differences along with equation [1.10] yield the expected transition frequencies and amplitudes (the double quantum transition is calculated using a higher order result from perturbation theory; cf. references (2) and (96)). The case shown in Table III is that for an AB system of nuclei (1), for which $|J| \simeq |\delta|$. If $|J| << |\delta|$, one may invoke the "AX approximation" (1-7) which allows that the off-diagonals of H_c are negligible; the results in Table III then apply with $\phi = \pi/2$.

$$H = \begin{bmatrix} \Delta'+J/4 & 0 & 0 & 0 \\ 0 & \delta/2-J/4 & J/2 & 0 \\ 0 & J/2 & -\delta/2-J/4 & 0 \\ 0 & 0 & 0 & -\Delta'+J/4 \end{bmatrix} \qquad [3.11]$$

With $\delta = (\omega_1 - \omega_2)$ and $\Delta' = (\omega_1 + \omega_2)/2$.

It is useful to use the above results to express the equilibrium spin density matrix in a more detailed form than in equation [3.3]. Note that only the static high-resolution NMR Hamiltonian must be involved in the equation [3.3], since if any perturbation $H_p(t)$ is present and not negligible, then the system can attain a steady-state configuration but <u>not</u> an equilibrium configuration. The form of [3.3] also implies that an eigenvalue basis of H is being employed;

Table III.

Eigenvalues and eigenvectors of the high-resolution NMR Hamiltonian for a system of two spin-1/2 nuclei, and the corresponding transition frequencies and amplitudes. The labelling of the transitions and eigenstates is as in figure 2. The angle ϕ is given by $\mathrm{Tan}\ 2\phi = J/\delta$ where $\delta = (\omega_1 - \omega_2)$, the parameter R is given by $R = (\delta^2 + J^2)^{1/2}$ and the frequency origin is defined by the expression $\Delta' = (\omega_1 + \omega_2) \equiv 0$.

Eigenvector	Eigenvalue
$\|1\rangle = \|\alpha\alpha\rangle$	$\Delta' + J/4$
$\|2\rangle = \mathrm{Cos}\phi\ \|\alpha\beta\rangle + \mathrm{Sin}\phi\ \|\beta\alpha\rangle$	$R/2 - J/4$
$\|3\rangle = -\mathrm{Sin}\phi\ \|\alpha\beta\rangle + \mathrm{Cos}\phi\ \|\beta\alpha\rangle$	$-R/2 - J/4$
$\|4\rangle = \|\beta\beta\rangle$	$-\Delta' + J/4$

Transition	Frequency	Amplitude
$\|3\rangle \rightarrow \|1\rangle$	$R/2 + J/2$	$1 - \mathrm{Sin}\ 2\phi$
$\|4\rangle \rightarrow \|2\rangle$	$R/2 - J/2$	$1 + \mathrm{Sin}\ 2\phi$
$\|2\rangle \rightarrow \|1\rangle$	$-R/2 + J/2$	$1 + \mathrm{Sin}\ 2\phi$
$\|4\rangle \rightarrow \|3\rangle$	$-R/2 - J/2$	$1 - \mathrm{Sin}\ 2\phi$
$\|4\rangle \rightarrow \|1\rangle$	0	---

however the following approximations may be made:

(a) since the energies represented by $\hbar H$ are much less than kT, the exponential may be given, to a good approximation, by the first two terms in its polynomial expansion (the high-temperature limit);

(b) since the nuclear Zeeman term contribution to H dominates by a considerable margin, H may be approximated by H_o; and

(c) since the Larmor frequency differences are much less than the Larmor frequencies, the Zeeman term H_o may be approximated by [3.8] instead of [3.9].

With these considerations, the equilibrium spin density matrix is given by the expression(s)

$$\rho^o \simeq 1/Z(\mathbb{1} - \hbar H/kT) \simeq 1/Z(\mathbb{1} - \hbar H_o/kT) \simeq \mathbb{1}/Z - CI_z \quad [3.12]$$

where $\mathbb{1}$ is the identity matrix, and, assuming identical nuclei,

$$C = \hbar\omega_1/ZkT \quad (\omega_1=\omega_2=\gamma_n H_o). \quad [3.13]$$

Consequently the basis product vectors are eigenvectors of ρ^o as required[+]. An example of ρ^o is given below for an AB system of spin-1/2 nuclei; since $C<<1$ and $Z\simeq 4$, the populations are all very close to 0.2500, as expected.

$$\rho^o \simeq 1/Z \begin{bmatrix} 1-C & 0 & 0 & 0 \\ 0 & 1 & 0 & 0 \\ 0 & 0 & 1 & 0 \\ 0 & 0 & 0 & 1+C \end{bmatrix} \quad [3.14]$$

[+] the computer programmes written used the AX approximation (1-7) and the first expression in [3.12]; this basis set may then be applied.

C. The Single Resonance Experiment.

In the previous section it was implied that the transitions observed in a single resonance experiment are given by the eigenvalue differences of H with intensities as determined from the selection rule [1.10]. The derivation of this selection rule follows from an application of perturbation theory in which it is assumed that a small rotating field perpendicular to $\underline{H}_o$ couples the energy levels but does not, to first order, produce population changes or frequency shifts. In this case the resonance phenomenon is readily interpreted since energy will be absorbed by the spin system only when the frequency of the perturbation is near the energy difference between two eigenstates. In fact it is not the energy of absorption which is detected; as stated previously the signal is a voltage induced in a receiver coil due to changes in the y-magnetization, which in turn occurs as a result of the absorption of energy. The results of Table III indicate, for example, that a system of two spin-1/2 nuclei possesses four resonance frequencies of the order of the Larmor frequencies of the nuclei. The case involving strong rf fields becomes more complicated since the perturbation Hamiltonian will compete more effectively with the relaxation processes and mix the eigenstates, and a more detailed analysis of the interactions is required.

It is often more convenient, in the experimental arrangement, to employ a sinusoidally oscillating rf field $\underline{H}_{rf}$ rather than a rotating field. This field is generally linearly polarized perpendicular to $\underline{H}_o$ and is taken as defining the negative x-axis:

$$\underline{H}_{rf} = - 2 H_1 \text{ Cos } \omega_1' t \ \underline{i} \qquad [3.15]$$

with amplitude $2H_1$ and frequency ω_1'. If $\underline{H}_{rf}$ is now interpreted as a superposition of two fields of amplitude H_1 and rotating in the opposite senses at $\pm\omega_1'$, then a well-known approximation (1-4) allows that, for $H_1 << H_o$, the only important field is that rotating in the same sense as the Larmor precession. The other part of the rf field gives rise to the Bloch-Siegert shift (121) which may be ignored for the cases of interest here[+]. With this approximation, the energy of interaction $-\underline{\mu} \cdot \underline{H}_{rf}$ between the magnetic moment and the rf field is given by the perturbation Hamiltonian $H_p(t)$ where

$$H_p(t) = \sum_n \omega_n (H_1/H_o) (I_{nx}\mathrm{Cos}\omega_1't + I_{ny}\mathrm{Sin}\omega_1't) \quad [3.16]$$

where, as before, the summation is over all those nuclei possessing spin angular momentum. Note that this equation contains an in-phase component (the cosine term) and an out-of-phase component (the sine term), which is reflected in the expression for the signal (Chapter II).

It was also stated previously that it is useful to transform the equations to an interaction representation in order to simplify the solution procedure for the equation of motion. The transformation used here is that yielding the frame rotating at the frequency of the rf field, and it may be obtained from the unitary operator (1-5,17,60):

[+]the Bloch-Siegert shift is proportional to $(H_1/H_o)^2$. This approximation will fail for some experiments, such as experiments done with the earth's magnetic field being the static field or pulse sequences requiring large pulse amplitudes. In any case, however, the subsequent equations are valid for the case of a rotating rf field. This approximation is not strictly required for the solution procedure.

$$U = \exp(i\omega_1' t\, I_z) \qquad [3.17]$$

where $I_z = \sum_n I_{nz}$. The transformed Hamiltonian H_p^r may be rewritten, using [3.16], [3.17], and the properties of the spin angular momentum operators (cf. Appendix A or references (3,122,123)), in the form

$$H_p^r = \sum_n (\omega_n/2)\ (H_1/H_o)\ (I_{n+} + I_{n-}) \qquad [3.18]$$

where $I_\pm = I_x \pm i\, I_y$. An alternate derivation of [3.18] follows using [3.15], with the Hamiltonian put into the form

$$H_p(t) = \sum_n (\omega_n/2)\ (H_1/H_o)\ [\exp(i\omega_1' t)+\exp(-i\omega_1' t)] \times (I_{n+} + I_{n-})\ . \qquad [3.19]$$

Introducing the transformation [3.17], it follows that

$$H_p^r = \sum_n (\omega_n/2)(H_1/H_o)[\exp(i\omega_1' t)+\exp(-i\omega_1' t)] \times [I_{n+}\exp(i\omega_1' t)+I_{n-}\exp(-i\omega_1' t)]\ . \qquad [3.18a]$$

In order to obtain the expression [3.18] from [3.18a], one requires the omission of terms of the form of $\exp(\pm 2i\omega_1' t)$, another version of the approximation described above for the rotating fields. The two approaches for the simplification of H_p^r to [3.18] therefore yield the same result, although the latter procedure provides a more convenient form for the extension to multiple resonance (vide infra).

It is now instructive to consider the effect of the above transformation on the equation of motion of the spin density matrix. It may be readily shown that the transformed spin density matrix $\rho^r = U\,\rho\,U^{-1}$ obeys the equation (7,17)

$$d\rho^r/dt = i[\rho^r, H_s^r] + (\partial\rho^r/\partial t)_{relax} \qquad [3.20]$$

where, using [3.2], [3.4], [3.7], [3.9] and [3.10],

$$H_s^r = U\,H_s(t)\,U^{-1} = U\,H\,U^{-1} + U\,H_p(t)\,U^{-1}$$
$$= H^r + H_p^r \qquad [3.21a]$$

with $$H^r = H_o^r + H_c^r \qquad [3.21b]$$

$$H_o^r = \sum_n (\omega_n - \omega_1')\, I_{nz} \qquad [3.21c]$$

$$H_c^r = H_c = \sum_{m<n}\sum J_{mn}\, \underline{I}_m \cdot \underline{I}_n \qquad [3.21d]$$

and $$H_p^r = \sum_n (\omega_n/2)\,(H_1/H_o)\,(I_{n+} + I_{n-})\ . \qquad [3.21e]$$

Thus the effect of this transformation is to remove the explicit time-dependence of the perturbing field; further since the frequency ω_1' is of the order of the Larmor frequencies, the derivative $d\rho^r/dt$ is "small". A final note is warranted, however, since high-resolution NMR spectra are often obtained by varying the frequency of the rf field (or the static field amplitude H_o; refer to the footnote on page 40). Consequently the above equations contain an implicit time-dependence, and as noted in section II.C, terms like $\exp(\pm i\omega_1' t)$ must be replaced by terms like

$$\exp\left(\pm i \int_0^t (\omega_o' + a\tau)\, d\tau\right) \qquad [3.22]$$

assuming a linear sweep rate of "a" radians/second/second. This consideration also requires modifications to the Hamiltonian in the rotating frame; specifically the term ω_1' in [3.21c] must be altered to $\omega_o' + at$ (see section II.C). In the interests of brevity of notation, however, these equations and some equations to follow will be written in the simpler form as above.

The matrix representation of H_p^r is shown below for an AB system of spin-1/2 nuclei, relative to the basis product set. Since $H_p/H_o \ll 1$, H_p^r is often written in the form $\omega_p/2(I_+ + I_-)$ where $\omega_p = \omega_n(H_p/H_o)$ (n being the index for either the A or the B nucleus). One may also invoke the AX approximation for equations [3.21]; as before this involves ignoring the off-diagonals of H_c^r. In addition, however, it is possible to simplify the perturbation Hamiltonian since only a few of the off-diagonals ρ_{ij}^r appearing in the expression for the signal differ from zero near, say, the Larmor frequency of the B nucleus. To show this in detail one must expand the commutators, etc. (cf. Appendix B, equation [B.8]) whereupon the terms involving ω_A vanish[+]. These simplifications are discussed more fully in the next section, where the use of a different transformation makes their applications more obvious.

$$H_p^r = \tfrac{1}{2}(H_1/H_o) \begin{bmatrix} 0 & \omega_B & \omega_A & 0 \\ \omega_B & 0 & 0 & \omega_A \\ \omega_A & 0 & 0 & \omega_B \\ 0 & \omega_A & \omega_B & 0 \end{bmatrix} \qquad [3.23]$$

[+] cf. Appendix B. These simplifications are based on an extension of the usual "AX approximation", which allows that the off-diagonals of H_c^r may be ignored if $|J_{AX}| \ll |\omega_A - \omega_X|$ (see references (1-6) for example).

D. The Double Resonance Experiment.

The experimental arrangement for multiple resonance cw NMR involves the use of more than one rf field aligned along an axis perpendicular to the static field $\underline{H}_o$. The corresponding perturbation Hamiltonian $H_p(t)$ is then given by the sum

$$H_p(t) = \sum_m H_m(t) \qquad [3.24]$$

where the summation index m runs over each of the rf fields. If each field is of the form $- 2 H_m \cos\omega_m' t \, \underline{i}$, as for the single resonance experiment, then

$$H_p(t) = \sum_m \sum_n (\omega_n/2)(H_m/H_o)[\exp(i\omega_m' t)+\exp(-i\omega_m' t)] (I_{n+} + I_{n-}) \qquad [3.25]$$

where m=2 corresponds to double resonance, m=3 to triple resonance, etc. The following discussion will be concerned solely with the double resonance experiment, with the convention that the index 1 corresponds to the observing (stimulating) field (whose frequency is being swept) and that the index 2 corresponds to the perturbing field (whose frequency is fixed).

The effect of a transformation to the frame rotating at ω_2' may be readily determined by manipulations of [3.25] similar to the case for single resonance. The required unitary operator is

$$U = \exp(i\omega_2' t \, I_z) \qquad [3.26]$$

and the equation of motion of the transformed spin density matrix $\rho^{r2} = U \rho U^{-1}$ becomes (18,77,103)

$$d\rho^{r2}/dt = i[\rho^{r2}, H_s^{r2}] + (\partial\rho^{r2}/\partial t)_{relax} \qquad [3.27]$$

with $$H_s^{r2} = H_o^{r2} + H_c^{r2} + H_1^{r2} + H_2^{r2} \qquad [3.28a]$$

$$H_o^{r2} = \sum_n (\omega_n - \omega_2') I_{nz} \qquad [3.28b]$$

$$H_c^{r2} = H_c^r = H_c \qquad [3.28c]$$

$$H_1^{r2} = \sum_n (\omega_n/2)(H_1/H_o)[\exp(i\omega' t)+\exp(-i\omega' t)](I_{n+}+I_{n-}) \qquad [3.28d]$$

and $$H_2^{r2} = \sum_n (\omega_n/2)(H_2/H_o)(I_{n+} + I_{n-}) \; . \qquad [3.28e]$$

Note that, as before, equations [3.28d] and [3.28e] have been simplified by ignoring terms of the form $\exp[\pm i(\omega_m'+\omega_n')t]$ $(m,n=1,2)$. Since [3.28e] is time-independent, it is clear that at least part of the time-dependence of the equation of motion [3.27] has been removed; the transformation is of particular use when $H_2 << H_1$ (18,77). The equation [3.28d] still retains some (explicit) dependence on time, with $\omega' = \omega_1' - \omega_2'$.

An alternate transformation, which will also prove useful, is given by the unitary operator

$$U = \exp(iH_o t) \qquad [3.29]$$

Denoting the transformed matrices here by the superscript "*", then the relevant equations are as follows:

$$d\rho^*/dt = i[\rho^*, H_s^*] + (\partial\rho^*/\partial t)_{relax} \qquad [3.30]$$

with $$H_s^* = H_c^* + H_1^* + H_2^* \qquad [3.31]$$

and where the elements of the Hamiltonians in [3.31] are related to the elements in [3.28] (for example) by the relations

$$(H_c^*)_{mn} = (H_c^{r2})_{mn} \exp(i\omega_{mn} t) \qquad [3.32a]$$

$$(H_1^*)_{mn} = (H_1^{r2})_{mn} \exp(i\omega_{mn} t) \qquad [3.32b]$$

and $$(H_2^*)_{mn} = (H_2^{r2})_{mn} \exp(i\omega_{mn}t) \qquad [3.32b]$$

where $\omega_{mn}=(E_m-E_n)/\hbar$ is the eigenvalue difference $(H_o)_{mm}-(H_o)_{nn}$ (7). This transformation is perhaps a little more difficult to interpret since both perturbation Hamiltonians are still time-dependent. Its usefulness may be made clear, however, by recalling that the general solution technique requires that the equation of motion of the spin density matrix be as "small" as possible. In the lab frame, the derivative is dominated by the commutator which is in turn dominated by the nuclear Zeeman term. Transformation to one of the rotating frames removed part of the Zeeman term and thereby reduced the magnitude of the derivative. Clearly the transformation [3.29] is of considerable merit since the entire Zeeman term has been eliminated from the equation of motion.

The corresponding matrices for the interaction representation Hamiltonians are given below for an AB system of spin-1/2 nuclei, relative to the basis product set.

$$H^* = H_o^* + H_c^* = \begin{bmatrix} J/4 & 0 & 0 & 0 \\ 0 & -J/4 & J/2e^- & 0 \\ 0 & J/2e^+ & -J/4 & 0 \\ 0 & 0 & 0 & J/4 \end{bmatrix} \qquad [3.33]$$

with $e^{\pm}=\exp[\pm i(\omega_A-\omega_B)t]$.

$$H_p^*(t) = H_1^* + H_2^* = \begin{bmatrix} 0 & \omega_B P_B & \omega_A P_A & 0 \\ \omega_B P_B^* & 0 & 0 & \omega_A P_A \\ \omega_A P_A^* & 0 & 0 & \omega_B P_B \\ 0 & \omega_A P_A^* & \omega_B P_B^* & 0 \end{bmatrix} \qquad [3.34]$$

with $$P_A = \tfrac{1}{2}\{(H_1/H_o)\exp[i(\omega_A-\omega_1')t]+(H_2/H_o)\exp[i(\omega_A-\omega_2')t]\}$$

and $$P_B \quad \tfrac{1}{2}\{(H_1/H_o)\exp[i(\omega_B-\omega_1')t]+(H_2/H_o)\exp[i(\omega_B-\omega_2')t]\} \quad [3.35]$$

and where P_A^* and P_B^* are the complex conjugates of P_A and P_B.

The AX approximation (including the "extension") is now realized with very little difficulty.+ For equation [3.33], recalling that the frequency difference $|\omega_A-\omega_B|$ is large, one may set the off-diagonals to zero since the rapid oscillations $e^{\pm}$ of these terms average its effect to zero. Similarly the perturbation Hamiltonian in [3.34] is simplified by modifying P_A and P_B; suppose, for example, that the "A" transitions are being observed as the "B" transitions are being perturbed. One then has that $|\omega_A-\omega_2'|$ and $|\omega_B-\omega_1'|$ are large, and consequently the terms involving these oscillations may be omitted. In this case H_p^* has the same form as [3.34] but with

$$\begin{aligned} P_A' &= \tfrac{1}{2}\{(H_1/H_o)\exp[i(\omega_A-\omega_1')t]\} \\ P_B' &= \tfrac{1}{2}\{(H_2/H_o)\exp[i(\omega_B-\omega_2')t]\} \end{aligned} \quad [3.35a]$$

replacing P_A and P_B. Finally, for the single resonance experiment (ie. $H_2 \equiv 0$), it follows that $P_B'=0$, and therefore that $H_p^*=H_1^*$ is

$$H_1^* = \begin{bmatrix} 0 & 0 & \omega_A P_A' & 0 \\ 0 & 0 & 0 & \omega_A P_A' \\ \omega_A P_A'^* & 0 & 0 & 0 \\ 0 & \omega_A P_A'^* & 0 & 0 \end{bmatrix} \quad [3.36]$$

where it is assumed that the observing frequency is near ω_A but far

+similar simplifications apply in the expression for the signal.

from ω_B (and $|J| << |\omega_A - \omega_B|$). For the rotating frame discussed in the previous section, one can now use [3.32b] to justify directly the statements made there for the (extended) AX approximation as applied to H_p^r, where some terms were omitted.

Finally, it is useful to point out here the two more common types of double resonance experiments. First of all, there is the spin-decoupling experiment where the perturbing frequency is centered at the Larmor frequency of nucleus B, for example, while the observing field records the response in the neighborhood of nucleus A. It can be shown that, for strong perturbation amplitudes H_2, the A nucleus behaves as if there were no B nucleus; that is the B nucleus has been "spin-decoupled" from the spin system.

The second common variation of the double resonance experiment usually employs somewhat weaker perturbing fields, with the perturbation frequency centered at <u>one</u> of the transitions. If, for example, one of the "B" transitions is perturbed, then the interesting part of the response occurs near the Larmor frequency of nucleus A; if that "B" transition is isolated, then one can interpret some of the resultant effects in terms of population redistributions, which in turn give rise to the nuclear Overhauser effect (120). In figure 3, for example, when transition 1 is perturbed, the pattern shown, with the transitions 3' and 3" attenuated (relative to the single resonance pattern displayed in figure 2) and the transitions 4' and 4" reinforced, is the expected result of an increase of the population of spin state $|1\rangle$ at the expense of $|3\rangle$ (the splitting of the transitions is a

"second-order" effect; see for example reference (77)). The transitions 3 and 4 in figure 2 are defined to be, respectively, regressively and progressively connected to the transition 1; an alternate definition is that the net change in the z-component of the spin angular momentum vector, ΔI_z, between the first and third of the connected spin states is $\Delta I_z=0$ for a regressive pair of transitions and $\Delta I_z=2$ for a progressive pair of transitions. Similar patterns as stated above are expected for other spin-tickling experiments, with respect to the relative intensity changes of regressive and progressive pairs of transitions. For the simulated spectra to be presented in Chapter V, both of these double resonance variations have been calculated.

E. The Pulse Experiments.

The major distinction between pulsed and continuous wave NMR lies not so much in the nature of the perturbation as in the manner in which the perturbation is applied. Thus, for example, the Hamiltonian of a pulse applied along the x-axis is, as before[+],

$$H_p^x(t) = \sum_n (\omega_n/2)(H_1/H_o)[\exp(+i\omega_1't)+\exp(-i\omega_1't)] \times (I_{n+} + I_{n-}) \qquad [3.37]$$

but with the stipulation that the amplitude H_1 of the rf field $-2 H_1 \cos \omega_1't \; \underline{i}$ is a step function with time. Consequently a pulse sequence varies from a cw experiment only in that, when a pulse is off, H_1 and $H_p^x(t) = 0$. Here the superscript x indicates explicitly that the rf field is directed along the x-axis since occasionally a pulse may be applied along the y-axis (or a rotating field is applied 90 degrees out-of-phase with a "x"-pulse). For an rf field given by $-2 H_1 \cos \omega_1't \; \underline{j}$, the corresponding Hamiltonian is

$$H_p^y(t) = i \sum_n (\omega_n/2)(H_1/H_o)[\exp(i\omega_1't)+\exp(-i\omega_1't)] \times (I_{n+} + I_{n-}) \qquad [3.38]$$

using the argument outlined in section 3.C .

As before, these equations are desired in an interaction representation, usually the rotating frame. Equations [3.17] and [3.20] to [3.21] hold therefore, but with

$$H_1^{yr} = i \sum_n (\omega_n/2)(H_1/H_o)(I_{n+} - I_{n-}) \qquad [3.39]$$

[+] both H_o and ω_1' are time-independent as well.

for a pulse along the y-axis.

It remains now to examine the step function nature of H_1 in order to describe completely the pulse experiments. For this problem, one defines a sequence of time intervals $\tau_{p1}-\tau_1-\tau_{p2}-\tau_2-\tau_{p3}-\ldots$ for which the rf field is on during the times τ_{pi} and off during the times τ_i. Further the pulse durations and amplitudes are adjusted so that[+]

$$\omega_n \, (H_1/H_o) \simeq \gamma H_1 \tau_p = \omega_p \tau_p = \pi/2, \pi, \ldots \quad [3.40]$$

ie. the pulses define an angle, usually some multiple of $\pi/2$, which corresponds to the angle through which the bulk magnetization vector is rotated by the rf field (cf. the Bloch equations, section I.B). The common experimental requirements are for τ_p of the order of a few microseconds with H_1 of the order of several gauss[+] (for cw NMR, H_1 rarely exceeds 10^{-3} gauss). The magnitudes of these parameters suggest a number of approximations available for the calculation of response: for example one often uses the following results:

$$\tau_{pi} << T_1, T_2, \tau_i \quad [3.41]$$

and

$$\omega_p >> |\omega_m-\omega_1'|, |\omega_m-\omega_n|, |J_{mn}| \quad [3.42]$$

so that, during a pulse, the high-resolution Hamiltonian (in the rotating frame) and the effects of relaxation may be ignored. These approximations may limit the range of applicability of the solutions thereby obtained, however, and they will not be required in the solution technique to be discussed below.

One may now describe a variety of pulse experiments by writing

---

[+] for homonuclear nonselective pulses. An equation analogous to [3.40] is derived in Appendix C for selective pulses.

a sequence of times τ_{pi} and τ_i, and some of the more common pulse experiments are described below. The sequence of times is also written using the notation, for example, π-τ-$\pi/2$ where the pulse times τ_{pi} are implicitly defined from [3.40] by the angle, and it is also assumed that a pulse is directed along the x-axis unless a superscript "y" is written with that pulse angle.

1. The Free Induction Decay (FID) Experiment.

This experiment involves a single $\pi/2$ pulse, and the interesting part of the signal is that immediately following the pulse. For a single spin-1/2 system, the signal decays at a rate $1/T_2$ (8) in a perfectly homogeneous static magnetic field, and the presence of any inhomogeneity hastens the rate of decay.

The FID pulse sequence is often employed as an alternate method whereby slow-passage unsaturated cw spectra are obtained, since the FID signal and the cw spectrum are Fourier transforms of one another (4,8,37,124). Mathematically, for a FID signal $S(t)$ where $t=0$ at the end of the $\pi/2$ pulse and $S(t<0)\equiv 0$, the cw signal is

$$S(\omega) = \int_{-\infty}^{+\infty} S(t)\, \exp(-i\omega t)\, dt \qquad [3.43]$$

where the absorption and dispersion modes are contained in the real and imaginary parts of $S(\omega)$, respectively (and as before). The inverse relation is

$$S(t) = \int_{-\infty}^{+\infty} S(\omega)\, \exp(+i\omega t)\, d\omega \,. \qquad [3.44]$$

An example of these relations is afforded by the single resonance absorption mode signal of a single spin-1/2 system (cf. [1.4])

$$S_{abs}(\omega) \propto \frac{T_2}{1 + (\omega_o-\omega)^2 T_2 2} \quad . \qquad [3.45]$$

The corresponding FID signal is of the form

$$S(t) \propto \exp(-|t|/T_2) \times \exp[i(\omega_o-\omega)t] \qquad [3.46]$$

where S(t) contains both in-phase and out-of-phase components (and where ω_1' is written as ω for convenience; ω_o is the Larmor frequency of the single nucleus). Equation [3.44] requires the response S(t) as $t \to \infty$; in practise (both experimentally and for theoretical calculations) one may limit the time to several multiples of T_2, beyond which the signal becomes vanishingly small (8). It has also been shown that the $\pi/2$ rotation is not essential for the use of Fourier transformations (37), and a number of modifications have been described to the simple FID experiment (see Farrar and Becker (8) for examples)

2. Pulse Experiments for the Measurement of T_1.

The pulse sequence $\pi-\tau-\pi/2$ was mentioned in Chapter I as a method whereby the spin-lattice relaxation time of simple systems could be measured. It was shown there that the signal amplitude immediately following the $\pi/2$ pulse obeys the relation (8):

$$S(\tau) \propto 1 - 2\exp(-\tau/T_1) \quad (\tau \ll \tau_p) \quad . \qquad [3.47]$$

For a system of independent (uncoupled) spins, the signal consists of a summation of terms like [3.47] for each nucleus in the molecule possessing different spin-lattice relaxation times, and the complicated pattern is more readily interpreted if one performs a Fourier transformation of the signal immediately following the $\pi/2$ pulse.

There obtains a spectrum similar to the usual cw spectrum, but with the intensities of the transitions following equations of the form of [3.47] (as a function of τ); for τ either very short or very long (compared to T_1), this pulse sequence resembles the FID experiment, while for intermediate values of τ one calculates spectra known as "partially relaxed Fourier transform spectra" (62-63). For coupled spin systems, however, the signal may be very difficult to interpret since it may not be possible to assign a single parameter T_1 to the transition(s) of a particular nucleus (cf. section 2.C). Finally, other experiments exist for the measurement of spin-lattice relaxation times, usually limited to simple spin systems, but they will not be discussed here (see, for example, reference (8)).

3. Spin-Echo Experiments.

Once again there exist a number of different pulse sequences for the study of spin-spin relaxation; however this work will be concerned only with two of the more common methods, namely the Carr-Purcell (CP) and the closely related Carr-Purcell-Meiboom-Gill (CPMG) spin-echo experiments (19,20). The pulse sequences are defined by

$$\pi/2 - \tau - \pi - 2\tau - \pi - 2\tau - \ldots.$$
$$\text{and} \qquad \pi/2 - \tau - \pi^{y} - 2\tau - \pi^{y} - 2\tau - \ldots. \qquad [3.48]$$

respectively for the CP and the CPMG experiments, the only difference being that in the latter pulse sequence the π pulses are directed along the negative y-axis instead of the negative x-axis. Now since the effect of the initial $\pi/2$ pulse is to rotate the magnetization into the y-axis, one obtains at first a FID signal which decays due

to spin-spin relaxation and due to the effects of inhomogeneity. It is possible to show that the effect of the π pulses (in either case) is to refocus the magnetization, less that which has irreversibly decayed due to spin-spin relaxation, at the times $t=2n\tau$ ($n=1,2,\ldots$), and that the echo amplitude at these times is independent of the static magnetic field and therefore any inhomogeneity in the static magnetic field (4,8,19,20)[+]. The signal for a single spin-1/2 system of nuclei obeys the equation (8,19,20):

$$|S(t=2n\tau)| \quad \propto \quad \exp(-|t|/T_2) \ . \qquad [3.49]$$

It is also possible to show that, for coupled spin systems characterized by a single spin-spin relaxation time (ie. the phenomenological model describes the effects of relaxation), the CP or CPMG experiments yield a signal whose value at times $t=2n\tau$ is independent of static field inhomogeneity[+] (cf. Appendix B). For these systems, however, the echo envelope does not trace out a simple exponential decay as in [3.49] since the presence of spin-spin couplings causes a modulation of the envelope. The CP and CPMG experiments have been applied to the measurement of spin-spin relaxation times for simple spin systems, and to the measurement of coupling constants for more complex spin systems; in addition chemical exchange parameters have

---

[+] assuming that molecular diffusion is negligible, a good approximation of the experimental conditions only if the pulse separation times τ are small (8,19,20). Some experiments have been devised for the measurement of diffusion rates, with the feature that the static field is purposely <u>not</u> inhomogeneous over the sample (see reference (8), Chapter 7).

been determined for some spin systems (coupled and uncoupled) using the spin-echo pulse sequences (23,24,47,80-84,108-112).

4. Selective Pulse Experiments.

It is possible, by means of a suitable arrangement of the experimental variables, to selectively perturb a given transition in a spin system by means of a pulse experiment. The pulse is selective in the sense that only the spin states connected by that particular transition are "aware" of the pulsing field. The definition and derivation of such a pulse is described in Appendix C, where it is found that the parameters defining the pulse obey the relation

$$\gamma_i H_1 \tau_p \lambda_{rs} = \pi/2, \pi, \text{ or } 2\pi, \ldots \quad [3.50]$$

with λ_{rs} and γ_i pertaining to the transition in question. If these conditions are met, and for the rf frequency centered at the transition connecting states $|r\rangle$ and $|s\rangle$, then the effect of a pulse is to alter the populations and the magnetizations associated with these states. It can be shown, for example,(Appendix C), that the effect of a selective π pulse applied to the transition 3 in figure 2 is to invert the populations of states $|1\rangle$ and $|2\rangle$. Compared to the equilibrium configuration, therefore, state $|1\rangle$ has become more populated at the expense of state $|2\rangle$.

Freeman, Wittekoek and Ernst (113) have studied the resultant response of an AB system of spin-1/2 nuclei to a selective π-τ-2π sequence of pulses. The π pulse is applied to, and inverts the population across, one transition and the 2π pulse monitors the magnetization appearing τ seconds later at the same or at another trans-

ition. A qualitative explanation of their findings may be made using the energy level diagram in figure 2. Suppose, for example, that the π pulse has been applied to the transition 3 as above. Consequently if one now monitors the magnetization at the progressively connected transition 2 with the selective 2π pulse, it is expected that the signal due to this transition would be enhanced compared to the application of a 2π pulse to a system in thermal equilibrium. On the other hand one predicts that the signal from the regressively connected transition 1 is attenuated relative to its equilibrium signal. It is also to be expected that in the limit of long pulse separation times, the system will have reverted to an equilibrium configuration at rates which will depend on the relaxation interactions. These effects have been observed, and Freeman et. al. (113) have been able to relate the rate of recovery of a signal to its equilibrium value to a series of rate equations for the populations, which in turn are dependent on the relaxation mechanisms. Their results indicate that a detailed analysis of the observed spectra may yield considerable insight into the nature of relaxation processes, and it is also to be expected that the development of experimental techniques for the generation of selective pulses will lead to a number of similar experiments.

F. Other High-Resolution NMR Experiments.

The experiments described above by no means exhaust the list of experiments which have been performed in high-resolution NMR. Other experiments include variations of the above cw and pulse experiments - for example "J-spectra" (125), the Hahn spin-echo pulse sequence (29), etc. - as well as some mixed cases such as periodically pulsed double resonance (126,127), transient nutations in double resonance (128), the Torrey pulse sequence (28) and so forth. In this dissertation, however, the simulations carried out are limited to the experiments discussed in parts C to E of this chapter, largely because it was felt that an in-depth study of a few experiments would be more rewarding than an attempt to consider all the possible variations of the NMR experiment (quite probably an open-ended task). Nevertheless, since it will be demonstrated below that the technique for the calculation of response accurately reproduces the features of the experiments considered, it seems only reasonable to predict that those experiments <u>not</u> considered could also be calculated by the same technique. The only modification required would be the specification of the appropriate perturbation Hamiltonian describing the experiment, or for other NMR experiments, such as the NMR of solids, the specification of the appropriate equations (such as the static dipolar Hamiltonian for solids).

G. Other Considerations.

Perhaps one of the best known complications observable in high-resolution NMR is that deriving from inhomogeneity in the static magnetic field. In cw NMR, inhomogeneity manifests itself as an extra broadening of the transitions in addition to the broadening due to relaxation, while in pulsed NMR inhomogeneity results in the disappearance of a FID signal at a rate faster than $1/T_2$ and it will also affect the width (but not the echo amplitude) of the spin echo in a CP pulse sequence.

Since these effects are observable, a complete formulation of the NMR experiment requires some method whereby inhomogeneity effects may be included into the calculations. One of the most direct methods of describing these features results from the realization that inhomogeneity causes deviations in the Larmor frequency of a nucleus, so that there results a spread in its resonance frequency. The effect is analogous to the spread caused by the transverse relaxation time T_2, and consequently the single resonance cw signal of a single spin-1/2 system of nuclei is often found in the modified form (2-6,8):

$$S_{abs}(\omega_1') \propto \frac{T_2^*}{1 + (\omega_o-\omega_1')^2(T_2^*)^2} \qquad [3.51]$$

where T_2^*, the effective spin-spin relaxation time, is defined by

$$(T_2^*)^{-1} = (T_2)^{-1} + (\gamma\Delta H_o). \qquad [3.52]$$

It is assumed in the derivation of [3.51] that the inhomogeneity distribution of the static field $-H_o\underline{k}$ is Lorentzian with a width at half-height of $(2\gamma\Delta H_o)$ radians/second. It also follows, from the Fourier

transform of [3.51], that the FID signal should be of the form

$$S(t) \quad \propto \quad \exp(-|t|/T_2^*) \exp[i(\omega_o - \omega_1')t] \quad . \qquad [3.53]$$

This concept may be extended to coupled spin systems and the spin density matrix description, provided that it is assumed that the inhomogeneity distribution is Lorentzian and that the simple phenomenological model [2.12] adequately describes relaxation effects. One then obtains the following modification of [2.12]+:

$$(\partial\rho/\partial t)_{relax} = (\rho^o - \rho)/T_{1_{diag}} + (-\rho/T_2^*)_{odiag} \qquad [3.54]$$

where T_2^* is defined by [3.53].

It is not immediately clear how the more complex Bloch-Wangsness-Redfield formalism would be modified by a similar argument. In addition, there exist a number of experiments for which the above description must necessarily fail. Two prominent examples are described below.

(a) In a double resonance spin-tickling experiment, it is found that the regressively-connected transitions are narrower than are the progressively-connected transitions. This fact has also been demonstrated theoretically (75,78,94), and is in disagreement with the above model which would not predict any asymmetry in the transitions due to the presence of inhomogeneity.

(b) In the spin-echo experiments, it is well-known that inhomogeneity

---

+ a proof of the validity of [3.54] with the preceding conditions may be found in reference (112). Abragam (4), however, discusses the cases for a simple spin-1/2 system for which an effective spin-spin relaxation time represents an inadequate model for the description of both spin-spin relaxation and inhomogeneity (see pages 49-53 of (4)).

and relaxation effects are separable, and it is possible to measure a natural spin-spin relaxation time T_2. Obviously [3.54] fails, since it does not allow a distinction between the contributions to the effective spin-spin relaxation time.

Since it is inadequate in the general case, [3.54] will be used sparingly in the following calculations. Although the model is entirely phenomenological in origin, it has the advantage of being very simple in form compared with other more general methods for the inclusion of inhomogeneity. Abragam (4), for example, proposed a method for the spin density matrix formalism in which he supposes that a system of spins in an inhomogeneous magnetic field may be described by a number of ensembles, each in a constant (but varying) homogeneous static magnetic field. The sample is then characterized by an averaged spin density matrix over all of these ensembles, with coupling between ensembles afforded by processes such as molecular diffusion across field gradients. Unfortunately this last consideration renders the model very unwieldy, and a more useful model uses the extra assumption that each ensemble is isolated[+]. The net signal $\overline{S}$ arising from such a group of ensembles is given by a summation of the signals due to each ensemble

$$\overline{S} = \sum_n S_n \qquad [3.56]$$

and each ensemble would follow an equation of motion as in [3.2] but

---

[+]the following development is similar to that discussed elsewhere, and corresponds to the "convolution integral" treatment. See, for example, references (8,28,29,34,78,80).

with different values for the magnitude of the static magnetic field. A more manageable form for [3.56] is

$$\overline{S} = \int_{-\infty}^{+\infty} d\beta\ S(\beta)\ G(\beta) \qquad [3.57]$$

where it is assumed that there is some distribution $G(\beta)$ of ensembles with corresponding signals $S(\beta)$ experiencing the same magnetic field of magnitude H. The variable β represents the deviation of the field from some central value of H_o:

$$\beta = H - H_o \qquad [3.58]$$

and it is required that the distribution be normalized:

$$\int_{-\infty}^{+\infty} d\beta\ G(\beta) = 1 . \qquad [3.59]$$

In general, an a priori deduction of the actual form of $G(\beta)$ is not possible, although it might be argued that since the equation [3.55] represents a Lorentzian distribution, one might have that

$$G_L(\beta) = (w/\pi)\ \ 1/(w^2+\beta^2) . \qquad [3.60]$$

This form for $G(\beta)$ assumes that the inhomogeneity of the static field follows a Lorentzian distribution whose full width at half-height is 2w gauss. Although this type of distribution is the one most commonly chosen (17,18), one might also argue that, say, a Gaussian distribution is also likely (28,29,80), with

$$G_G(\beta) = (w^2\ \pi\ \ln 2)^{-\frac{1}{2}}\ \exp(-\beta^2/w^2\ \ln 2) \qquad [3.61]$$

where ln2 is the natural logarithm of 2 and the parameter 2w is once again the half-height width of the Gaussian distribution. In the calculations to follow, the parameter w may be reported either in the units of gauss, or in the units of hertz; the relating equation is simply

$$\text{width} \quad \propto \quad 2w \text{ (gauss)} \quad = \quad 2\gamma w/2\pi \text{ (hertz)} \qquad [3.62]$$

where γ is the gyromagnetic ratio of the nucleus being observed. Typical values for proton NMR in a "good" magnetic field are $w \simeq 1.5 \times 10^{-5}$ gauss $\simeq 0.06$ hertz, with $H_o = 10^4$ gauss and $\gamma_p H_o = 42.577$ megahertz.

It is instructive to consider those cases for which equation [3.57] may be simplified. Consider first of all a single resonance cw experiment, and suppose that the inhomogeneity is small, ie. $w << H_o$. One would then expect that the signals due to two ensembles in static fields of magnitude $H_o+\beta_1$ and $H_o+\beta_2$ are virtually identical except for a small frequency shift $\gamma(\beta_1-\beta_2)$, where the nuclei have a gyromagnetic ratio γ. This approximation allows the simplification of [3.57] to

$$\overline{S}(\omega_1') = \int_{-\infty}^{+\infty} d\beta \; S(\omega_1'; \beta) \; G(\beta) \qquad [3.63a]$$

$$\simeq \int_{-\infty}^{+\infty} d\beta \; S(\omega_1'+\gamma\beta; 0) \; G(\beta) \qquad [3.63b]$$

where $S(\omega_1'; \beta)$ denotes the response of the ensembles in the field $H_o+\beta$ at an rf frequency ω_1', and where $S(\omega_1'+\gamma\beta; 0)$ denotes the response of the ensemble in the central field H_o at a frequency $\omega_1'+\gamma\beta$. Note that the last equation represents a considerable simplification of the problem since it requires only one solution of the equation of motion of a spin density matrix, namely the "central" spin density matrix, whereas the first equation implies that an infinite number be solved.

It is also possible to apply equation [3.63b] to the double resonance experiment, provided that the above stipulation remains valid; specifically one requires that the signals deriving from different

ensembles differ only by a small frequency shift. While this is true for some double resonance experiments, there are cases when the signals from two different ensembles may vary by more than a frequency shift. This occurs, for example, in a spin-tickling experiment, where it may be shown (78,94,129) that for perturbations with $\gamma H_2 \simeq T_2^{-1}$, small offsets in its frequency become important. When this experiment is applied to a given spin system, then two ensembles in slightly different static fields will experience the same perturbation amplitude but, since their Larmor frequencies will be (slightly) different, the effective frequency offset of the perturbation will also be different. Consequently if this offset is important, one must use [3.63a] instead of [3.63b]. In the following calculations, it was always assumed that [3.63b] was valid, solely from a consideration of required computer execution time (see Chapter IV).

Unfortunately the above restriction applies to the majority of the pulsed NMR experiments. In this case, the signal due to one ensemble is given by expressions like the following FID signal

$$S(t;\beta) \quad \propto \quad \exp(-|t|/T_2) \quad \exp[i(\omega_o+\gamma\beta-\omega_1')t] \quad .$$

Consequently two ensembles in different fields will oscillate at different rates, and (particularly for multispin systems) one is forced to use the equation

$$\overline{S}(t) \quad = \quad \int_{-\infty}^{+\infty} d\beta \; S(t;\beta) \; G(\beta) \qquad [3.64]$$

where $S(t;\beta)$ is the response of the ensemble in the field $H_o+\beta$ at time t. This expression has been employed for the calculations in

pulsed NMR, but only when inhomogeneity effects must be reproduced.

In the above discussion, it has been assumed implicitly that the inhomogeneity of the static magnetic field occurs only along the z-axis. In addition, other complicating effects have been ignored; for example the inhomogeneity in the magnitude of the rf field(s), the assumption that the frequency of an rf field is monochromatic, etc. Usually these effects are small (but recall, for example, the footnote on page 73) or else they can be made small by a judicious choice of the experimental variables, and they will not be considered further here. It might be noted, however, that various modifications of the formalism might be developed to cover those situations where other complicating effects are observable.

CHAPTER IV. A DYNAMIC METHOD FOR THE CALCULATION OF RESPONSE

A. Introduction.

It has been shown that, in order to describe completely an NMR experiment, it becomes necessary to solve two important types of problems:

(a) the system of coupled linear first order differential equations for the equation of motion of the spin density matrix:

$$d\rho/dt = i[\rho, H_s(t)] + (\partial\rho/\partial t)_{relax} \qquad [4.1]$$

where the exact nature of the experiment is contained in the perturbation Hamiltonian. It was also mentioned that [4.1] reduces to a system of simultaneous linear equations as a result of the steady-state approximation; however the general problem is an initial value problem in the sense as defined by standard texts on numerical analysis (for example references (130-132)). An initial value is readily found by postulating that, at the start of a given experiment, the spin system is in a state of thermal equilibrium so that

$$\rho(t=0) = \rho^o . \qquad [4.2]$$

(b) The integrals over the inhomogeneity distributions, of the general form

$$\overline{S} = \int_{-\infty}^{+\infty} d\beta\ S(\beta)\ G(\beta) \qquad [4.3]$$

where it may be assumed that the function $G(\beta)$ is analytic, and where the signal $S(\beta)$ is a discrete set of points obtained from solutions

to the first problem.

For the experiments outlined in the previous chapter, there are a number of related problems which are of interest here, namely

(c) the filtering of the double resonance signal in order to extract the Fourier component of interest, and

(d) the evaluation of the Fourier transform of a discrete set of points in order to calculate Fourier transform spectra.

Note that the solutions to the last three problems are, of necessity, numerical since their starting data is obtained from the discrete set of points generated by numerical solutions to the first problem. Consequently a consideration of importance to all the above problems is the question of the accuracy and the convergence characteristics of the calculations. In general a converged solution is not always accurate because of the important distinction between the two types of computational errors[+] - those due to truncation and those due to round-off. Suppose, for example, that some function is approximated at some point by a Taylor series expansion. The truncation error is then that error associated with cutting off the infinite formula after some finite number of terms so that the resultant approximation converges to the desired value within some limit of precision. Now in this last statement, it is assumed that the actual calculations have been performed with an infinite number of significant figures so that the calculations are exact; round-off error is that error associated with the use of a finite number of digits. It follows that if

---

[+] lucid discussions of these types of errors may be found in most texts on numerical analysis; see for example references (130-133).

round-off error exceeds truncation error, then the resultant solution may converge, but to an inaccurate value.

This undesirable occurrence may be avoided, however, if round-off error can be made sufficiently small so that it cannot affect the result within the accuracy desired. In the above example, suppose further that it is known that a desired accuracy of 0.1% is attained after exact calculations using r terms. If there are required 10^n calculations to evaluate this result, and if round-off error in each calculation affects the last digit, then the accumulated round-off errors could affect the last n significant figures of the result (but may not since round-off errors are random in nature). Consequently, if the number of digits retained in the calculations is at least n+3, it follows that the round-off error will not affect the result within the desired accuracy of 0.1%.

It will be assumed that the following calculations are always accurate if they converge, ie. that round-off error is always negligibly small. This assumption is rendered plausible by the use of double precision arithmetic (ie. for an IBM 360, fifteen significant figures) in problems where round-off may become important[+]. The remainder of this chapter is devoted to a discussion of the procedures developed for the solution of the problems mentioned above.

[+]this assumption may be validated by a careful analysis of the computed results. In the above example, if the Taylor series expansion were performed with r, 2r, 4r, ... terms, one would expect a systematic convergence of successive results if round-off error is negligibly small; whereas if round-off error is not small, then successive results could display a random convergence pattern (or no convergence).

B. Solution of the Equation of Motion.

The initial value problem defined by [4.1] and [4.2] may be solved by a variety of numerical methods, many of which are described in some detail in standard texts on numerical analysis (see, for example, references (130-133)). The choice of a method is based on considerations such as the accuracy required, the execution time for the solution of a given problem, the computer storage requirements, etc., and the choice of a "best" method for a given problem is neither obvious nor uncomplicated. It was decided that a satisfactory approach is that offered by the Gill modification (134) of a fourth-order Runge-Kutta method.+ The particular advantages of the Runge-Kutta-Gill (RKG) algorithm may be stated as follows:

(a) the method is self-starting and relatively simple to translate into a computer language;

(b) the amount of storage required is minimal (134,135);

(c) the Gill modification (134) significantly reduces round-off errors; and

(d) the step-size required is continuously variable, a particularly useful feature for the calculation of pulsed NMR spectra (see below).

+other methods such as the Milne predictor-corrector formulae (131-135) were also studied for the calculation of cw spectra. It was found that equally-accurate results could be obtained with a slight reduction in computational times, but at the expense of larger storage requirements. The relative simplicity of the RKG formula then weighted the decision in its behalf.

The main disadvantage of the RKG algorithm is that truncation errors cannot be readily estimated, so that proof of convergence of the solutions becomes a formidable task. Fortunately this problem is largely circumvented (see below).

1. The Runge-Kutta-Gill Algorithm.

In order to gain some insight into the workings of the RKG method, consider for simplicity Euler's method (130) as applied to a single initial value problem, whose defining equations are

$$dY/dt \equiv Y'(t) = F(t;Y) \qquad [4.4a]$$

and

$$Y(t=0) = Y_o \qquad [4.4b]$$

where t is the independent variable. The differential equation may be transformed into an integral equation, yielding

$$Y(t) = Y_o + \int_0^t F(t;Y)\, dt \quad . \qquad [4.5]$$

In Euler's method, the integral in [4.5] is approximated by a rectangular area of length h and of height $F(0;Y_o)$, so that

$$Y_h = Y_o + h\, F(0;Y_o) \quad . \qquad [4.6]$$

After a number of repetitions of [4.6], the general expression is

$$Y_{n+1} = Y_n + h\, F(t_n;Y_n) \qquad [4.7]$$

where $t_n=nh$ and where the Y_n refer to the approximations to the exact solution $Y(t_n)$. In another interpretation, this equation follows from the Taylor series expansion

$$Y(t_{n+1}) = Y(t_n) + h\, Y'(t_n) + h^2/2!\, Y''(t_n) + \ldots \qquad [4.8]$$

where the formula is truncated after the term linear in h. It follows, therefore, that if the higher order derivatives of the function Y(t) are zero, then Euler's method is exact; ie. by definition Euler's

method is of order unity.

It is convenient to regard the Runge-Kutta method as a generalization of Euler's method in the sense that one retains higher order terms in the Taylor series expansion. One has, for example, formulae of the general fourth-order Runge-Kutta method in the form (131-135)

$$Y_{n+1} = Y_n + K \qquad [4.9a]$$

with $$K = \sum_{i=1}^{4} w_i K_i \qquad [4.9b]$$

and $$K_i = h\, F(t_n + a_i h;\ Y_n + \sum_{j=1}^{i-1} b_{ij}\, K_j)\ . \qquad [4.9c]$$

Here the constants w_i, a_i and b_{ij} are chosen such that a Taylor series expansion in powers of h for $Y(t_{n+1})$ is identical with a Taylor series expansion of hK, up to and including terms of the order of h^4. Thus one obtains a fourth-order approximation for $Y(t_{n+1})$ by means of four recursive evaluations of the derivative Y' at various positions of the independent variable t, where $t_n \le t \le t_{n+1}$.

It turns out that there are more constants than there are restraints and defining equations, so that there exists a family of fourth-order Runge-Kutta formulae (131-135). It has been shown that the Gill modification possesses two additional advantages over other Runge-Kutta formulae, namely the storage requirements are at a minimum and round-off error is considerably reduced (134,135). The final form of this refinement may be expressed by the following algorithm (134,135):

$$\begin{aligned} K_1 &= h\, F(t_n, Y_n) & Z_1 &= Y_n + (K_1 - 2Q_o)/2 \\ K_2 &= h\, F(t_{n+h/2};\ Z_1) & Z_2 &= Z_1 + (K_2 - Q_1)(1-c) \\ K_3 &= h\, F(t_{n+h/2};\ Z_2) & Z_3 &= Z_2 + (K_3 - Q_2)(1+c) \end{aligned} \qquad [4.10a]$$

and $\quad K_4 = h\,F(t_{n+1};\, Z_3) \qquad Z_4 = Z_3 + (K_4 - 2Q_3)/6$

where $c = (2)^{-1/2}$ and where the constants Q_o to Q_4 are defined by

$$Q_o = 0 \text{ for } n=0; = Q_4 \text{ for } n>0.$$

$$Q_1 = Q_o + 3\,[(K_1 - 2Q_o)/2] - K_1/2$$

$$Q_2 = Q_1 + 3\,[(K_2 - Q_1)(1 - c)] - (1 - c)K_2 \qquad [4.10b]$$

$$Q_3 = Q_2 + 3\,[(K_3 - Q_2)(1 + c)] - (1 + c)K_3$$

and $\quad Q_4 = Q_3 + 3\,[(K_4 - 2Q_3)/6] - K_4/4$.

The constants Q_i are introduced to compensate for round-off error[+], and hence Q_o is initially zero and (approximately) equal to the value of Q_4 from the previous integration step. Note also that at any time in the integration, only three storage locations are required (for K_i, Z_i and Q_i), and it follows that a fourth-order approximation to $Y(t_{n+1})$ is given simply by (135)

$$Y(t_{n+1}) \simeq Y_{n+1} = Z_4 \,. \qquad [4.10c]$$

Thus one proceeds from the initial value Y_o at time t=0 to some arbitrary result Y_{n+1} at time $t=t_{n+1}$ after n integrations with a constant step-size h (although [4.10] does not limit h to be a constant value throughout the integration process).

This algorithm is almost ready for application to the solution of the equation of motion of the spin density matrix. An initial difficulty is that the equations [4.1] and [4.2] define a system of

[+] it has been observed that at the end of a RKG integration, $|Q_4|$ is of the order of 10^{-14} times smaller than $|Z_4|$ (after convergence), indicating that round-off error has (probably) been negligible.

coupled initial value problems; however this complication is readily overcome by interpreting the variables K, Q, Y and Z in [4.10] as matrices, and associating the matrix ρ with Y and the function F(t,Y) with the derivative $d\rho/dt$. The fact that the density matrix and its derivative are Hermitian can also be put to good use here: not all of the elements of ρ need be integrated since if ρ_{ij} is known, then so is $\rho_{ji} = \rho_{ij}^*$. Consequently one can simplify the system of n^2 differential equations to a system of $n(n+1)/2$ differential equations by solving only, for example, those elements appearing in the upper triangle of the density matrix. One then interprets Y, F, etc. as a set of vectors whose elements must be ordered systematically, according to the relationships expressed by ρ and $d\rho/dt$.

2. Convergence of the Algorithm.

It remains now to show that the RKG method does in fact converge to the required solutions. This is a non-trivial problem even for a single differential equation whose analytical solution is known. It is known, however, that a necessary and sufficient condition for convergence is that (130)

(a) a unique solution exists, and

(b) the numerical method is consistent.

The first condition seems intuitively obvious, and in fact it may be easily shown that the problems of interest here do possess unique solutions (cf. Henrici (130), page 14). It may also be shown that the RKG algorithm is consistent (130,131,134,135), that is in the limit as h tends to zero, the truncation error introduced at <u>each</u> step also

tends to zero, and therefore the numerical solution obtained is consistent.

These results state that the RKG algorithm can converge, but there is no indication of the actual magnitude of the step-size which may be employed and still yield converged solutions. One requires a finite step-size in the integration process in order that the computation time be finite (and also so that round-off error will not grow too large), and this brings up the important question of stability of the algorithm, as applied to the NMR problem. For the purposes here, a definition of stability is that it is a measure of the rate of convergence of a given problem using a given numerical method and using a finite step-size. In general this problem is insoluble for a system of equations; however it has been shown (136) that a reliable estimate to an upper limit of h is given by the eigenvalues of the Jacobian whose elements J_{ij} are defined by[+]

$$J_{ij} = \partial F(t;Y_i)/\partial Y_j \qquad [4.11]$$

where $F(t;Y_i)=dY_i/dt$ and Y_i is an element of the vector Y (corresponding to some element ρ_{mn} of the spin density matrix). The largest

[+] the independent variable t lies somewhere within the region $(0,t_{n+1})$ for an integration to the value Y_{n+1}. In the following results, it is assumed that the Jacobian is a slowly varying function of t so that one can arbitrarily choose some intermediate value (cf. Karim (136)). It has also been confirmed that the magnitude of the eigenvalues depend weakly on t, so that the results obtained should be reasonable for all values of t.

possible value for the step-size h is then determined by the largest eigenvalue λ_k of the Jacobian, since it can be shown (136) that if the product $h\lambda_k$ lies with the complex space shown in figure 5, then the problem is stable.

Calculations of this nature were performed using the equation of motion as defined in [4.1] and with the relaxation term as given by [2.12]. It follows that the Jacobian is anti-Hermitian except for real terms on the diagonal which are related to the relaxation times, and that the eigenvalues are indeterminably complex functions of the parameters and variables describing a given experiment (relaxation times, Larmor frequencies, rf amplitudes and frequencies, etc.). It was possible, however, to make the conclusions and deductions listed below.

(a) In the lab frame, the differential equations [1.4] possess eigenvalues whose imaginary part is of the order of the Larmor frequencies, and as a result one requires exceedingly small values of h for stability. In an interaction representation, however, the eigenvalues are dramatically smaller, and therefore the step-size may be considerably larger. For this reason, an interaction representation represents an obvious improvement to the initial value problem (cf. Lawson (137)), although this conclusion may follow in a more intuitive fashion by comparison of the relevant equations of motion. Consider the double resonance cw experiment for example; in the lab frame the Hamiltonian contains terms of the form $\exp(i\omega_1't)$, whereas in the interaction representation the same term is altered to the form $\exp(i\Delta\omega_1't)$ where

Figure 5.

Plot of the stability region of the fourth-order Runge-Kutta method for the solution of a system of differential equations (Karim (136)). The solution is stable if and only if the product $h\lambda_k$, where λ_k is the largest eigenvalue of the Jacobian (see text) and where h is the step-size, lies within the complex region R in the plot. The boundaries of R cut the real axis (Re) at 0 and $-2.785\cdots$, and the imaginary axis (Im) at $\pm(8)^{1/2}$.

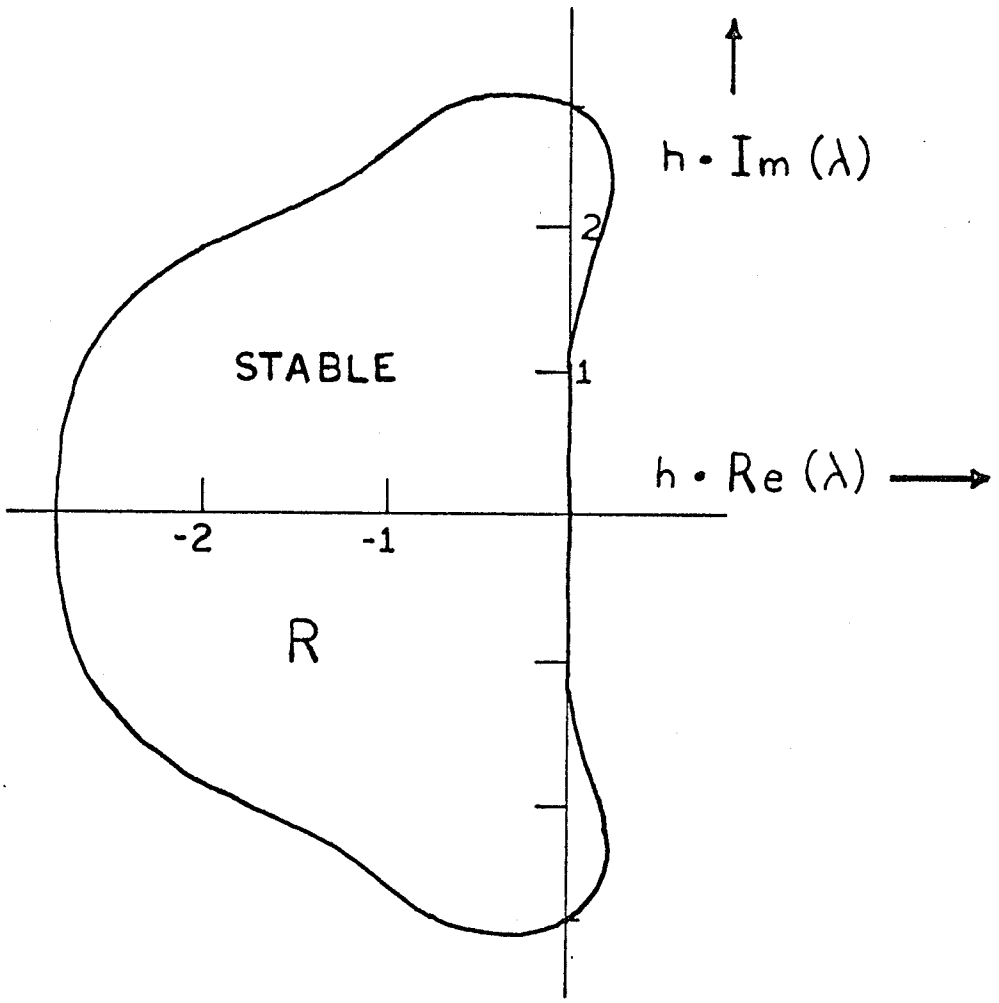
h • Im (λ)
2
STABLE
1
h • Re (λ)
-2
-1
R

ω_1' and $\Delta\omega_1'$ are, respectively, of the order of the Larmor frequencies and of the order of the Larmor frequency differences. Now it seems only logical that if these oscillations are to be reflected by the integration procedure for ρ, then the step-size must be of the order of a period of the oscillation, and consequently the interaction representation allows the use of a much larger step-size.

(b) The real part of the eigenvalues are of the order of $(-T_1)^{-1}$ or $(-T_2)^{-1}$; consequently one requires the presence of a relaxation term in order to evaluate numerically the initial value problem. This prohibits, for example, the calculation of "stick" spectra.

(c) In the interaction representation, the effective stability region is usually determined by the imaginary parts of the eigenvalues (unless the relaxation times are very large), which depend in a complex manner on the coupling constants, Larmor frequency differences, the rf amplitudes, etc. In general the step-size decreases as these parameters increase[+], and it is often found that one parameter may effectively determine the largest eigenvalue. In cw NMR, this parameter is usually the largest frequency difference, while in nonselective pulsed NMR the limiting parameter may be the amplitude of the pulsing field when the pulse is "on", and a frequency difference when the pulsing field is "off".

[+] at a first glance, it may seem that these calculations are effectively restricted to homonuclear spin systems (ie. $\Delta\omega_1'$ is small). It is possible, however, to introduce the AX approximation which removes the fast oscillations present; in light of the previous discussion, therefore, an AX system may be more stable than its AB counterpart.

Unfortunately these results are plagued by the fact that only estimates are obtained for the magnitude of h guaranteeing convergence. A more practical approach is obtained by comparing results using a step-size h with the results obtained using a step-size h/2. If the differences are negligible[+], then it may be assumed that the solutions have converged. It has also been found that the initial value problems are "stiff" in the sense that slight variations (less than about 10%) in h may result in a converged solution or in a solution which obviously diverges. The divergence may appear, often within a few steps in the integration process, either as a rapid deviation of the norm of the density matrix from unity and/or as a signal which rapidly approaches an absolute limiting value of infinity. Consequently it is possible to find useful values of h very quickly, and in fact it is not too difficult to localize an upper limit.

The calculated spectra reproduced in this thesis have all been obtained from solutions of the equation of motion of the spin density matrix in an interaction representation, and in each case convergence was guaranteed by the efficacious procedure mentioned above. It turns out that this procedure is computationally the most expensive of the various routines employed for the calculations, and therefore the choice

---

[+]negligible is interpreted here as meaning that plots of the signal using a step-size h and h/2 deviate by less that 0.1% at <u>any</u> point in the integration routine. This requires, of course, that round-off error is not important; however its effects were never noticed, an expected result since the routine used double precision arithmetic throughout.

of the parameters and variables for a given calculation were often determined with the aim of reproducing a variety of spectral features within a reasonable amount of computer time. The following list may be taken as representative of the actual execution times required for the calculation of some spectra present in successive discussions[+].

Experiment	h (sec.)	Execution time	Examples
single resonance	0.03	3½ minutes	Fig. 23a
double resonance	0.03	7 minutes	Fig. 34d, 41f
nonselective CP	$10^{-6}/10^{-2}$	1 minute	Fig. 13a
selective pulses	0.0025	1½ minute	Fig. 57a.

Three computer programmes were written in FORTRAN IV (copies are presented in Appendix D) for the solution of the initial value problems defined by systems of two spin-1/2 nuclei, and for the experiments listed in sections C to E of the previous chapter. Most of the single resonance spectra and all of the pulse spectra were obtained from calculations performed in the rotating frame, while the double resonance spectra and some of the single resonance spectra employed the equations for the interaction representation. The step-size was held constant for the cw calculations in order to simplify the data for later

[+]for cw spectra, the execution time varies directly with the range of the frequency scan and inversely with the rate of scan. Consequently it is not possible to apply this dynamic method (nor is it required) for those cases where the sweep rate tends to zero. For the nonselective pulse experiment, the smaller step-size applies when the pulse is on and the larger step-size when the pulse is off.

manipulation, while for the nonselective pulsed NMR simulations, the step-size was varied since the rf amplitude was the limiting parameter (determining the largest eigenvalue of the Jacobian) when it is non-zero, ie. when the pulse is on. For the selective pulse sequence calculations, however, only one step-size was used since, apparently, the rf amplitude is never the determining parameter.

The result of these calculations is then the spin density matrix, in an interaction representation, as a discrete function of the time (for cw NMR, the observing rf frequency may be interpreted as the independent variable). That is, one obtains the list of matrices:

$$\rho^i(t=0);\ \rho^i(t_1);\ \rho^i(t_2);\ \ldots\ldots;\ \rho^i(t_n);\ \ldots\ldots \qquad [4.12]$$

which vary with the nature of the differential equations describing the experiment being calculated. The programmes then evaluate the set of numbers for the signal:

$$S(t=0);\ S(t_1);\ S(t_2);\ \ldots\ldots;\ S(t_n);\ \ldots\ldots \qquad [4.13]$$

from the expression appropriate to the type of detector desired and in the representation in which the spin density matrix has been calculated. Finally, the data in [4.13] is filtered (for double resonance), integrated so as to include the effects of inhomogeneity (unless [3.54] has been employed), Fourier transformed (for those pulse experiments), and, lastly, plotted.

A concluding point should be mentioned with respect to the step-size and the plotting programme. One requires a plot with a sufficient density of points so that the discrete set of points for the signal

appears as a continuous function when plotted against some scale of time or frequency. This consideration may, therefore, place a new upper limit on the step-size for the convergence of the RKG routine. For most of the plots, however, it was found that the step-size is effectively determined by the RKG routine; in fact it often proved convenient to discard every other calculated point (for example) in the list [4.13] since the greater density is superfluous.

C. Solution of the Inhomogeneity Integrals.

1. Introduction.

In the previous chapter, inhomogeneity of the static magnetic field was introduced into the density matrix formalism by two different methods. The first and simplest method, given by equation [3.54], is of no further concern here since inhomogeneity effects are included in the equation of motion of the spin density matrix. The second method incorporates inhomogeneity through an equation of the form

$$\overline{S} = \int_{-\infty}^{+\infty} d\beta\ S(\beta)\ G(\beta) \qquad [4.14]$$

where $G(\beta)$ is analytical and $S(\beta)$ consists of a set of numbers which are a function of the time or frequency.

Before considering the different cases for pulsed and cw NMR, a few preliminary remarks concerning [4.14] are in order. First of all, the integral equation must be put into a form suitable for evaluation by techniques available in numerical analysis. This is readily achieved by rewriting the integral as a summation, yielding

$$\overline{S} \simeq \sum_{\beta} \beta\ G(\beta)\ S(\beta). \qquad [4.15a]$$

This result is exact in the limit as the parameter β tends to zero (cf. reference (138), Chapter 1). Now since $G(\beta)$ tends to zero as $\beta \to \pm\infty$, it is possible to contract the limits of the integral to finite values; in practise it is found that useful limits are $\beta \simeq \pm 3w$ where $2w$ is the full width of the distribution at its half-height (ie. in the numerical evaluations presented below, it was determined that for

β outside these limits, $G(\beta)$ was sufficiently small that the signal from the corresponding ensembles was negligible in the sense as described in the footnote on page 96). Now the summation [4.15a] is in a form suitable for adaptation to a computer language; suppose, for example that the interval (-3w,3w) is split into an even number of 2n equal parts, each with length given by L=3w/n. Equation [4.15a] now becomes

$$\bar{S} = L \sum_{k=-n}^{n} S(\beta_k)\, G(\beta_k) \equiv L \sum_{k=-n}^{n} f_k \qquad [4.15b]$$

where $\beta_k = 3wk/n = Lk$. [4.15b] actually represents a rectangular quadrature formula, whereby the function f is approximated by a step function of value f_k in each of the interval segments.

The problem of convergence is now solved in a manner similar to that in the RKG algorithm; that is one estimates $\bar{S}$ using first 2n+1 points and segments of length L, then using 4n+2 points and segments of length L/2, etc., until successive estimates $\bar{S}(L)$ converge within the accuracy required. An alternate test for convergence is afforded by the Richardson extrapolation (130-133) which states that if $\bar{S}(L)$ and $\bar{S}(L/2)$ are two estimates to an integral, then a better estimate is given by the expression

$$2 \{ \bar{S}(L/2) - \bar{S}(L)/2 \} . \qquad [4.16]$$

It is also possible to devise different forms of quadrature for the evaluation of the integral in [4.14]. The programmes written for the evaluations in this thesis use either of the two equations given below[+] (130-132)

[+] other methods were also attempted, for example the Gauss-Hermite quadrature formulae (132) which require integrals of the form

(a) the trapezoid rule, given by

$$\overline{S}(L) = L/2 \{ \sum_{k=-n}^{n} 2f_k - (f_{-n} + f_n) \} \qquad [4.17]$$

which corresponds to approximating the function in each interval by a trapezoid, and

(b) Simpson's compound rule, given by

$$\overline{S}(L) = L/3 \{ f_{-n} + 4f_{-n+1} + 2f_{-n+2} + \ldots + 2f_{n-2} + 4f_{n-1} + f_n \} \qquad [4.18]$$

which corresponds to approximating the function by a series of parabolas.

A final note must be mentioned with respect to these numerical approximations. Since the integral now involves a discrete set of points, the normalization condition [3.59] must be altered to the following expression:

$$\sum_{k=-n}^{n} G(\beta_k) = 1 \qquad [4.19]$$

2. The Pulsed NMR integrals.

The application of 4.18 to the expression for the net signal $\overline{S}$ follows directly for the pulsed NMR simulations. As implied by

---

$\int_{-\infty}^{+\infty} f(x)\exp(-ax^2)\,dx$. It appears that this particular quadrature would lend itself to cases with a Gaussian distribution; however a surprising result was that Simpson's rule converges within a fewer number of points. [4.18] was therefore used for the pulsed NMR calculations, while the form of [4.17] lent itself to the cw integrals.

equation [3.64], one requires 2n+1 solutions to the equation of motion of the spin density matrix at each of the 2n+1 values of k in order to obtain the approximation [4.18]. Typical examples of the convergence pattern are shown in figures 6 and 7, where the signal from a Carr-Purcell pulse sequence is integrated over a Gaussian distribution of inhomogeneity with $2w = 1.67 \times 10^{-3}$ gauss. Note that figures 6a and 7a may be interpreted as the signal due to a perfectly homogeneous static magnetic field; for the calculations with inhomogeneity it represents the signal from the "central" ensemble. Figures 6b-d and 7b-d have a step-size of, respectively, L = w (7 points), L = w/2 (13 points) and L = w/4 (25 points); the Richardson formula indicates that the last spectrum in each case is a converged spectrum (the result with L = w/8 for figure 6, not shown here, confirms this conclusion). In general it is found that the number of points required increases with the width of the distribution and the RKG routine must be applied a large number of times whenever [3.65] is to be evaluated[+]. This is an unfortunate (but unavoidable) result since the required computer time is substantially increased

[+] in order to halve the step-size from, say, L to L/2, one must calculate first 2n+1 points and then 4n+2 points. For example, with n=3,

$$\bar{S}(L) = L/3 \{f_{-6} + 4f_{-4} + 2f_{-2} + 4f_{0} + \ldots + 4f_{4} + f_{6}\}$$

$$\bar{S}(L/2) = L/6 \{f_{-6} + 4f_{-5} + 2f_{-4} + 4f_{-3} + \ldots + 4f_{5} + f_{6}\} .$$

Now if suitable bookkeeping arrangements are made in the programmes (see Appendix D), then only 2n+2 new evaluations are required (f_1, f_3, etc.) in the process, and the execution time is therefore reduced.

Figure 6.

Convergence of the inhomogeneity integrals for the signal of a phase-sensitive detector for a Carr-Purcell sequence of pulses ($\pi/2$-τ-π-2τ-π-2τ-...) applied to a system of two magnetically equivalent nuclei. The parameters are $H_o=10^4$ gauss, $\omega_1/2\pi = \omega_2/2\pi$ = 42.577 megahertz, $J/2\pi$ = 0.0, $T_1=T_2=1.0$ seconds, H_1 = 3.2724 gauss (the pulse duration time τ_p is 17.94 and 35.88 microseconds, respectively, for the $\pi/2$ and the π pulses) and $\omega_1' = \omega_1$. The pulse separation time τ is 0.25 seconds and the inhomogeneity distribution is assumed to be Gaussian with $2w = 1.67\times10^{-3}$ gauss (the rms width is 10^{-3} gauss). Figure 6a is the calculated signal of the central ensemble, or it represents an approximation to the integral in [4.14] using one point. The plots 6b to 6d represent further estimates of the integral, using 7 points, 13 points and 25 points respectively, in the approximation formula from Simpson's rule (equation [4.18]).

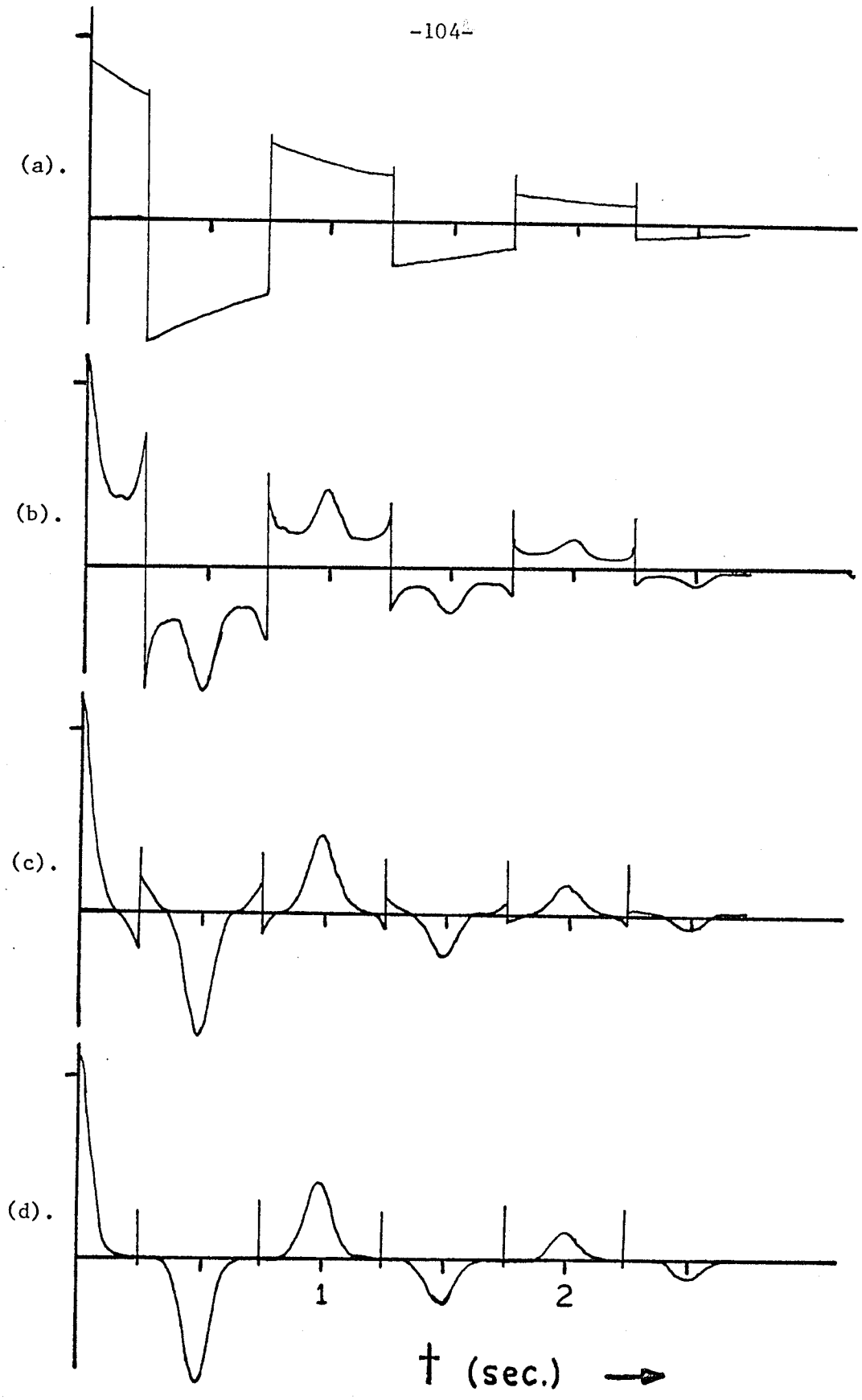
(a).
(b).
(c).
(d).
1
2
t (sec.)

Figure 7.

Convergence of the inhomogeneity integrals for the signal from a phase-sensitive detector for a Carr-Purcell sequence of pulses applied to a system of two magnetically inequivalent nuclei. The parameters are as for figure 6, but with $\omega_2/2\pi = \omega_1/2\pi +$ 2.0 hertz, $J/2\pi = 1.0$ hertz and $\omega_1'/2\pi = \omega_1/2\pi + 10.0$ hertz. The plots 7a to 7d represent estimates to the net signal using, respectively, one point, 7 points, 13 points and 25 points in equation [4.18] , assuming a Gaussian distribution of inhomogeneity with a width $2w = 1.67 \times 10^{-3}$ gauss.

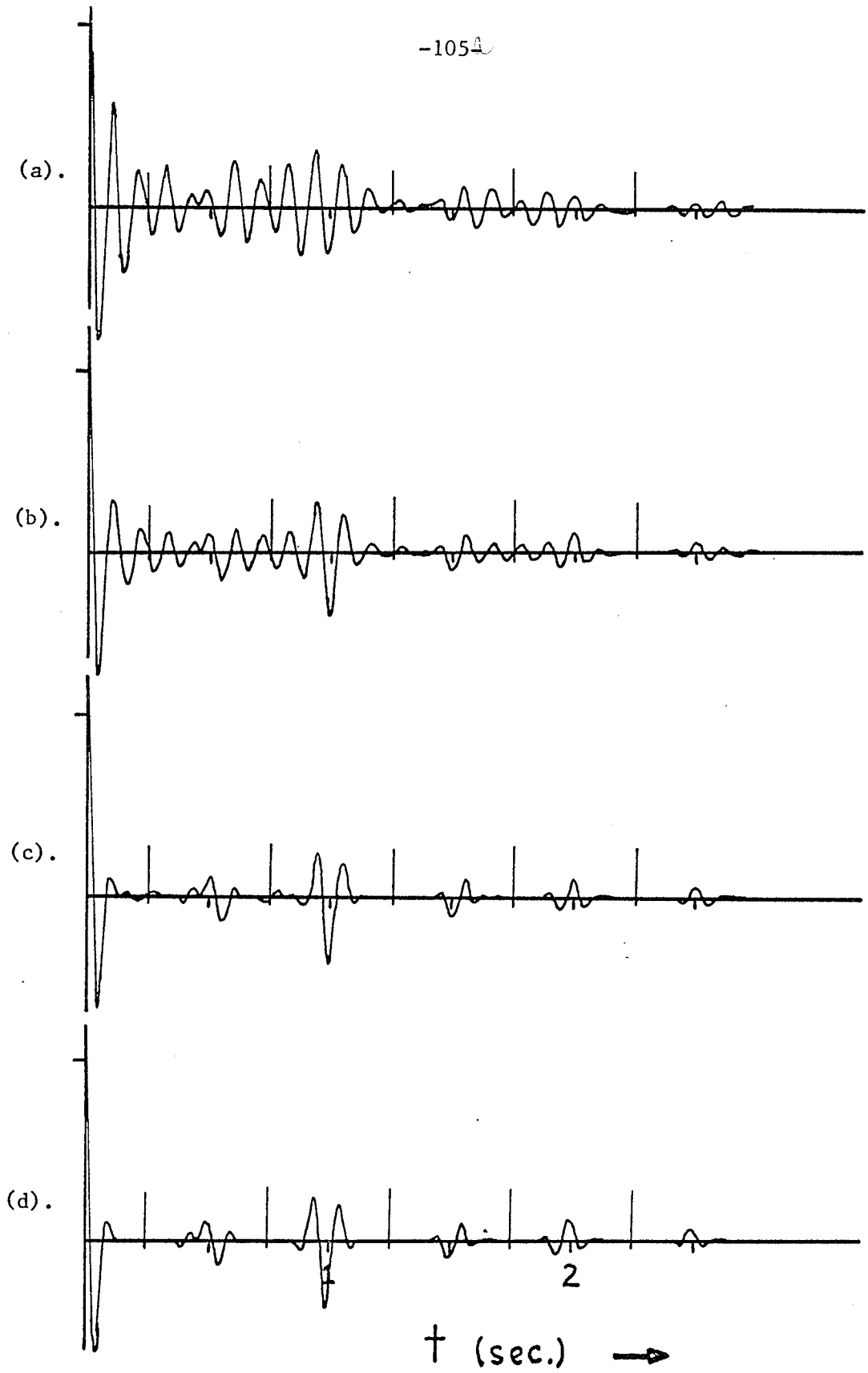
(a).
(b).
(c).
(d).
1
2
t (sec.)

when the entire signal of the system is of interest. Note, however, that the signal for the CP sequence behaves as expected; that is the relative signal amplitudes at the times t=2n (n=1,2,3,...) are independent of inhomogeneity (compare 6a and 6d or 7a and 7d). Consequently if one is interested in the (relative) amplitudes at these times, only the "central" spin density matrix need be calculated. Other simplifications for the Fourier transform spectra of some pulse sequences will also be discussed below.

3. The Continuous Wave NMR Integrals.

For cw NMR, it was shown that one need solve only the equation of motion of the central spin density matrix, provided that the approximation yielding

$$S(\omega_1'; \beta) \simeq S(\omega_1'+\gamma\beta; 0) \qquad [4.20]$$

is valid. The quadrature formula used in this case is [4.17] and it remains to describe how the step-sizes are determined so as to assure that the calculations converge to the desired integrals.

From equation [4.20], each point in the expression [4.17] is separated by the amount $\gamma\beta$ (radians/second) where γ is the gyromagnetic ratio of the species yielding a signal near the frequency ω_1', and where β is the inhomogeneity parameter in some finite range (the range is always greater than (-3w,3w); in this case, it was more convenient to restrict the range by requiring that, at the limits $\pm\beta'$, the corresponding value $G(\beta')$ is less than 1% of the value for $G(\beta=0)$). Now for frequency swept cw spectra, the separation in frequency units between two adjacent points in the calculated signal is

given by the product (ah) where a (in radians/second/second) is the sweep rate of the observing frequency and where h (in seconds) is the step-size used by the RKG algorithm. In all cases presented in this thesis, these points are much closer together than the (approximate) separation $\gamma w/8$ expected for convergence (by analogy with the pulsed NMR integrals; if however a is very large, then this may require that the step-size of the RKG routine be decreased). In practise, convergence is guaranteed by means of the following procedure: given the signal from the central ensemble, denoted here by $S(\omega_1')$, one has the set of points

$$\ldots;\ S(\omega_1'-8ah);\ S(\omega_1'-7ah);\ \ldots\ldots;\ S(\omega_1');\ \ldots\ . \quad [4.21]$$

A first estimate to $\overline{S}(\omega_1')$ is made by applying [4.17] to, say, every eighth point in some finite range (greater than (-3w,3w)). Successive estimates are then made by using [4.17] with every fourth point, every second point, etc., in the same range until the results converge (the time-consuming method mentioned above for pulsed NMR was also attempted for one single resonance experiment, and both approaches for that experiment gave identical results).

A sample of this procedure is presented in figure 8. The first two spectra, 8a and 8b, represent respectively the "central" ensemble and the net signal after converged integration over a Lorentzian distribution of half-height width equal to 0.12 hertz (1.693×10^{-5} gauss), and the normalization condition [4.19] is evidenced by the fact that the areas under the curves are approximately equal. Figures 8c and 8d display the effect of increasing the number of points by (about) a

Figure 8.

Convergence of the inhomogeneity integrals for the absorption mode signal of a single resonance experiment applied to a system of magnetically inequivalent nuclei. The parameters are $\omega_1/2\pi$ = 56.4 megahertz, $\omega_2/2\pi = \omega_1/2\pi + 2.0$ hertz, $J/2\pi = 1.0$ hertz, a dipole-dipole relaxation mechanism with T_D=0.94 seconds, H_1 = 0.01 milligauss and the sweep rate $a/2\pi$ is 0.05 hertz/second. Spectrum 8a is the signal from the central ensemble, and spectrum 8b is the net signal obtained by using [4.17] with 75 points over a finite range of (about) ±3w, where 2w=0.12 hertz is the full width at half-height of an assumed Lorentzian distribution of inhomogeneity. The spectra in 8c and 8d were obtained using 25 and 55 points, respectively, over the same range, and spectrum 8e was obtained using 55 points over a range of (about) ±1.5w. The horizontal lines in 8b to 8e have been added to the plots to aid in visual comparisons. The frequency origin is defined to be at ω_1, the sweep is in the direction indicated by the arrow, the horizontal scale is 1.0 hertz/division, and the vertical scale is constant for each plot.

Note: for this figure and for the following cw spectra, the sweep rate $a/2\pi$ is always greater than zero, unless otherwise specified, and frequency increases in the direction of the arrow. If $a/2\pi$ is less than zero, then frequency increases in the direction <u>opposite</u> to that indicated by the arrow.

(a).

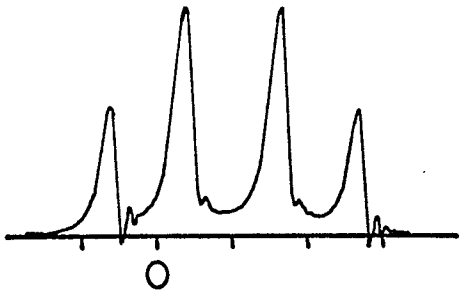

(b).

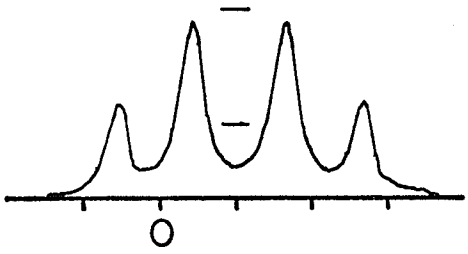

$\nu \rightarrow$

(c).

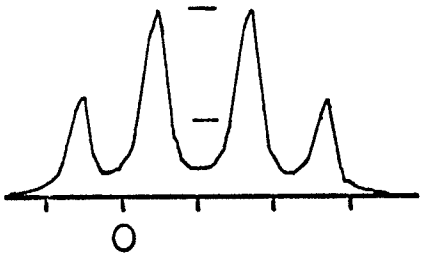

(d).

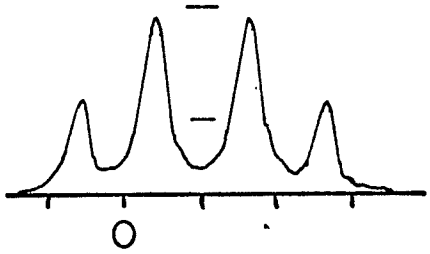

(e).

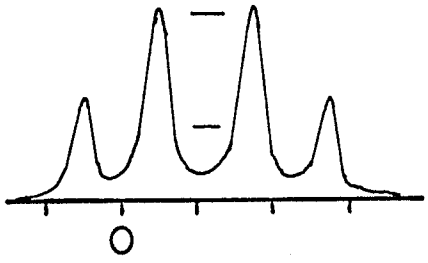

factor of two; the approach to convergence is accompanied by a broadening of the peaks and by a decrease in their intensities. Finally, the effect of the range of the integration may be demonstrated by a comparison of plots 8d and 8e. The calculations leading to the latter plot have the same number of points as 8d, but the limits of the integral have been halved to about ±1.5w. Note that the spectrum in 8d has essentially converged (cf. 8b); other calculations with limits greater than that for 8d do not show appreciable differences.

4. Fourier Transform Integrals.

Although it may not be obvious, the use of the approximation [4.20] represents a considerable saving in terms of computer execution time, as compared to the corresponding calculations for inhomogeneity in pulsed NMR. The overriding cost, as mentioned before, is largely determined by the number of RKG solutions required, and this consideration led to the investigation of the case of the FID signals and their Fourier transforms[+]. If it is the actual FID signal which is interesting, then of course the required expression is [4.14]. Often, however, it is the Fourier transform of the FID signal which is of interest, since this transform yields the usual unsaturated slow passage spectrum. One might then argue that a Fourier transform spectrum with inhomogeneity effects included might be calculated by either of the two following methods:

[+]this discussion also applies to partially-relaxed Fourier transform spectra.

(a) the FID signal is computed, including effects of inhomogeneity, and the Fourier transform spectrum is evaluated from this net signal, or,

(b) the FID signal from the "central" ensemble is computed, its Fourier transform evaluated, and then inhomogeneity effects are introduced using the simplification [4.20] for cw spectra.

Actual calculations using both methods verified the above conclusions; therefore it is possible to calculate Fourier transform spectra, including inhomogeneity effects, without recourse to the computationally more expensive procedure required for pulsed NMR calculations. A typical example of the Fourier transform of the FID due to a system of two spin-1/2 nuclei is shown in figure 9a (compare with figure 49 below). In this particular case, the spectrum was obtained using the first procedure outlined above (ie. using equation [4.14]), although identical results are expected by following the second procedure. For comparison, the spectrum deriving from a slow passage single resonance experiment in the limit of a weak rf field (ie. no saturation), and with the same parameters as for 9a, is presented in figure 9b. Except for the presence of effects attributable to a finite (but slow) sweep rate, the two spectra are identical, indicating that the two different methods of calculating inhomogeneity effects are at least consistent.

Figure 9.

A Fourier transform spectrum and the equivalent single resonance spectrum for a system of magnetically inequivalent nuclei. The parameters defining the FID signal are given in figure 49 (below), and the parameters describing both spectra are $H_o=10^4$ gauss, $\omega_1/2\pi$ = 42.577 megahertz, $\omega_2/2\pi = \omega_1/2\pi + 2.0$ hertz, $J/2\pi = 1.0$ hertz and $T_1=T_2=10.0$ seconds. Spectrum 9a corresponds to the infinitely slow passage unsaturated limit, and 9b has been calculated with the sweep rate $a/2\pi = 0.025$ hertz/second. Inhomogeneity has been included in 9a through a calculation of the net FID signal (ie. the first procedure mentioned on page 110), and in 9b through an application of equation [4.20]; in both cases the inhomogeneity distribution is Gaussian with a full width at half-height of $2w= 8.33\times10^{-5}$ gauss. The frequency origin is defined to be at ω_1, the sweep direction for 9b is in the direction indicated by the arrow, and the horizontal scale is 1.0 hertz/division.

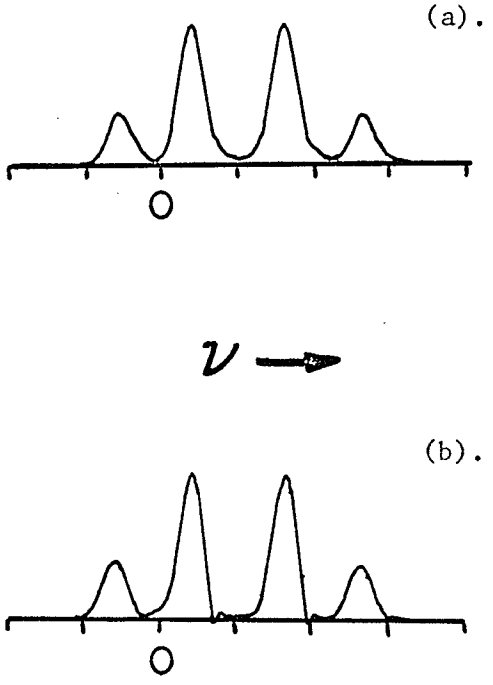
(a).
O
ν
(b).
O

D. Filtering of the Double Resonance Signal.

It was mentioned that the signal detected by the receiver in a double resonance experiment is complicated by the presence of the two rf fields. It may be shown (cf. Appendix B) that the actual signal, after demodulation, is of the form

$$S = S_o + S_1(\Delta\omega') + S_2(2\Delta\omega') \qquad [4.22]$$

where $\Delta\omega' = \omega_1' - \omega_2'$ is the frequency difference between the two rf fields. The interesting part of the signal is S_o[+], the stationary part of the response, and in a conventional NMR spectrometer this component is separated out by means of a narrow-pass filter.

Since the signal calculated from the RKG routine is of a discrete nature, it is convenient to simulate such a filter directly in order to remove the unwanted oscillating components (cf. Bloch (85)). This result is achieved by the rather straight-forward approach of averaging S over a period of the oscillation $\Delta\omega'$ (and also, therefore, $2\Delta\omega'$)[++]. Writing S(t) and $S_o(t)$ for the total and stationary signals at time t (which corresponds to some frequency ω_1' of the observing field), then the appropriate equation for the averaging is

$$S_o(t) = \sum_{k=-n}^{n} S(t+nh) \qquad [4.23]$$

where the period p of the oscillation is given by

[+] see, for example, references (18) and (139).

[++] the method is in fact a crude approximation to a Fourier analysis which is complicated by the fact that the frequency components involved are time-dependent (cf. Appendix B).

$$p = 2\pi/\Delta\omega' \qquad [4.24]$$

and where

$$n = p/h \qquad [4.25]$$

is the number of points from the RKG integration process within that period. Now obviously n should be very large to give a reliable average; this requirement may set a new upper limit to the step-size h of the RKG algorithm (if, for example, $\Delta\omega'/2\pi = p \leq h^{-1}$), although the case rarely arose in the examples presented here (where it was required that n be ≥ 2). On the other hand, n cannot be too large since then the signal $S_o(t)$ corresponding to some frequency ω_1' will be given by an average over a large range of frequencies near ω_1'. As a consequence of this last consideration, and since equation [4.23] will fail at observing frequencies near the perturbing frequency (ie. $\Delta\omega' \to 0$; note, however, that the spectrometer filter also "fails" in this limit), no attempts were made to calculate the filtered signal when $\Delta\omega'$ is small.

It is also important to note that the points S(t+nh) in [4.23] are required to be at the same frequency ω_1'. This is not the case since two adjacent points S(t) and S(t+h) vary in frequency by the amount (ah) where a is the sweep rate and h the step-size. Furthermore, since the points S(t+nh) are discrete in nature, and since n is of necessity finite, the set of points represent a random-like sampling of the signal and the averaging process will not be exact. If, however, the entire set of points for the signal is "filtered" or averaged several times, then it is to be expected that these deficiencies will eventually disappear, and that a converged result for the filtered signal will be

reached. This sequence of events is illustrated in figure 10, where the spectra 10a to 10d are the calculated signals obtained after applying [4.23] a different number of times. The original signal is not reproduced here since $\Delta\omega'/2\pi \simeq 100$ hertz, and the "spectrum" on a similar scale would appear as a series of closely spaced near-vertical oscillations which effectively swamp out the stationary part of the signal. In the spectra presented in figure 10, it is clear that only a few applications of the averaging are required to produce a converged result; further it was observed that the result is stable in the sense that if the filtering were repeated, for up to one hundred times, the final spectrum would be identical with 10d.

The actual parameters used in the calculation of the spectra in figure 10 describe an AX system, and one may invoke the AX approximations as discussed in section D of Chapter III. When one performs the simplifications of the perturbation Hamiltonian (and the static Hamiltonian and the signal), it turns out that the observed signal is as given in 10d; ie. the signal is already "filtered". This result may be rationalized by realizing that the AX approximation allows the omission of terms involving the rapid oscillations $\exp[\pm i(\omega_1'-\omega_2)t]$ and $\exp[\pm i(\omega_2'-\omega_1)t] \simeq \exp(\pm i\Delta\omega' t)$, which apparently are responsible for the oscillations in the signal. Since this signal is identical with 10d, one may argue that either the filtering routine converges to the required solution and/or that the AX approximation is valid[+].

[+] another useful cross-check for the accuracy of the filtering routine is made possible by the fact that the double resonance spectrum should

Figure 10.

An example of the convergence of the filtering routine, for the absorption mode signal of a system of magnetically inequivalent nuclei. The parameters are $H_o=10^4$ gauss, $\omega_1/2\pi$ = 42.577 megahertz, $\omega_2/2\pi = \omega_1/2\pi$ + 100.0 hertz, $J/2\pi$ = 1.0 hertz and $T_1 = T_2^* = 4.0$ seconds. The observing field is swept at 0.025 hertz/second with an amplitude of 0.0005 milligauss, and the perturbing rf field is centered at the frequency ω_2 with an amplitude of 1.174×10^{-2} milligauss. The zero of the frequency axis is defined to be at ω_1, the sweep is in the direction indicated by the arrow, and the horizontal scale is 1.0 hertz/division. The filtering routine has been applied once, twice, five times and ten times respectively in spectra 10a to 10d; the latter spectrum is a converged spectrum.

(a).

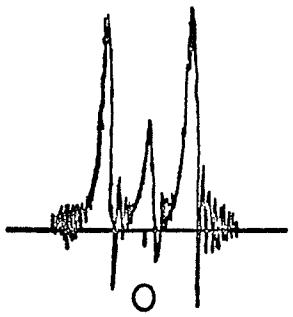

(b).

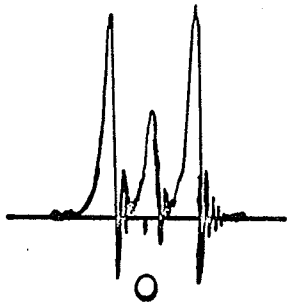

$\nu \longrightarrow$

(c).

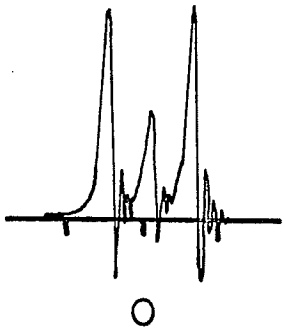

(d).

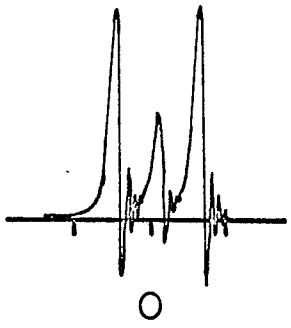

A concluding remark should be made concerning the order of the filtering and the calculation of inhomogeneity integrals. Equations [4.22] and [4.23] are meant to imply that the "filtering" is to be carried out first; however actual calculations have demonstrated that the order is not important. In practise, however, since the filtering routine usually requires a greater density of points for convergence than does the inhomogeneity routine, normally the filtering process should be carried out first. Note also that both of these routines "lose" points at the beginning and at the end of the set of numbers for the signal. Consequently if one requires the signal over some frequency range (a,b), it is necessary to perform the RKG integration procedure over a slightly larger range ($a-\delta$, $b+\delta$).

---

resemble the corresponding single resonance spectrum if the perturbing rf frequency is far removed from any of the transitions. Some results presented below illustrate that after filtering such a double resonance spectrum, one obtains a plot essentially identical to the single resonance spectrum, as required for consistency.

E. Evaluation of the Fourier Transforms.

The equation to be solved here is the integral for the Fourier transformation, of the form

$$S(\omega_1') \quad \propto \quad \int_0^\infty S(t)\ \exp(-i\ \omega_1' t)\ dt \qquad [4.26]$$

where S(t) is a discrete set of points for the signal, with time t=0 defined as the time at the end of a $\pi/2$ pulse. The problem is in fact very similar to the experimental problem since both cases involve a signal which has been sampled at random points in time.

Equation [4.26] is numerically evaluated after manipulations as before; that is one first rewrites the integral using some quadrature formula, and then contracts the upper limit to some finite value. The formula used here is Simpson's compound rule ([4.28]) with the step-size L given by the difference between two adjacent points in the list for the signal. It is well-known that one requires a step-size less that $1/\omega_{max}$, where ω_{max} is the largest frequency difference encountered in S(t), if the Fourier transform is to yield the required spectrum (cf. reference (8)). For values of L larger than this value, the phenomenon known as "frequency fold-back" (8) may occur; however this situation is never encountered here since the step-size required by the RKG routine guarantees a sufficient density of points for the convergence of the Fourier transforms.

The second consideration of interest here is that concerning the upper limit required in the numerical approximation to the integral in [4.26]. An example of the variation of the calculated Fourier

transform spectra with this limit is shown in figure 11, where 11a and 11b display the effect of using an upper limit which is too small. This effect is overcome by the calculations reproduced in 11c and 11d by requiring that the upper limit, t_{max}, is such that $|S(t_{max})| < |S(t=0)| \times 10^{-4}$. This same situation may occur experimentally if the signal is not sampled for a long enough period of time following the pulse, and often the effects are overcome by analytical approximations known collectively as apodization (8). Practical limits for the value of t_{max} are $t_{max} \simeq 3T_2^*$ (8), where T_2^* is the effective spin-spin relaxation time for the spin system.

For the alternate scheme proposed for the evaluation of these spectra, that is the scheme where one has the parameter T_2 and inhomogeneity effects are included <u>after</u> the Fourier transform, the corresponding practical limit is $t_{max} \simeq 3T_2$. It follows that, since $T_2 \geq T_2^*$, the RKG integration routine must be carried to greater lengths of time than for the first scheme (method (a) on page 110), although the alternate scheme ((b) on page 110) still represents a considerable saving in execution time.

Figure 11.

Convergence of the Fourier transformation routine, for the Fourier transform of the FID signal of a system of two magnetically equivalent nuclei. The parameters defining the pulse are given in figure 48 (below), and the parameters defining the spin system are $\omega_1/2\pi = \omega_2/2\pi = 42.577$ megahertz, $J/2\pi = 0.0$ and $T_1 = T_2 = 10.0$ seconds. A Gaussian inhomogeneity distribution with half-height width $2w=8.33 \times 10^{-5}$ gauss has been assumed, and inhomogeneity integration has been carried out using the method (a) outlined on page 110. The absorption mode signal, 11a, and its corresponding dispersion mode signal, 11b, were obtained using an upper limit $t_{max} \simeq 1.5$ seconds. The spectra in 11c and 11d have been calculated with $t_{max} \simeq 4.5$ seconds and the plots show the predicted convergence pattern (see text) since $t_{max} > 3T_2^*$ (from equation [3.52], $T_2^* \simeq 0.77$ seconds). The zero of the frequency axis is defined to be at ω_1 and the horizontal scale is 1.0 hertz/division.

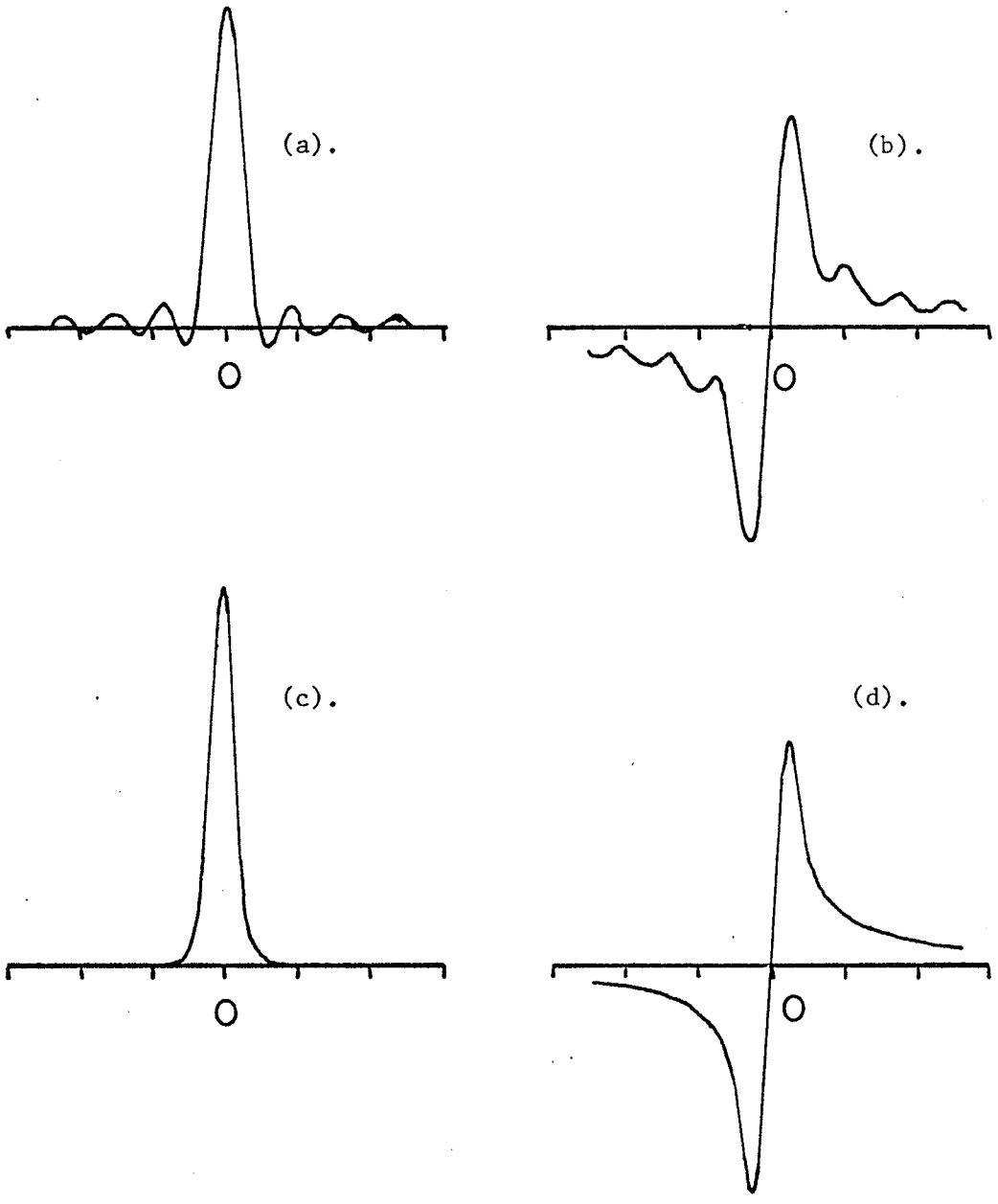
(a).
O
(b).
O
(c).
O
(d).
O

CHAPTER V. SOME SIMULATED HIGH-RESOLUTION NMR SPECTRA

A. Introduction.

This chapter is devoted to a presentation and discussion of a number of spectra which were calculated using the techniques described in the previous chapter. Some of these calculations have appeared previously in the literature (114-116). Listings of the relevant programmes are given in Appendix D, and it may be assumed that the various approaches employed for the different problems possess converged solutions, unless otherwise stated.

A few general comments concerning these calculations should be mentioned at this time. First of all, these spectra are variously referred to as "simulations" of the NMR experiment as opposed to "theoretically-calculated" spectra. This is meant to imply that the solutions obtained here are more closely related to the actual experimental conditions than are other methods of solution. Thus, for example, the computed double resonance spectra simulate the double resonance cw experiment in the sense that one requires "new" parameters describing the frequency sweep, the demodulation of the signal, the filter, etc., all of which are involved in the usual experimental arrangement necessary for the actual recording of a double resonance spectrum.

A second point to be made is that direct quantitative comparison with experimental results is often difficult to realize since in many cases a given experimental spectrum reproduced in the literature is incompletely defined with respect to all the experimental parameters

and variables. A typical example is afforded by the experimentalist who is interested in using cw NMR as a tool in structural elucidations. For such studies it may well be that the only important requirement is that a given spectrum is representative of the unsaturated slow passage limit for the determination of transition frequencies and amplitudes, and parameters such as relaxation times, the rf amplitude, sweep rates, the type of inhomogeneity distribution and its half-height width, etc., are often not of any interest. As a result, these parameters may not be listed and/or not determined (or they may be indeterminable), so that the problem of simulation of such a spectrum is complicated by the presence of a number of unknown variables. Although it may be possible to estimate reasonable values for these variables, in general it was felt that qualitative comparisons of the calculated spectra with similar experimental results would suffice to show the accuracy of the technique. This procedure is followed in most of the discussion presented below, although a few cases are also mentioned for which more quantitative comparisons are possible.

Another related consideration is the number of different spin density matrix models available for the description of the NMR experiment. Those of interest here have been discussed in some detail, and they vary depending on the manner in which the effects of relaxation and inhomogeneity are included in the formalism. In the plots reproduced below, three models have been employed; they are referred to as models A, B or C where the appropriate equations for a given model are listed below.

(a) Model A - the phenomenological equations [2.12] and [3.54] for the description of both relaxation and inhomogeneity effects (used only for simulations of cw experiments).

(b) Model B - the phenomenological equation [2.12] for relaxation effects, and convolution integrals of the form of [3.57] for the description of inhomogeneity.

(c) Model C - relaxation is described using the Bloch-Wangsness-Redfield formalism (ie. equation [2.23]) with the mechanisms of interest as expressed in Table I, and inhomogeneity integrals of the form of equation [3.57].

These different models are not compared systematically in the ensuing discussion, principally because there is a lack of experimental spectra to serve as a basis for comparison, and also because the main objective of this dissertation is the development of a general dynamic method for the calculation of response in NMR as opposed to the development of a "best" model (the models used here have been discussed in some detail; see for example the references listed in Chapters II and III). In the evolution of this technique, the first model, model A, was originally employed (114) inasmuch as it allowed the presentation of the main numerical problem with a minimum of complexity; furthermore, the resultant expressions, being phenomenological in origin, are relatively easy to interpret. This model possesses obvious shortcomings, however, since any simulations using an effective spin-spin relaxation time must fail for those experiments, such as the Carr-Purcell pulse sequence, for which the

effects of relaxation and inhomogeneity are separable[+]. In addition model A implicitly assumes that the distribution of the ensembles is Lorentzian, which may not be the case.

These conclusions led to the extended model B (115) which is somewhat more general since relaxation and inhomogeneity are treated in a manner which is more consistent with the actual experimental conditions. Nevertheless, one would expect similar results in the simulation of unsaturated cw NMR spectra, provided that a suitable correlation is made between the parameters T_2, T_2^* and w (using equation [3.52] for example).

Both models A and B are restricted to those experiments for which the effects of relaxation are either unimportant or only of qualitative interest (unless the spin system is a system of single spin-1/2 nuclei), so that the phenomenological equations [2.12] are

---

[+]Abragam (reference (4), pages 50-52) points out that the effects of inhomogeneity and relaxation in cw NMR vary differently as a function of the rf amplitude, and are therefore separable. The effect of inhomogeneity of the static field is to broaden a transition by a constant amount, whereas the broadening due to natural spin-spin relaxation depends weakly on the strength of the rf field through the "saturation factor" (cf. equation [1.4]) (1-6). Consequently these two sources of line broadening yield different effects as a function of the rf amplitude, and it follows that an effective spin-spin relaxation time cannot adequately describe both spin-spin relaxation and inhomogeneity for all cases.

adequate. The last model, C (116), represents yet another extension (or generalization) to enable the simulation of some experiments which are designed to yield explicit information on the nature of the relaxation processes. This last model is more complicated than models A or B because of the complexity of the Bloch-Wangsness-Redfield formalism; however some observed spectra with sufficient known parameters are available so that more quantitative comparisons are possible. This might be taken to imply that model C is the "best" model; however the spectra to be presented below will shed more light on this question and a brief consideration of the usefulness of a given model is deferred until the last chapter.

The remainder of this chapter is given over to four sections dealing with the simulations for single resonance, double resonance, nonselective pulse sequences, and a selective pulse sequence. Within each section, the simulations may involve any or all of the three models, and some comparisons may be made.

Finally it should be restated that the calculated spectra are all of systems of two spin-1/2 nuclei, with the actual parameters chosen corresponding to the NMR of protons. The variations of the spin systems include, using the notation of Pople et. al. (1), A_2 systems (essentially equivalent to a single spin-1/2 system), AX systems and AB systems, where the protons are magnetically equivalent ($\omega_1=\omega_2$), magnetically inequivalent with $|\omega_1-\omega_2| >> |J_{12}|$ and magnetically inequivalent with $|\omega_1-\omega_2| \simeq |J_{12}|$, respectively.

B. Simulations of the Single Resonance Experiment.

In the following plots, calculated single resonance spectra are presented as a function of the sweep rate, the amplitude of the observing rf field, the relaxation parameters, etc., in an attempt to show some of the more interesting features that this dynamic technique is capable of reproducing. Before considering these results, however, it is appropriate to explain here the source of an apparent anomaly which occurs in all of the cw simulations.

1. The Initial Transients.

An essential requirement for the numerical solution of the equation of motion of the spin density matrix is that the differential equations be cast into the form of an initial value problem. This was achieved by assuming that, at time t=0, the spin system is in a state of thermal equilibrium (thereby implying that the rf field is not present for some time $t < 0$). The cw spectra are now obtained by allowing that an rf field of finite amplitude and with a frequency near the transitions of interest is suddenly switched on, and as a result the spin system experiences a sudden perturbation. This perturbation is in fact similar to the conditions defining the Torrey experiment (8,28) (the arrangement described by Torrey utilizes rf fields of much stronger amplitudes, and the rf frequency is constant during a given experiment), and therefore it is to be expected that there would result oscillations similar in nature to the Torrey transients (8,28). For a single spin-1/2 system,

these transients may be characterized by the Bloch equations (28); one predicts, for example, that the initial amplitude of the oscillations varies directly with the strength of the rf field, and that the oscillations should decay at a rate determined by the extent of inhomogeneity and both of the relaxation times T_1 and T_2.

In figures 12a to 12c, there are present on the extreme lhs some initial transients which are attributed to the source described above. Some calculations using a time-independent rf frequency tend to support this conclusion, as does the behaviour of the transients with, for example, increasing the amplitude of the rf field[+]. The anomaly now becomes clear since similar effects have not been reported in experimental cw spectra[++]. It is not too difficult to explain the apparent conflict, however. Briefly, the difference between the simulated spectra and the observed spectra derives from the rather artificial initial conditions chosen for the simulations, since an experimental spectrum is usually not recorded until the rf field has been "switched on" for a long time. Thus any initial transients would have decayed sufficiently so as not to appear in the recorded spectrum.

With this last fact in mind, the undesirable (and usually uninteresting) initial transients have not been reproduced in the

---

[+] this behaviour has been utilized as a method for the determination of rf amplitudes (17,102,103,140).

[++] it is predicted that such transients would be observed if the experimental conditions are made to correspond with the conditions for the simulations.

Figure 12.

A_2 spectra as a function of the rf amplitude, using model A. The parameters are $H_o=10^4$ gauss, $\omega_1/2\pi = \omega_2/2\pi = 42.577$ megahertz, $J/2\pi = 0.0$ and $T_1=T_2^*=2.0$ seconds. The zero on the frequency axis is at $\omega_1' = \omega_1$, the horizontal scale is 1.0 hertz/division and the sweep direction is as indicated by the arrow. The sweep rate is $a/2\pi = +0.05$ hertz/second and the rf amplitude is (a) 0.005 milligauss; (b) 0.010 milligauss; (c) 0.050 milligauss; (d) 0.100 milligauss and (e) 0.500 milligauss.

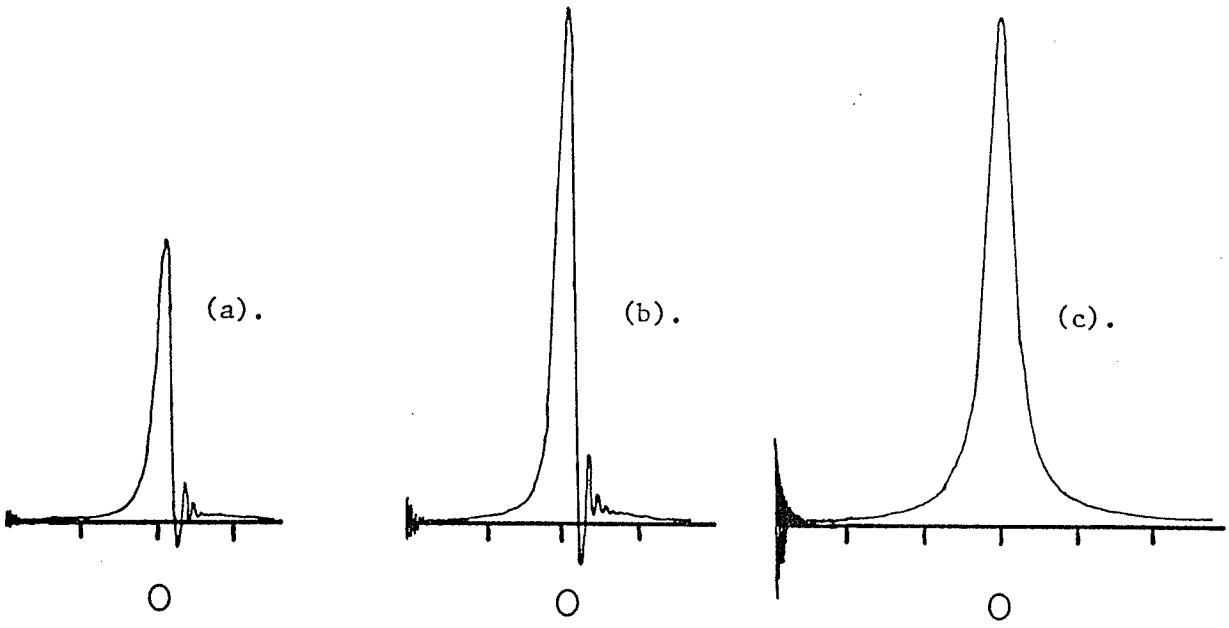

$\nu \rightarrow$

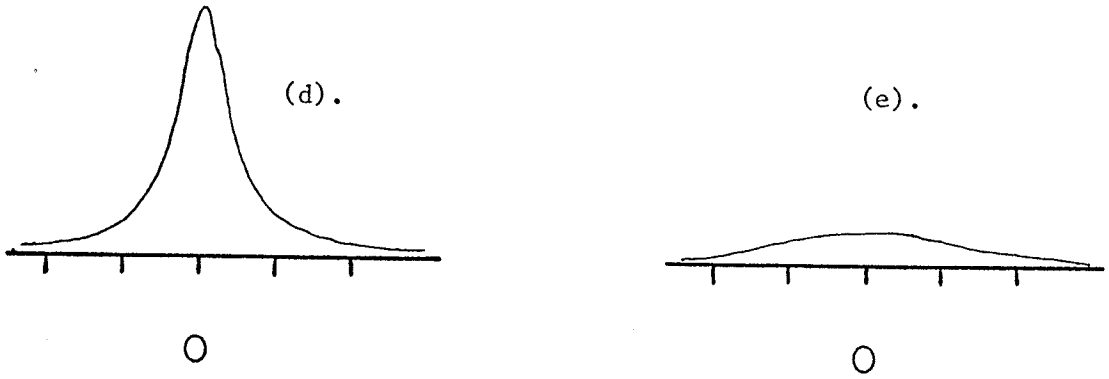

remainder of the cw plots. One important consequence which results, however, is that a given calculated cw spectrum must begin at a frequency slightly removed from the starting point of interest in order that any initial transients will not superimpose on the spectrum. The actual distance required depends in a complex manner on the parameters defining the simulation, and it is best determined by trial calculations (although the initial transients will decay before any ringing effects in the unsaturated limit, so that reasonable estimates are often possible).

2. Simulations of A_2 Systems.

The plots presented in figure 12 display the effect of different strengths of the rf field on the calculated spectra of an A_2 system, using model A. The results are in good qualitative agreement with corresponding solutions to the Bloch equations (cf. equation [1.4] and references (1-6)), which predict a broadening due to saturation as the rf amplitude becomes large. The first two spectra, 12a and 12b, are in the limit of no saturation, and in fact the field used in 12a is somewhat less than the optimal value for a maximum unsaturated absorption mode signal. Saturation occurs when $\gamma^2 H_1^2 T_1 T_2^* \simeq 1$, or for the parameters in figure 12, when $H_1 \gtrsim 0.02$ milligauss (cf. equation [1.4]).

Also shown in figures 12a and 12b are transients following the passage of the rf field through the Larmor frequency. This phenomenon, known as "ringing" or the "wiggle" effect, is displayed in figures 13 and 14, where the rf sweep rate and the effective spin-

Figure 13.

A_2 spectra as a function of the sweep rate, using model A. The parameters are as for figure 12, but with H_1 fixed at 0.01 milli-gauss, and with the sweep rate $a/2\pi$ equal to 0.025, 0.050, 0.100, 0.200, 0.400 and 0.800 hertz/second, respectively, for (a) to (f). The frequency has been swept in the direction indicated by the arrow, except for the right-most spectrum in 12c which has been calculated using a sweep in the opposite direction (ie. $a/2\pi = -0.100$ hertz/second).

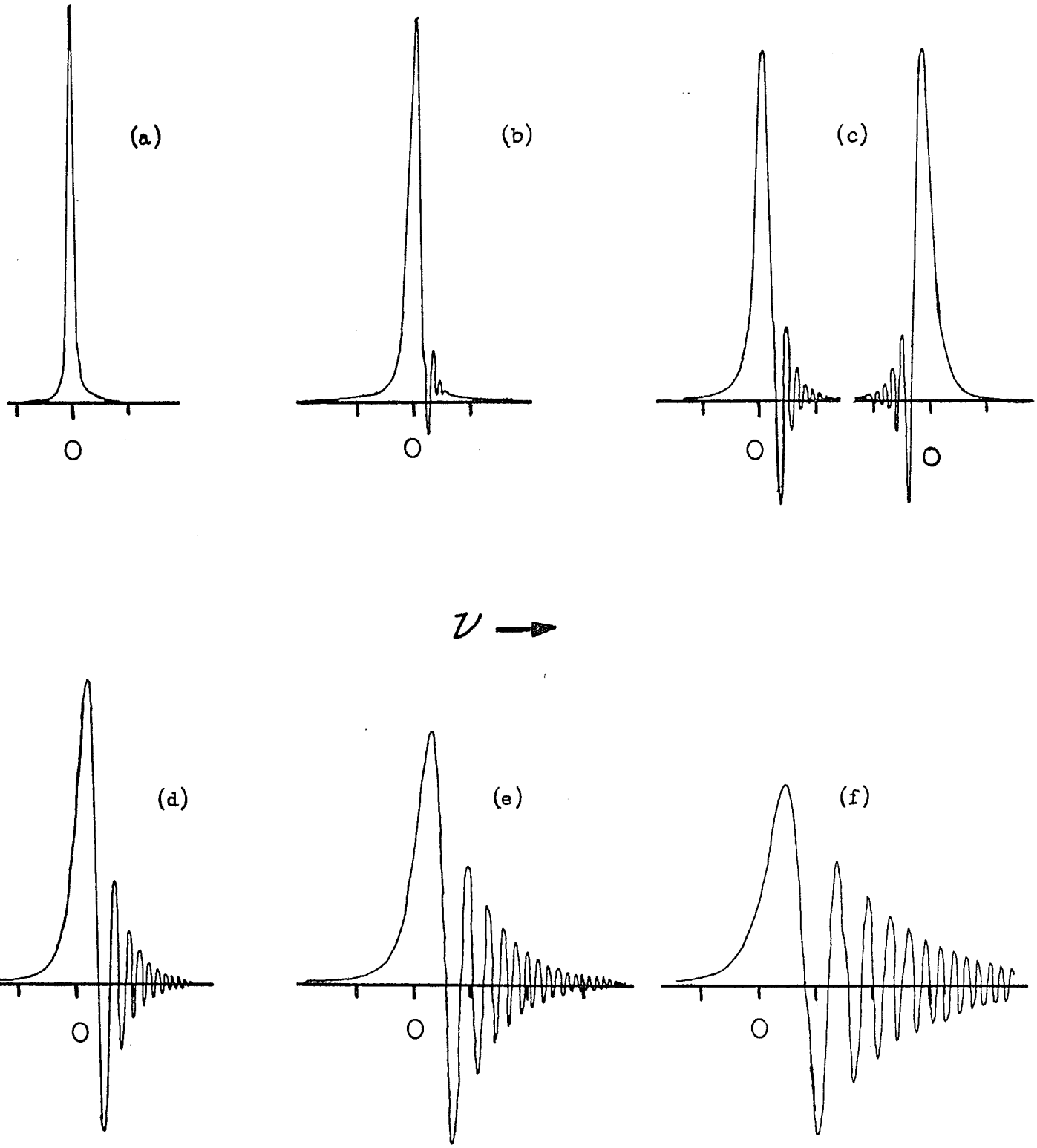
(a)
(b)
(c)
O
O
O
O
$\nu \rightarrow$
(d)
(e)
(f)
O
O
O

Figure 14.

A_2 spectra as a function of the relaxation times, using model A. The parameters are as for figure 12, but with H_1 fixed at 0.01 milligauss and the sweep rate is 0.05 hertz/second. The spectrum in 14a has $T_1=T_2^*=4.0$ seconds, and 14b has $T_1=T_2^*=0.50$ seconds. For these simulations, the spin-spin coupling constant $J/2\pi$ = 3.0 hertz, although no effects are observable if the magnitude or the sign is varied.

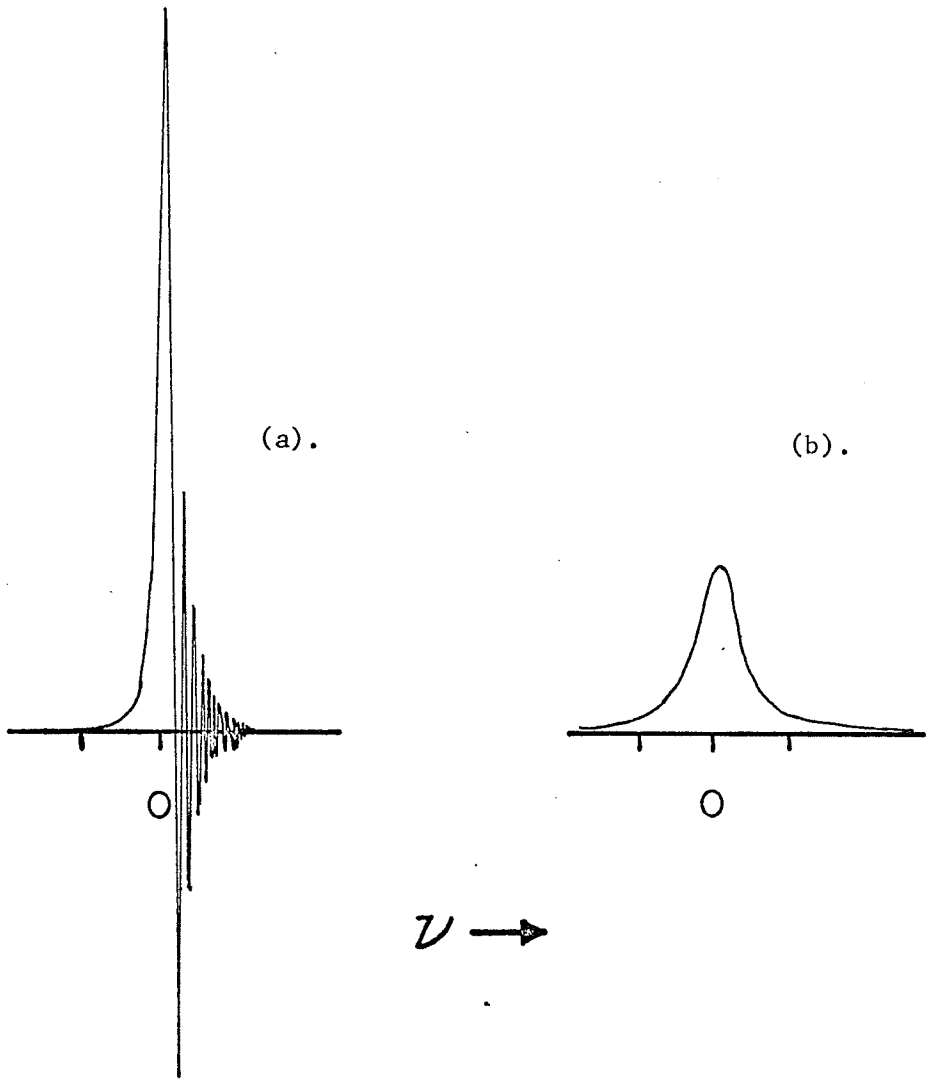
(a).
(b).
O
O
ν

spin relaxation time have been varied[+]. Typical experimental spectra are also shown in figures 15a and 15b for comparison. If the plots displayed in figures 12 to 14 are analyzed in some detail, it may be concluded that the length of time for which the wiggles persist varies directly with the magnitude of the sweep rate (and is independent of the direction of the sweep), directly with the effective spin-spin relaxation time, and inversely with the strength of the observing rf field. Furthermore, the transition tends to broaden and its maximum is shifted towards the sweep direction as the sweep rate is increased.

These effects are also in agreement with observed spectra[++] and with the predictions of the Bloch equations (1-6,9,25-27), and a simple explanation of some of these features may be readily realized by recalling that the absorption process is accompanied by a rotation of the macroscopic magnetization vector in the x'y' plane, which in turn induces a voltage in the detector coil. The Bloch equations predict that this component of the magnetization will decay to zero at a rate determined by the effects of relaxation and inhomogeneity of the static field. Now if the rf field is swept through resonance quickly enough, then some magnetization may persist in the x'y' plane, and consequently there will be induced in the detector an interference pattern, with the interference arising because the magnetization and the detector rotate at different frequencies (the detector is referenced to the frequency of the rf field). The wiggles

---

[+] the A_2 spectra in figure 14 were calculated with $J \neq 0$; however no observable effects are apparent, as expected (1-6).

[++] experimental spectra are further complicated by the presence of radiation damping (4), not accounted for in these calculations.

Figure 15.

Experimental spectra of a single spin-1/2 system of nuclei. The first two plots display the ringing observed after the rf field has been swept through the Larmor frequency, with the sweep rate being much slower for 15b than for 15a. The discontinuities in the wings of the peak in 15b are attributed to spectrometer instabilities (taken from Becker (6), figure 2.8). The pattern displayed in figure 15c is that deriving from a fast scan through two transitions which are relatively close together on the frequency scale, and the interference of the wiggles from each transition gives rise to the beat effect (taken from Emsley et. al. (3), figure 2.8).

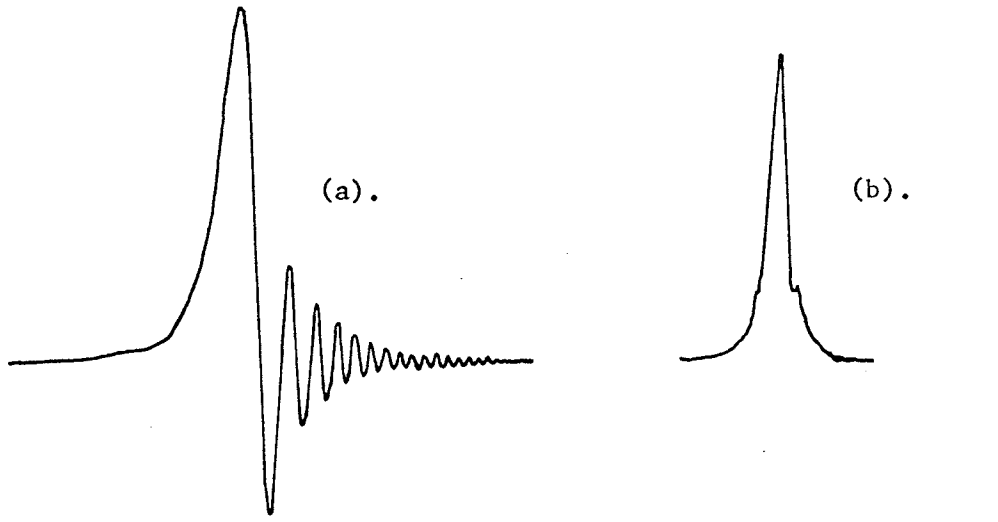
(a).
(b).

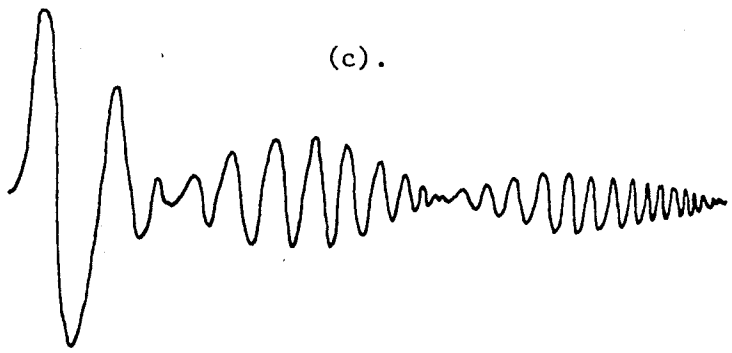
(c).

therefore depend, in the manner predicted above, on the magnitude of the sweep rate and the effective spin-spin relaxation time. The effect of the strength of the rf field follows from a similar argument: since the signal is broadened as H_1 begins to saturate the transition, the ringing pattern tends to become lost in the wing of the absorption peak, although some distortion may be present (as compared to a similar spectrum obtained using a slower sweep rate).

The spectra in 13a and 14b may also be compared quantitatively with the Bloch equations with respect to their half-height line widths. Model A was derived in analogy with the Bloch equations, and therefore one predicts that spectra calculated in the slow passage unsaturated limit possess full half-height line widths given by $(1/\pi T_2^*)$ hertz. For the parameter T_2^* in figures 13a and 14b, the predicted line widths are 0.16 and 0.64 hertz respectively, in good agreement with the actual widths of the simulated spectra (the other spectra are broadened to somewhat greater extents due to the effects of saturation and/or the finite sweep rate).

Another effect closely related to the ringing phenomenon is shown in figure 16, where two transitions occur relatively close together on the frequency axis. The ringing of the first peak produces rather severe distortions in the second peak in figures 16a and 16b; and as the sweep rate is increased still more, there appears the phenomenon known as wiggle-beats (10). The beats shown in 16c and 16d derive from the interference of the wiggles from each peak, and analytical approximations have revealed that it is possible to

Figure 16.

The wiggle-beat effect for a system of two uncoupled spin-1/2 nuclei whose transitions are near-degenerate. The parameters are, using model A, $H_o=10^4$ gauss, $\omega_1/2\pi$ = 42.577 megahertz, $\omega_2/2\pi = \omega_1/2\pi$ + 0.50 hertz, $J/2\pi$ = 0.0 hertz, $T_1=T_2^*=2.0$ seconds, and the rf amplitude H_1 is fixed at 0.010 milligauss. The sweep rate $a/2\pi$ is equal to 0.05, 0.20, 0.50 and 0.75 hertz/second, respectively, for the spectra (a) to (d). The zero of the frequency axis is defined to be at $\omega_1'=\omega_1$, the horizontal scale is 1.0 hertz/division and the sweep direction is as indicated by the arrow.

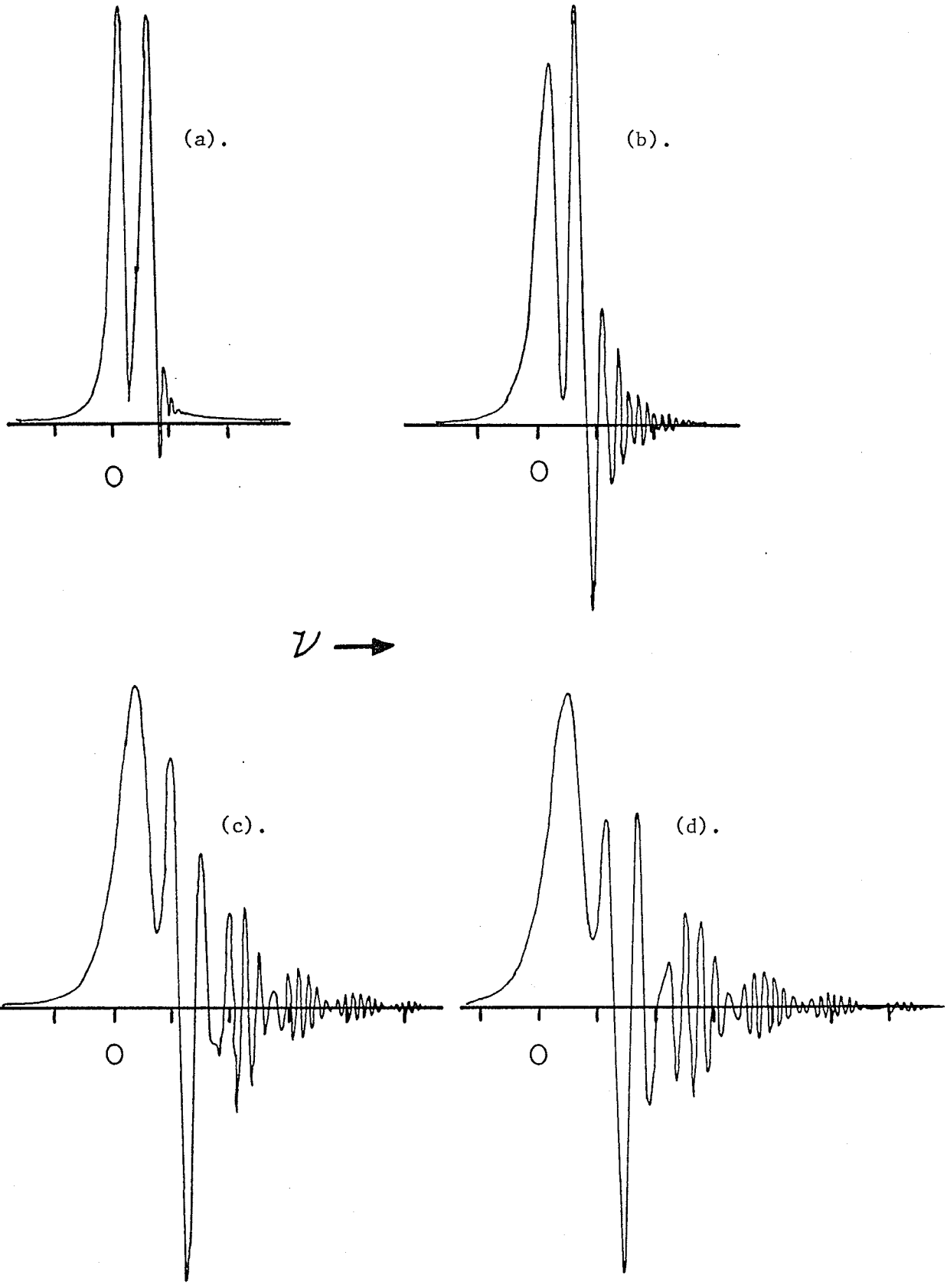
(a).
O
(b).
O
ν
(c).
O
(d).
O

obtain estimates for the splitting between two transitions through an analysis of the beats (cf. references (1-6,10), for example). In figure 16c, for example, the two beat maxima near 3.0 hertz are separated by about 1.0 hertz or 2.0 seconds in time. Consequently the period of the beats is (about) 2 seconds, yielding an estimated splitting of 0.5 hertz, in complete agreement with the parameter actually used in the simulation. An example of these effects is also shown in figure 15c which is experimental in origin.

In each case, the calculated spectra discussed in this section have been obtained using model A. Further examples of A_2 spectra using model B are postponed to the next section, where additional features are described before the two models are compared.

2. Simulations of AB Systems.

The ringing patterns due to a system of AB nuclei are displayed in some of the following figures. In figure 17, the sweep rate parameter has been varied, and the spectra would eventually show the complicated effects of wiggle-beats for a fast enough sweep rate. For the unsaturated slow passage limit, it is predicted that the intensities of the innermost and outermost transitions of the AB system chosen are in the ration 1 : 2.62 (cf. Table III and references (1-6)). The ratio of the corresponding peak areas in figure 17a approaches closely this value; however as the sweep rate increases (or as broadening due to saturation occurs), the measured ratio varies because of asymmetric distortions of the transitions.

Figure 17.

AB spectra as a function of the sweep rate, using model A. The parameters are $H_o=10^4$ gauss, $\omega_1/2\pi$ = 42.577 megahertz, $\omega_2/2\pi$ = $\omega_1/2\pi$ + 2.0 hertz, $J/2\pi$ = 1.0 hertz, $T_1=T_2^*=2.0$ seconds and the rf amplitude is fixed at 0.010 milligauss. The sweep rate $a/2\pi$ is 0.025, 0.050, 0.100, and 0.200 hertz/second respectively, for the spectra (a) to (d). The zero of the frequency axis is defined to be at $\omega_1'=\omega_1$, the horizontal scale is 1.0 hertz/division and the sweep direction is as indicated by the arrow.

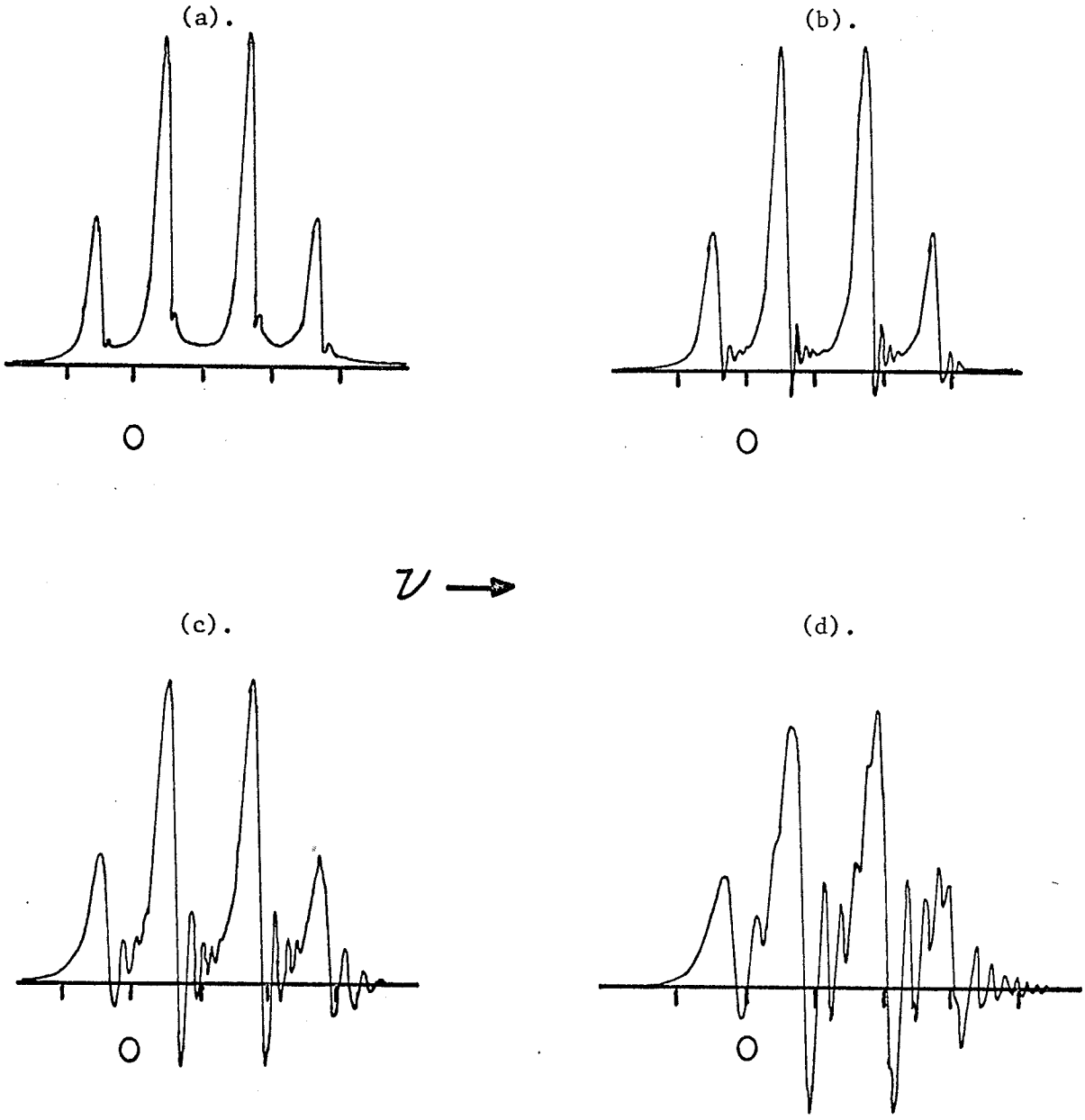
(a).
(b).
O
O
ν →
(c).
(d).
O
O

These distortions are also responsible for the deviation of the measured half-height line widths from their expected value of $(1/\ T_2^*)$ hertz (for each transition; cf. Table II), although the spectrum in figure 17a approaches the expected value.

The spectra illustrated in figure 18 display the effect of increasing the amplitude of the rf field on the spectra of the same AB system, also calculated using model A^+; similar experimental results are shown in figure 19. Initially the peaks are somewhat broadened, with the outermost lines growing in amplitude relative to the innermost lines (the vertical scale is constant for each spectrum in figure 18). An alternate description of this effect is that the central two transitions tend to saturate before the outer two transitions; a feature also displayed by the first two experimental spectra in figure 19. As the rf power is increased still more, there appears at the midpoint of the unsaturated quartet the double quantum transition (cf. Table III), as shown in figures 18c to 18h and 19c. The intensity of the double quantum transition grows much faster than do the intensities of the single quantum transitions as H_1 increases, and its half-height line width is less than that of the unsaturated single quantum transitions (cf. Table II). Since the relaxation time of this transition is less than the relaxation time of a single quantum transition, one also expects the observed patterns of ringing and saturation (as compared to the

---

+note that the spectra are independent of the sign of J and of the sign of the frequency difference $(\omega_2-\omega_1)$, an expected result (cf. references (1,2) for example).

Figure 18.

AB spectra as a function of the rf amplitude H_1, using model A. The parameters are as for figure 17, but with the sweep rate fixed at 0.05 hertz/second, and with the rf amplitude H_1 equal to 0.010, 0.025, 0.0375, 0.050, 0.0625, 0.075, 0.100, and 0.500 milligauss, respectively, for spectra (a) to (h). Identical spectra have been obtained with $J/2\pi = -1.0$ hertz and/or $\omega_2/2\pi = \omega_1/2\pi - 2.0$ hertz (with an apparent shift in origin for the second case).

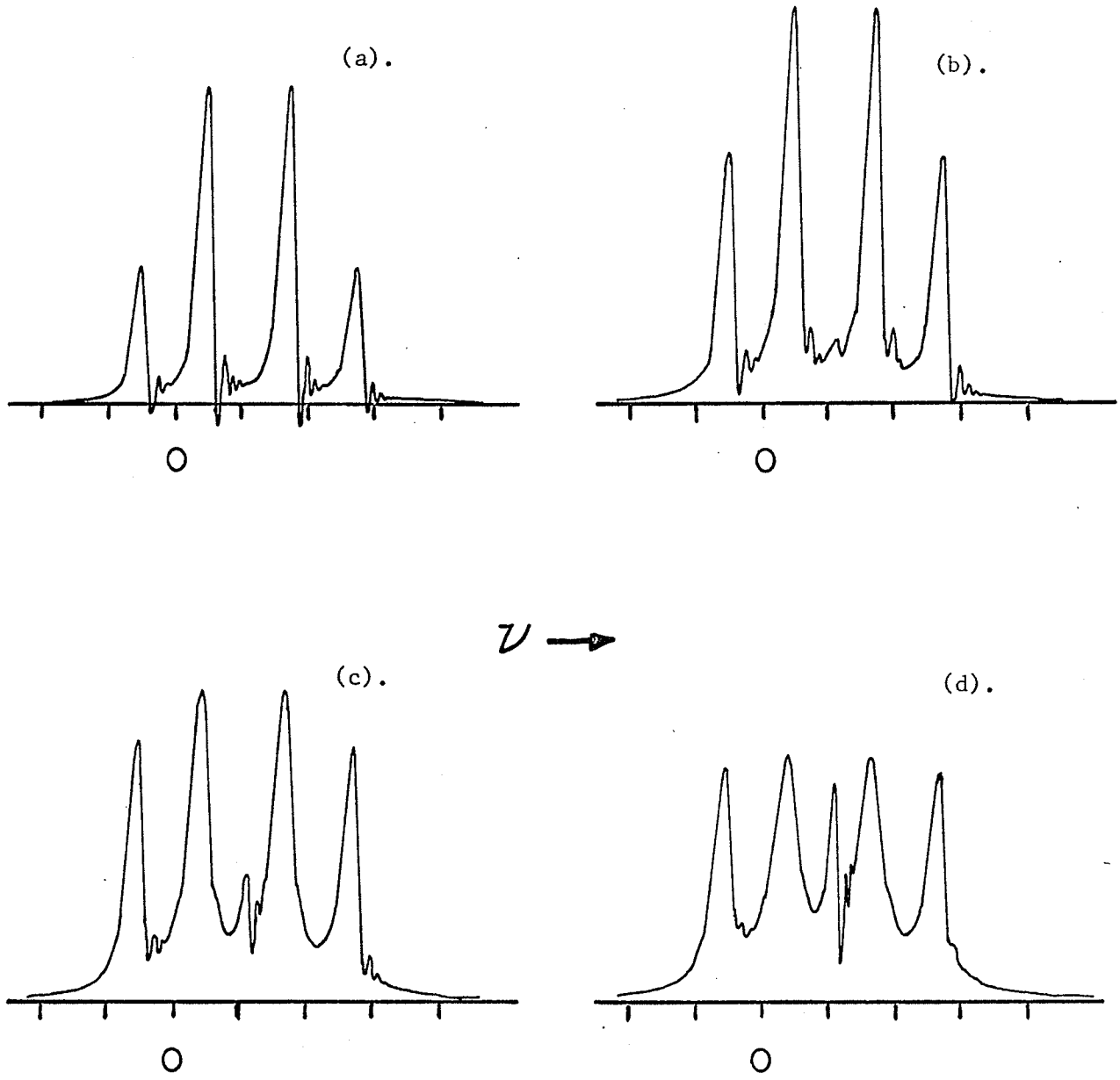
(a).
(b).
O
O
ν →
(c).
(d).
O
O

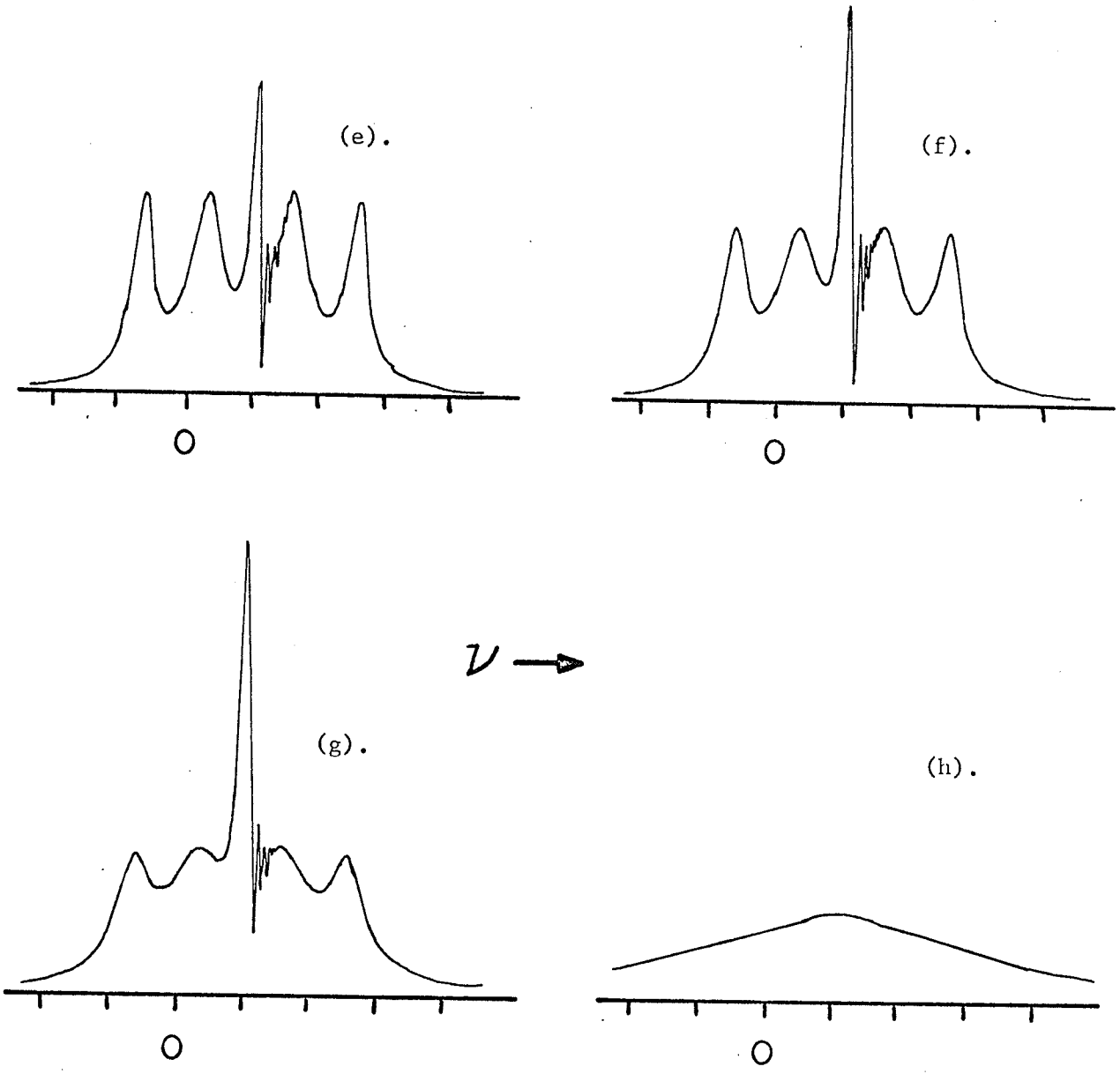
(e).
(f).
O
O
ν
(g).
(h).
O
O

Figure 19.

Experimental spectra of an AB system of spin-1/2 system of nuclei using a fixed sweep rate of 5 hertz/minute. The rf amplitude in (a) is weak enough to preclude the possibility of saturation effects, and in (b) and (c) the rf amplitude has been increased by factors of (approximately) 3.4 and 11.5 respectively (taken from Anderson (79)).

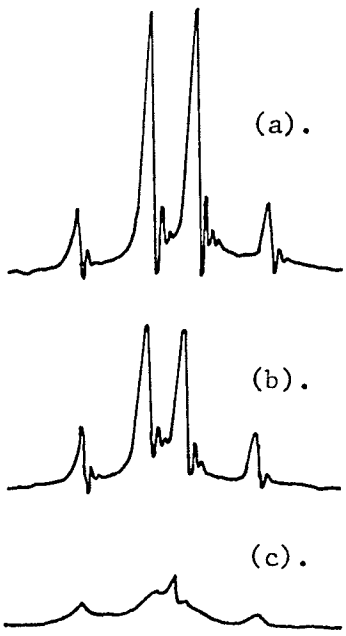
(a).
(b).
(c).

single quantum transitions). These features are experimentally well-known, and in excellent agreement with the predicted results of other theoretical calculations (see, for example, the discussions in references (2,4,17,96)).

The spectra presented in figure 20 display the effect of an intramolecular exchange process on the line shape of an AB system of nuclei. The model used here is actually similar to model A, but with the equation of motion [2.11] modified to the following form (14,16,97-99):

$$d\rho/dt = i[\rho, H_s] + (\partial\rho/\partial t)_{relax} + (\partial\rho/\partial t)_{exch}$$

and with

$$(\partial\rho/\partial t)_{exch} = k\,(P\rho P - \rho)$$

where the matrix P corresponds to the "exchange operator" and k to the rate of exchange (in radians/second). The spectra 20a to 20f have been calculated using various exchange rates, and the effects of increasing sweep rates are shown in the series (b,g,h) and (d,i,j). The spectra show the typical broadening effects as the chemical exchange rate increases; in particular there are two coalescence points near $k \simeq |J|$ and $k \simeq |\omega_1 - \omega_2|$.

It might be relevant at this point to consider the accuracy of the preceding spectra, calculated using model A, in a more quantitative sense. As mentioned previously, in-depth comparisons of the various models and experimental results are not attempted here; however it is worthwhile to pursue briefly the important question as

Figure 20.

AB spectra as a function of the intramolecular exchange rate parameter k and for some different sweep rates, using an extension of model A (see text). The parameters are as for figure 17 but with the rf amplitude fixed at 0.010 milli-gauss in each spectrum, and with the sweep rate equal to 0.050 hertz/second for (a) to (f), 0.200 hertz/second for (g) and (i), and 0.400 hertz/second for (h) and (j). The exchange rate k is equal to 0.10, 0.50, 1.00, 2.50, 5.00, and 10.00 radians/second for (a) to (f), respectively. The series (b,g,h) have the same exchange rate of 0.50 radians/second for different sweep rates, and the series (d,i,j) have the same exchange rate of 2.50 radians/second for different sweep rates. The vertical scaling is constant for each of the spectra in this figure.

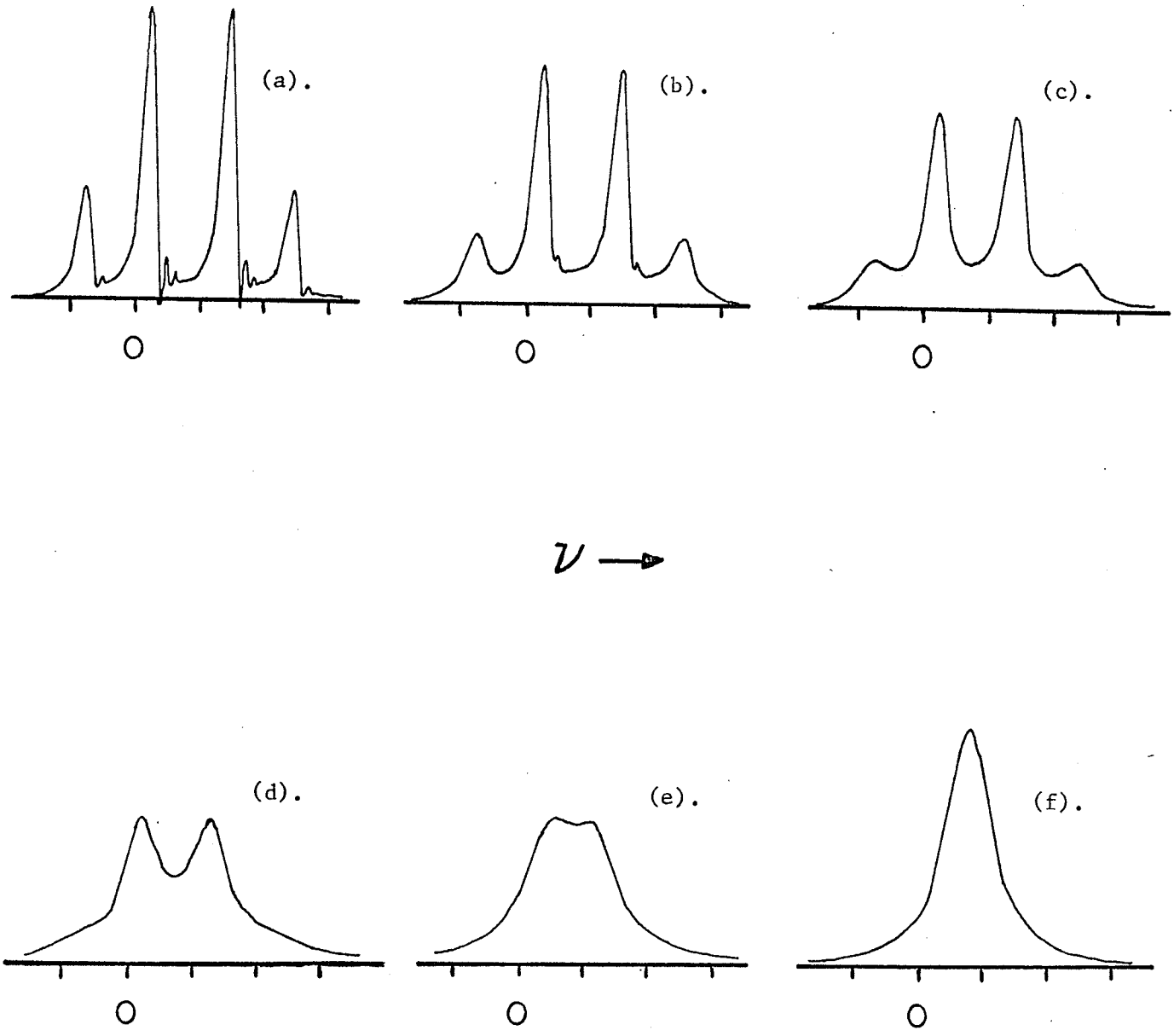
(a).
(b).
(c).
O
O
O
ν
(d).
(e).
(f).
O
O
O

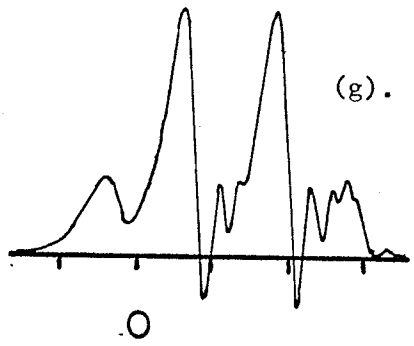

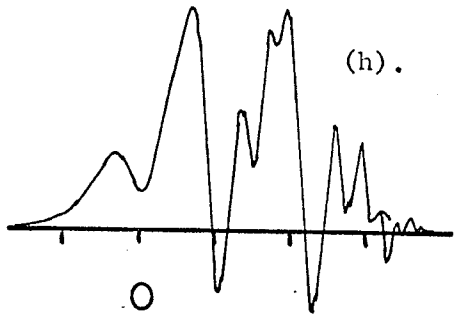

$\nu \longrightarrow$

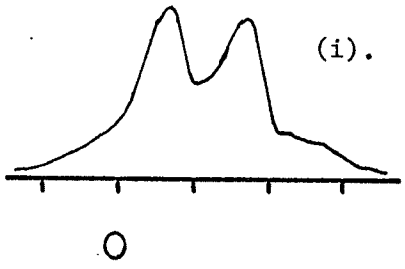

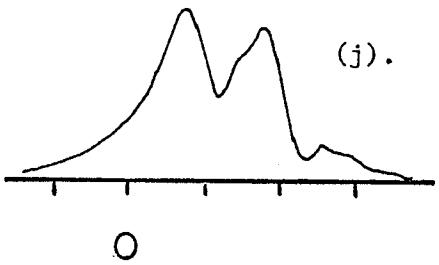

to the efficaciousness of model A in describing the effects of relaxation and inhomogeneity, especially in light of the discussion in the footnote on page 123. There it was stated that inhomogeneity and relaxation (specifically spin-spin relaxation) produce different effects but to different degrees, depending, for example, on the rf amplitude. The problem here, then, is to exhibit the limitations of model A insofar as the use of an effective spin-spin relaxation time is concerned. To this end, it will be assumed that a basis of comparison is given by model B which should describe the actual situation more closely. In figure 21, two spectra are shown which possess the same parameter list as in figures 12a and 12c, except that the effective spin-spin relaxation time T_2^* has been replaced by the natural spin-spin relaxation time T_2 and a Lorentzian inhomogeneity convolution integral with a full width at its half-height of 2w (ie. using model B, with the parameters T_2 and w adjusted so that $(T_2^*)^{-1} = (T_2)^{-1} + 2\pi w$ where w is in hertz; cf. equation [3.52]). The pair 12a and 21a are in close agreement (detailed comparison reveals the same effects as stated below for 12c and 21b, but to a lesser degree) as is to be expected, since the amplitude H_1 is well below the required value for saturation effects to become important. On the other hand, the pair 12c and 21b differ somewhat, especially with respect to their half-height line widths (about 0.38 hertz for 12a and 0.34 hertz for 21b) and with respect to the behaviour of the absorption line in the wings of the peak (with 21b being much narrower than 12c). The first result is consistent with the footnote on page 123, and the second

Figure 21.

A comparison of models A and B. The spectra reproduced in this figure have been calculated using model B and with the corresponding parameter list for the pairs (12a and 21a) and (12c and 21b), except that T_1=2.00 seconds and T_2=8.13 seconds for the simulations here. The inhomogeneity distribution was chosen to be Lorentzian with a full width at half-height of 2w = 0.12 hertz; note that the estimates for the width of the transitions, given by $(1/\pi T_2^*)$ hertz for model A and by $(1/\pi T_2 + 2w)$ hertz for model B is 0.16 hertz in both calculations using model A or model B. The pair (12a and 21a) are virtually identical, while the pair (12c and 21b) show considerable divergence, particularly in the behaviour of the peaks in their wings.

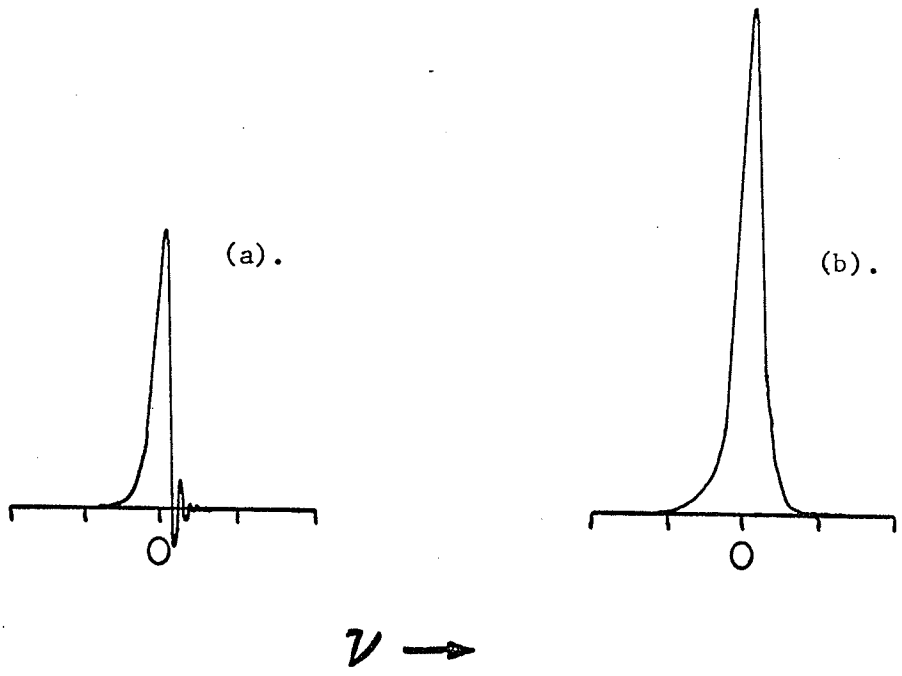
(a).
(b).
O
O
ν →

result would appear to be intuitively obvious; ie. the ringing patterns (or the distortions due to a finite sweep rate) are affected differentially by the relaxation processes and by the presence of inhomogeneity as a function of the amplitude of the observing rf field. Similar effects are predicted and have been observed for the spectra of an AB system; for example in the limit of unsaturated slow passage conditions, the spectra using either model A or model B are essentially identical, whereas for fast passage and/or strong rf fields the two models differ as for the case of A_2 spectra.

One therefore concludes that model A must necessarily fail whenever saturation effects or sweep rate effects are observable. Nevertheless, the preceding plots using model A can be salvaged as a result of the following considerations:

(a) the above spectra are at least qualitatively successful in the reproduction of many of the features of cw spectra, and they appear to be quantitatively exact in the unsaturated slow passage limit; and/or

(b) if the effective spin-spin relaxation time is reinterpreted as the natural spin-spin relaxation time, then all of the above spectra are accurate (or more exactly, as accurate as model B) for systems with that relaxation time and in a perfectly homogeneous static magnetic field or for systems in which inhomogeneity effects are negligible compared with the effects due to spin-spin relaxation.

With this last point in mind, the previous calculated spectra may be adjusted to compensate for the alternate scheme whereby the

effects of inhomogeneity are included into the calculations. In figures 22 and 23, inhomogeneity has been accounted for by employing equation [3.63b], assuming a Gaussian distribution with different half-height line widths (the results for rectangular[+] and Lorentzian distributions, not shown here, differ mostly in the behaviour of a transition at its wings; it has been found that the wings fall off more quickly in the order of distributions Lorentzian, Gaussian, rectangular). These simulations show similar effects to the results obtained using model A; for example as the extent of inhomogeneity increases (compare with the results of decreasing the parameter T_2^*), the transitions tend to broaden and the degree of ringing is reduced[++]. The spectra in figures 22 and 23 do not possess a constant vertical scale; however the normalization condition [4.19] is reflected in the original plots by a decrease in the absorption signal intensities as the parameter 2w increases, so that the area under the curves remains (approximately) constant. Note also that the measured half-height line widths behave as expected; for example in the series 22a to 22f the observed and calculated full line widths at half height (the calculated widths, equal to $(1/\pi T_2 + \gamma w/2\pi)$ hertz with w expressed in units of gauss, are given in brackets) are 0.08 (0.03), 0.11 (0.10), 0.21 (0.21), 0.39 (0.39), 0.56 (0.56) and

[+] a rectangular distribution is defined such that $G(\beta) = 0$ for $|\beta| > w$, and $G(\beta) =$ constant for $|\beta| \leq w$.

[++] the initial Torrey-like transients are also attenuated to a greater degree in equivalent calculations using model B instead of model A.

Figure 22.

A_2 spectra as a function of the inhomogeneity parameter 2w, using model B and equation [3.63b] with a Gaussian distribution of inhomogeneity. The parameters are $H_o=10^4$ gauss, $\omega_1/2\pi = \omega_2/2\pi =$ 42.577 megahertz, $J/2\pi = 0.0$, $T_1=T_2=10.0$ seconds, and the rf amplitude and frequency sweep rate are fixed at 0.001 milligauss and 0.025 hertz/second respectively. The zero of the frequency axis is at $\omega_1'=\omega_1$, the horizontal scale is 1.0 hertz/division, the direction of the frequency scan is as indicated by the arrow, and the vertical scaling is not constant, with the spectra being amplified in the order (a) to (f). The full half-height line width 2w of the inhomogeneity distribution is equal to 0.0 (ie. the signal from the "central" ensemble), 1.67×10^{-5}, 4.16×10^{-5}, 8.32×10^{-5}, 12.48×10^{-5} and 16.67×10^{-5} gauss, respectively, in the spectra (a) to (f). The width of the distributions in units of hertz range from 0.07 hertz in (b) to 0.71 hertz in (f).

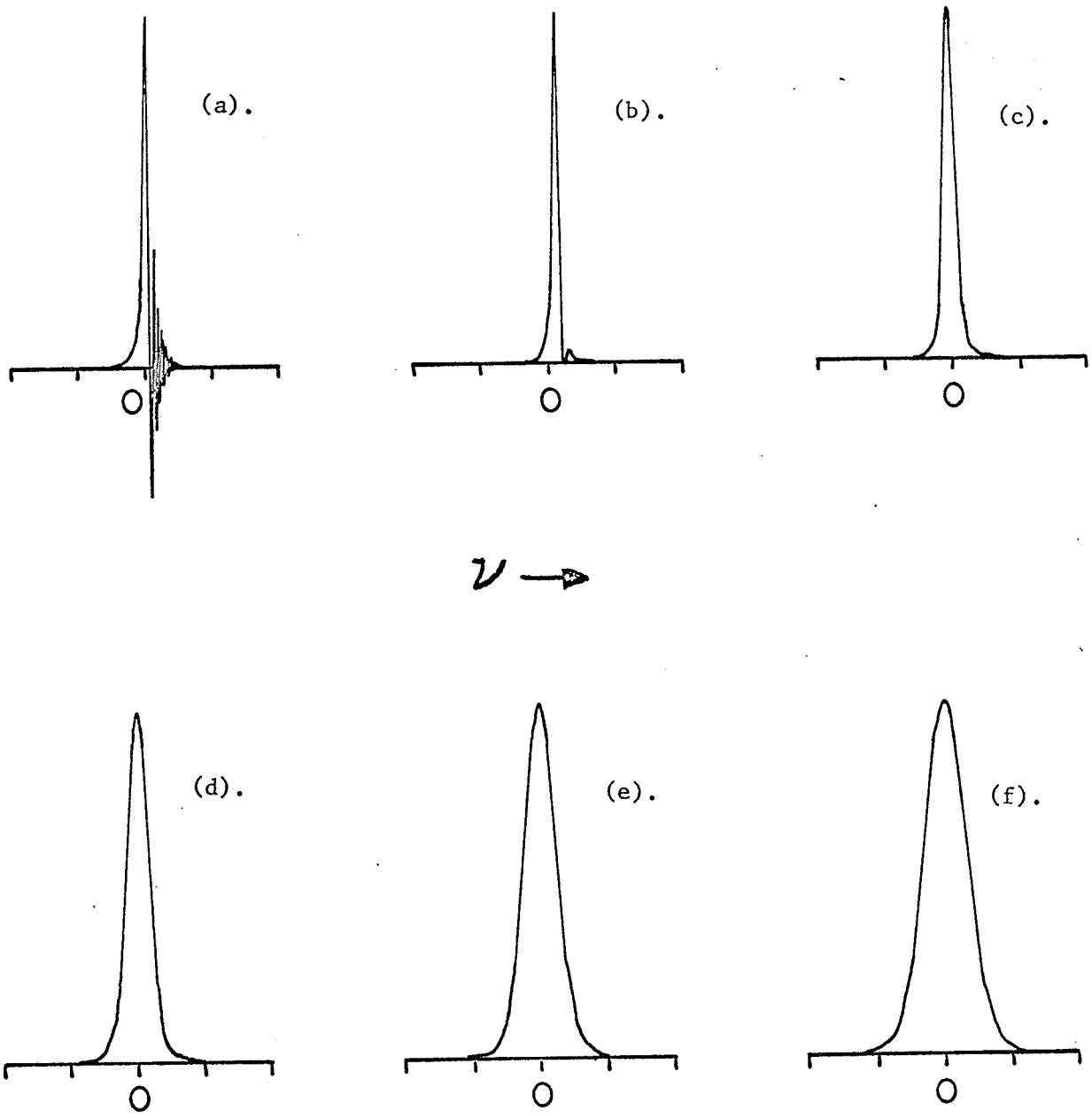
(a).
(b).
(c).
O
O
O
ν →
(d).
(e).
(f).
O
O
O

Figure 23.

AB spectra as a function of the inhomogeneity parameter 2w, using model B and equation [3.63b] with a Gaussian distribution of inhomogeneity. The parameters are $H_o=10^4$ gauss, $\omega_1/2\pi$ = 42.577 megahertz, $\omega_2/2\pi = \omega_1/2\pi + 2.0$ hertz, $J/2\pi$ = 1.0 hertz, $T_1=T_2=$ 10.0 seconds, and the rf amplitude and frequency sweep rate are fixed at 0.001 milligauss and 0.025 hertz/second, respectively. The zero of the frequency axis is defined to be at $\omega_1'=\omega_1$, the horizontal scale is 1.0 hertz/division, the direction of the frequency scan is in the direction indicated by the arrow, and the vertical scaling is not constant. The full half-height line width 2w of the inhomogeneity distribution is equal to 0.0, 1.67×10^{-5}, 4.16×10^{-5}, 8.32×10^{-5}, 12.48×10^{-5} and 16.67×10^{-5} gauss, respectively, for the spectra (a) to (f) (the width in hertz ranges from 0.07 hertz in (b) to 0.71 hertz in (f)).

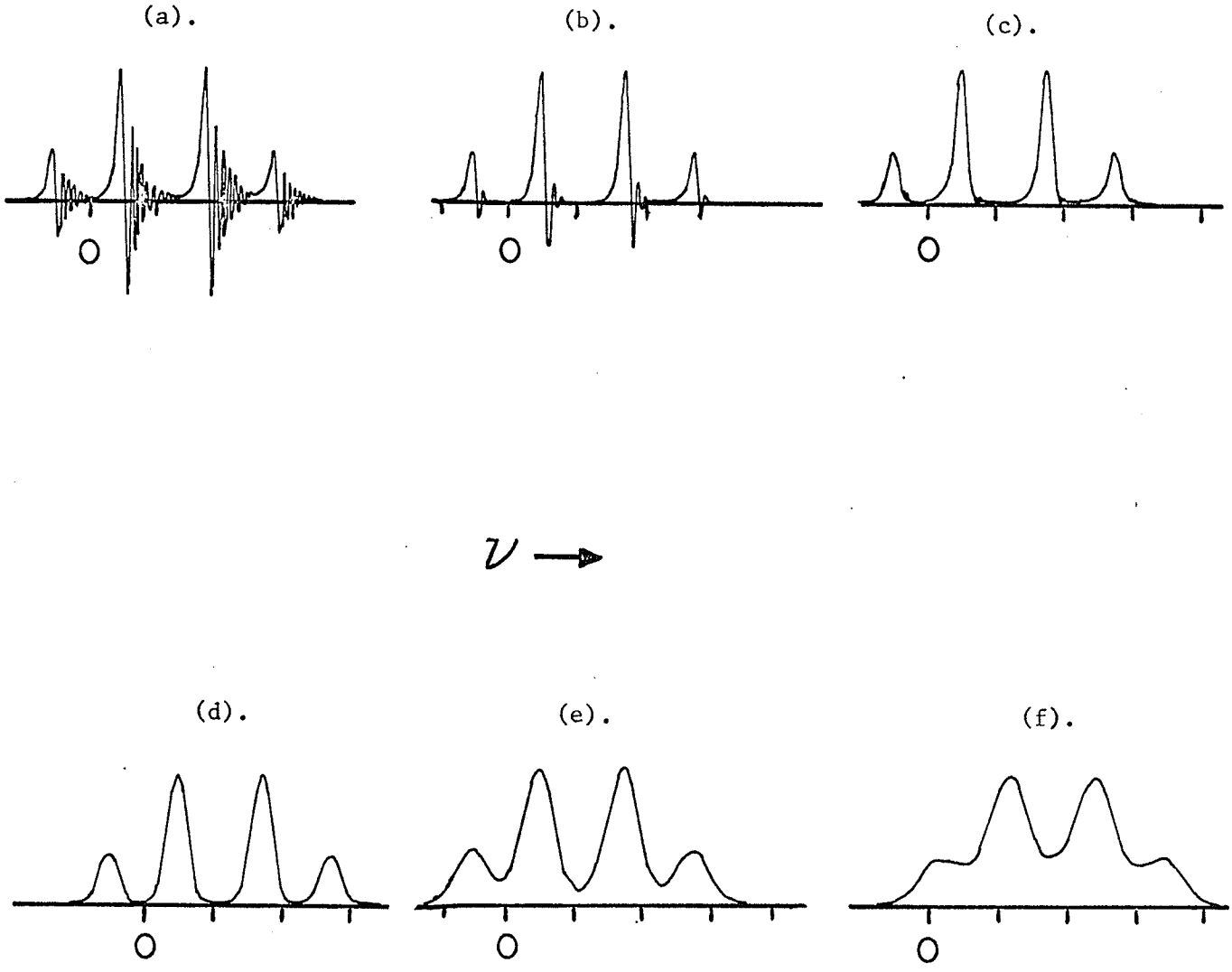
(a).
(b).
(c).
O
O
O
ν →
(d).
(e).
(f).
O
O
O

0.74 (0.74) hertz, respectively, for the spectra 22a to 22f. These comparisons reveal that there is appreciable disagreement only for those cases where ringing might be expected to produce observable distortions in the line shape. Finally, it may be seen from the spectra in figure 23 that each of the transitions in an AB system of nuclei is broadened identically (except for those effects due to a finite sweep rate) by the inhomogeneity. This is an expected result, however, because of the manner in which inhomogeneity is introduced into the formalism.

In figure 24, there are presented the absorption mode signals of an AB system of nuclei as a function of the amplitude of the observing rf field, calculated using model B (and equation [3.63b]) and with a Lorentzian distribution of inhomogeneity. These spectra are qualitatively similar to the spectra in figure 18; note however that the parameter lists do not correspond exactly (in particular the parameters T_2^*, T_2 and w are not adjusted). The principal divergence between the spectra in figure 18 and in figure 24 occurs when the amplitude of the rf field becomes large enough to cause saturation.

Similar spectra, shown in figures 25 to 27, have been evaluated using model C with the mechanisms discussed previously, namely the RFUC, RFC and DD relaxation mechanisms. The relaxation parameters were chosen so that, in the limit of weak rf fields, the half-height line widths of the transitions are identical (cf. Table II; the calculated spectra, not shown here, with H_1=0.003 milligauss are essentially indistinguishable). From a detailed comparison of these spectra, the following conclusions may be drawn (cf. Harris and Worvill (102)

Figure 24.

AB spectra obtained using the phenomenological description for relaxation (equation [2.12]) and with inhomogeneity described by equation [3.63b]; ie. using model B. The parameters are $H_o \simeq 1.32 \times 10^4$ gauss, $\omega_1/2\pi$ = 56.4 megahertz, $\omega_2/2\pi = \omega_1/2\pi + 2.0$ hertz, $J/2\pi$ = 1.0 hertz, $T_1 = T_2 = 1.667$ seconds, a Lorentzian distribution of inhomogeneity with the width parameter 2w = 0.12 hertz, and the rf frequency sweep rate $a/2\pi$ is fixed at 0.05 hertz/second for (a) to (e) and (g), and at 0.20 hertz/second for (f). The amplitude of the observing rf field is 0.0132, 0.026, 0.053, 0.078, 0.106, 0.106 and 0.212 milligauss for spectra (a) to (g), respectively. The zero of the frequency axis is at $\omega_1' = \omega_1$, the horizontal scale is 1.0 hertz/division and the direction of the frequency scan is as indicated by the arrow.

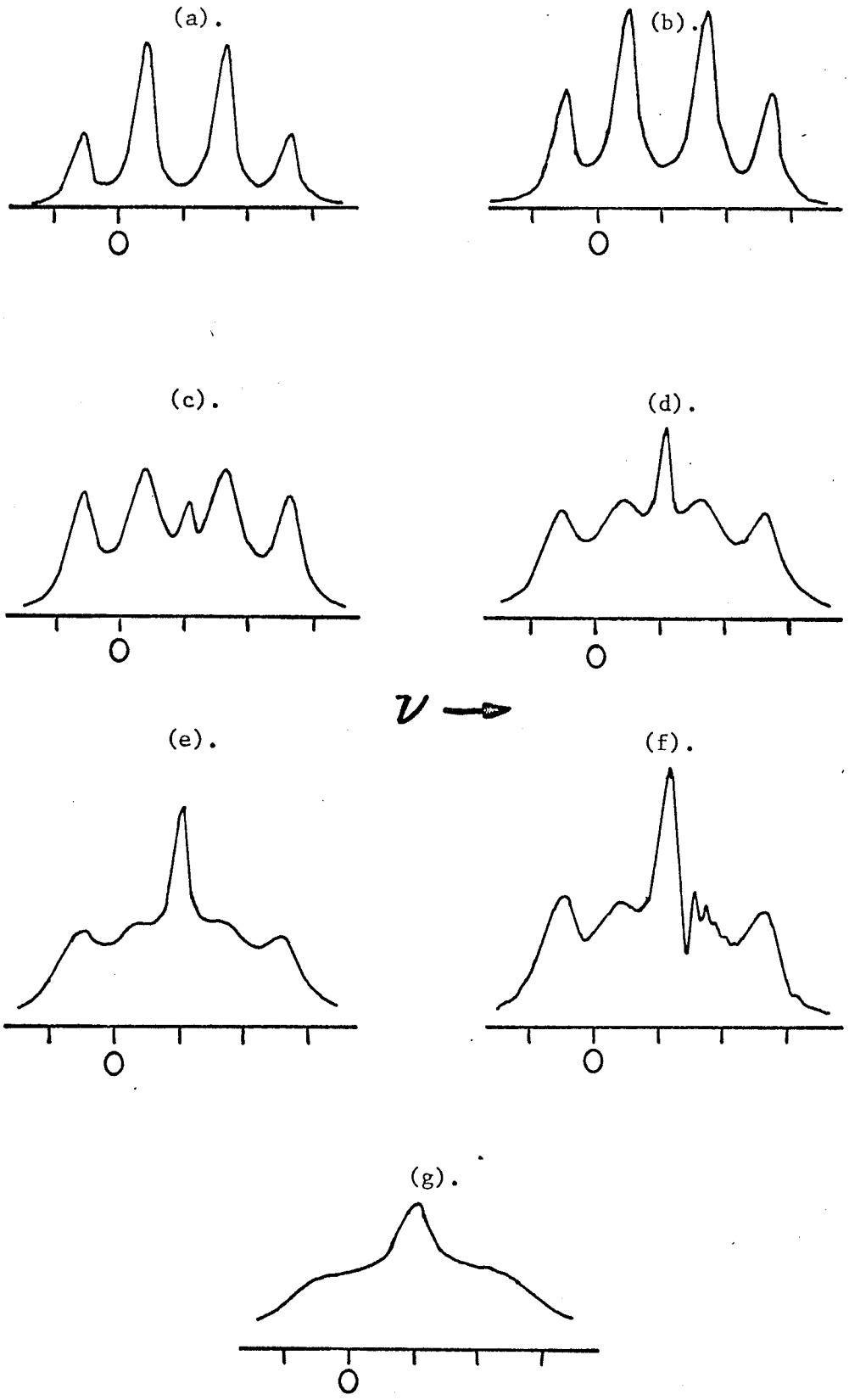
(a).
(b).
(c).
(d).
ν
(e).
(f).
(g).
O

Figure 25.

AB spectra obtained using the RFUC relaxation mechanism (see text), ie. using model C. The parameters are as for figure 24 but with $\omega_s/2\pi$ = 0.096 hertz, η = 0.0 and r = 0.0. The sweep rate is (as for figure 24) 0.05 hertz/second for (a) to (e) and for (g), and 0.20 hertz/second for (f). The amplitude of the observing field is as for figure 24, with H_1 = 0.0132, 0.026, 0.053, 0.078, 0.106, 0.106 and 0.212 milligauss for plots (a) to (g), respectively.

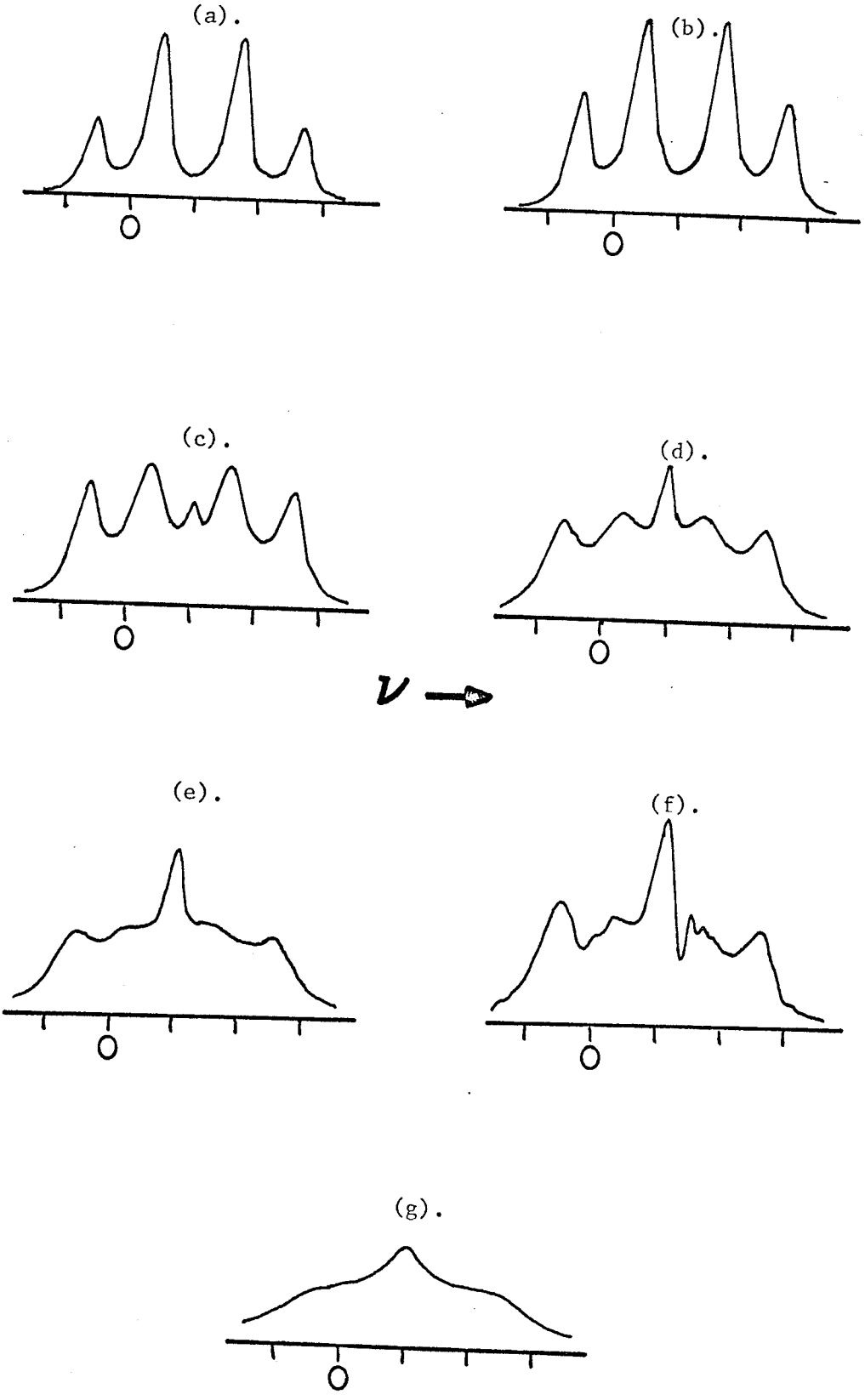
(a).
(b).
(c).
(d).
ν
(e).
(f).
(g).

Figure 26.

AB spectra obtained using the RFC relaxation mechanism (see text), ie. using model C. The parameters are as for figure 24 but with $\omega_s/2\pi$ = 0.096 hertz, η = 0.0 and r = 1.0 . The sweep rate and the amplitude of the observing rf field are as for the corresponding spectra in figure 24 (and figure 25).

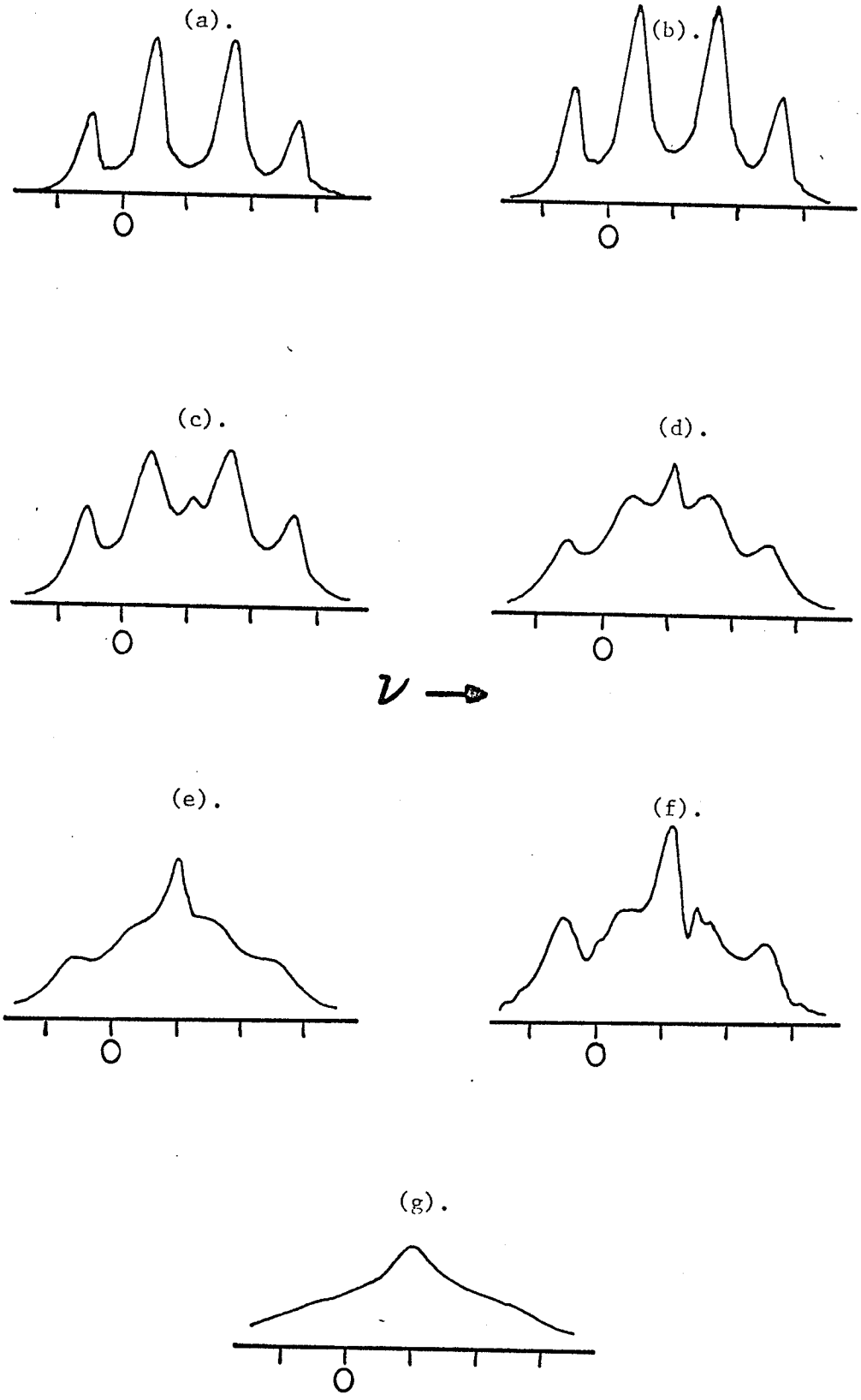
(a).
(b).
(c).
(d).
ν
(e).
(f).
(g).

Figure 27.

AB spectra obtained using the DD relaxation mechanism (see text), ie. using model C. The parameters are as for figure 25 but with T_D = 0.940 seconds. The sweep rate and the amplitude of the observing rf field are as for the corresponding spectra in figure 24 (and figures 25 and 26).

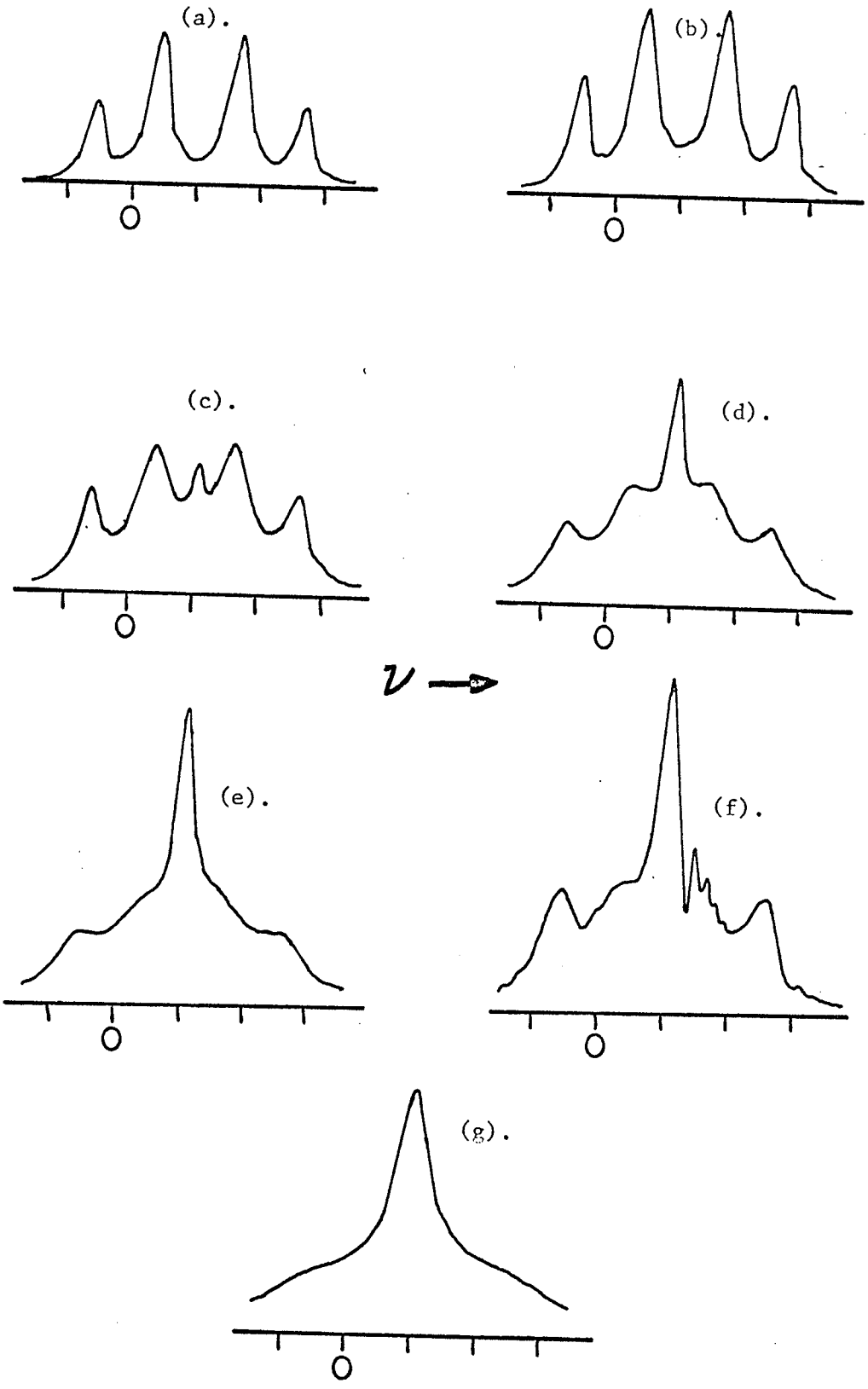
(a).
(b).
(c).
(d).
ν
(e).
(f).
(g).
O
O
O
O
O
O
O

and the discussion in section II.4).

(a) In the unsaturated slow passage limit, the calculated line shape is independent of the mechanism responsible for the relaxation, and in fact model B (or, it is expected, model A) yields identical results. This limit is approached by the first spectrum in each of the figures 24 to 27.

(b) As a function of the rf amplitude, model B has some of the characteristics of model C for the RFUC and DD mechanisms.

(c) The distinctive difference between the DD mechanism and the RFC or RFUC mechanisms is shown in the behaviour of the double quantum transition (4,17,102). As predicted in Chapter II, the double quantum transition is less saturated and sharper (relative to the single quantum transitions) for the system which is relaxed by means of the dipole-dipole interactions.

(d) The RFUC and RFC mechanisms show differential effects with respect to the relative rates of saturation of the inner and outer transitions, with the RFUC mechanism resembling the DD mechanism and model B.

(e) It appears that effects attributable to the finite sweep rate depend on the relaxation mechanism employed, although the patterns are very complex and not readily correlated.

It is also possible to calculate spectra which fall "between" the limiting cases of the RFC and RFUC mechanisms (in principle, the RFUC mechanism with $r = 0$ is not the lower limit of r, since the definition [2.27c] allows that $-1 \leq r \leq 1$), or which derive from an independent combination of dipolar and isotropic random field interactions. Some examples of these calculations are shown in figure 28, with the

Figure 28.

AB spectra obtained using "intermediate" relaxation mechanisms (see text). The parameters are as for figure 24 but with $\omega_s/2\pi$ = 0.096 hertz, η = 0.0 and r = 1/3 for spectra (a) and (b); $\omega_s/2\pi$ = 0.096 hertz, η = 0.0 and r = 2/3 for spectra (c) and (d); and an independent mixture of the RFC and DD mechanisms for (e) and (f) with $\omega_s/2\pi$ = 0.048 hertz, η = 0.0, r = 1.0, and T_D = 1.88 seconds. The sweep rate is fixed at 0.05 hertz/second in each case, and the amplitude of the observing rf field is 0.053 milligauss for (a), (c) and (e) (cf. spectrum (c) of figures 24 to 27) and 0.106 milligauss for (b), (d) and (f) (cf. spectrum (e) of figures 24 to 27). In the limit of a weak observing field, these spectra (and the spectra using the parameters in figures 24 to 27) are independent of the relaxation mechanism.

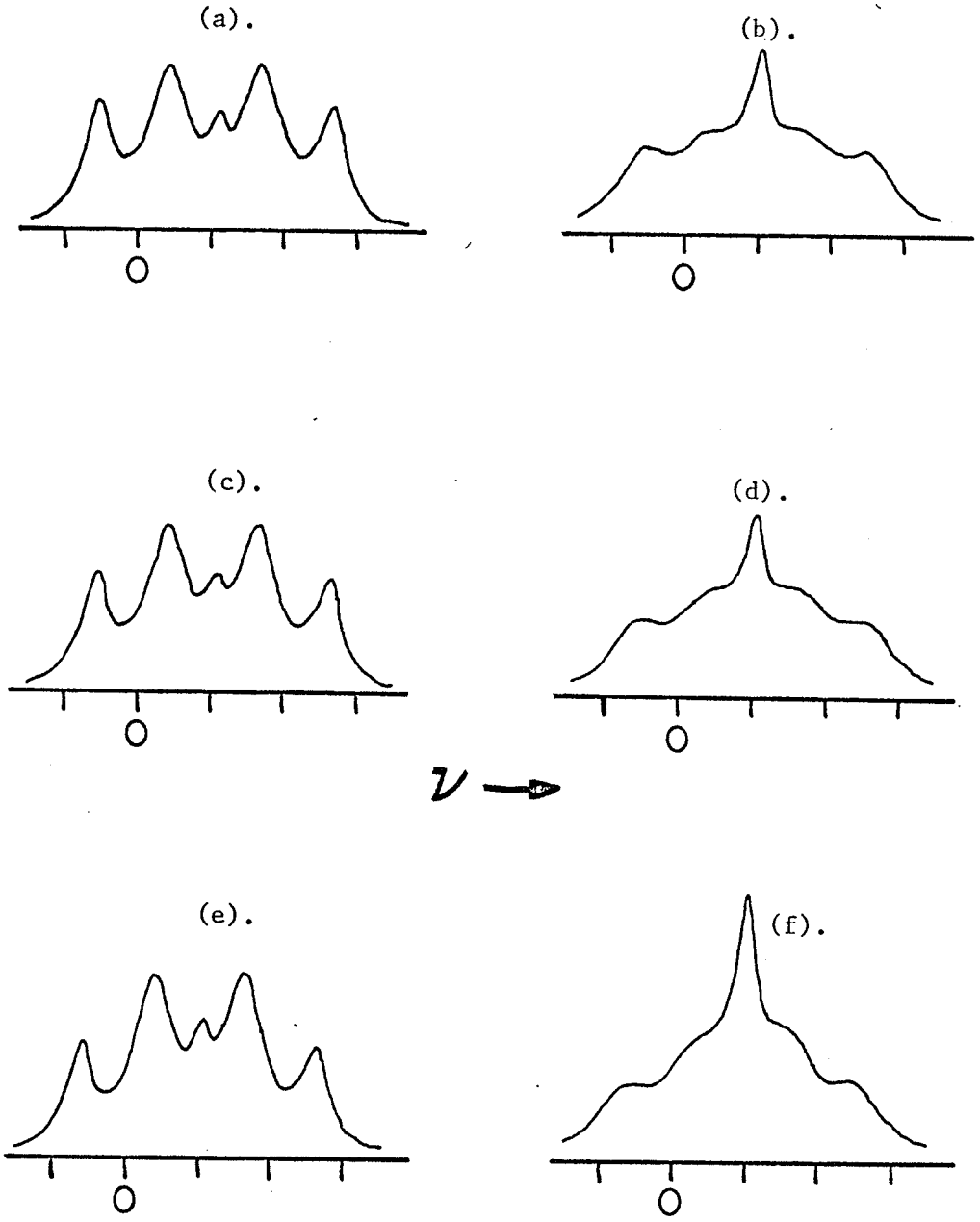
(a).
(b).
(c).
(d).
ν
(e).
(f).
O
O
O
O
O
O

parameters of (a), (c) and (e) corresponding to the parameters of spectrum (c) of figures 24 to 27 (except for the relaxation parameters), and with the parameters of (b), (d) and (f) corresponding to the parameters of spectrum (e) of figures 24 to 27.

The above conclusions tend to support recent studies on the feasibility of distinguishing between the different relaxation mechanisms, by means of a careful and detailed analysis of the single resonance spectra as a function of the rf power (see, for example, reference (102)). The calculated spectra also indicate that, in principle, relaxation might be studied through an analysis of the ringing patterns obtaining with relatively fast sweep rates.

The last series of spectra in this section is concerned with related studies carried out by the late R.A.Hoffman for the extraction of the relaxation parameters of an AB system of protons, where it is assumed that the only interaction of significance is that due to isotropic random fields[+]. Before proceeding to these spectra[++], however, it is necessary to resolve a preliminary problem,

---

[+] the sample was doped with a paramagnetic impurity so that any intramolecular dipolar interactions were effectively "swamped" out (17).

[++] note that the experimental spectra were obtained with a sweep rate of 0.01 hertz/second (17), whereas the calculated spectra were evaluated using a sweep rate of 0.05 and 0.20 hertz/second in order to reduce the required computational time; however reasonable "extrapolations" to a slower sweep rate are possible, so that some direct comparisons may be attempted.

namely that of the type of inhomogeneity distribution describing the experimental conditions. Hoffman (17) assumed that a Lorentzian distribution with a half-height width of 0.12 hertz is adequate, and this assumption is sustained by a comparison of the calculated spectra in figure 29 with the corresponding experimental spectrum in figure 30c[+] (the centermost plot in 30c is the experimental spectrum, while the rightmost and leftmost plots are the calculated spectra due to Hoffman (17) with and without a Lorentzian distribution of inhomogeneity, respectively). Given that the width is 0.12 hertz, the Lorentzian distribution is clearly in closer agreement with the experimental spectrum than are the Gaussian distribution or the rectangular distribution (not shown here), and it is also clear that the inclusion of inhomogeneity results in line shapes which are more consistent with experiment.

The simulations reproduced in figure 31 have been calculated using a Lorentzian distribution (with $2w = 0.12$ hertz), and the results are in good agreement with the corresponding experimental spectra shown in figure 30. These calculations are very similar to the calculations performed by Hoffman (17), with the principal difference deriving from the manner in which the equation of motion of the (identical) spin density matrix model is solved. Hoffman's assumption of the steady-state approximation limits the validity of his calculations to the slow passage limit, and therefore any effects

[+]the majority of the calculated spectra in figure 31 are not very sensitive to the type of distribution used, largely because the broadening of the transitions is dominated by relaxation effects.

Figure 29.

AB spectra obtained using model C as a function of the type of inhomogeneity distribution. The parameters are $H_o \simeq 1.32 \times 10^4$ gauss, $\omega_1/2\pi = 56.4$ megahertz, $\omega_2/2\pi = \omega_1/2\pi + 4.90$ hertz, $J/2\pi = 12.45$ hertz, and an isotropic random field relaxation mechanism with $\omega_s/2\pi = 0.204$ hertz, $\eta = 0.0$ and $r = 0.66$. The amplitude of the observing rf field is fixed at 0.0411 milligauss for each spectrum, and the frequency sweep rate $a/2\pi$ is 0.05 hertz/second for (a), (c) and (e), and 0.20 hertz/second for (b), (d) and (f). The spectra (a) and (b) represent simulations in a perfectly homogeneous static magnetic field, while the pair (c) and (d) and the pair (e) and (f) have been calculated using [3.63b] for a Lorentzian and a Gaussian distribution respectively; in both cases the distributions possess a full width at their half-height of 0.12 hertz. The zero of the frequency scale is at $\omega_1' = \omega_1$, the horizontal axis is scaled in units of 1.0 hertz/division and the direction of the frequency scan is as indicated by the arrow. Only parts of the spectra, those containing the two centermost transitions, have been reproduced here.

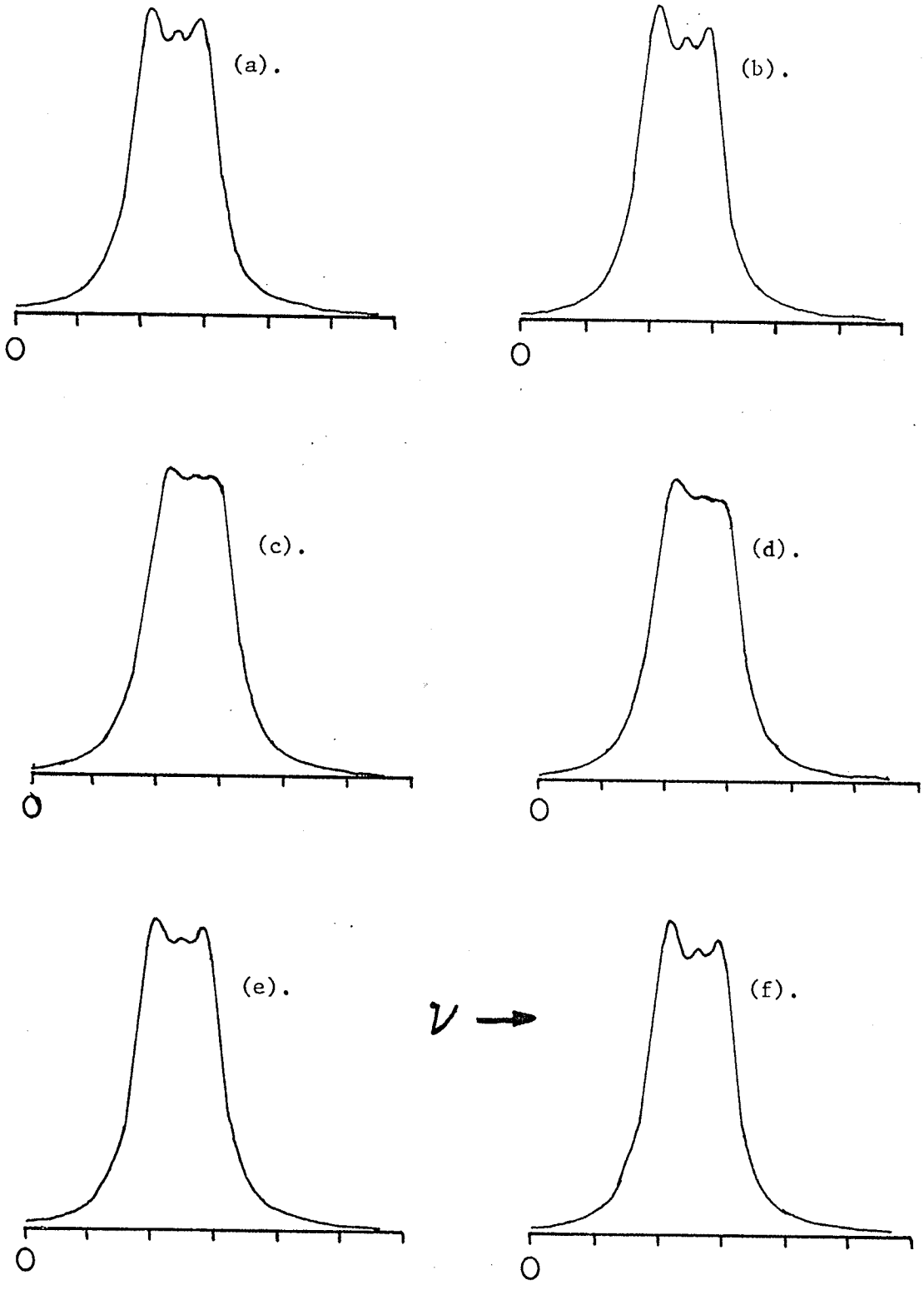
(a).
(b).
(c).
(d).
(e).
(f).
O
O
O
O
O
O
ν

Figure 30.

Experimental spectra for various strengths of the observing rf field, used for the study of an isotropic relaxation mechanism (taken from Hoffman (17), figures 17, 18, 19, 21, 22 and 23). The parameters describing the spin system have been determined by Hoffman (17), and are as in figure 29. The sweep rate is 0.01 hertz/second and the amplitude of the rf field, expressed in hertz as $\gamma H_1/2\pi$ is 0.056, 0.156, 0.175, 0.220, 0.311 and 0.622 hertz, respectively, in spectra (a) to (f). The centermost plot in 30c is the experimental spectrum, while the rightmost and leftmost plots are theoretical spectra calculated with and without a Lorentzian distribution of inhomogeneity with a width of 0.12 hertz respectively (17). Only the two central transitions of the AB system have been reproduced here.

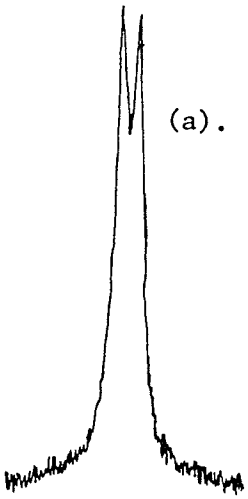

(a).

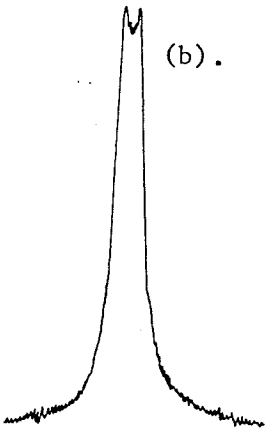

(b).

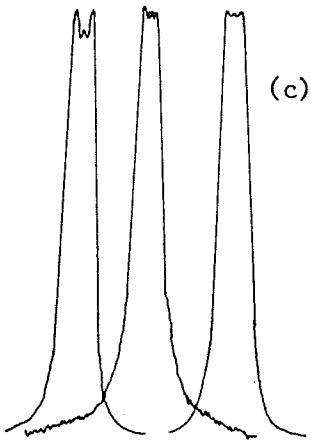

(c).

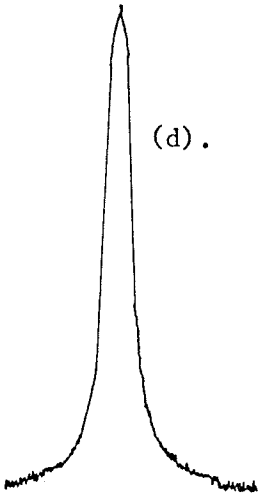

(d).

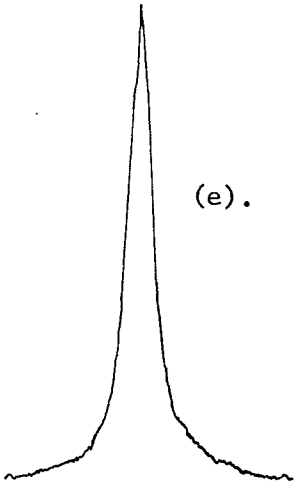

(e).

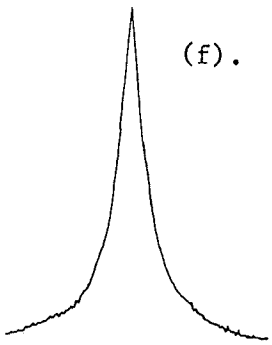

(f).

Figure 31.

Simulations of the single resonance experiments used for the study of relaxation (cf. figure 30). The parameters are as in figure 29, except that a Lorentzian distribution of width 0.12 hertz has been assumed for each spectrum. The first column of spectra (a,c,e,g,i,k) have a sweep rate of 0.05 hertz/second, and the second column (b,d,f,h,j,l) have a sweep rate of 0.20 hertz/second. The rf amplitude, expressed as $\gamma H_1/2\pi$ is equal to 0.056 hertz for (a) and (b); 0.156 hertz for (c) and (d); 0.175 hertz for (e) and (f); 0.220 hertz for (g) and (h); 0.311 hertz for (i) and (j); and 0.622 hertz for (k) and (l). Only the central portion of the spectrum has been reproduced here.

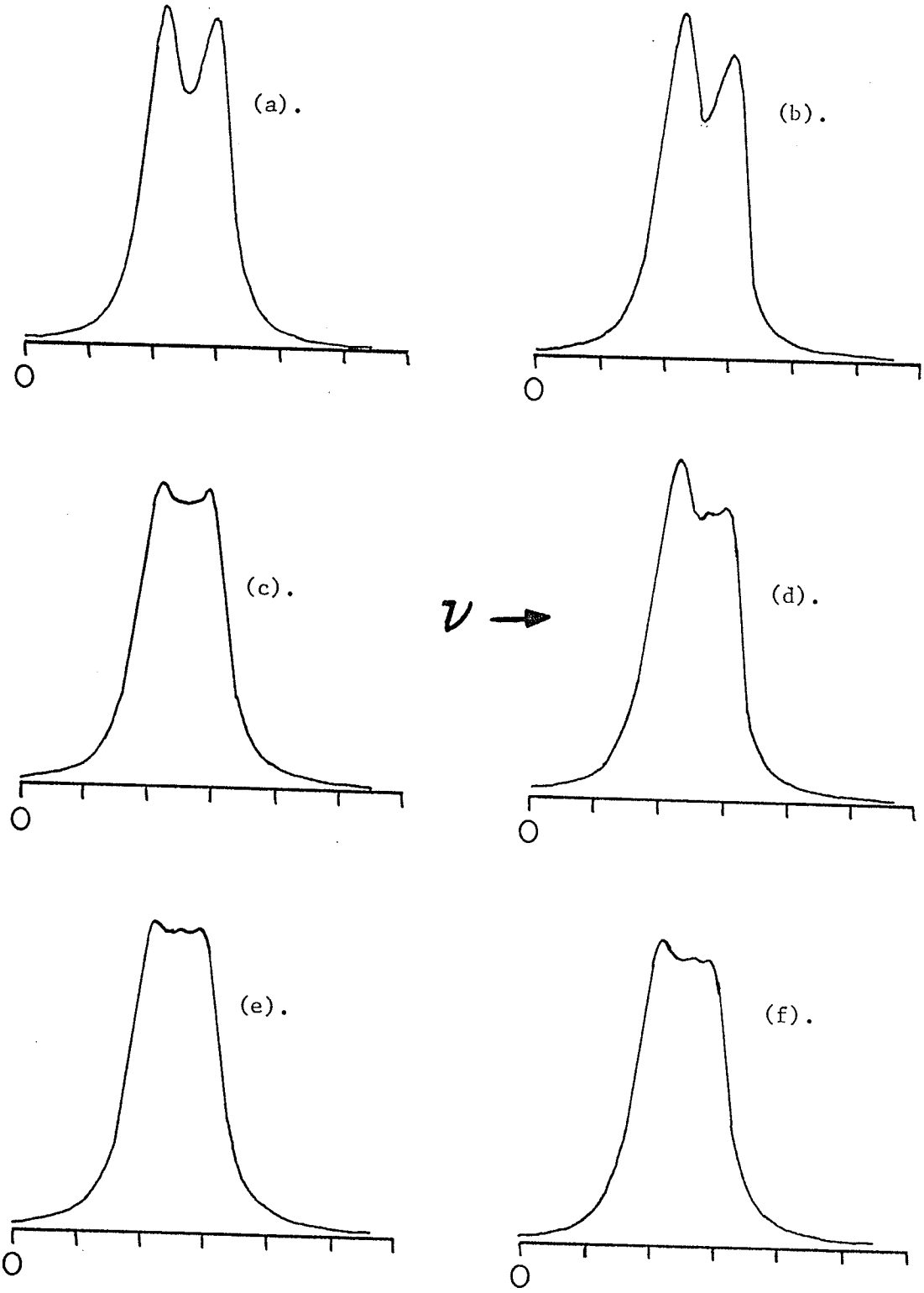
(a).
(b).
(c).
(d).
(e).
(f).
O
O
O
O
O
O
ν

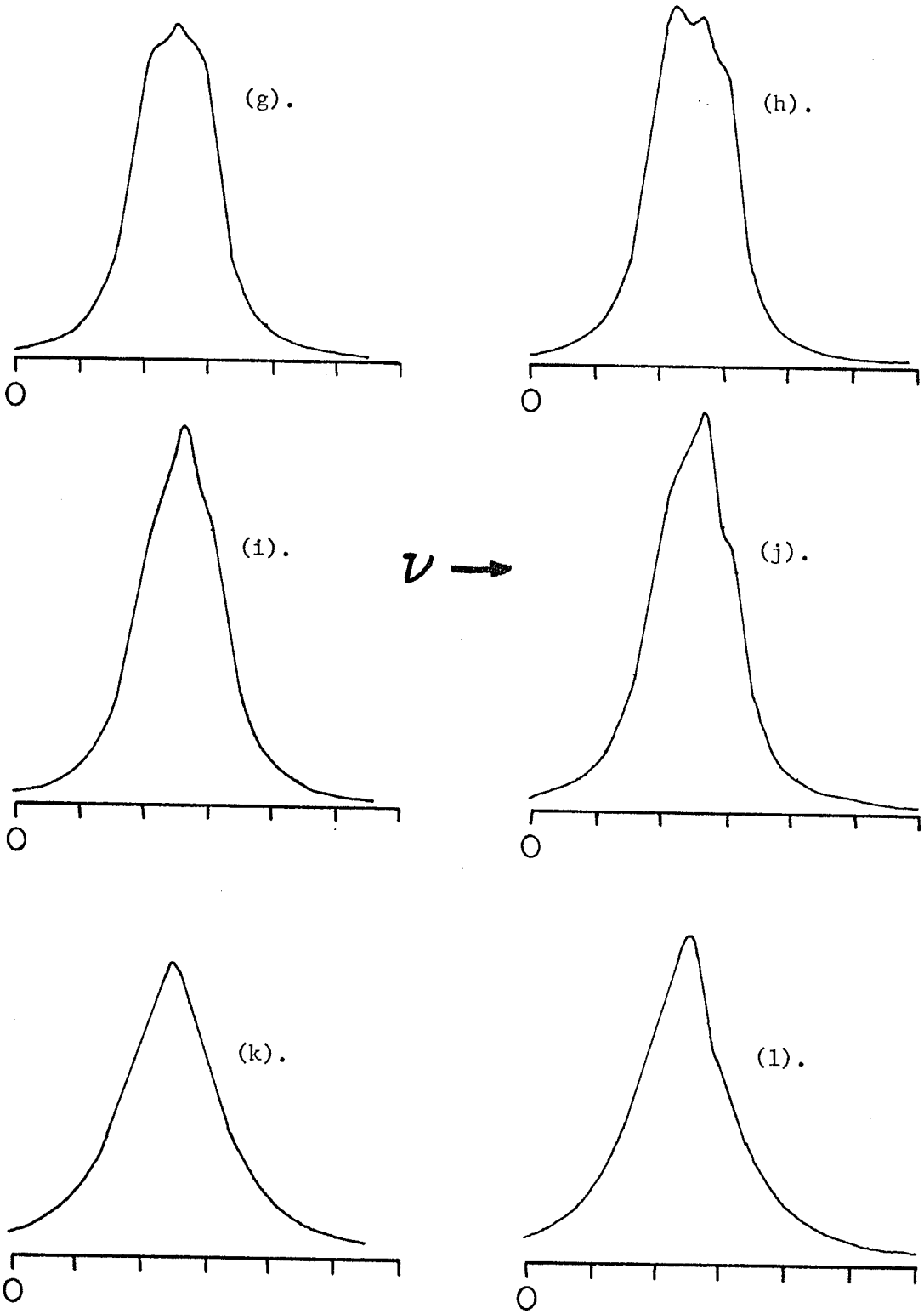
(g).
(h).
(i).
(j).
(k).
(1).
O
O
O
O
O
O
ν

of a finite sweep rate cannot be reproduced. The present simulations allow for a finite (linear) sweep rate, and in fact some effects are observable in the experimental spectra in figures 30a and 30c, where there is present a degree of asymmetry in the spectra. Note, for example, that Hoffman's calculated spectra in 30c are symmetric, while the simulated spectra in 31e and 31f possess the same type of asymmetry as the center experimental spectrum reproduced in figure 30c. Hoffman points out that, although the agreement between his calculated and observed spectra may seem impressive, the slow passage (steady-state) assumption is inadequate since "spectra recorded at the sweep rate of 0.02 Hz/sec. ... differ observably from those recorded with the slowest sweep speed available" (0.01 hertz/second). The technique presented in this dissertation is unique in its ability to lift the steady-state approximation for the calculation of cw spectra.

C. Simulations of the Double Resonance Experiment.

Most of the calculated spectra presented in this section have been obtained using model A, and the discussions in the previous section concerning its accuracy are again demonstrated here. As before, the initial Torrey-like transients are not reproduced, although it should be noted that the presence of two rf fields (both switched on at time t=0) yields a more complicated pattern than was observed for the single resonance spectra, and that the "filter" may attenuate these oscillations, depending on their frequency. Finally it is assumed that the perturbing rf field is coherent as opposed to incoherent (cf. Ernst (144)).

1. Simulation of an A_2 system.

The first case of interest here is the effect of the perturbing field on an A_2 system of spin-1/2 nuclei, which can be regarded as a single spin-1/2 system (the results are independent of the sign or magnitude of the coupling constant). The results, shown in figure 32, display that there appear two transitions, one on each side of the perturbing rf frequency and with opposite intensities (the central portions of the spectra have not been calculated due to the limitation of the filtering routine mentioned previously; the plots are in fact composites of two separate calculations). The splitting between the peaks varies directly with the power of the perturbing rf field and with the magnitude of the frequency offset $|\omega_2'-\omega_1|$ where ω_2' is the perturbing rf frequency and ω_1 $(=\omega_2)$ is the Larmor frequency of the nuclei. These conclusions also follow from experimental spectra,

Figure 32.

Double resonance simulations of an A_2 system, using model A. The parameters are $H_o \simeq 1.41 \times 10^4$ gauss, $\omega_1/2\pi = \omega_2/2\pi = 60.0$ megahertz, $J/2\pi = 0.0$ hertz, $T_1 = T_2^* = 1.00$ seconds, and the observing rf field is swept at a linear scan rate of 0.025 hertz/second with an amplitude of 0.0141 milligauss. The zero of the frequency axis is at $\omega_1' = \omega_1$, the horizontal scale is 2.0 hertz/division, and the direction of the frequency scan is as indicated by the (horizontal) arrow. The vertical arrows approximate the location of the perturbing rf frequency; in spectra (a) and (b), the perturbation frequency is fixed at $\omega_2'/2\pi = \omega_1/2\pi + 1.67$ hertz, while the perturbation amplitude increases from a value of $\gamma H_2/2\pi = 3.53$ hertz in (a) to a value of 4.44 hertz in (b). For spectra (c) and (d), the perturbation amplitude is fixed at the value $\gamma H_2/2\pi = 3.53$ hertz, while the perturbation frequency changes from $\omega_2'/2\pi = \omega_1/2\pi + 2.0$ hertz in (c) to $\omega_2'/2\pi = \omega_1/2\pi + 3.0$ hertz in (d). Due to a limitation of the filtering routine, each spectrum actually consists of a composite of two separate calculations, each calculating the line shape on one side of the perturbation frequency.

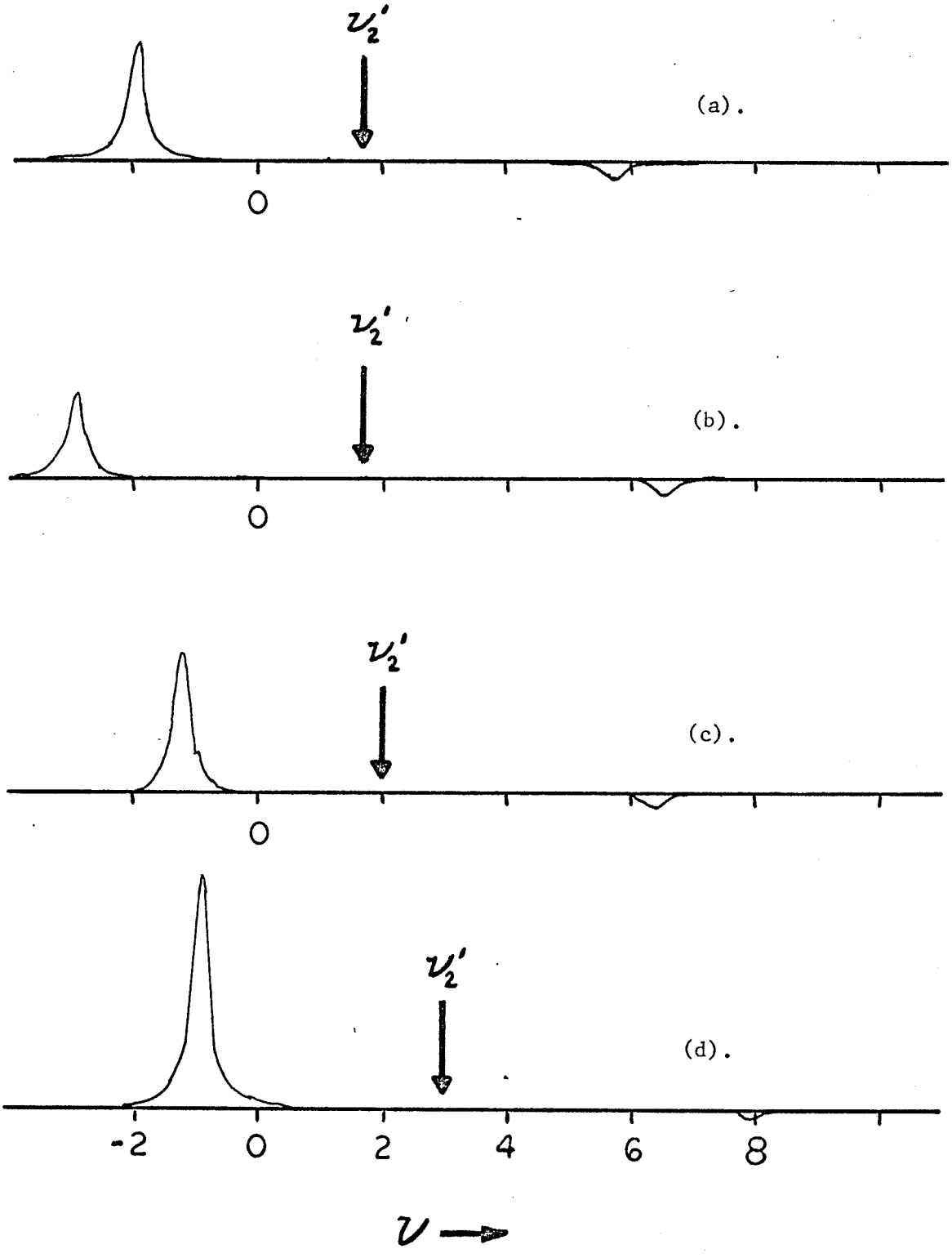
ν_2'
(a).
0
ν_2'
(b).
0
ν_2'
(c).
0
ν_2'
(d).
-2
0
2
4
6
8
$\nu \longrightarrow$

examples of which are shown in figure 33; Bloch (85) and Baldeschwieler (88) have also derived theoretical expressions displaying this dependence. Actually plots 32a and 32b were meant to be simulations of the experimental spectra in 33a and 33b respectively; however the differences may be readily attributed to uncertainties in the guesses for some of the parameters (such as the effective spin-spin relaxation time, the sweep rate, etc.). An obvious difference, for example, is that the directions of the frequency sweep are in the opposite sense.

2. Simulations of AX Systems.

In figures 34 and 35, there are presented simulations of the spin-decoupling experiments applied to systems of nuclei which are in the AX limit ($|J| << |\omega_1-\omega_2|$). The calculations have employed model A with and without the AX approximation described in Chapter III (but with identical results after convergence). Once again there is good agreement with observed spectra, examples of which are shown in figure 36: when $H_2=0$, the spectrum is a symmetric doublet, and as H_2 increases in magnitude, the doublet diverges and a new transition appears at their midpoint. Eventually, for H_2 large ($\gamma H_2 > |J|$; see, for example, references (75,76)), the intensities of the outermost lines become vanishingly small and the system is "decoupled" in the sense that the A nucleus is apparently not coupled to the X nucleus. These simulations may also be compared more quantitatively with the theory advanced by Anderson and Freeman (75) or by Freeman and Whiffen (76); for example with $\gamma H_2/2\pi J = 1$, their predicted intensity ratios are approximately 1 : 7.9 : 1 and the two outermost peaks are split by approximately 2.24J. The corresponding simulations in 34d and 35d

Figure 33.

Experimental spectra of the double resonance experiment as applied to a system of single spin-1/2 nuclei. Spectra (a) and (b) show that the splitting between the two transitions increases as the strength of the rf perturbation is increased from (a) to (b) (taken from Baldeschwieler (88)). Spectra (c) to (e) display the dependence of the splitting on the position of the perturbation frequency; as ω_2' approaches the Larmor frequency ω_1 of the nuclei, the splitting decreases, as shown in the sequence (c) to (e) (taken from Baldeschwieler and Randall (77)). Spectra (a) and (b) are meant to have the same parameter list as for 32a and 32b, respectively, but some poor "guesses" have been made for some of the parameters (see text).

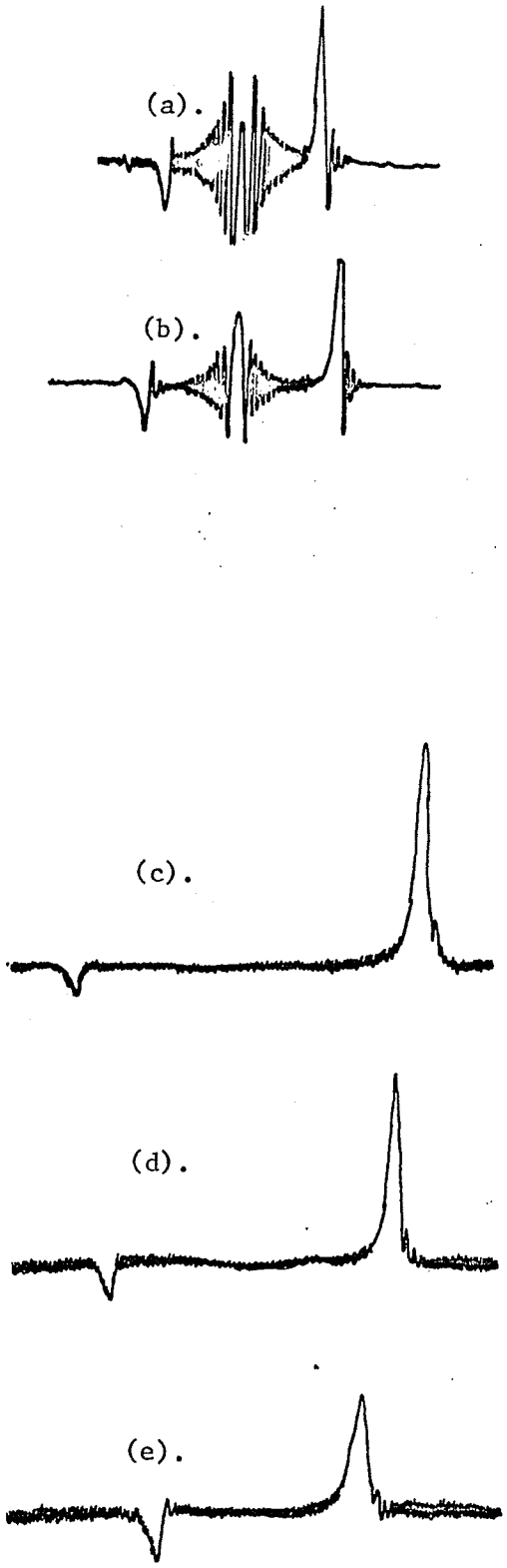
(a).
(b).
(c).
(d).
(e).

Figure 34.

Simulations of the spin-decoupling experiment as applied to a system of AX nuclei, using model A, and with only the "A" portion of the spectrum reproduced. The parameters are $H_o=10^4$ gauss, $\omega_1/2\pi$ = 42.577 megahertz, $\omega_2/2\pi = \omega_1/2\pi$ + 100.0 hertz, $J/2\pi$ = 1.0 hertz, $T_1=T_2^*=4.00$ seconds, and the observing rf field is swept at a rate of 0.025 hertz/second with an amplitude of 0.0005 milligauss. The zero of the frequency axis is at $\omega_1'=\omega_1$, the horizontal scale is 1.0 hertz/division and the direction of the frequency scan is as indicated by the arrow. In spectra (a) to (e), the perturbation frequency ω_2' is centered at the Larmor frequency of the X nucleus (ω_2) and the perturbation amplitude, in dimensionless units defined by the expression $\gamma H_2/J$, is equal to 0.0 (ie. single resonance), 0.025, 0.50, 1.00 and 2.00, respectively.

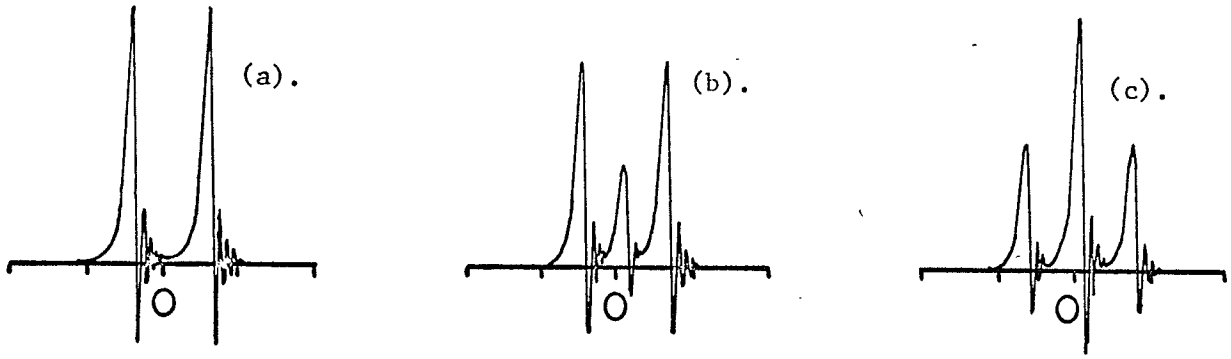

$\nu \rightarrow$

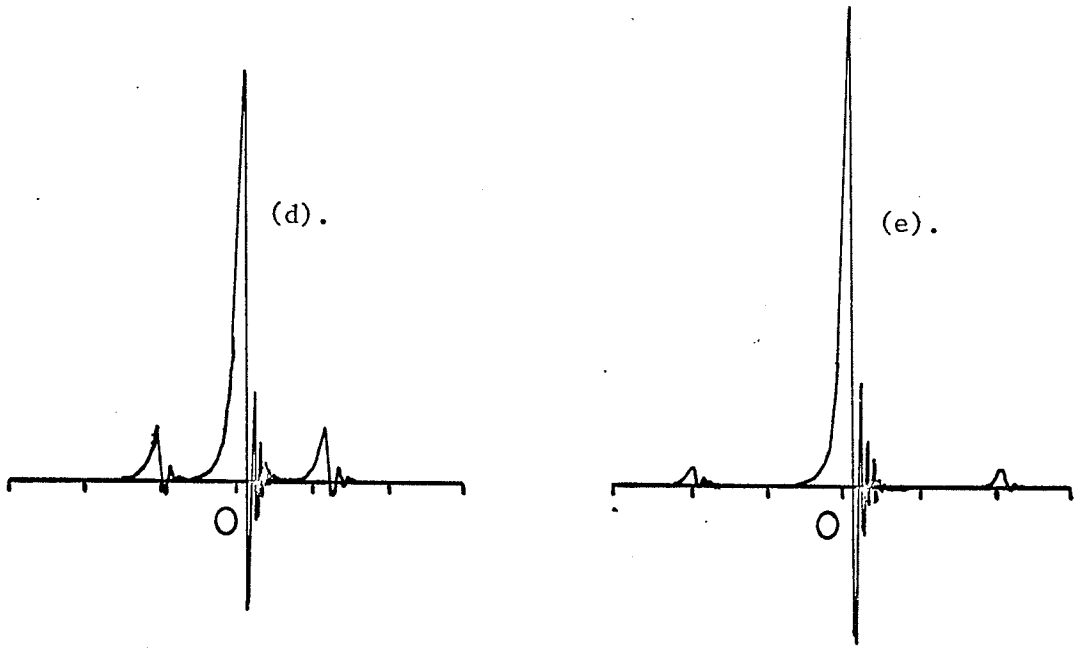

Figure 35.

Simulations of the spin-decoupling experiment as applied to a system of AX nuclei, using model A. The parameters are as for figure 34, except that the relaxation times have been decreased to $T_1=T_2^*=2.00$ seconds, and the observing rf amplitude is 0.005 milligauss. The perturbation rf field is centered at ω_2 and its amplitude (in units of $\gamma H_2/J$) is equal to 0.0, 0.25, 0.50, 1.00 and 2.00, respectively, for spectra (a) to (e) (as for figure 34).

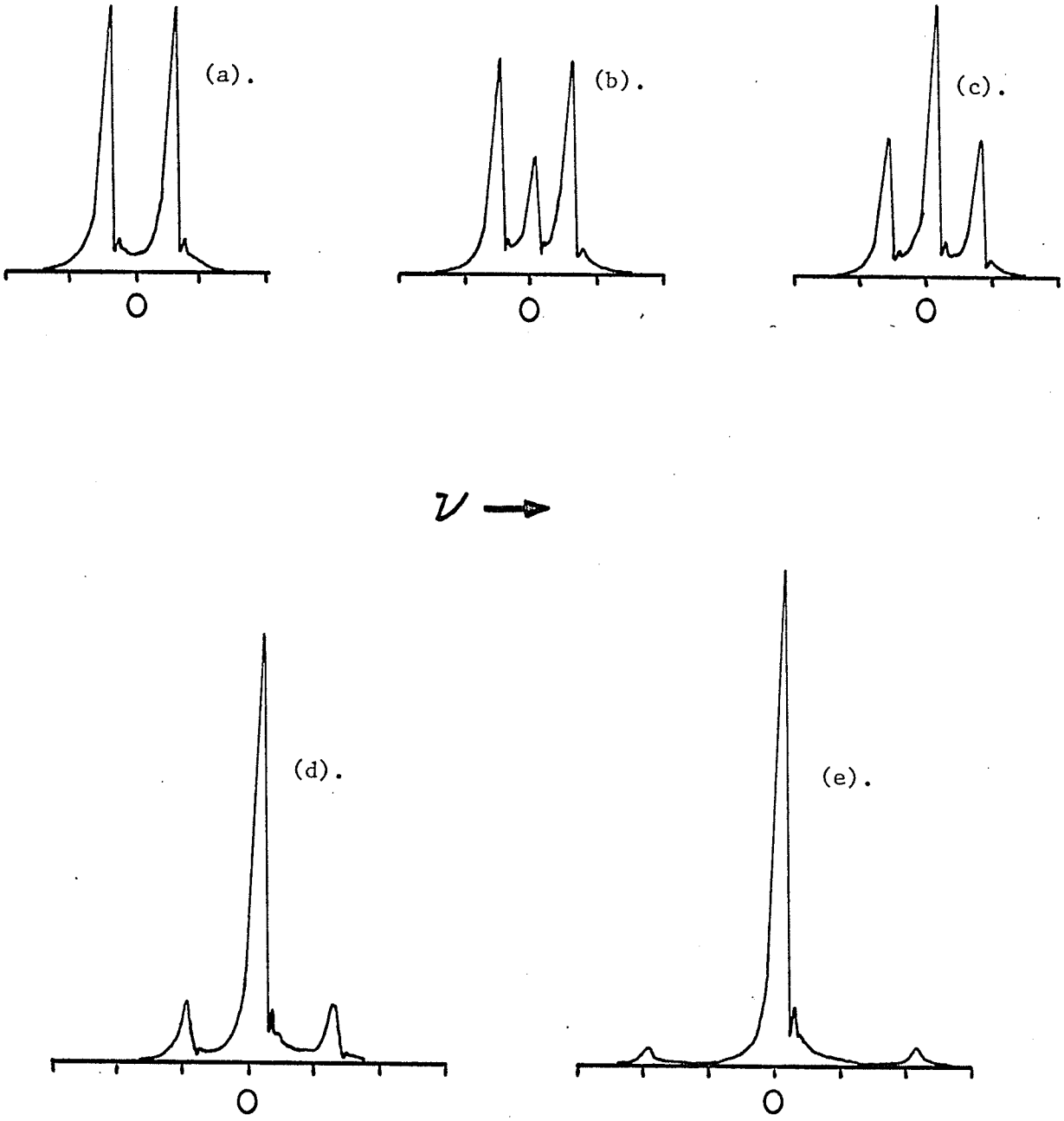
(a).
(b).
(c).
O
O
O
ν
(d).
(e).
O
O

Figure 36.

Experimental spectra displaying the spin-decoupling experiment as applied to an AX system of spin-1/2 nuclei (taken from Bloom and Schoolery (143)). The perturbation amplitude, in units of $\gamma_X H_2/J$ (the spin system is heteronuclear) is equal to 0.257, 0.463, 0.632 and 0.792 in spectra (a) to (d), respectively.

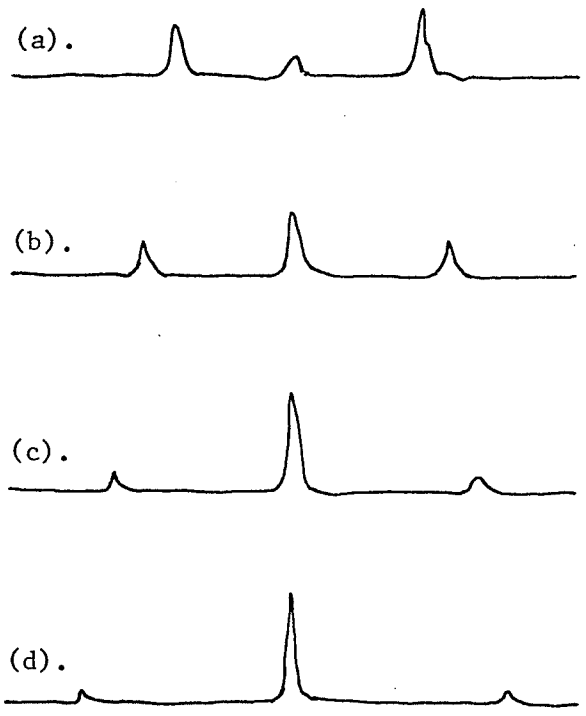
(a).
(b).
(c).
(d).

show the expected splitting (the peaks are slightly shifted in their absolute frequency due to a finite sweep rate), although the intensity ratios are somewhat different (for example, triangulation gives the ratio of approximately 1 : 7.5 : 1 for 35d). These latter discrepancies, however, may be attributed to the finite sweep rate and/or saturation by the observing rf field (neither of which are allowed by the other calculations (75,76); see also the discussion below).

The spectra in figure 37 are simulations of the double resonance experiment for which the rf perturbation is varied in frequency but fixed in amplitude. These results may also be compared favorably with experimental results and with other theoretical calculations (see, for example, references (75,76)); for example one proceeds from the partially decoupled spectrum in 37a to a spin-tickled spectrum in 37e (see also below) to the spectrum in 37f for which the frequency of the perturbation field is so far removed from any of the transitions so as to have no apparent effect on the spectrum (note that 37f and the single resonance spectrum 34a are identical; however the presence of a nonzero amplitude H_2 in 37f necessitates the use of the filtering routine[+]). Actually there may be some discrepancies between the calculated intensities in figure 37 and the calculated intensities of, for example, reference (75). The difficulty here lies in the fact that their equations are valid only for rf fields which

[+] cf. section IV.4 . No filtering is required if the AX approximation is employed, but calculations with and without the AX approximation yield identical results.

Figure 37.

Simulations of double resonance AX spectra for various positions of the perturbation frequency, using model A. The parameters are as for figure 34, but with the amplitude of the rf perturbation fixed at $\gamma H_2/J = 0.25$ (or $H_2 = 0.0587$ gauss). The frequency of the perturbation field is offset from the Larmor frequency of the X nucleus by the amount $\omega_2'/2\pi - \omega_2/2\pi = 0.0$, +0.100, +0.200, +0.300, +.500, and +2.00 hertz, respectively, in spectra (a) to (f). Spectrum 37f and spectrum 34a are essentially identical.

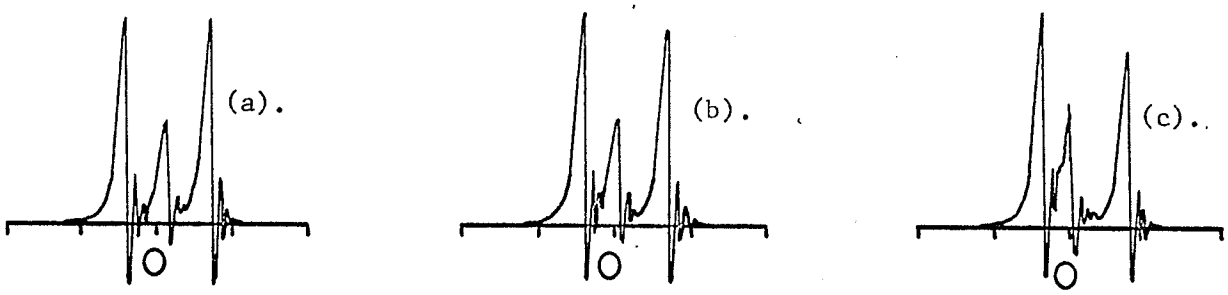

$\nu \rightarrow$

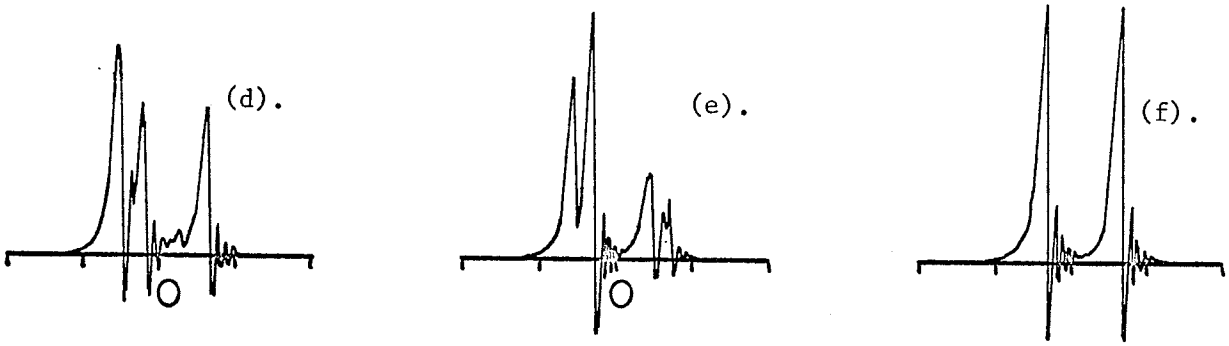

are so weak so as to produce negligibly small population transfers. Using the Bloch equations (cf. equation [1.4]) as an estimate, saturation and, therefore, population changes should occur when $\gamma^2 H_2^2 T_1 T_2^*$ approaches unity. This is the case for the spectra in figure 37, since, for that parameter list, $\gamma^2 H_2^2 T_1 T_2^* > 1$ if $H_2 > 0.01$ milligauss.

The transfer of populations due to the perturbing rf field gives rise to the phenomenon known as the nuclear Overhauser effect (4,74-77,85,120,142), and the spectra in figure 38 show more examples of this phenomenon in greater detail. These spectra are simulations of the spin-tickling experiment[+], with the rf perturbation frequency centered at one of the X transitions while the A transitions are observed. The intensity changes (cf. spectrum 35a, the corresponding single resonance spectrum) are readily interpreted from a consideration of the corresponding energy level diagram: for example if transition 4 in figure 2 is perturbed, then the partial saturation which occurs would tend to boost the population of spin state $|3\rangle$ at the expense of spin state $|4\rangle$. Subsequently it is expected that the

[+]the usual distinction between the spin-tickling and spin-decoupling experiments is made with respect to the rf power, with $\gamma H_2 / \mathbf{J} < 1$ defining a tickling experiment and $\gamma H_2 / \mathbf{J} \geq 1$ defining a decoupling experiment. These definitions are not rigorously upheld in the naming of the spectra in this thesis; rather the two experiments are differentiated by the location of ω_2'. If ω_2' coincides with a Larmor frequency, then the spectrum is called a decoupling simulation, whereas if ω_2' coincides with some transition frequency, the spectrum is called a tickling simulation.

Figure 38.

Simulations of the spin-tickling experiment applied to an AX system, using model A. The parameters are as for figure 34, except that $T_1=T_2^*=2.00$ seconds and the observing rf amplitude is fixed at 0.005 milligauss (as in figure 35). The frequency of the perturbing rf field is set at $\omega_2'/2\pi = \omega_2/2\pi +$ 0.5 hertz (the outermost X transition, or line 4 in figure 2) for spectra (a) to (c), and at $\omega_2'/2\pi = \omega_2/2\pi - 0.50$ hertz (the innermost X transition or line 3 in figure 2) for (d). The amplitude of the perturbation field in units of $\gamma H_2/J$ is 0.125 for (a), 0.250 for (b), and 0.500 for (c) and (d). Except for the effects attributed to the finite scan rate (0.025 hertz/second), spectra (c) and (d) are mirror images of one another. The corresponding single resonance spectrum is in figure 35a.

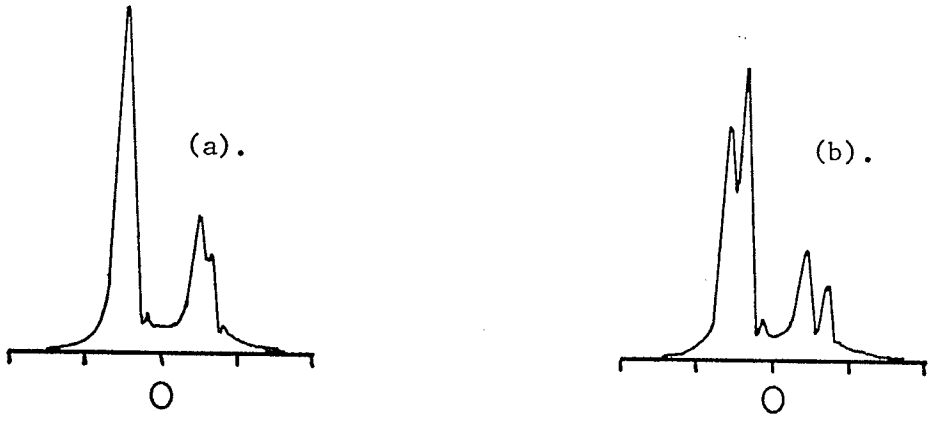

$\nu \longrightarrow$

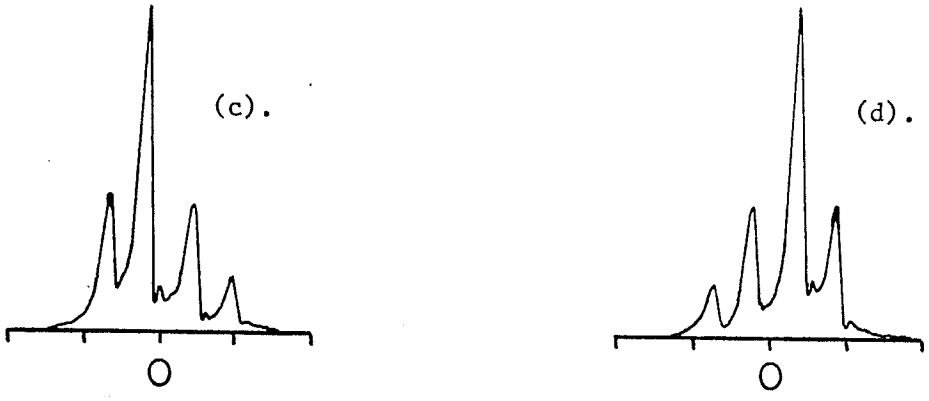

progressively-connected transition 1 will be enhanced in intensity, while the regressively-connected transition 2 will be attenuated; this is the case shown in figures 38a to 38c, although the latter two spectra are complicated by the presence of splitting of each transition. The opposite pattern occurs if transition 3 is perturbed, an example being the spectrum 38d. In general, a progressively-connected transition (ΔM_z=1) increases in intensity while a regressively-connected transition (ΔM_z=0) is attenuated (ΔM_z being the net change in M_z between the three connected levels).

Two additional features should be mentioned with regard to the spin-tickling experiments simulated in figure 38. First of all, the two A transitions are split into a pair of doublets as either one of the X transitions is perturbed, with the degree of splitting varying directly with the amplitude of the perturbing field (spectra 38c and 38d are mirror images except for the effects due to the finite sweep rate)[+]. Finally, it also appears that the doublet originating from the transition regressive to the perturbed line is better resolved than is the progressively-connected doublet; this is displayed in 38b and to a lesser extent in 38a. These results are generally in agreement with the experimental work and theoretical calculations of Freeman and Anderson (75) except for intensity differences; however further comments concerning the differential behaviour of regressive

[+] note that the splitting is identical for the doublet pairs in 38c and 34d, while the splitting is slightly different for the pair of doublets in 34b. This may be due to the finite sweep rate, but an alternate possibility is discussed below.

and progressive transitions are deferred to a later discussion.

3. Simulations of AB Systems.

The spectra presented in figure 39 are examples of the spin-decoupling experiment applied to an AB system of spin-1/2 nuclei. The results are much the same as for the decoupling of an AX system, except that the spectra are asymmetric and the central peak eventually splits into a doublet. This would indicate that an AB system can never be completely decoupled since some residual splitting always exists. The experimental spectra reproduced in figures 40a to 40d do not show this splitting because the spectral parameters approach the AX limit ($|J|/|\omega_1-\omega_2| \simeq 0.10$) and because the rf power of the perturbation field has not been taken to sufficiently high values. The corresponding theoretical calculations (93) do show, however, that the central peak does split into an asymmetric doublet and that the splitting increases with the amplitude H_2, in accordance with the simulations in figure 39f to 39h.

The spectra displayed in figures 41 and 42 are simulations of the spin-tickling experiment for an AB system; the rf frequency is centered respectively at the weaker and the stronger of the "B" transitions (lines 4 and 3, respectively, in figure 2). Two features are immediately discernable; first of all the nuclear Overhauser effect (behaving as before) and, secondly, the degree of splitting of the connected transitions varies directly with the amplitude of the perturbing rf field and with the intensity of the transition being perturbed. In the series 41c to 41f, for example, the two

Figure 39.

Simulations of the spin-decoupling experiment applied to an AB system of nuclei, using model A, and with only the "A" part of the spectrum reproduced here. The parameters are $H_o=10^4$ gauss, $\omega_1/2\pi$ = 42.577 megahertz, $\omega_2/2\pi = \omega_1/2\pi$ + 8.0 hertz, $J/2\pi$ = 2.0 hertz, $T_1=T_2^*=2.0$ seconds, and the frequency of the observing rf field is swept at 0.05 hertz/second with an amplitude of 0.01 milligauss. The zero of the frequency axis is at $\omega_1'=\omega_1$, the horizontal scale is 1.0 hertz/second and the direction of the frequency sweep is as indicated by the arrow. The frequency ω_2' of the perturbing rf field is centered at ω_2, and its amplitude is equal to 0.0 (ie. the single resonance spectrum), 0.050, 0.100, 0.250, 0.300, 0.350, 0.500 and 0.755 milligauss, respectively, in the series of spectra (a) to (h). The "ripples" in the central peak of spectrum (c) are attributed to an incomplete filtering of the signal.

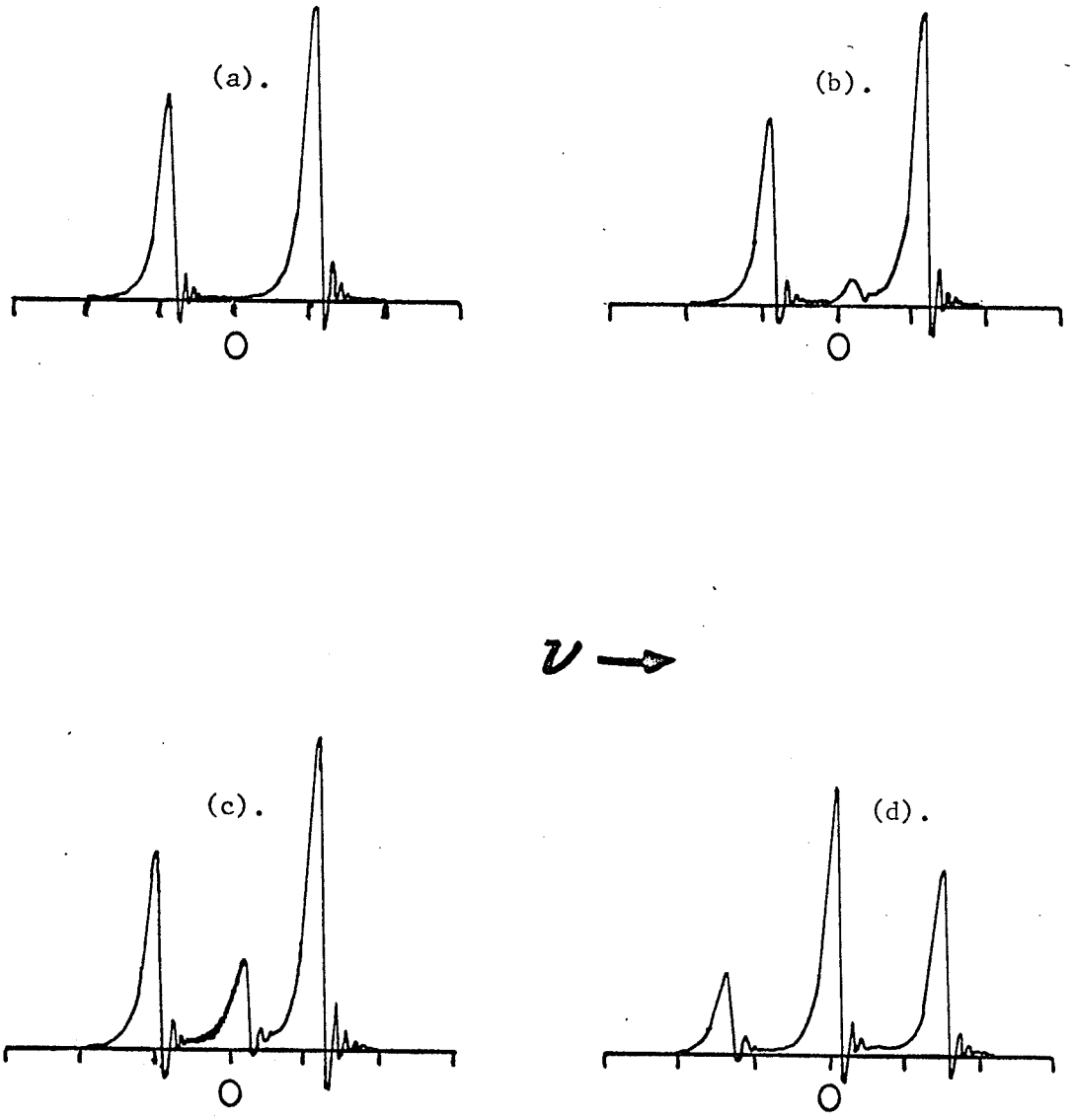
(a).
O
(b).
O
ν →
(c).
O
(d).
O

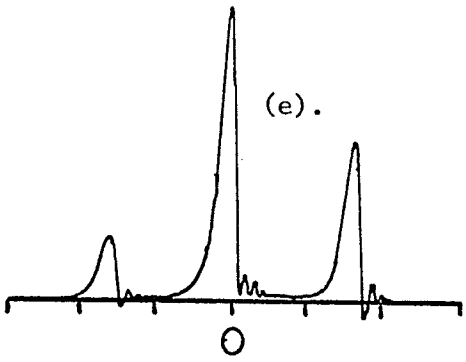

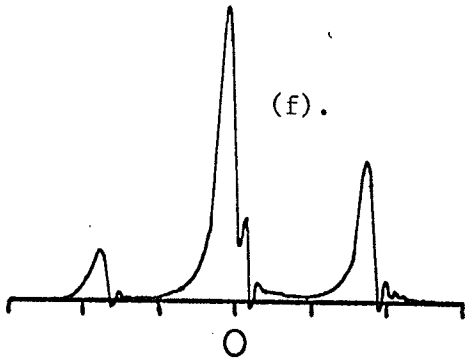

$\nu \rightarrow$

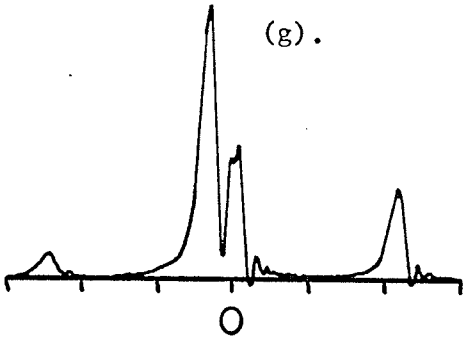

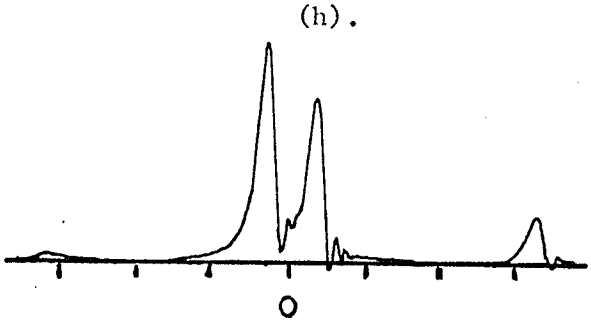

Figure 40.

Experimental double resonance spectra of an AB system of spin-1/2 nuclei. The spectra (a) to (d) are examples of the spin-decoupling experiment (from Wakefield and Memory (93)), with the rf perturbation amplitude, in units of $\gamma H_2/2\pi$, equal to 0.0, 2.0, 5.0 and 15.0 hertz, respectively. The spectra (e) to (g) are examples of the spin-tickling experiment (from Freeman and Anderson (75)), with spectrum (e) being the single resonance spectrum. The spectra in (f) and (g) are double resonance spectra obtained using the same rf perturbation amplitude, with its frequency centered at the first and second transition, respectively. The transition regressively connected to the perturbed transition is denoted by the label "R".

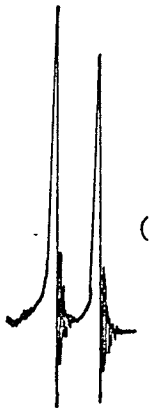

(a).

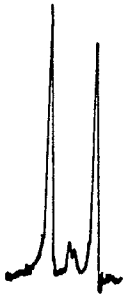

(b).



(c).

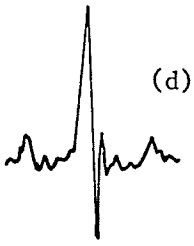

(d).

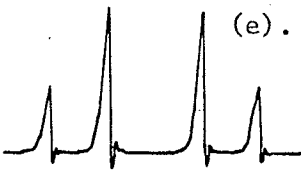

(e).

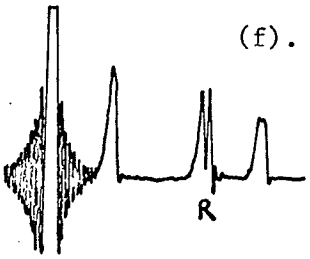

(f).

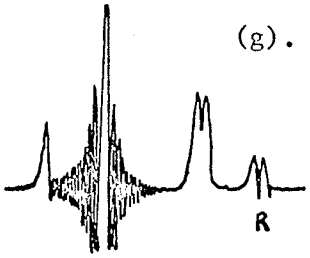

(g).

Figure 41.

Simulations of the spin-tickling of an AB system, using model A. The parameters are as for figure 39, but with the frequency of the perturbation field centered at the outermost "B" transition (transition 4 in figure 2), or $\omega_2'/2\pi = \omega_1/2\pi + 9.123$ hertz. The amplitude of the perturbing rf field is equal to 0.010, 0.025, 0.050, 0.075, 0.100 and 0.250 milligauss, respectively, in spectra (a) to (f). The regressively-connected transition is indicated by the label "R".

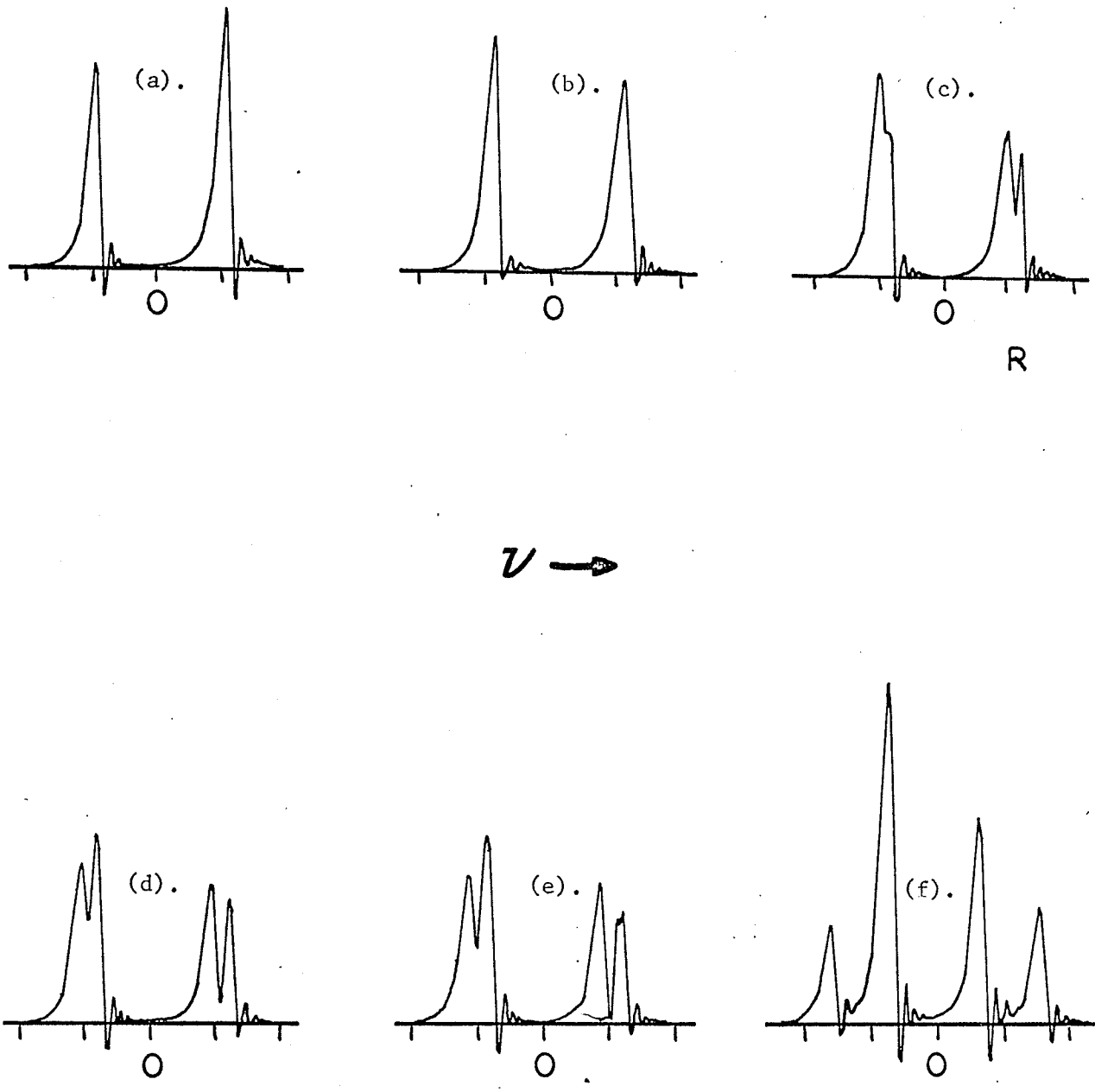
(a).
O
(b).
O
(c).
O
R
ν
(d).
O
(e).
O
(f).
O

Figure 42.

Simulations of the spin-tickling of an AB system, using model A. The parameters are as for figure 39 (and figure 41), but with the frequency of the perturbation field centered at the innermost "B" transition (transition 3 in figure 2), or $\omega_2'/2\pi = \omega_1/2\pi +$ 7.123 hertz. The amplitude of the perturbing field is equal to 0.010, 0.025, 0.050, 0.075, 0.100 and 0.250 milligauss, respectively, in the spectra (a) to (f) (compare with figure 41). The regressively-connected transition is indicated by the label "R".

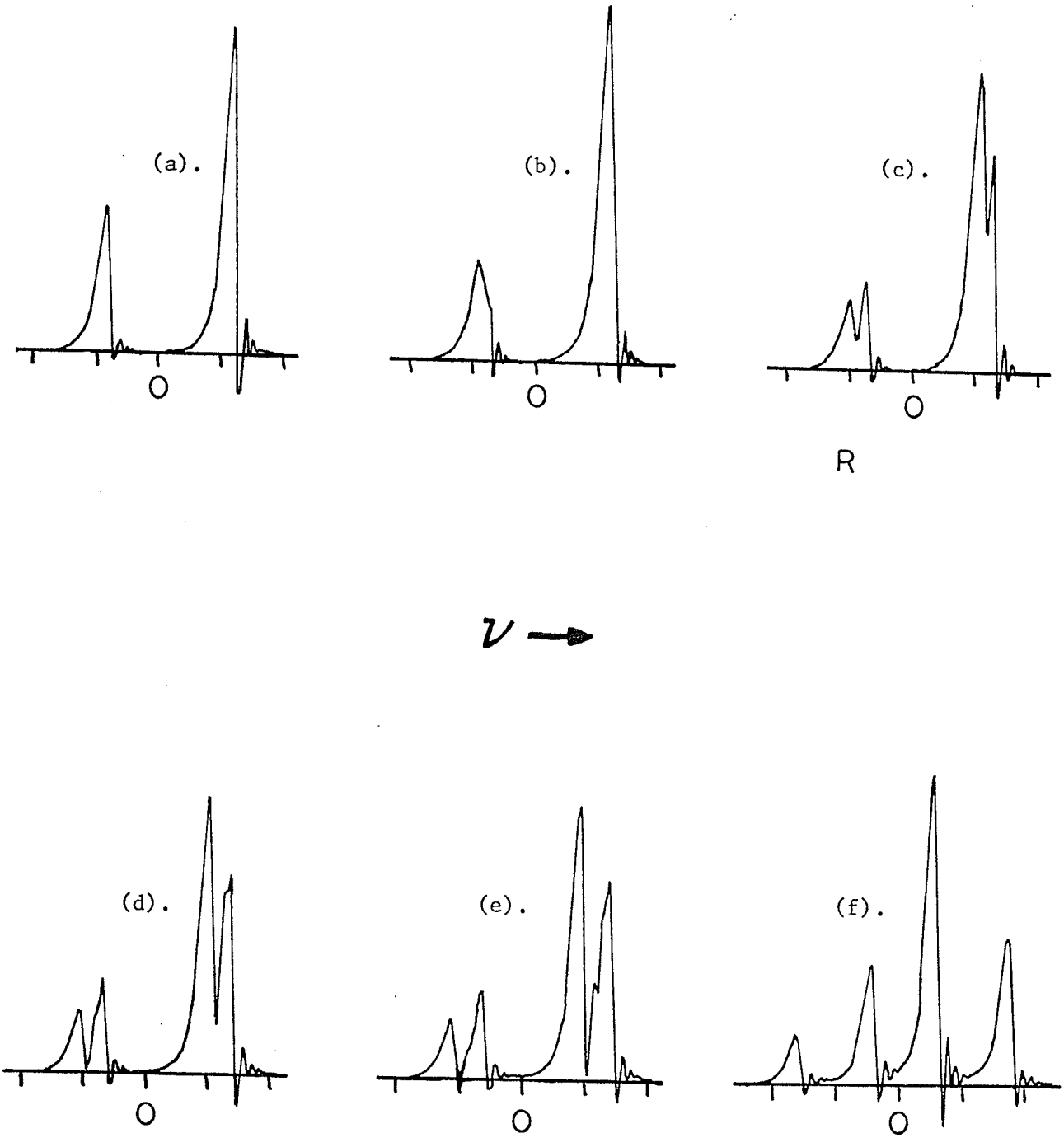
(a).
O
(b).
O
(c).
O
R
ν
(d).
O
(e).
O
(f).
O

transitions are split more as H_2 increases, while comparisons between 41c and 42c or between 41d and 42d etc. reveal that the spectra in figure 42 are split to a greater extent. This latter dependence was not observed in the case of the AX spectra, since the two "X" transitions have equal intensities. These features have been described in the theory developed by Freeman and Anderson (75), and some of their experimental spectra have been reproduced in figures 40e to 40g for comparison.

These experimental spectra also show an apparent asymmetry in the extent to which the doublets are resolved; this feature is observed in the simulated spectra in figures 41 and 42. In each case, the regressively-connected transition (denoted by the symbol "R") is that which is best-resolved, and Anderson and Freeman (75) originally attributed this asymmetry to differential broadening caused by inhomogeneity in the static magnetic field. In this sense the spectra in figures 41 and 42 are surprisingly accurate when it is recalled that inhomogeneity is introduced phenomenologically through the effective spin-spin relaxation parameter T_2^* (ie. model A). Consequently the first consideration of the applicability of model A mentioned on page 146 might be successfully altered to those cases for which only the observing rf field is in the unsaturated limit, with no similar restriction placed on the perturbing field (assuming that the two frequencies never coincide). If, however, the second consideration on page 146 is applied, then it appears that the regressive/progressive asymmetry is present even in the limit of zero inhomogeneity, since now T_2^* is reinterpreted as only a relaxation

time.

This last problem warranted more careful study, and the spectra appearing in figure 43 are simulations obtained using model C; in particular inhomogeneity is accounted for by the simplified equation [3.63b]. These calculations indicate that, even in perfectly homogeneous static magnetic fields, there is present some asymmetry in the degree of resolution of the transitions regressively and progressively connected to the perturbed transition. Figure 43b also indicates that the presence of inhomogeneity is to make the effect of the asymmetry more obvious[+]. Furthermore, a more detailed study of the splittings of the regressive/progressive doublets indicates that the regressive doublet is split slightly more than the progressive doublet for those cases where H_2 is just strong enough to produce a detectable splitting (see, for example, the spectra 38b, 41d, 42d, 43b); for larger amplitudes H_2 any differences tend to vanish (for example, figures 41f and 42f).

In fact, all of these observations are in agreement with later, more detailed studies on the double resonance spin-tickling experiment (78,94,129). Lippmaa and Rodmar (129), for example, have experimentally verified the prediction of Sinivee (94) that the regressive/progressive doublets are <u>not</u> split identically for values of H_2 just sufficiently strong to produce an observable splitting

[+] not shown here are results for an AX system calculated using model B and equation [3.63b] and for which similar conclusions may be made. Recall also that if [3.63b] is employed, then this implies that <u>all</u> transitions are broadened <u>equally</u> (cf. page 150).

Figure 43.

Simulation of the spin-tickling experiment for an AB system, using model C, and showing the asymmetry of the regressive and progressive pair of doublets. Only the "B" part of the spectrum is reproduced here. The parameters are $H_o \simeq 2.35 \times 10^4$ gauss, $\omega_1/2\pi = 100.0$ megahertz, $\omega_2/2\pi = \omega_1/2\pi + 9.85$ hertz, $J/2\pi = 2.80$ hertz, and an RFUC relaxation mechanism with $\omega_s/2\pi = 0.0334$ hertz, $\eta = 0.0$ and $r = 0.0$. The amplitude of the observing field is 0.0012 milligauss and the rate of frequency scan is -0.20 hertz/second. The zero of the frequency axis is at $\omega_2' = \omega_1$, the horizontal scale is 2.0 hertz/division and the direction of the frequency scan is as indicated by the arrow. The amplitude of the perturbing rf field is 0.1104 milligauss, and its frequency is centered at the outermost "A" transition (line 1 in figure 2), or $\omega_2'/2\pi = \omega_1/2\pi - 1.595$ hertz. Spectrum (a) is the calculated response with no inhomogeneity effects, and spectrum (b) is the same spectrum but with a Lorentzian distribution of inhomogeneity with a full width at half-height of 0.12 hertz (using equation [3.63b]). The regressively-connected doublets are denoted by the label "R".

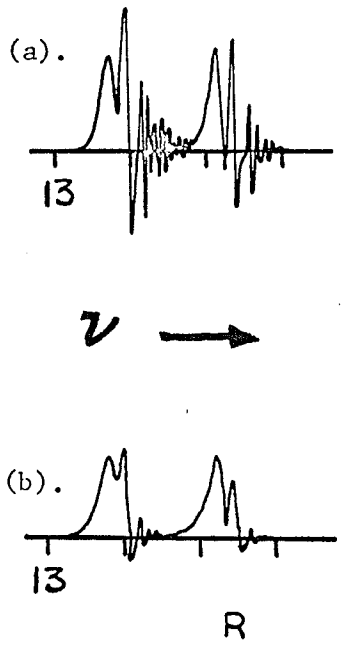
(a).
13
ν
(b).
13
R

(the theory developed by Sinivee indicates that the differential splitting is a relaxation effect). Finally, the more detailed study by Freeman at. al. (78) indicates that the simplification [3.63b] is not always an adequate approximation in double resonance (nor is model A). This follows since the effect of inhomogeneity is to shift the Larmor frequency of all the nuclei by a constant amount, and in double resonance this produces variations in the frequency offset $|\omega_2'-\omega_i|$ of the perturbation frequency ω_2' from the transition ω_i being perturbed. For weak perturbation amplitudes, these frequency offsets are important (78,94), and therefore one should use the computationally-expensive equation [3.63a] for the calculation of those spectra. The calculations reproduced here have all been obtained using either model A or model C and [3.63b]. For the former simulations, if T_2^* is reinterpreted (as before) to be the natural spin-spin relaxation time, then those spectra are representative of a perfectly homogeneous field. When model C is employed, it is assumed that the equation [3.63b] is adequate, although detailed comparisons have not been attempted.

The spectra in figure 44 are simulations for which the double quantum transition of the preceding AB system is perturbed while the "A" transitions are observed; similar patterns are to be expected for the "B" transitions. A consideration of the energy level diagram may explain much of the observed behaviour; for example as H_2 increases, the transitions are attenuated since saturation of the spin states occurs. By analogy with the previous spin-tickling experiments, both the "A" transitions are split into doublets since both

Figure 44.

Simulation of the double resonance of an AB system, using model A, for which the double quantum transition is being perturbed. The parameters are as for figure 39 but with $\omega_2'/2\pi = \omega_1/2\pi + 4.00$ hertz (ie. the line "DQ" in figure 2). The transitions shown are the "A" transitions; the "B" part of the spectrum is essentially identical to its "A" counterpart. The amplitude of the perturbing field is equal to 0.100, 0.175, 0.1875, 0.200, 0.225 and 0.250 milligauss, respectively, in the series of spectra (a) to (f).

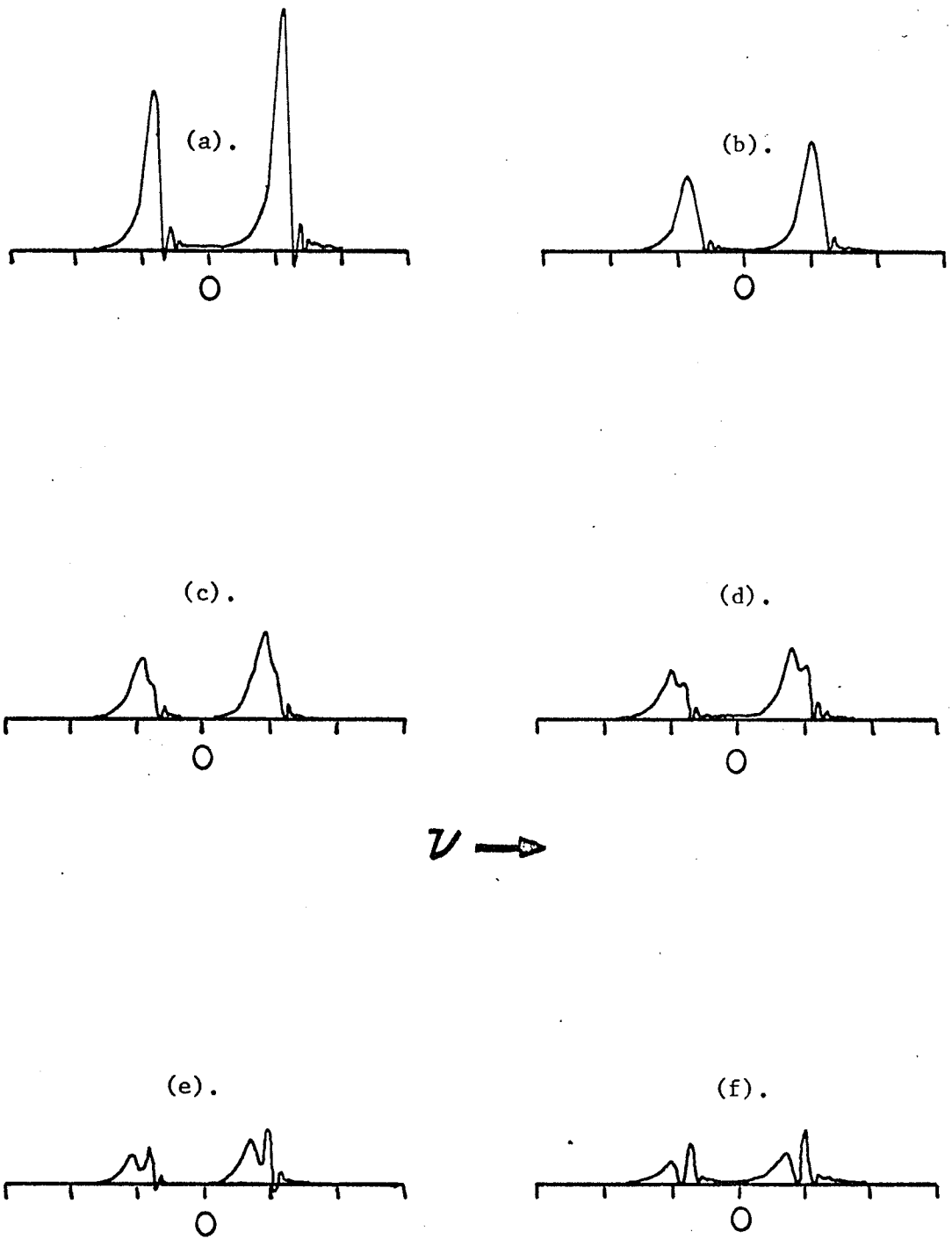
(a).
(b).
(c).
(d).
ν
(e).
(f).

share an energy level with the perturbed transition; in addition both transitions are of the same "type", with $\Delta M_z = \pm 1$, and therefore the resolution of the doublets is the same. These results are in agreement with experimental observations (144) and with other theoretical calculations (145,146).

The remaining simulations of this AB system, reproduced in figure 45, display the continuous progression of spectra obtained when the amplitude of the perturbing field is constant and its frequency is set at different positions near the Larmor frequency of the B nucleus. As for the AX system, for ω_2' far removed from any transition, the spectrum is essentially a single resonance spectrum (compare spectra 45a and 37a), except that the signal must be filtered. Note that the spectra 45c and 45g resemble the spin-tickling spectra 41e and 42e respectively, while 45e approaches the partially-decoupled spectrum 39c. Finally, the plot 45i resembles the spectrum in figure 44a, for ω_2' at the frequency of the double quantum transition.

The last two figures discussed in this section are concerned with spin-tickling experiments designed for the elucidation of the mechanisms responsible for relaxation in proton NMR. The simulated spectra, shown in figure 46, have been obtained using model C^+ for the DD, RFC and RFUC mechanisms, and these results may be compared with the experimental spectra of Krishna and Nageswara Rao (106) which have been reproduced in figure 47. For 47c and 47d, the

---

+ the spectra are calculated with H_2 below and well-above the splitting threshold and it is expected that equation [3.63b] is adequate for the description of inhomogeneity (cf. references (78,94)).

Figure 45.

Simulations of the double resonance of an AB system for various positions of the perturbing rf frequency, using model A. The parameters are as for figure 39 except that the amplitude of the perturbing rf field is fixed at 0.100 milligauss. The frequency offset $\omega_2'/2\pi-\omega_1/2\pi$ of the perturbing field is equal to 10.00, 9.40, 9.00, 8.80, 8.20, 7.40, 7.10, 6.75, and 4.00 hertz, respectively, for the spectra (a) to (i). The following spectra also fit into this series: figure 41e (between (b) and (c)); figure 39c (between (e) and (f)); and figure 42e (between (f) and (g)). Note that when the perturbation frequency is far removed from any transition, as in 45a, the spectrum is essentially the corresponding single resonance spectrum (shown in figure 39a).

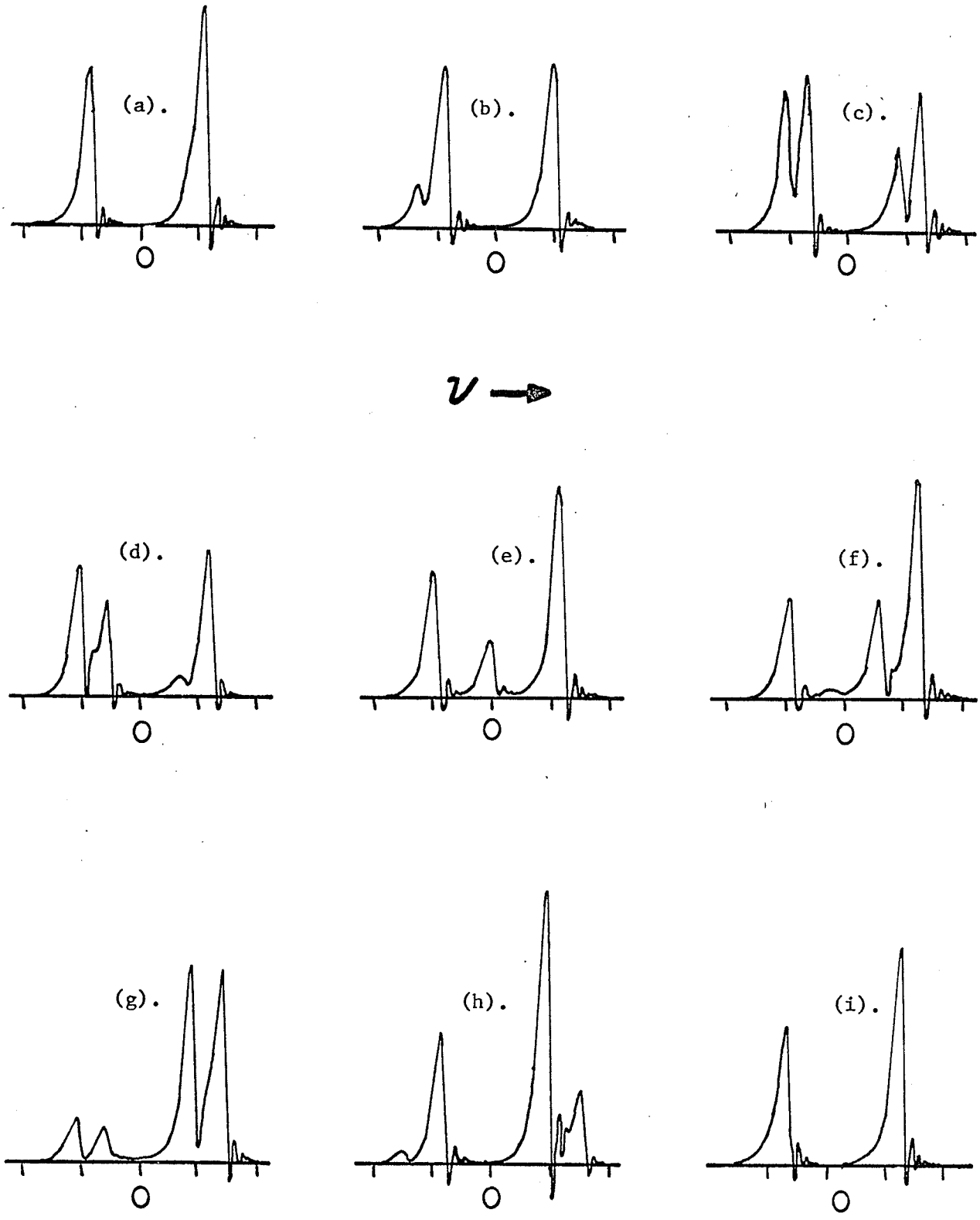
(a).
(b).
(c).
ν
(d).
(e).
(f).
(g).
(h).
(i).

Figure 46.

Simulations of a double resonance experiment used for the study of relaxation mechanisms (cf. figure 47), using model C. The parameters are as for figure 43, except that when an "A" transition is being perturbed, the "B" part of the spectrum is shown and vice versa. For spectra (a) to (f), the amplitude of the perturbing rf field is equal to 0.01104 milligauss with the frequency offset $\omega_2'/2\pi-\omega_1/2\pi$ equal to +8.645 hertz for (a) to (c) (ie. the innermost "B" transition or line 3 in figure 2), and to -1.595 hertz for (d) to (f) (ie. the outermost "A" transition or line 1 in figure 2). For spectra (g) to (i), the amplitude of the perturbing rf field is equal to 0.5520 milligauss with the frequency offset equal to 11.445 hertz for (g) to (i) (ie. the outermost "B" transition or line 4 of figure 2), and to -1.595 hertz for (j) to (l). The relaxation mechanisms are, by columns from left to right, DD with T_D = 2.71 seconds for (a,d,g,j); RFC with $\omega_s/2\pi$ = 0.0334 hertz and η = 0.0 for (b,e,h,k); and RFUC with $\omega_s/2\pi$ = 0.0334 hertz and η = 0.0 for (c,f,i,l). All spectra have been calculated with a Lorentzian distribution of inhomogeneity (using [3.63b]) whose half-height width 2w is equal to 0.12 hertz.

Note: the four rows of spectra are meant to be simulations of the spectra in figure 47, for different relaxation mechanisms. Row 1 corresponds to spectrum 47a, row 2 to spectrum 47b, etc.

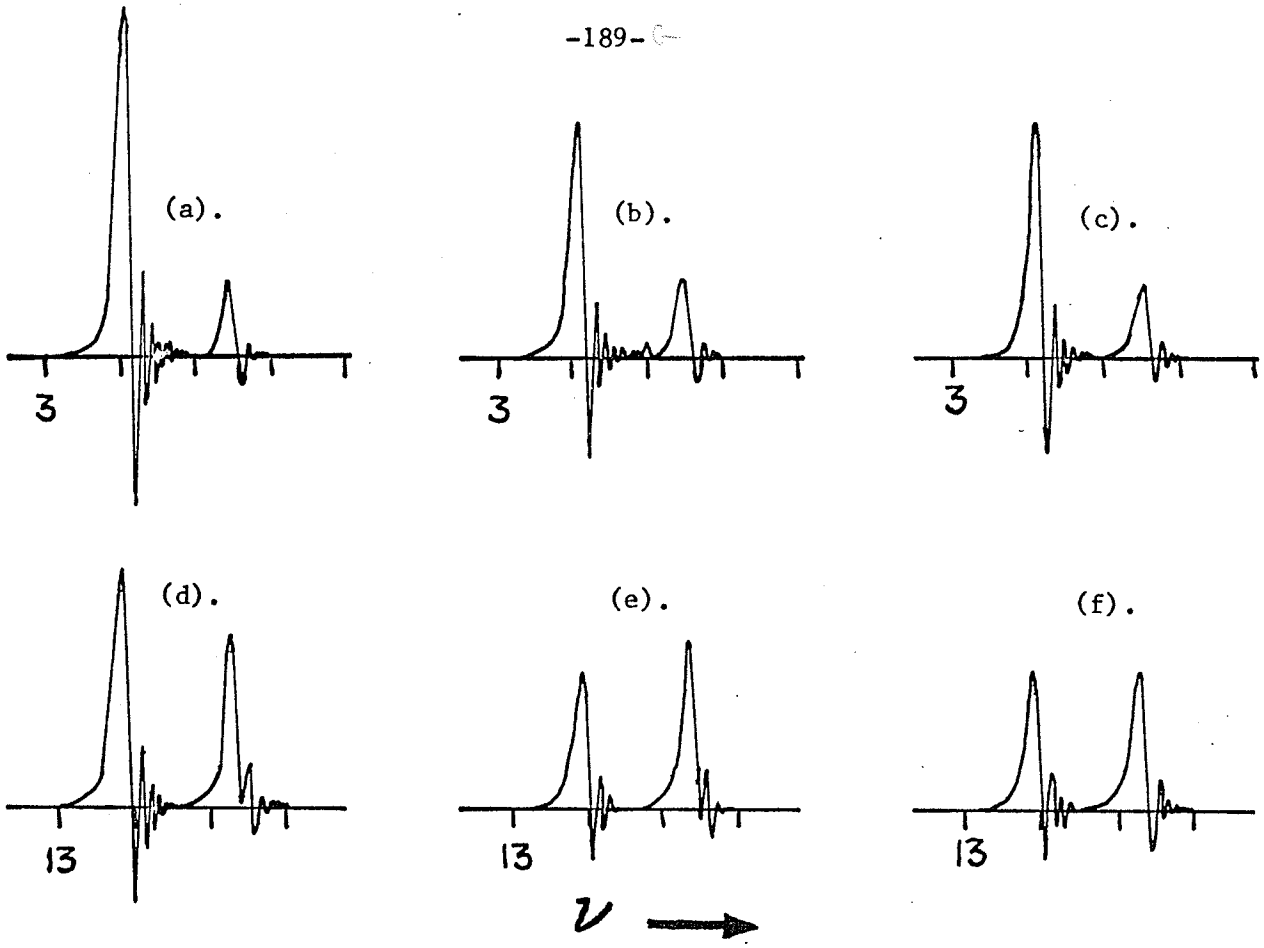
(a).
3
(b).
3
(c).
3
(d).
13
(e).
13
v
(f).
13
(g).
3
(h).
3
(i).
3
(j).
13
(k).
13
(l).
13

Figure 47.

Experimental double resonance spectra of an AB system of spin-1/2 nuclei (taken from Krishna and Nageswara Rao (106)). The spectral parameters are (106) $\omega_1/2\pi$ = 100.0 megahertz, $\omega_2/2\pi = \omega_1/2\pi$ + 9.85 hertz and $J/2\pi$ = 2.80 hertz. The frequency offset of the perturbing rf field is as indicated by the vertical arrows, and the amplitude of the perturbing rf field is equal to 0.01104 milligauss for (a) and (b), and to 0.5520 milligauss for (c) and (d). The spectra (a) to (d) have been simulated in figure 46, with 47a corresponding to the first row of spectra in figure 46, 47b to the second row, etc.; according to Krishna and Nageswara Rao (106) the spin system is relaxed predominately by means of an RFUC mechanism. The stick spectra shown below spectra (c) and (d) are the theoretical intensities and frequencies, as calculated by Krishna and Rao (106).

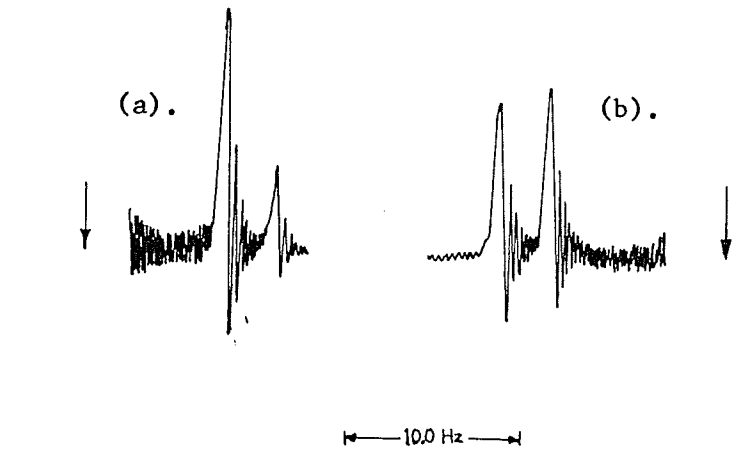
(a).
(b).
10.0 Hz

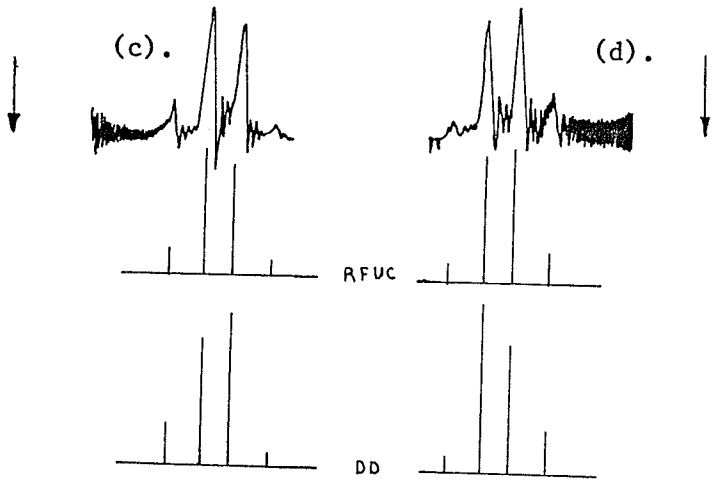
(c).
(d).
RFUC
DD

calculated stick spectra (from reference (106)) have been included to aid in the comparisons. Detailed analysis has revealed that the experimental spectra in figure 47 are relaxed, predominately, by means of an RFUC relaxation mechanism (106).

This conclusion appears to be the case after a comparison of the spectra in figures 46 and 47; for example the relative peak areas of 47a and 47b are best "fit" by the corresponding simulated spectra for the RFUC mechanism in 46c and 46f. It is clear that some discrepancies do occur, particularly when H_2 is large; however it should be pointed out that a number of parameters are not available for the simulations - notably the sweep rate(s) and an estimate for the type and width of the inhomogeneity distribution present[+]. This may explain, for example, the difference in peak maxima in 46i and 47c, although it is noted that the peak areas of spectrum 46i are in good agreement with the intensities of the calculated stick spectra for figure 47c (for the RFUC model). Once again this dynamic calculation technique appears to be invaluable in simulating these spectra, particularly because the effects of fast passage conditions are decidedly evident, and therefore the steady-state approximation cannot be acceptable (note that the calculated stick spectra in figure 47 have been modified in an attempt to compensate for sweep rate effects (106)).

[+]in addition it appears that the filtering of the experimental spectra is not quite as good (!) as for the simulated spectra.

D. Simulation of Some Nonselective Pulse Experiments

1. Introduction.

It was previously mentioned that there exists a wide variety of pulse experiments, and that the present calculations have been restricted to only a few pulse sequences which presumably display the overall generality of the technique. The spectra and plots reproduced below, however, do not exhaust the actual range of experiments simulated; some calculations are not presented in detail because the entire signal and/or the resultant plots are relatively uninteresting. Some such examples, along with the observed results, are listed below.

(a) The $\pi-\tau-\pi/2$ pulse sequence was applied to A_2 and AB systems of nuclei, using model B. Inhomogeneity effects were not considered[+], and the signal immediately following the $\pi/2$ pulse obeys the equation (8):

$$S(\tau) = S_o (1 - 2\exp(-\tau/T_1))$$

where S_o is the signal amplitude obtained with $\tau=0$ (in practise, it is deduced that the simulated results obey a given relation since, in this case for example, a plot of $\ln\{S(\tau)-S_o\}$ vs τ yields a straight line whose slope and intercept yield the expected values for T_1).

(b) The Hahn $\pi/2-\tau-\pi/2$-echo pulse sequence applied to an A_2 system gives the expected result that the signal at time $t=2\tau$ obeys the

---

[+]inhomogeneity was considered in one case, yielding results similar to figure 3.4 of reference (8) for a Gaussian distribution with different widths (and using equation [3.65]).

relation (8,29):

$$S(t=2\tau) \quad \propto \quad \exp(-2\tau/T_2)$$

ignoring diffusion. Inhomogeneity effects were also ignored since the Hahn pulse sequence is designed to negate the presence of any inhomogeneity, but only at time $t=2\tau$.

(c) The two types of Carr-Purcell experiments, applied to an A_2 system, obey the relation

$$S(t=2n\tau) \quad \propto \quad \exp(-2n\tau/T_2) \qquad (n=1,2,3,\ldots)$$

where n is the echo number (inhomogeneity was ignored for the same reason as for the Hahn experiment, but see also figure 50 below). The first variation of the CP experiment, the single-shot method, is concerned only with the first echo (n=1), and the pulse sequence is repeated for various values of τ. The second variation, called the multi-shot method, uses the pulse sequence $\pi/2\text{-}\tau\text{-}\pi\text{-}2\tau\text{-}\pi\text{-}2\tau\text{-}\pi\text{-}$ ... with echos appearing at times $t=2n\tau$. The Meiboom-Gill modification (20) of the Carr-Purcell experiment yields identical results for the same A_2 system, except for the relative signs of the echo maxima when a phase-sensitive detector is employed (the echos are always positive for a diode detector): for the CP experiment, the first and every other echo is negative and the even echos are positive, while for the CPMG experiment every echo is positive. This last observation is also in good agreement with experiment (see, for example, references (8,19, 20)), and corresponds to a refocusing of the net magnetization along the positive or negative x-axis (the detector axis).

2. Simulations of the FID Experiment.

The first pulse experiment to be considered in detail is that yielding the free induction decay (FID) signal. This experiment is of special interest here since the various techniques developed can be readily checked for consistency; for example in the discussion concerning figure 9 it was shown that the Fourier transform of the FID signal yields an unsaturated slow passage cw spectrum (as expected) which is very similar to the spectrum obtained using the single resonance simulation. It was also shown that the two different methods of inclusion of inhomogeneity resulted in a similar broadening effect for those spectra (in figure 9).

Examples of the FID signals and their corresponding absorption mode Fourier transforms are shown in figures 48 and 49. The first two spectra in figure 48 differ in the position of the pulsing rf frequency relative to the Larmor frequency of the A_2 nuclei; in 48a the frequencies coincide and in 48b they differ by 10.0 hertz. The latter spectrum displays an interference pattern as the magnetization and the detector (referenced to the rf frequency ω_1') alternately come in and out of phase at the rate of 10 hertz, although the envelope traced out by the maxima in the oscillations is the same as for 48a. Figure 48a actually represents the response of the in-phase component of a phase-sensitive detector; the corresponding out-of-phase component is everywhere zero. On the other hand, figure 48b represents the out-of-phase response, and the corresponding in-phase signal consists of similar oscillations (having the same envelope) which are 90 degrees out of phase with the out-of-phase oscillations. This last pattern is

Figure 48.

Free induction decay signals and a Fourier transform spectrum of an A_2 system of nuclei, using model B. The parameters are $H_o=10^4$ gauss, $\omega_1/2\pi = \omega_2/2\pi = 42.577$ megahertz, $J/2\pi = 0.0$, $T_1=T_2=10.0$ seconds and a Gaussian distribution of inhomogeneity with width $2w = 8.33\times10^{-5}$ gauss (0.354 hertz). Plots (a) and (b) are the in-phase and out-of-phase components, respectively, of the FID signal obtained following a $\pi/2$ pulse of amplitude $H_1=3.2724$ gauss and of duration $\tau_p=17.94$ microseconds. The frequency of the pulsing field is equal to the Larmor frequencies in (a), and to $\omega_1/2\pi + 10.0$ hertz in (b). The spectrum (c) is the Fourier transform of the FID signal in plot (a).

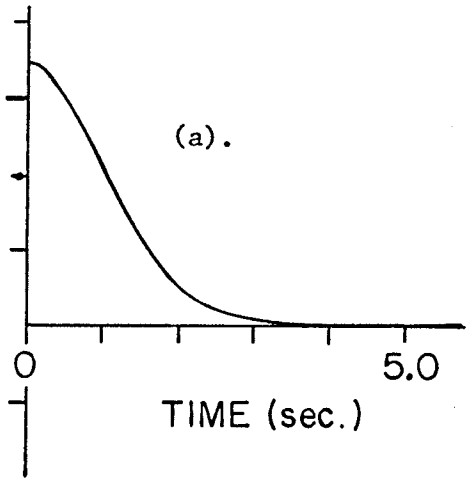
(a).
0
5.0
TIME (sec.)

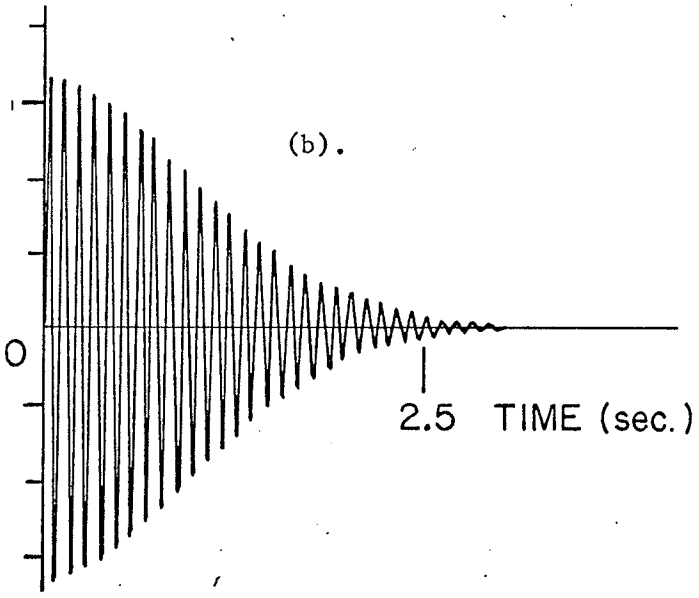
(b).
0
2.5
TIME (sec.)

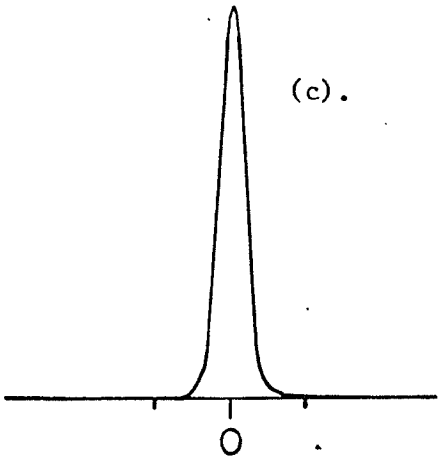
(c).
0

Figure 49.

Free induction decay signals and a Fourier transform spectrum of an AB system of nuclei, using model B. The parameters are $H_o=10^4$ gauss, $\omega_1/2\pi$ = 42.577 megahertz, $\omega_2/2\pi = \omega_1/2\pi$ + 2.0 hertz, $J/2\pi$ = 1.0 hertz, $T_1=T_2=10.0$ seconds and a Gaussian distribution of inhomogeneity with $2w = 8.33\times10^{-5}$ gauss (0.354 hertz). Plots (a) and (b) represent the in-phase component of the FID signal following a $\pi/2$ pulse of amplitude 3.2724 gauss and of duration 17.94 microseconds. The frequency of the pulsing field, ω_1', is equal to ω_1 in (a), and to $\omega_1/2\pi$ + 10.0 hertz in (b). The spectrum (c) is the Fourier transform of the FID signal in (b) (compare with figure 9).

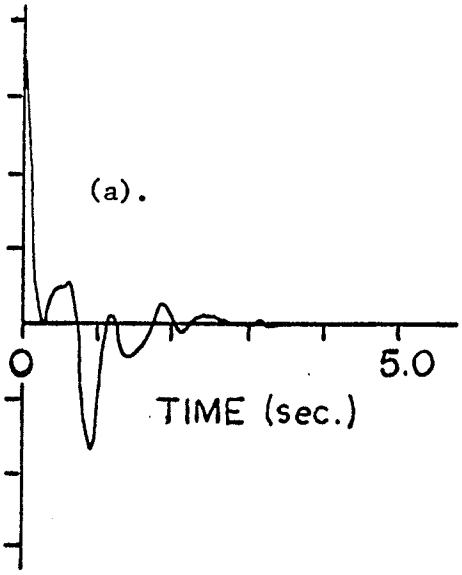
(a).
0
5.0
TIME (sec.)

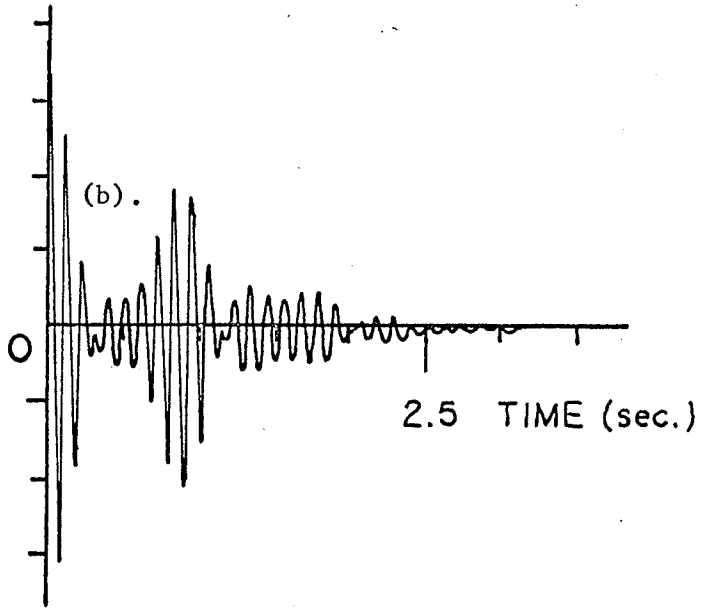
(b).
0
2.5 TIME (sec.)

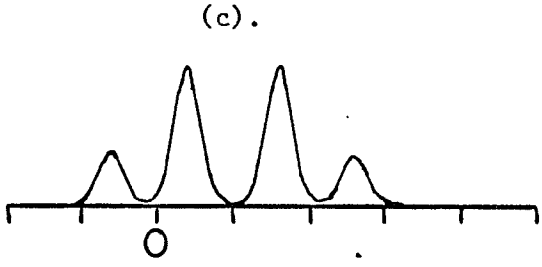
(c).
0

always present in the FID signal of an AB system since the pulsing frequency can never be set simultaneously at both Larmor frequencies, although the oscillations are somewhat simplified in 49a when ω_1' is centered at one of the Larmor frequencies (compare with 49b). Both of the FID signals in 49a and 49b represent the in-phase response, the out-of-phase response behaves as for figure 48b. These oscillations are analogous to the ringing observed in cw NMR, and they may be explained in a similar fashion.

The FID plots in figures 48 and 49 were all obtained using model B and with equation [3.65]. The Fourier transforms have been evaluated from these FID signals, although it was pointed out that a more convenient method is to include inhomogeneity effects after the Fourier transformation (cf. Chapter IV.E). It should also be mentioned that the origin of the Fourier transform spectra is actually relative to the pulsing (detector) frequency ω_1'; for example in figure 49c the frequency "zero" is actually -10.0 hertz from the rf frequency. In addition, note that the real part of the Fourier transform in [4.26] is independent of the sign of the frequency, so that in fact one can also obtain an absorption mode spectrum identical to 49c but +10.0 hertz from ω_1' and (apparently) backwards (the imaginary part of the transformation is, however, antisymmetric). This may lead to very confusing transforms; for example the Fourier transformation of figure 49a yields <u>two</u> AB absorption spectra which are mirror images about ω_1.

The variation of the FID signal with inhomogeneity of the static magnetic field is not shown explicitly here, although the effects may be deduced from the spectra in figures 50 and 51 which are meant to

Figure 50.

Simulations of the Carr-Purcell experiment applied to an A_2 system of nuclei, using model B, for different widths of an inhomogeneity distribution. The parameters are $H_o=10^4$ gauss, $\omega_1/2\pi = \omega_2/2\pi =$ 42.577 megahertz, $J/2\pi = 0.0$, and $T_1=T_2=1.00$ seconds. Plots (a) to (d) have the frequency of the pulsing field centered at ω_1, while for plot (e), $\omega_1'/2\pi = \omega_1/2\pi + 10.0$ hertz. The amplitude of the pulsing field is 3.2724 gauss, with the pulse durations being 17.94 and 35.88 microseconds, respectively, for a $\pi/2$ pulse and a π pulse. The $\pi/2$ pulse initiates the experiment at time t=0, and 0.25 seconds after the end of this pulse (at approximately time t= 0.25 seconds) a π pulse is applied to the system. Successive π pulses follow 0.50 seconds after a preceding π pulse, with the echo amplitude at the midpoint of two π pulses being independent of inhomogeneity. The inhomogeneity distribution is Gaussian, and the width parameter 2w is equal to 0.0 for (a) (ie. the "central" ensemble); $8.33\text{x}10^{-5}$ gauss for (b); $8.33\text{x}10^{-4}$ gauss for (c); and $1.67\text{x}10^{-3}$ gauss for (d) and (e). The near-vertical traces correspond to the calculated response during a pulse; in all cases it is the in-phase response which has been plotted. The convergence pattern for (d) has been displayed in figure 6.

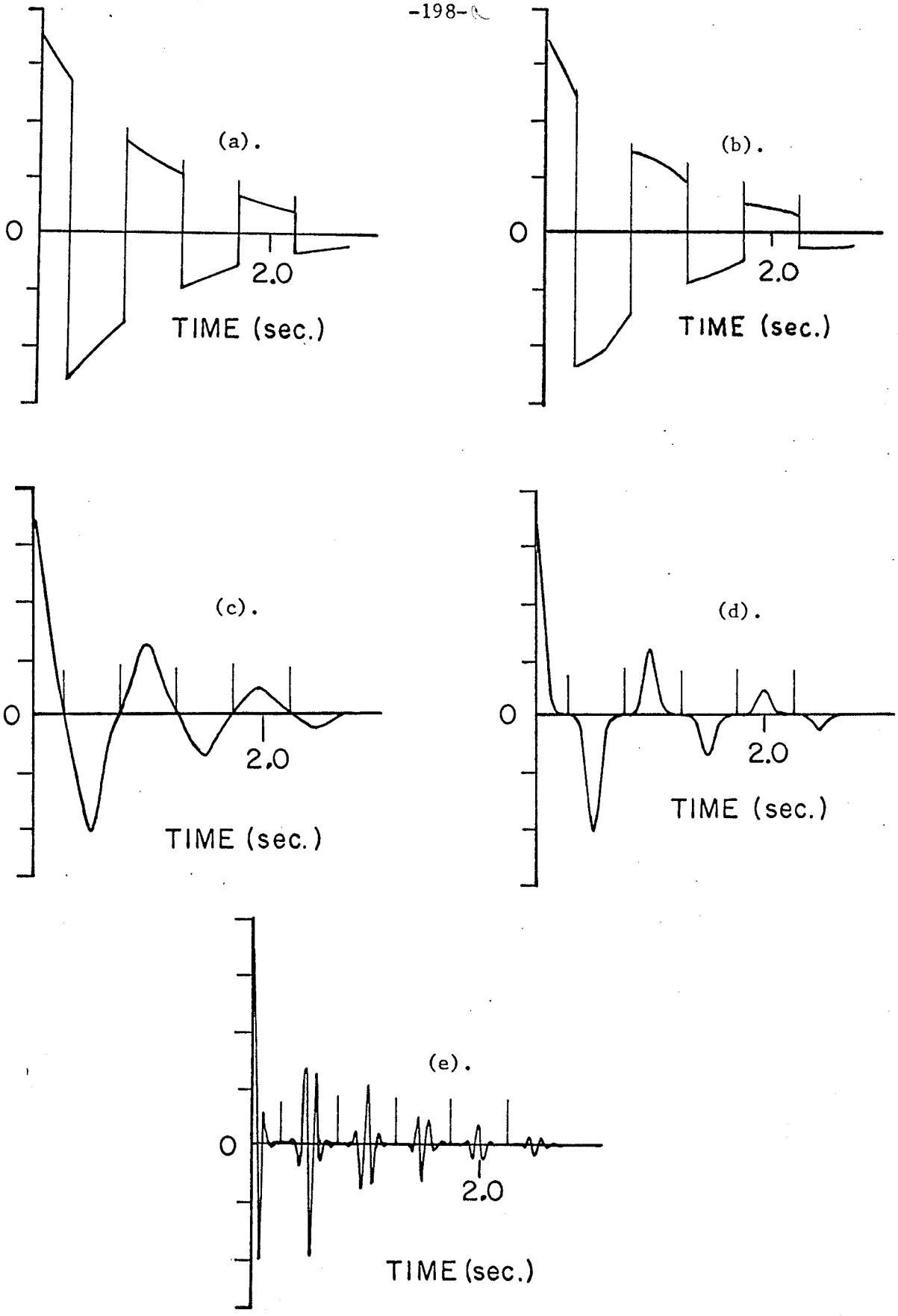
(a).
0
2.0
TIME (sec.)
(b).
0
2.0
TIME (sec.)
(c).
0
2.0
TIME (sec.)
(d).
0
2.0
TIME (sec.)
(e).
0
2.0
TIME (sec.)

Figure 51.

Simulations of the Carr-Purcell experiment applied to an AB system of nuclei, using model B, for different widths of an inhomogeneity distribution. The parameters are $H_o=10^4$ gauss, $\omega_1/2\pi$ = 42.577 megahertz, $\omega_2/2\pi = \omega_1/2\pi$ + 2.0 hertz, $J/2\pi$ = 1.0 hertz, and $T_1=T_2$ = 1.00 seconds. Plots (a) and (b) have the frequency of the pulsing field centered at ω_1, while for plot (c), $\omega_1'/2\pi = \omega_1/2\pi$ + 10.0 hertz. The amplitudes, durations and separations of the pulses are as for figure 50; as before the echo amplitude at the midpoint of two π pulses is independent of inhomogeneity. The inhomogeneity distribution is Gaussian and the widths 2w are $1.67\text{x}10^{-4}$ gauss for (a) and $1.67\text{x}10^{-3}$ gauss for (b) and (c). The near-vertical traces correspond to the calculated response during a pulse; in all cases it is the in-phase response which has been plotted. The convergence pattern for (c) has been displayed in figure 7.

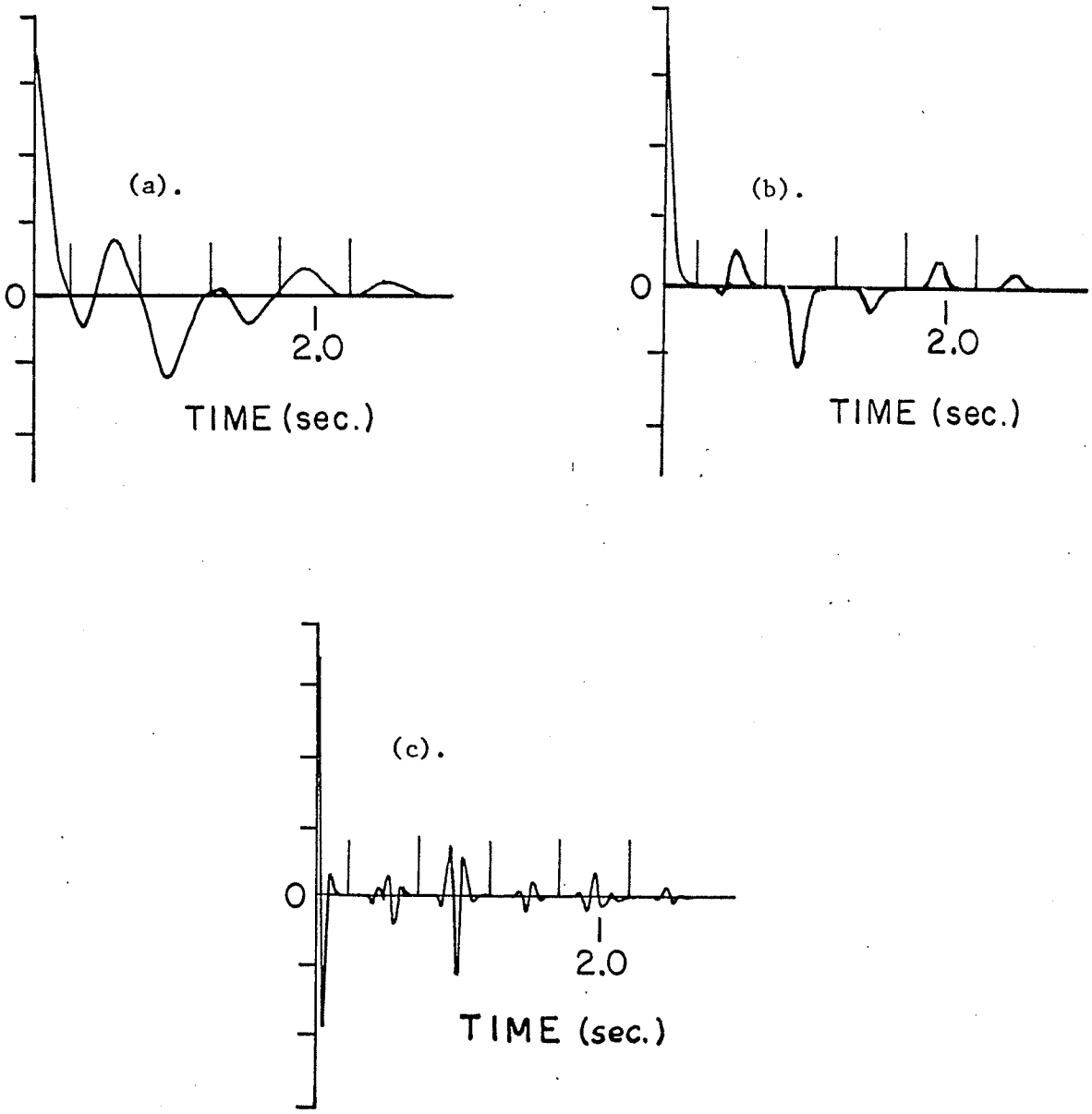
(a).
0
2.0
TIME (sec.)
(b).
0
2.0
TIME (sec.)
(c).
0
2.0
TIME (sec.)

display the effect of variations in the extent of inhomogeneity for a Carr-Purcell experiment. Since, however, the first pulse of the CP pulse sequence is the required $\pi/2$ pulse, the signal immediately following that pulse is a FID signal, and therefore the spectra in figures 50 and 51 show the first 0.25 seconds of the FID. In the perfectly homogeneous field used to evaluate 50a, it appears that the FID signal follows a simple exponential decay (an expected result), and the presence of a Gaussian distribution in 50b results in a faster rate of decay which follows a Gaussian-like curve. As the width of the inhomogeneity is increased to greater extents, the signal is attenuated still faster, and in 50d the entire FID signal is contained in the 0.25 second interval. Except for variations in scale due to the different relaxation times, the FID signals in figures 50d and 50e are qualitatively similar to 48a and 48b, respectively. Similar observations may also be made for the FID portion of the signals displayed in figure 51, and for the experimental spectra reproduced in figure 52.

3. Simulations of Some Spin-Echo Experiments.

The spectra reproduced in figures 50 and 51, as mentioned, are simulations of the CP pulse sequence applied to A_2 and AB systems of nuclei; only the first five echos have been calculated for $\tau = 0.25$ seconds. A few general observations are immediately apparent, and they are listed below.

(a) The near-vertical traces in figures 50 and 51 represent the actual response of the detector <u>during</u> the pulses (hidden in the vertical axis of the spectra in figures 48a, 49a and 49b is the response of the system to a $\pi/2$ pulse, when the magnetization is rotated from along

Figure 52.

Experimental spectra of the Carr-Purcell experiment applied to a single spin-1/2 system of nuclei. Plots (a) and (b) display the effect of inhomogeneity on the echo: for the more inhomogeneous field in (b), the echo is sharper. Plot (c) displays the observed pattern for the multishot experiment; note that the FID signal (following the first pulse) is Gaussian in form, and that the echo maxima follow an exponential decay curve (taken from Carr and Purcell (19)).

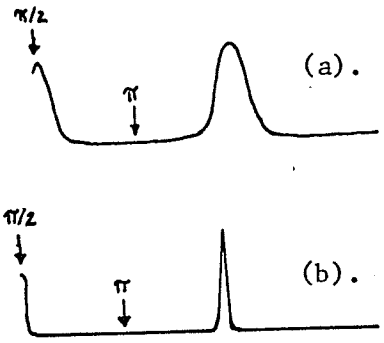
π/2
π
(a).
π/2
π
(b).

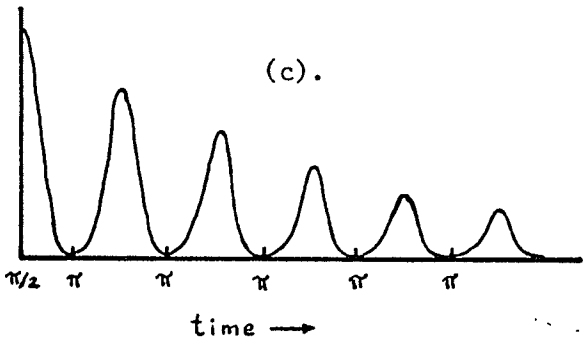
(c).
π/2
π
π
π
π
π
time

the z-axis into the y-axis). These effects are not observed experimentally (see, for example, the experimental plots in figure 52) since the detector is effectively saturated during the pulse (8) and no response may be detected.

(b) As the inhomogeneity width parameter 2w is increased, the echo is "sharpened"; this feature is also displayed in the experimental spectra in figures 52a and 52b.

(c) The different widths of the inhomogeneity distributions do not alter the relative amplitudes $|S(t=2n\tau)|$ as expected; for example at t = 2.0 seconds, the fourth echo, the amplitudes are identical for 50a to 50e or for 51a to 51c. Thus if one is interested only in the signals at those times, then they may be evaluated by executing the RKG procedure only once, that is for the "central" ensemble. The first spectrum in figure 50 is in fact the calculated signal from the "central" ensemble, which is then used in the calculations yielding the spectra 50b to 50d.

(d) The amplitudes $|S(t=2n\tau)|$ for the A_2 system in figure 50 decay exponentially at the rate $1/T_2$. This fact was also mentioned on page 193, and it is also displayed in the experimental spectrum 52c; note, however, that the simulated signals in figure 50 are for a phase-sensitive detector (as opposed to a diode detector in figure 52c), so that the echos alternate in sign at $t=2n\tau$.

(e) The amplitudes $|S(t=2n\tau)|$ for the AB system in figure 52 do not decay exponentially. This effect is well-known (2,4,8,19,20,23,24,29 80-83,108-112) and is a result of the presence of the coupling constant, which produces modulations in the echo envelope.

This last phenomenon yields a technique for the determination of the spin-spin coupling constant of multispin systems (see, for example, references (23) and (83)). Figure 53 displays in more detail the simulated echo envelope for the Carr-Purcell pulse sequence applied to an AB system of nuclei; from top to bottom the three plots represent the modulus of the signal at times $t=2n\tau$ for the first three echos ($n=1,2,3$), as a function of the pulse separation time τ. The calculations have been carried out for different values of T_2 using model B, but with inhomogeneity effects being ignored for the reasons discussed above.

The first two plots in figure 53 may be compared with those in figure 54, which are the envelopes of theoretical and experimental results obtained by Powles and Hartland (23) for the same AB system. Powles (82) has derived the expression (see also Appendix B)

$$|S(2\tau)| = |(\delta^2/R^2)\mathrm{Cos}J\tau + (J^2/R^2)\mathrm{Cos}R\tau\mathrm{Cos}J\tau + (J/R)\ \mathrm{Sin}R\tau\mathrm{Sin}J\tau|\ \exp(-2\tau/T_2) \qquad [5.3]$$

where $R=(\delta^2+J^2)^{1/2}$ and $\delta = (\omega_1-\omega_2)$, which describes the modulation of the first echo. The derivation of this equation assumes that relaxation may be accounted for in a phenomenological manner, and that the pulse durations are negligibly small (cf. Appendix B), so that relaxation may be ignored during the pulses. Equation [5.3] has been computed and compared with the first-echo-plots in figure 53 for different values of T_2, and in each case the agreement is excellent. Typically, with $T_2=100$ and for $\tau=0.5$ seconds, the simulation and [5.3] are identical to within about 0.05%. There is some

Figure 53.

Modulation of the echo envelopes for the first three echos of a Carr-Purcell experiment applied to an AB system of nuclei, obtained using model B but without consideration of inhomogeneity. The pulse sequence is $\pi/2$-τ-π-2τ(echo 1)-π-2τ(echo 2)-π-2τ(echo 3); the detector employed is a diode detector, and the parameters defining the pulses are as in figure 51 (with $\omega_1'=\omega_1$). Parameters for the spin system are $\omega_1/2\pi$ = 21.5 megahertz, $\omega_2/2\pi = \omega_1/2\pi$ + 3.97 hertz, $J/2\pi$ = 3.87 hertz, and the plots (a) to (c) have T_2 (and T_1) equal to 100.0, 0.40 and 0.20 seconds, respectively.

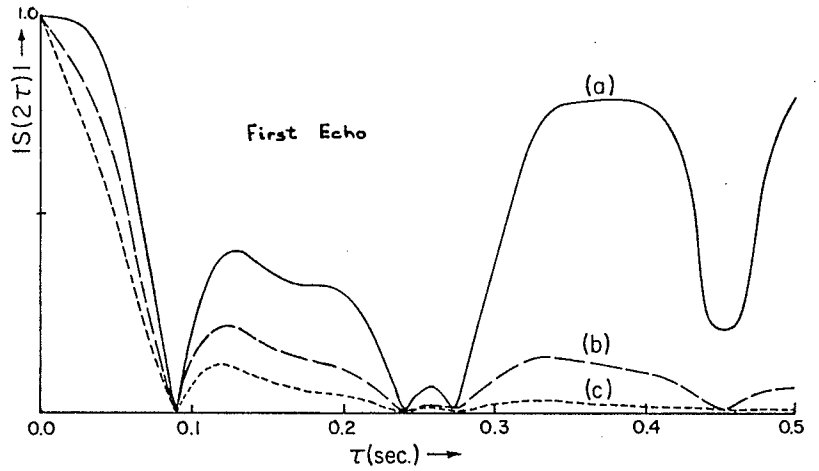
1.0
|S(2τ)| →
First Echo
(a)
(b)
(c)
0.0
0.1
0.2
0.3
0.4
0.5
τ(sec.) →

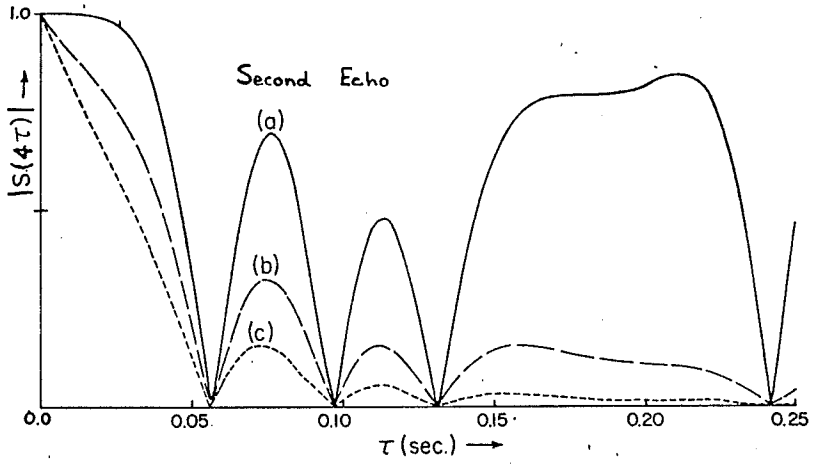
1.0
|S(4τ)| →
Second Echo
(a)
(b)
(c)
0.0
0.05
0.10
0.15
0.20
0.25
τ (sec.) →

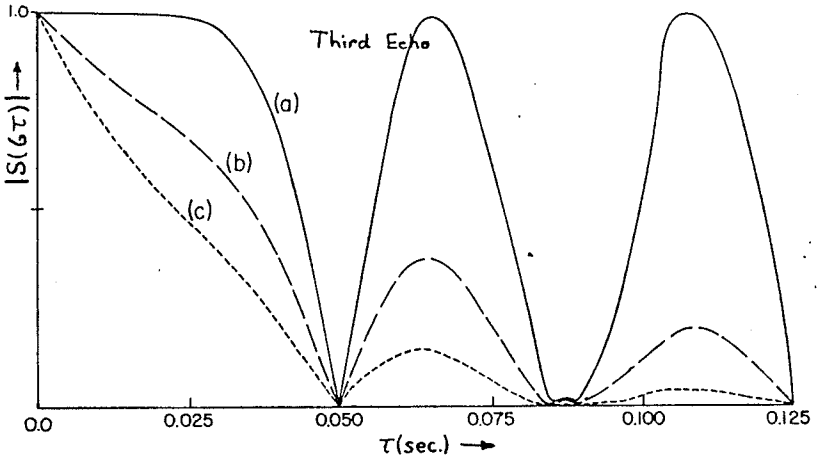
1.0
|S(6τ)| →
Third Echo
(a)
(b)
(c)
0.0
0.025
0.050
0.075
0.100
0.125
τ(sec.) →

Figure 54.

Modulation of the echo envelopes for the first and second echos of a Carr-Purcell experiment applied to an AB system of spin-1/2 nuclei, with the spectral parameters $\omega_1/2\pi$ = 21.5 megahertz, $|\omega_2/2\pi - \omega_1/2\pi|$ = 3.97 hertz and $J/2\pi$ = 3.87 hertz (cf. figure 53). The solid line represents the experimentally-determined modulation, and the dashed line is the calculated modulation with relaxation effects ignored (ie. equation [5.3] with $T_2 = \infty$) (taken from Powles and Hartland (23)). Note: the original plots were labeled on the vertical axis as "echo amplitudes" (23) (see text).

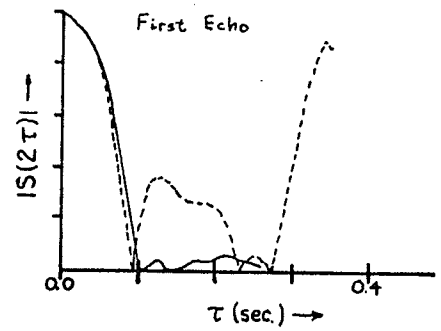
First Echo
|S(2τ)| →
0.0
0.4
τ (sec.) →

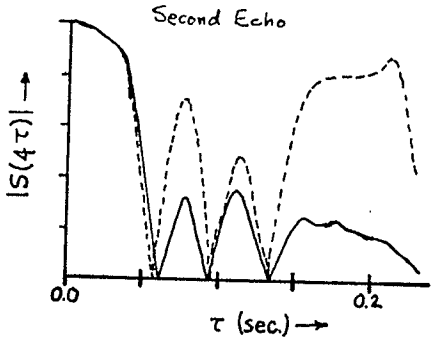
Second Echo
|S(4τ)| →
0.0
0.2
τ (sec.) →

divergence of the results for larger values of τ and for smaller values of T_2; this pattern may be explained by the fact that only the present calculations are able to account for relaxation during the pulses. Excellent agreement is also found between these simulations and the theoretical expressions of Powles and Hartland (23) for the second and third echos.

The experimental plots shown in figure 54 (the solid lines) are obviously not in good agreement with the theoretical plots (the broken lines), even if relaxation is taken into consideration as in figure 53. Powles and Hartland (23) have attempted to explain this disagreement in terms of sample impurities and attenuations due to diffusion (which is not simulated here). Another possibility is suggested by the plots in figure 51, where it is shown that the echo maxima do not always occur at the times $t=2n\tau$. Now some results presented in other papers (see, for example, Powles and Strange (47)) show experimental spectra on a much more compacted scale compared to, say, figure 51a or 52c, which suggest that the above fact may well have gone unnoticed[+]. If one assumes that this is the case, then

[+]the time scale is so compressed that the echos are very nearly vertical lines, and it would be difficult to estimate accurately the times $t=2n\tau$ in order to pick out the signal amplitudes $|S(t=2n\tau)|$. Note, however, that the original plots (23) reproduced in figure 54 are labeled along the vertical axis as "echo amplitudes" rather than specifying "echo amplitudes at time $t=2n\tau$". Hahn and Maxwell (80) have also reproduced similar plots for their $\pi/2$-τ-$\pi/2$ spin-echo

the experimental plots in figure 54 always overestimate the real value for $|S(t=2n\tau)|$, which is a step in the right direction for explaining the disagreement between experimental and theoretical results.

Similar plots and observations have been obtained for the CPMG experiment, using either a diode or a phase-sensitive detector. As mentioned previously, the CPMG and CP experiments may show some differences in the signs of the echo if a phase-sensitive detector is used; for example the second maxima of the first echo in figure 53 is actually negative for the CP experiment and positive for the CPMG experiment (using a phase-sensitive detector). Note, however, that the echos are not always positive for an AB system when one uses a phase-sensitive detector and the CPMG pulse sequence, in contrast to the same situation applied to an A_2 system.

This fact is displayed in figure 55, which represents a variation of the CPMG experiment applied to the same AB system as in figure 53. In this case, there is plotted the signal $S(t=2n\tau)$ as a function of the number, n, of the echo (recall that, in figure 53, the value of τ is varied and one plots $|S(t=2n\tau)|$ for the first echo, the second echo, etc., as a function of τ), for two different values of τ and for different relaxation times. Two important features are commented on below.

(a) for τ small, explicitly for $\tau << |J|^{-1}$ ($\simeq$0.04 seconds), there is

---

experiment, but the vertical axis is (suggestively) labeled "maximum echo amplitude" whilst their theory does not necessarily imply that the maxima occur at the times $t=2n\tau$ for any case other than a single spin-1/2 system of nuclei.

Figure 55.

Envelope of the echo amplitude at time $t=2n\tau$ vs n, the number of the echo, for a Carr-Purcell-Meiboom-Gill pulse sequence, employing a phase-sensitive detector. The spectral parameters are as in figure 53. The curves (a) and (d) have T_2 (and T_1) equal to 1.00 seconds with τ = 0.025 seconds and 0.050 seconds, respectively. Curves (b) and (c) have T_2 (and T_1) equal to 0.40 seconds and τ equal to 0.025 and 0.050 seconds respectively. Curves (a) and (b) show small deviations from an exponential curve (with characteristic times of 1.00 and 0.400 seconds, respectively).

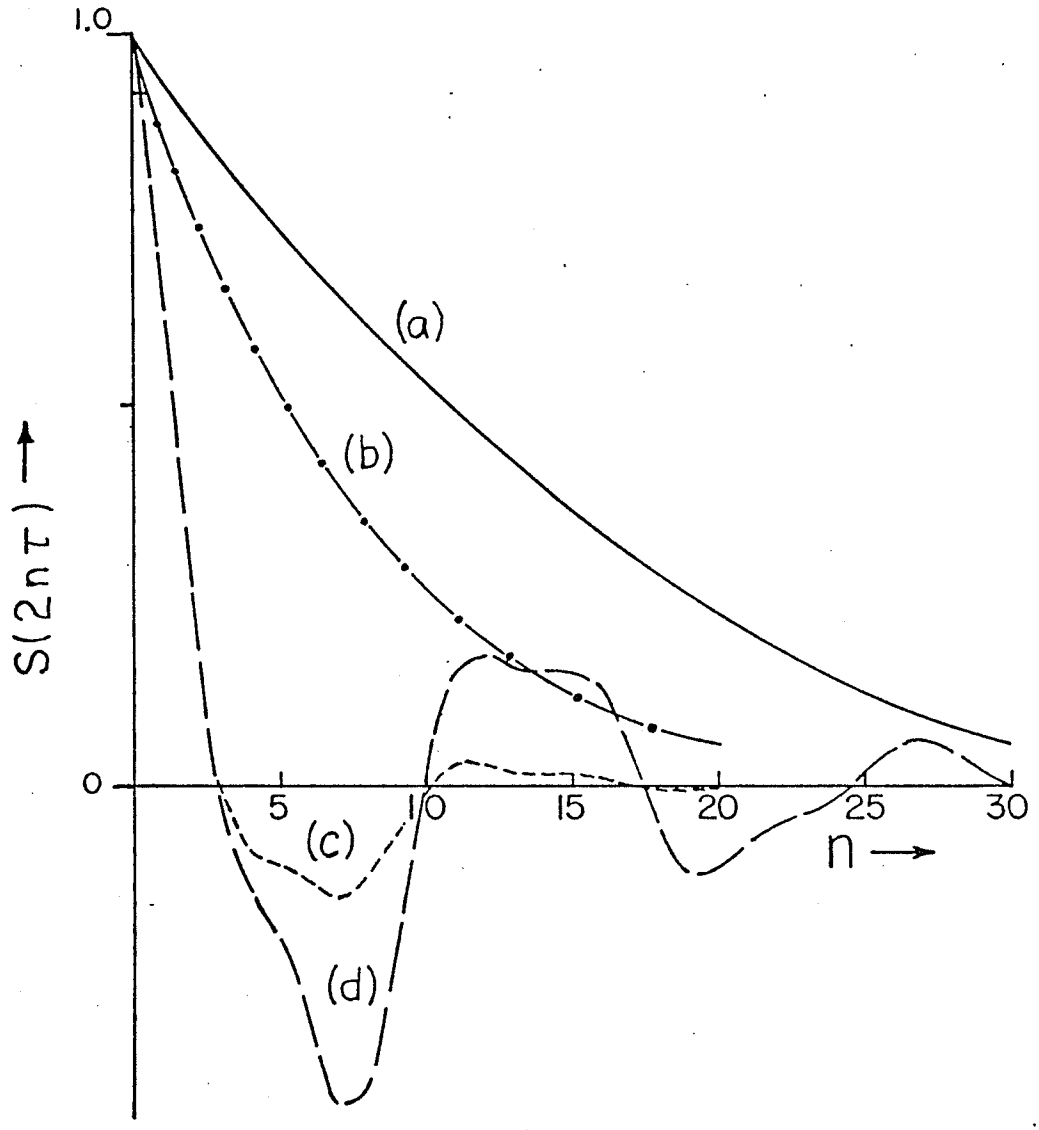
1.0
0
S(2nτ)
(a)
(b)
(c)
(d)
5
10
15
20
25
30
n

no apparent modulation of the echos[+], as shown in curves (a) and (b) of figure 55. Furthermore, the echo maxima decay at the rate $1/T_2$, as was observed (and as expected) for the case of an A_2 system of nuclei. A qualitative interpretation of this result obtains if one allows that, for τ small, the coupling constant does not have sufficient time to produce a large effect on the signal, and therefore the system resembles an A_2 system. A more quantitative argument follows from [5.3] by allowing that the product $J\tau$ approaches zero. (b) For τ large ($\tau > |J|^{-1}$), the usual situation reverts, that is there is not obtained an exponential decay but rather a modulation due to the effect of the spin-spin coupling constant. This is the case observed for the plots in figure 53 (and figure 54), although for the first portions of those plots, with τ small, the curves are exponential in nature.

Finally, it should be emphasized that the plots in figure 55 are not characteristic only of the CPMG pulse sequence. As before, one can also obtain similar plots for the CP experiment, except for some variations in the signs of the echos if a phase-sensitive detector is employed.

4. Simulation of a Partially-Relaxed Fourier Transform Experiment.

The last nonselective pulse experiment which will be discussed here is actually a variation of the π-τ-$\pi/2$ pulse sequence which has

---

[+]expanded plots of the curves (a) and (b) of figure 55 reveal small ripples on the exponential decays, since the value of $\tau = 0.025$ seconds does not quite satisfy the required inequality.

been mentioned elsewhere as a method for determining the spin-lattice relaxation time. Generally this method is limited to systems of magnetically equivalent nuclei, although recent extensions include the study of systems of uncoupled magnetically inequivalent nuclei (see, for example, references (8,61-62)) through an evaluation of the Fourier transform of the FID-like signal immediately following the $\pi/2$ pulse. These spectra are known as partially relaxed Fourier transforms, and in figure 56 there are reproduced simulations of this pulse sequence applied to an AB system of (coupled) nuclei (using model C, but with inhomogeneity introduced after the Fourier transformation of the signal from the central ensemble, using [3.63b]).

These results are readily interpreted by using the fact that a nonselective π pulse inverts the spin populations (cf. Appendix C) but does not create a net magnetization in the xy plane (except during the pulse). In the following time period of length τ seconds, therefore, only relaxation of the spin-lattice type occurs, and the longer τ the closer will the system approach its equilibrium configuration. This limit is almost reached in figure 56 for $\tau = 4.8$ seconds, so that the $\pi/2$ pulse acts on a system almost in thermal equilibrium, and one obtains the usual Fourier transform spectrum. At the other limit, for τ very small, the pulse sequence approaches the FID experiment which utilizes a $3\pi/2$ pulse, and once again one obtains the usual Fourier transform spectrum but with inverted intensities (unless a diode detector is employed). The intermediate transforms in figure 56 display the effects obtained when the spin system is in intermediate stages

Figure 56.

Calculated partially-relaxed Fourier transform spectra of the FID signal following the $\pi/2$ pulse in a nonselective π-τ-$\pi/2$ sequence of pulses applied to an AB system of spin-1/2 nuclei, for various pulse separation times (using model C but with the effects of inhomogeneity included after the Fourier transform of the "central" ensemble, using [3.63b]). The parameters are $H_o=10^4$ gauss, $\omega_1/2\pi$ = 42.577 megahertz, $\omega_2/2\pi = \omega_1/2\pi + 2.0$ hertz, $J/2\pi$ = 1.0 hertz, and an RFC relaxation mechanism with $\omega_s/2\pi$ = 0.096 hertz and η = 0.0 for (a), and η = 0.333 for (b). The amplitude and duration times for the pulses are as for figure 49, and all spectra are given with a Lorentzian distribution of inhomogeneity with a full width at half-height of 0.12 hertz. The zeroes of the frequency scales are at the Larmor frequency ω_1, the scales of the horizontal axes are 1.0 hertz/division and the direction of increasing frequency is as indicated by the arrow (ie. nucleus B resonates to the left of nucleus A; left corresponding to a higher frequency).

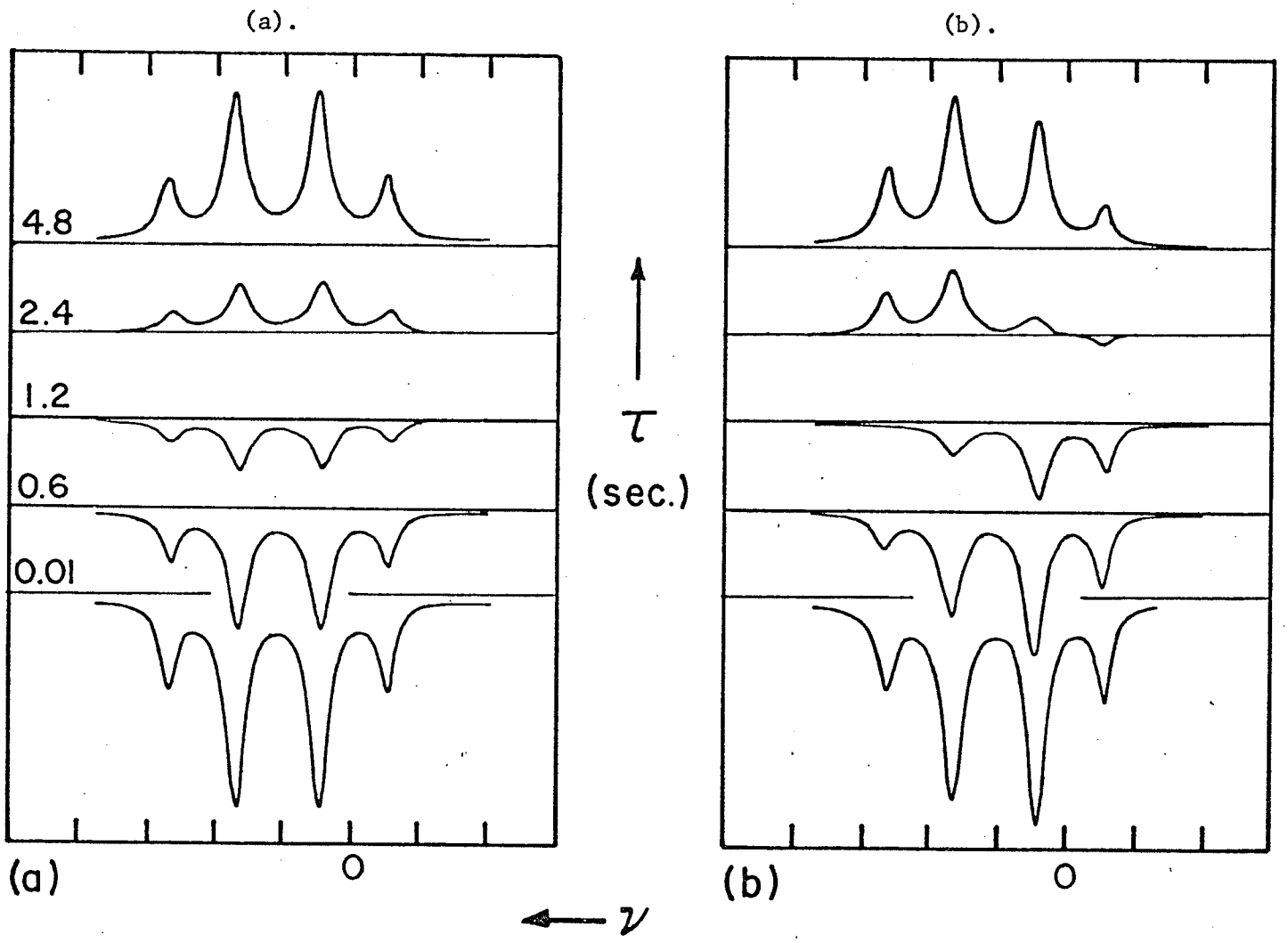
(a).
(b).
4.8
2.4
1.2
0.6
0.01
τ
(sec.)
(a)
0
(b)
0
ν

in its approach to thermal equilibrium.

The differences between the spectra in 56a and in 56b follow from the types of relaxation mechanisms causing the spin-lattice type relaxation. In figure 56b, the parameter η is greater than zero, which corresponds to the fact that the B nucleus interacts more strongly with the external random field than does the A nucleus (cf. equation [2.27b]). This is reflected in the corresponding expressions for the rate of relaxation of the spin states (whose populations are the diagonal elements of the spin density matrix; the required expressions have been given in Table II), and subsequently, therefore, in the Fourier transform spectra. Note, for example, that the two "A" transitions (near the zero of frequency) relax less quickly than do the two "B" transitions. On the other hand, the spectra in 56a do not show any similar asymmetry since the parameter $\eta = 0$, and therefore both nuclei relax at the same rate. This latter pattern is also to be expected (and has been observed) for the DD mechanism and for any external isotropic random field mechanism with $\eta = 0$.

It is believed that similar experimental spectra for a coupled spin system have not been published, likely because of difficulties in calculating theoretical spectra and/or in interpreting the results. Nevertheless this simple nonselective pulse experiment could prove useful in the determination of the strength of interactions and the asymmetry parameter for the mechanisms discussed in Table II (and, probably, for other relaxation mechanisms). The present technique allows a method whereby the experiment may be simulated; however a more practical approach to the problem would probably require a more

workable method for describing the intensity changes of each transition as a function of the pulse separation time τ. Some possibilities come immediately to mind: for example one could express the relaxation parameters in terms of generalized longitudinal relaxation times (17,85), or else one could derive appropriate rate equations for the populations in the same manner as did Freeman, Wittekoek and Ernst (113) for their related selective pulse experiment. These possibilities must be examined however, and the present dynamic technique for the calculation (simulation) of response allows an applicable method for the testing of the accuracy of a given approximation.

To sum up this section, it is worthwhile to briefly sum up the advantages afforded by this dynamic technique. A number of different pulse experiments have been simulated; in each case the solution procedure was essentially identical and most of the restrictive assumptions required by other methods of calculation were not required. Thus this technique is both more general and more accurate than are the other methods of calculation. This led to a plausible explanation of some difficulties observed with the fitting of echo envelopes for a Carr-Purcell experiment applied to a multispin system, for example, since the entire signal is calculable here. In addition, this dynamic technique allows the simulation of experiments which are yet to be performed; one example which was calculated suggests a new approach to the study of relaxation mechanisms (in fact no other method of calculation allows the incorporation of the more theoretical models for the description of relaxation; cf. Appendix B).

E. Simulation of a Selective Pulse Experiment.

A recent publication by Freeman, Wittekoek and Ernst (113) offers a final, more sophisticated test of the dynamic technique developed in this dissertation for the calculation of response in NMR. The pulse experiment is selective in the sense that only one transition in an AB system of spin-1/2 nuclei is perturbed by the pulses (cf. Appendix C), and the parameters defining the pulses exclude the possibility of using the methods developed for nonselective pulses for any calculations of this experiment.+

The first effect to be considered is that due to inhomogeneity in H_o. Shown in figure 57 are two spectra representing the calculated signal deriving from a sequence of selective pulses applied to one transition of an AB system of nuclei. Figure 57a is the response of the "central" ensemble; that is it represents the response of a system in a perfectly homogeneous static magnetic field. The spectrum 57b is the calculated response of the same system in a Lorentzian distribution of inhomogeneity, and two major differences are apparent:

(a) the oscillations, which are attributed to the presence of near-neighbour lines (63,113), are attenuated by the presence of the inhomogeneity, an intuitive result; and

(b) there is an apparent "overshoot" of the π or 2π pulses which is enhanced for the inhomogeneous calculations. This feature is explained

---

+principally because relaxation may not be ignored during the pulses, which may last for several seconds or longer. Freeman and Wittekoek (63) have presented some calculations for simple spin systems, using the Bloch equations (and which may not be extended).

Figure 57.

The effect of inhomogeneity on a selective pulse sequence applied to an AB system of nuclei. The parameters are $\omega_1/2\pi$ = 60.0 megahertz, $\omega_2/2\pi = \omega_1/2\pi$ + 20.8 hertz, $J/2\pi$ = 5.7 hertz, and a relaxation mechanism which is an independent combination of the isotropic random field mechanism and the intramolecular dipole-dipole mechanism with $\omega_s/2\pi$ = 0.00249 hertz, r = 0.67, η = -0.0416 and T_D = 87.8 seconds. At position I, a 2π pulse of amplitude 0.1045 milligauss, duration 2.0 seconds and frequency $\omega_1'/2\pi = \omega_1/2\pi$ + 18.33 hertz establishes the equilibrium magnetization of the transition at that frequency (the innermost "B" transition or line 3 in figure 2). After the system has re-established equilibrium, at position II, a π pulse of the same amplitude and frequency but of duration 1.0 seconds inverts the populations of the spin states connected by that transition. One second later, at position IV, the magnetization at that frequency is rendered observable by another 2π pulse with the parameters as before. This pulse sequence is used to determine $R_o(X,\overline{X})$ (see text). Figure 57a is the response from the "central" ensemble (ie. a perfectly homogeneous field), and 57b is the net signal from a Lorentzian distribution of ensembles whose full width at half-height is 0.12 hertz (using [3.65]). The oscillations appearing in the calculated response are attributed to the presence of neighbouring transitions (113); no "filtering" has been included in these simulations.

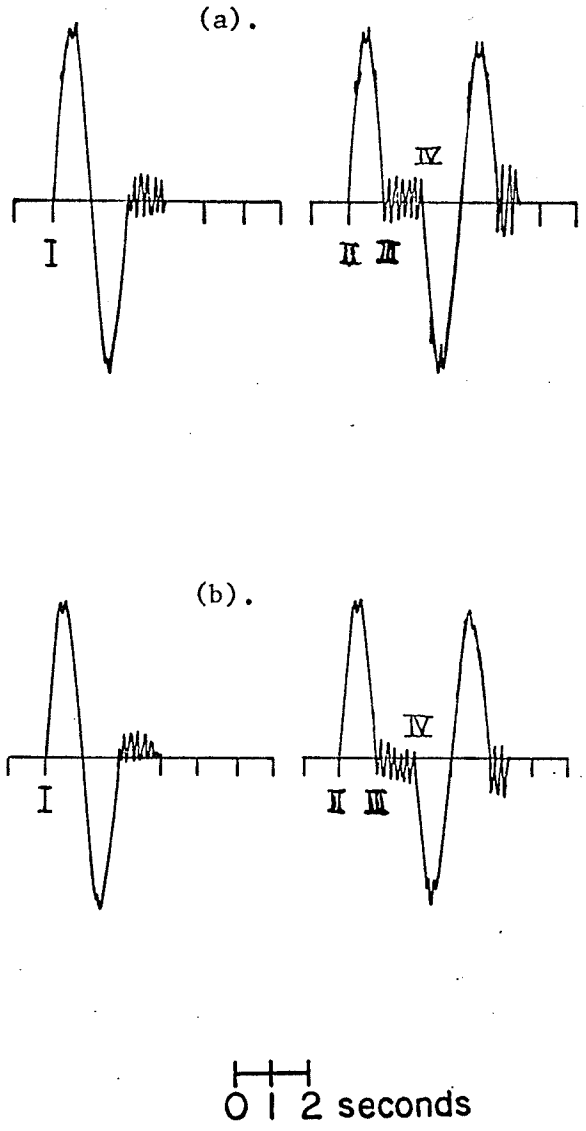
(a).
I
II III
IV
(b).
I
II III
IV
0 1 2 seconds

by Freeman and Wittekoek (63) in terms of the inhomogeneity; however a certain amount of "overshoot" also occurs in the case for a perfectly homogeneous field. This last case is readily explained by the fact that the equation

$$\gamma_i H_1 \lambda_{ij} \tau = \tau\pi \qquad (\tau=1 \text{ or } 2 \text{ seconds})$$

defining the pulse (cf. Appendix C) is derived by ignoring the effect of relaxation during the pulse. Therefore some overshoot should occur since the magnetization being rotated is subject to relaxation and since the above equation does not account for this fact.

The spectra presented in figure 57b and in figure 58 are simulations of a selective pulse experiment used to characterize the nature of the relaxation processes in an AB system of spin-1/2 nuclei (113). The method employs a selective π pulse applied to and inverting the populations across one transition (cf. Appendix C); one then monitors the magnetization appearing either at that same transition and/or at another transition by means of a selective 2π pulse. Some equations have been developed (113) relating the rate of recovery to equilibrium of the inverted populations, in terms of the mechanisms previously discussed in Chapter II. It is then assumed that the initial rate of recovery, $R_o(X,\overline{Y})$, of transition X to an inversion of transition Y has a simple exponential solution, and a series of measurements of $R_o(X,\overline{Y})$ has led to an elucidation of the relaxation parameters (113).

In each of the spectra, the first response amplitude during a selective 2π pulse, starting at position I, is used to determine the equilibrium magnetization of the line X which is being monitored. After the system has regained thermal equilibrium, a selective π pulse inverts the populations

Figure 58.

Simulation of a selective pulse sequence applied to an AB system of nuclei, using model C. The parameters are as for figure 57 (except for some pulse parameters described below), and in each case a Lorentzian distribution of inhomogeneity with $2w = 0.12$ hertz has been assumed. As for figure 57, a 2π pulse at position I establishes the equilibrium magnetization of the transition at frequency $\omega_1/2\pi + 18.333$ hertz. At position II, a π pulse of amplitude 0.1045 milligauss for (a) and of amplitude 0.1369 milligauss for (b) inverts the populations across the transitions progressively and regressively connected to that transition, respectively (the pulse duration is 1.00 seconds). During this π pulse, the frequency of the pulsing field, relative to $\omega_1/2\pi$, has been altered to 2.467 hertz for (a) (the innermost "A" transition or line 2 in figure 2) and to -3.233 hertz for (b) (the outermost "A" transition or line 1 in figure 2). At position III, the detector is again referenced to the transition at frequency 18.333 hertz (the innermost "B" transition or line 3 in figure 2), and four seconds later a 2π pulse of amplitude 0.1045 milligauss and of duration 2.00 seconds (as before) monitors the magnetization at that frequency. These experiments are used to measure $R_o(X,\bar{Y})$ where X and Y are progressively and regressively connected, respectively, in plots (a) and (b). The oscillations appearing in the response is attributed to the presence of neighbouring transitions (113) (see also the experimental spectra in figure 59).

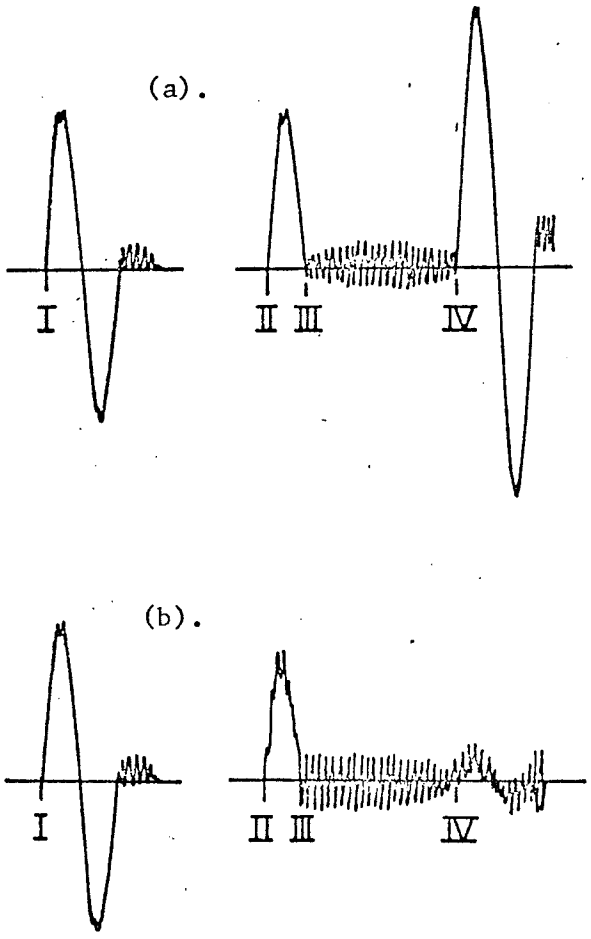
(a).
I
II III
IV
(b).
I
II III
IV
0 1 2 seconds

across transition Y, and at position III, the detector is again referenced to the frequency of transition X. Finally, at position IV, the magnetization at transition X is monitored by means of a selective 2π pulse. This sequence of events is repeated experimentally for different values of τ, where it must be assumed that τ is small enough so that the points thereby obtained lie on that part of the solution where $R_o(X,\overline{Y})$ follows an exponential curve.

The patterns displayed in figures 57 and 58 are readily interpreted in terms of the energy level diagram in figure 2. In each case, the monitored "X" transition is line 3, and one inverts the populations across transitions 3, 2 and 1, respectively, in figures 57, 58a and 58b. For the simulation in 57a, the signal observed at position IV is initially in the negative direction and it is slightly weaker than is the signal at position I; these features are consistent with the fact that the inverted populations have partially relaxed towards equilibrium. The simulations 58a and 58b show, respectively, the monitored response of line 3 after the transitions progressively and regressively connected have been "inverted", and consequently the corresponding signals are enhanced and attenuated, in that order, relative to the equilibrium signal. Figures 58a and 58b are meant to be simulations of the experimental spectra reproduced in figures 59a and 59b, and on comparison it may be seen that there is good qualitative agreement even though some of the guessed parameters are probably erroneous (for example the type and the width of the inhomogeneity distribution, the pulse separation times τ, etc.; note in particular that Freeman et. al. (113) use experimental methods to

Figure 59.

Experimental spectra for a selective sequence of pulses applied to an AB system of spin-1/2 nuclei. The spectral parameters and the pulse parameters are as for figure 58 (but see the discussion in the text); in particular 58a is meant to be the simulated response for the experimental situation yielding 59a, and 58b is meant to correspond to 59b. Note that the scale in 59a and 59b is not constant (as is the case for 58a and 58b); the response to the first 2π pulse should be identical for both (a) and (b) if the scales are identical. Note also that the position III in these plots does not exactly correspond to the position III in figure 58. Taken from Freeman, Wittekoek and Ernst (113).

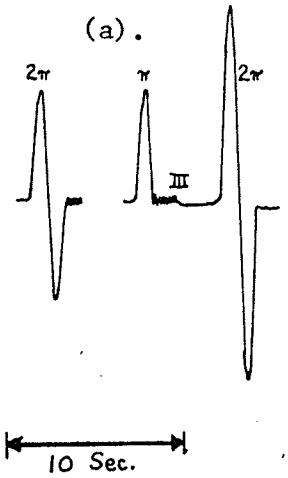
(a).
2π
π
2π
III
10 Sec.
(b).
2π
π
2π

determine a π or 2π pulse). Obviously more thorough calculations are required if quantitative comparisons are to be made; however for even qualitative agreement this dynamic technique represents a unique method for the calculation of these experiments. More quantitative calculations might also be in order since Freeman et. al. (113) point out that their equations for $R_o(X,\overline{Y})$ are derived assuming an exponential solution for τ small. They validate this assumption through a series of consistency checks and error comparisons, however this dynamic method offers a (unique) direct check of their equations through a simulation of the actual experimental conditions. In addition, this method would allow the calculation of the entire recovery envelope, including any non-exponential sections.

CHAPTER VI. CONCLUSIONS

1. Introduction.

In the preceding discussion, a dynamic method has been presented for the calculation of response in high-resolution NMR. The spin system has been described using the spin density matrix formalism, outlined in Chapter II, and two general types of models were mentioned for the description of relaxation effects. The first model is phenomenological in origin, while the second model derives from a more theoretical approach and is explicitly dependent on the type of interactions responsible for the relaxation. In fact the technique is independent of the actual model employed; for example one could also obtain dynamic solutions to the Bloch equations by the same general method.

In Chapter III, the high-resolution NMR Hamiltonian was discussed, and the spin density matrix formalism was more completely described by specifying the perturbation Hamiltonians characterizing a number of experiments. The concept of inhomogeneity of the static magnetic field was also taken into consideration, and methods for its inclusion were explored.

The actual dynamic method for the solution of the pertinent differential equations was discussed in some detail in Chapter IV. It was noted there that the major problem, from the viewpoint of required computational time, was the solution of an initial value problem which represents an NMR experiment. The Runge-Kutta-Gill algorithm was chosen to solve this problem, and the convergence characteristics of the routine were described. A number of numerical approaches

for the solution of related problems were also presented.

Finally, in Chapter V, the dynamic technique was put to a practical test. A variety of the more common NMR experiments were simulated, and a general conclusion is that these simulations and, in fact, the associated theory describing a system of spins, are accurate in the prediction of the observed response of a spin system to a variety of experimental conditions. The calculations were restricted to systems of two spin-1/2 nuclei (nominally protons), and not all the possible experimental variations were simulated. It is felt, however, that in general this dynamic technique may be applied to the calculation of any spin system, subjected to virtually any experimental conditions, with the principal practical consideration being that of the computer time required.

2. Extensions of the Simulations.

With respect to this last pragmatic consideration, a few general comments are in order. First of all, it is apparent that the Bloch-Wangsness-Redfield equations are required for the exact description of relaxation in NMR. This model, however, is somewhat undesirable since the resultant initial value problems are somewhat more complex and as a result more computer time is required. For this reason, the phenomenological model may be more convenient to employ for the description of relaxation, provided that it describes relaxation effects with sufficient accuracy. It was shown that the phenomenological models (both A and B) were adequate for the calculation of cw line shapes in the unsaturated limit or when relaxation effects dominate any effects

due to inhomogeneity in the static magnetic field. These models are also found to be adequate for most of the pulse experiments which have been simulated. Extensions to more complex spin systems are therefore readily realized by the choice of this relatively simple model for relaxation[+], provided that one desires only a qualitative description of relaxation (and inhomogeneity), or providing that any inherent limitations of that model are not exceeded.

The numerical problems may also be made more feasible, with respect to computer time, for the calculation of response in more complex spin systems by introducing various approximations into the equations for a given model. Two distinct possibilities are immediately suggested, one of which is the reduction of the order of the set of differential equations describing the equation of motion of the spin density matrix. This may be accomplished, for example, by assuming weak rf fields (ie. no saturation) so that the diagonal elements of ρ may be approximated by their corresponding values for thermal equilibrium (ie. their corresponding differential equations are "solved" by means of a partial steady-state approximation). Alternatively (or in addition), if some or all of the transitions are well-separated, then only a few of the off-diagonal elements need be considered at a given position of the frequency (see Appendix B for example): the corresponding differential

---

[+]detailed studies of relaxation are usually limited to simple spin systems (cf. reference (18)). It was shown in section V.B that the major differences between the phenomenological models and the theoretical models appear as (slight) variations in transition intensities.

equations of the remaining elements may be set to zero and/or ignored completely (near that frequency). It follows that, since the order of the set of differential equations is reduced, the required execution time will also be reduced (by a factor proportional to the cube of the order of the system of equations).

The second possibility is that the actual set of differential equations may be altered or rearranged so that the eigenvalues of the Jacobian are smaller in magnitude. This led to the use of the interaction representations as opposed to, for example, the equivalent expressions in the Schrödinger representation. In addition, the differential equations were modified for some double resonance simulations by invoking the AX approximation, which gave identical results but at a considerable saving in execution time (for the RKG routine). This last approximation is in fact not entirely limited to AX systems; similar approximations might be successfully applied to an AB system. The "extended" AX approximation, for example, deals with the perturbation Hamiltonian (while the usual AX approximation is concerned with the high-resolution NMR Hamiltonian), and the simplifications made for the double resonance of the AX system, which may then be applied to an AB system, correspond to allowing that only one of the two nuclei is "aware" of the perturbing rf field. It follows that computer execution time is again reduced (particularly for the RKG routine) since these simplifications reduce the order of magnitude of the eigenvalues of the Jacobian (but without affecting the accuracy of the simulations).

Finally, the numerical problems might be made more feasible by the use of other methods of solution. There are, for example, many

different numerical methods for the solution of an initial value problem, aside from the RKG method. Unfortunately the complicated nature of the NMR problem does not lend itself to a preliminary guess at a "best" numerical method; for example for the integration routine one must proceed by trial in order to find an alternate scheme whose convergence characteristics and computer requirements are better than the RKG algorithm.

It might therefore be concluded that not only are extensions to the calculation of more complex spin systems possible in principle, but also that they should be achieved without the need for a dedicated computer. To this end, the dynamic method outlined in this thesis should find use whenever other methods of calculation of response fail or are insufficiently accurate. One novel application of the dynamic method was described in Chapter V, where the spectra for a partially-relaxed Fourier transform pulse sequence were calculated in advance of similar experimental results. This aspect opens up a whole new realm of applications, namely the simulation of an experiment before it is attempted experimentally in order to determine whether or not that experiment will prove useful. One important area for this application is the field of selective pulse experiments; the dynamic method presented here is uniquely capable of the calculation of the response of a multispin system to a sequence of selective pulses. One interesting possibility, for example, is a selective π pulse followed τ seconds later by a nonselective $\pi/2$ pulse and a Fourier transformation. From a first analysis of the energy level diagram, one predicts that the resultant spectra (for an AB system)

would resemble the spectra in figure 56 except that only one transition would be inverted, while the regressively and progressively connected transitions would show significant intensity changes (recall that the selective π inverts only a pair of populations). The exact response of this experiment, including the effects of inhomogeneity, may be calculated in order to determine whether or not the spectra are sensitive enough to a given relaxation mechanism so that relaxation studies are feasible. One may readily suggest other similar pulse sequences in anticipation of the development of experimental techniques enabling their realization.

Aside from the simulation of the NMR experiment, this dynamic technique may also be applied (and has been applied) to other problems. The principal feature of the method derives from the fact that a given differential equation need not be solved by the assumption of a steady-state condition, and the principal reason for its success is that one has available high-speed computers for the numerical solutions. It does not take a great deal of foresight to predict the rapid growth of similar calculations.

APPENDICES.

A. The Spin Angular Momentum Vector Operators[+]

Although the exact nature of the source of the magnetic moment is not fully understood, it is well-known that the phenomenon may be described by a vector quantity called the spin angular momentum vector operator $\underline{I}$. The properties of $\underline{I}$ are obtained by analogy with the orbital angular momentum operator, and one has the definitions

$$\underline{I} = (I_x, I_y, I_z) \qquad [A.1]$$

with the commutation relations

$$\begin{aligned} [I_x, I_y] &= i I_z \\ [I_y, I_z] &= i I_x \\ [I_z, I_x] &= i I_y \end{aligned} \qquad [A.2]$$

where i is the imaginary number, $I^2 = I_x^2+I_y^2+I_z^2$, and the units are taken to be $\hbar$. It follows that I^2 and only one of the components of $\underline{I}$ possess a complete set of simultaneous eigenvectors. By convention, I_z is the component chosen; I_x and I_y must then be given by expectation values.

The description of spin angular momenta deviates here from the development of orbital angular momentum since there is no classical analogue for the eigenstates of spin angular momentum. It is possible,

---

[+] more complete discourses may be found in a number of references (for example (2,122,123)). The discussion here lists briefly the more important equations which are required in this thesis.

however, to generate a complete set of eigenvectors using the raising and lowering operators $I_{\pm}$ defined by

$$I_{\pm} = I_x \pm i I_y \qquad [A.3]$$

and obeying the commutation relations

$$\begin{aligned} [I_{\pm}, I^2] &= 0 \\ [I_{\pm}, I_{\mp}] &= \pm 2 I_z \\ [I_z, I_{\pm}] &= \pm I_{\pm} \end{aligned} \qquad [A.4]$$

It can be shown that, given an eigenvector $|a,b\rangle$ with a the eigenvalue of I^2 and b the eigenvalue of I_z, the following important relations hold (2,122,123):

$$I_{\pm} |a,b\rangle = [(a-b)(a\pm b+1)]^{1/2} |a,b\pm 1\rangle \qquad [A.5]$$

and that $a=I(I+1)$ where I is the spin quantum number and $b=m$ where m is the magnetic quantum number with permissible values $m=-I,-I+1, \ldots I-1$, or I. The raising and lowering operators generate new eigenstates of I^2 and I_z such that the eigenvalue of I_z is increased or decreased by unity. The generation process may be repeated until $m= \pm I$, at which point $I_{\pm} |I,m=\pm I\rangle = 0$, by definition. The eigenvalue equations for I^2 and I_z may be therefore be written as

$$\begin{aligned} I^2 |I,m\rangle &= I(I+1) |I,m\rangle \\ I_z |I,m\rangle &= m |I,m\rangle \end{aligned} \qquad [A.6]$$

where the complete set of 2I+1 (symbolic) eigenvectors $|I,m\rangle$ of I_z are orthogonal. A system with the spin quantum number I=1/2, for example, is spanned by two eigenvectors, commonly denoted as $|\frac{1}{2},\frac{1}{2}\rangle =$

$|\alpha\rangle$ and $|\tfrac{1}{2},-\tfrac{1}{2}\rangle = |\beta\rangle$, and the order of the "spin-space" is two.

Finally, these commutation relations may be used to derive some useful transformations. One important transformation, for example, is that given by the unitary operator $\exp(i\phi I_z)$, for which (2,17,122)

$$\begin{aligned}
\exp(i\phi I_z)\, I_{\pm}\, \exp(-i\phi I_z) &= \exp(\pm i\phi)\, I_{\pm} \\
\exp(i\phi I_z)\, I_x\, \exp(-i\phi I_z) &= I_x \cos\phi - I_y \sin\phi \\
\exp(i\phi I_z)\, I_y\, \exp(-i\phi I_z) &= I_x \sin\phi + I_y \cos\phi \\
\exp(i\phi I_z)\, I_z\, \exp(-i\phi I_z) &= I_z \,.
\end{aligned} \qquad [A.7]$$

When $\phi = \omega_1 t$, this transformation is that to the familiar rotating frame, often used to simplify the NMR Hamiltonian.

For systems with more than one spinning nucleus, the total spin angular momentum is given by vector addition rules. Using the subscript j to correspond to the j'th nucleus, then for a system of N nuclei possessing spin angular momentum,

$$\underline{I} = \sum_{j=1}^{n} \underline{I}_j \,. \qquad [A.8]$$

One can then derive commutation relations similar to [A.2] and [A.4], but with the definition that

$$[I_{jr},\ I_{ks}] = 0 \quad j\neq k;\ r,s=x,y,z,+,- \qquad [A.9]$$

ie. operators corresponding to different nuclei commute. The eigenvectors of $I_z = \sum_j I_{jz}$ and $I^2 = \underline{I}\cdot\underline{I}$ are now given by tensor products of the eigenstates for each I_{jz} and $I_j^{\,2}$; one denotes, for example, an eigenstate by $|I_1,m_1;I_2,m_2;\cdots\rangle$, with

$$\begin{aligned}
I_{jz}\, |I_1,m_1;I_2,m_2;\ldots.\rangle &= m_j\, |I_1,m_1;I_2,m_2;\ldots.\rangle \\
I_j^{\,2}\, |I_1,m_1;I_2,m_2;\ldots.\rangle &= I_j(I_j+1)\, |I_1,m_1;I_2,m_2;\ldots.\rangle
\end{aligned} \qquad [A.10]$$

These equations are somewhat simplified for a system of two spin-1/2 nuclei, which is the case of interest here. The $2^N=4$ eigenvectors are commonly denoted as $|\alpha\alpha>$, $|\alpha\beta>$, $|\beta\alpha>$ and $|\beta\beta>$, where it is understood that the first symbol within the ket applies to the first nucleus and the second symbol to the second nucleus. The matrix representations of I_z and I^2 may be readily evaluated, yielding:

$$I_z = \begin{bmatrix} 1 & 0 & 0 & 0 \\ 0 & 0 & 0 & 0 \\ 0 & 0 & 0 & 0 \\ 0 & 0 & 0 & -1 \end{bmatrix} \qquad I^2 = \begin{bmatrix} 2 & 0 & 0 & 0 \\ 0 & 1 & 1 & 0 \\ 0 & 1 & 1 & 0 \\ 0 & 0 & 0 & 2 \end{bmatrix} . \qquad [A.11]$$

The eigenvalues of I^2 are therefore (2,2,2,0) with the corresponding eigenvalues of I_z equal to (1,0,-1,0). One then has two spin-spaces with I=0 or I=1 and spanned by one or three eigenvectors of I_z, respectively.

Although the use of the corresponding eigenvectors of I_z and I^2 diagonalize their matrices, it is often convenient to work in the basis product set $|\alpha\alpha>$, $|\alpha\beta>$, etc. mentioned above. This basis set yields simple matrix representations of I_+ and I_-; for example

$$I_+ = \begin{bmatrix} 0 & 1 & 1 & 0 \\ 0 & 0 & 0 & 1 \\ 0 & 0 & 0 & 1 \\ 0 & 0 & 0 & 0 \end{bmatrix} \qquad I_- = \begin{bmatrix} 0 & 0 & 0 & 0 \\ 1 & 0 & 0 & 0 \\ 1 & 0 & 0 & 0 \\ 0 & 1 & 1 & 0 \end{bmatrix} . \qquad [A.12]$$

It is also possible to deduce extensions to equations like [A.7] for systems of more than one spin; for example the unitary transformation $\exp(i\phi I_z)$ yields an equation identical with [A.7], but with

all components I_z, I_+, etc. now being given by summations like [A.8]. The more complex transformation $\exp(i\phi I_y)$ to an interaction representation may also be simplified, yielding equations of the form:

$$\exp(i\phi I_y)\ I_{\pm}\ \exp(-i\phi I_y) \quad = \quad \sum_j \exp(i\phi I_j)\ I_{j\pm}\ . \qquad [A.13]$$

Equations like the transformations [A.7] and [A.13] will find important applications in the manipulations of the high-resolution NMR Hamiltonian.

B. Methods of Solution Using the Steady-State Approximation.

The signal in an NMR experiment is given by the trace of the spin density matrix with the raising operator

$$S \propto \mathrm{tr}\ (\rho\ I_+)\ \exp(-i\omega_1' t) \quad . \qquad [B.1]$$

This expression reduces to a number of off-diagonals ρ_{ij} which must be evaluated from the equation of motion in order to calculate S. As shown previously, the problem is often transformed to an interaction representation in which most of the time-dependence of the transformed spin density matrix ρ^i is removed; this resultant expression is set to zero by invoking the steady state approximation. In the following discussion, a number of different NMR experiments are described using this approximation, with the objective being to present some simple closed analytical expressions for their observables.

1. Single Resonance.

In the rotating frame, the signal for an AB system of two spin-1/2 nuclei is given by equation [2.35]

$$S(\omega) \qquad \rho^r_{21} + \rho^r_{31} + \rho^r_{42} + \rho^r_{43} \qquad [B.2]$$

with respect to the basis product set, and where the superscript "r" denotes the rotating frame. The required expressions for the equation of motion and the Hamiltonians are given in [3.20] and [3.21], with

$$H_p{}^r = \sum_n \omega_n/2\ (H_p/H_o)\ (I_{n+} + I_{n-}) \simeq \omega_p\ (I_+ + I_-) \quad [B.3]$$

where $\omega_p = \omega_1/2\ (H_p/H_o) \simeq \omega_2/2\ (H_p/H_o)$. For weak rf fields (ie. no saturation effects or $\omega_p << 1/T_1, 1/T_2$), it is possible to approximate the commutator $[\ \rho^r, H_p{}^r]$ by the expression

$$[\rho^r, H_p{}^r] \simeq [\rho^o, H_p{}^r] . \qquad [B.4]$$

ρ^o may be approximated by equation [3.12], yielding

$$[\rho^r, H_p{}^r] \simeq C\,(I_- - I_+) \qquad C=(\hbar\omega_{12}\omega_p)/(2ZkT) \qquad [B.5]$$

using [A.4], [A.9] and [B.3].

The remainder of the commutator, $[\rho^r, H^r]$, may be evaluated directly, and the resultant equations for the elements in [A.1] are

$$\begin{aligned}
(\rho_{21}^r)^{\cdot} \equiv 0 &= -\rho_{21}/T_2 + i[\rho_{21}(-\Delta-\delta/2+J/2)-\rho_{31}J/2+C] \\
(\rho_{31}^r)^{\cdot} \equiv 0 &= -\rho_{31}/T_2 + i[\rho_{31}(-\Delta+\delta/2+J/2)-\rho_{21}J/2+C] \\
(\rho_{42}^r)^{\cdot} \equiv 0 &= -\rho_{42}/T_2 + i[\rho_{42}(-\Delta+\delta/2-J/2)-\rho_{43}J/2+C] \\
(\rho_{43}^r)^{\cdot} \equiv 0 &= -\rho_{43}/T_2 + i[\rho_{43}(-\Delta-\delta/2-J/2)-\rho_{42}J/2+C]
\end{aligned} \qquad [B.6]$$

where the derivatives are set equal to zero using the steady-state approximation and where the substitutions $\Delta=(2\omega_1'-\omega_1-\omega_2)/2$ and $\delta = (\omega_1-\omega_2)$ have been introduced. Note also that the superscripts "r" have been dropped and that relaxation has been described using the phenomenological model [2.12].

These equations are linear in the required elements of ρ^r for the signal, and since only pairs are coupled, it is a simple matter to obtain analytical solutions. The absorption mode signal, for example, is

$$\begin{aligned}
S_{abs}(\omega_1') &\propto \text{Imag}\,(\rho_{21} + \rho_{31} + \rho_{42} + \rho_{43})/(C/T_2) \\
&\propto \sum_{\mathbf{s}} (2\Delta^2 \mp 4\Delta J + \delta^2/2 + 2J^2)/N(\pm)
\end{aligned} \qquad [B.7a]$$

where $N(\pm) = \Delta^4 \mp 2\Delta^3 J + \Delta^2(-\delta^2/2+J^2+1/T_2^2) \pm \Delta(\delta^2 J/2 - 2J/T_2^2) + \delta^4/16+(\delta^2+J^2)/2T_2^2+1/T_2^4$ [B.7b]

and where the symbol $\sum_s$ is meant to indicate that the two terms in [B.7] with upper and lower signs are to be added.

In the AX limit ($|J| \ll |\delta|$), equations [B.6] and [B.7] simplify: upon ignoring the off-diagonal elements in H_p^r and evaluation of the commutator, one obtains equations of the form+

$$(\rho_{21}^r)^{\cdot} \equiv 0 = -\rho_{21}/T_2 + i[\rho_{21}(-\Delta-\delta/2+J/2) + C)] \quad [B.8]$$

for each off-diagonal in [B.2]. Since the equations are not coupled, the absorption mode signal is simply

$$S_{abs}(\omega_1') \propto \frac{T_2}{1+(-\Delta-\delta/2+J/2)^2T_2^2} + \frac{T_2}{1+(-\Delta+\delta/2+J/2)^2T_2^2} + \ldots . \quad [B.9]$$

The signal then consists of four peaks of equal intensity at the frequencies $\Delta=\pm\delta/2\pm J/2$, and each with a half-height line width of $2/T_2$ seconds^{-1} (compare with [1.4]). Furthermore, provided that the transitions are non-degenerate and well-separated (ie. $2/T_2$ is less than the frequency difference between adjacent transitions), then each transition $|i> \rightarrow |j>$ may be associated with one of the off-diagonal elements ρ_{ij}^r, since only the term for that element has a maximum at that frequency. For the above AX case, the following pairings

---

+note that the "B" transition ρ_{21} is in fact independent of the Larmor frequency of the A nucleus since $-\Delta-\delta/2 = \omega_B-\omega_1'$.

between a transition frequency Δ and a matrix element ρ^r_{ij} are readily found: ($\rho^r_{43} \rightarrow \Delta=-\delta/2-J/2$), ($\rho^r_{21} \rightarrow \Delta=-\delta/2+J/2$), ($\rho^r_{42} \rightarrow \Delta=\delta/2-J/2$), and ($\rho^r_{31} \rightarrow \Delta=\delta/2+J/2$). Assuming that $\delta>J>0$, then these transitions are listed in the order of figure 2, proceeding from right to left.

Note that if the relaxation is described using the theoretical models, then the above off-diagonals are, in general, coupled by their relaxation terms. If, however, the transitions are well-separated, then one expects a result similar to [B.9]; the appropriate relaxation parameters for the expected half-height line widths have been listed in Table II for the relaxation models of interest here (compare with the discussion of Hoffman (17), section VI, B).

For more complicated spin systems in the unsaturated limit, analytical solutions are difficult to obtain since more than just pairs of elements are coupled. Once again, however, for well-separated transitions, Hoffman (17) has shown that the absorption mode signal may be put in the form of [B.9]

$$S_{abs} \propto \sum_{\alpha} \sum_{\alpha'} \frac{|\langle\alpha'|I_+|\alpha\rangle|^2 \, R^{-1}_{\alpha\alpha'\alpha\alpha'}}{1 + R^{-2}_{\alpha\alpha'\alpha\alpha'} \, (\omega_{\alpha\alpha'} - \omega_1')^2} \qquad [B.10]$$

where the indices α and α' represent eigenstates of the static Hamiltonian H and $\omega_{\alpha\alpha'} = H_{\alpha\alpha} - H_{\alpha'\alpha'}$. The appropriate elements appearing in [B.1] are selected from the double summation by the term $\langle\alpha'|I_+|\alpha\rangle$ and the $R_{\alpha\alpha'\alpha\alpha'}$ are the Redfield relaxation matrix elements (or that term premultiplying $\rho_{\alpha'\alpha}$ in $(\partial\rho_{\alpha'\alpha}/\partial t)_{relax}$). [B.10] reduces to [B.9] for an AX system; in particular $R_{\alpha\alpha'\alpha\alpha'} = -1/T_2$ for all $\alpha \neq \alpha'$.

When the perturbing rf field is allowed to be large enough to produce saturation effects, the equations again become quite complex

even for simple spin systems. Since the approximation [B.5] is no longer valid, for example, one finds terms of the form

$$(\rho_{21}^{r})^{\cdot} \equiv 0 = -\rho_{21}/T_2 + i[\rho_{21}(-\Delta-\delta/2+J/2)-\rho_{31}J/2 + \omega_p(\rho_{23}-\rho_{41}+\rho_{22}-\rho_{11})] \quad . \qquad [B.11]$$

The list of elements required for the signal, in general, are coupled to every other element of the spin density matrix, and the solutions are much more difficult to obtain. Hoffman (17) has derived some simple expressions, assuming the "simple-line" approximation (4) which allows that only one transition (including any multiple-quantum transitions) is perturbed by the rf field at any time (ie. a variation of the "well-separated" transitions approximation). These expressions are as for [B.10] except that there appear, in the denominator, the extra term

$$\omega_p^2 \, |\langle\alpha'|I_+|\alpha\rangle|^2 T_{2\alpha\alpha'} \, T_{1\alpha\alpha'} \qquad [B.12]$$

(compare with equation [1.4]). Here $-T_{2\alpha\alpha'} = R^{-1}_{\alpha\alpha',\alpha\alpha'}$, and the term $T_{1\alpha\alpha'}$ is a "generalized longitudinal relaxation time" (4,17,85) which is, in general, a function of the decay rates for <u>each</u> energy level (for the simple phenomenological model, $T_{2\alpha\alpha'} = T_2$ and $T_{1\alpha\alpha'} = T_1$). Another similar approximation[+] is possible which allows simple expressions for multiple quantum transitions (17). If, for example, the double quantum transition of a system of nuclei is well-separated from

[+] all transitions, including multiple quantum transitions, are "well-separated" in the sense that the half-height line widths are much smaller than frequency differences between adjacent transitions.

the single-quantum transitions, then the absorption signal follows an expression of the form (17)

$$S_{abs} \propto \sum_{\gamma}\sum_{\gamma'} \frac{(\tfrac{1}{2}T_{2\gamma\gamma'})|K_{\gamma\gamma'}|^2}{1 + (\tfrac{1}{2}\omega_{\gamma\gamma'},-\omega_1')^2(\tfrac{1}{2}T_{2\gamma\gamma'})^2} \qquad [B.13a]$$

where $$K_{\gamma\gamma'} = \left| \sum_{\beta} \frac{\langle\gamma|I_+|\beta\rangle\langle\beta|I_+|\gamma'\rangle}{\omega_{\gamma\beta} - \omega_{\beta\gamma'}} \right|^2 \qquad [B.13b]$$

and where two quanta of frequency $\tfrac{1}{2}\omega_{\gamma\gamma'}$ are required to give the double quantum transition. The line width at half-height is related to $\tfrac{1}{2}T_{2\gamma\gamma'}$ as opposed to $T_{2\alpha\alpha'}$ for a single quantum transition. It can be shown that the only nonzero element of K for a system of two spin-1/2 nuclei is K_{14}, that is the transition connects $|\alpha\alpha\rangle$ with $|\beta\beta\rangle$. The corresponding spin density matrix element is ρ^r_{41} which becomes large for $\Delta=0$, and consequently the elements appearing in the expression for the signal also become finite through coupling with ρ^r_{41} (refer to equation [B.11]). It can also be shown that $K_{14} \to 0$ as the AX limit is approached (ie. the double quantum transition is forbidden for an AX system) and that the element ρ^r_{32} has no physical significance (17).

It should be pointed out that there is not much to be gained by equations like [B.10] or [B.13] since similar results may be obtained using the simpler indirect approach. For more general applications, only the density matrix description will yield accurate results for the line shapes of a spectrum. It becomes clear, however, that general analytical solutions for the single resonance signal, even for simple two spin-1/2 systems, are often not known. Consequently one must resort to numerical methods of solution of the simultaneous linear equations

(see for example references (13,16,17,65,66,98,99,102))[+]

$$d\rho^r/dt \equiv 0 = i[\rho^r, H^r] + (\partial\rho^r/\partial t)_{relax}. \quad [B.14]$$

The order of this system of equations is in general n^2 where n is the number of spin states; for example an AB system of spin-1/2 nuclei (N=2) requires the solution of $n^2=2^{2N}=16$ simultaneous equations. The problem simplifies in the unsaturated limit, for example the AB case described above reduced to a system of four simultaneous equations. It has been shown that (17), in general, the number of coupled equations to be solved in the unsaturated limit equals the number of allowed single resonance transitions. Finally, it should be repeated that the steady-state approximation allows the identity on the lhs of [B.14], and that this approximation effectively restricts the description of the NMR single resonance experiment to those employing (infinitely) slow passage conditions.

2. Double Resonance.

The double resonance experiment calls for the use of two rf fields, one of which is usually strong enough to compete with the relaxation. In light of the preceding section, it appears that analytical solutions are difficult to obtain, even for simple spin systems, and therefore this discourse will be concerned only with an outline of the steps by which the numerical problems are obtained.

[+]these equations are actually linearly dependent by virtue of $tr(d\rho^r/dt) = 0$; however one of the equations for $(d\rho^r_{ii}/dt)$ may be replaced by the equation $tr(\rho^r) = 1$ (the normalization condition).

The general technique for the description of the double resonance experiment involves the approximation that ρ may be partitioned as

$$\rho \simeq \rho^{o} + \chi(t) + \eta(t) \qquad [B.15]$$

where $\chi(t)$ and $\eta(t)$ describe the deviation from equilibrium of the spin density matrix, caused by the presence of the perturbing and observing rf fields, respectively. In a frame rotating at the frequency of the second (perturbing) rf field, one has that H^{r2} is time-independent (see equations [3.26] to [3.28]), and a logical approximation is that χ^{r2} is also stationary. This is certainly true for $H_1^{r2}=0$ (ie. there is only one rf field; compare with equation [B.14]) so that this approximation yields

$$\rho^{r2} = \rho^{o} + \chi^{r2} + \eta^{r2}(t). \qquad [B.16]$$

Suppose for the moment that the observing field is zero, and hence that $\eta(t)=0$; the steady state approximation then yields the linear simultaneous equations (cf. [B.14])

$$d\rho^{r2}/dt = d\chi^{r2}/dt \equiv 0 = i[\chi^{r2}, H^{r2} + H_2^{r2}] - i\,C'\,[H_o, H_2^{r2}] + (\partial\rho^{r2}/\partial t)_{relax} \qquad [B.17]$$

where $C'=\hbar/ZkT$ (using the first expansion term [3.12] for ρ^{o}). Equation [B.17] represents n^2 simultaneous equations in the elements of χ (but recall the footnote on the previous page) which may be solved by numerical techniques (cf. references (88,89,104-107)).

If it is now allowed that the observing field is nonzero, but that [B.16] and solutions to [B.17] are valid, then one has

$$d\rho^{r2}/dt \simeq d\eta^{r2}/dt \simeq i[\eta^{r2}, H^{r2}+H_2^{r2}] + i[\rho^{r2}, H_1^{r2}]$$

$$(\neq 0) \qquad + (\partial\rho^{r2}/\partial t)_{relax} \qquad [B.18]$$

using [B.16], [B.17] and [3.27]. Another steady-state approximation is now obtained (18) by assuming that the diagonal elements $\eta_{\alpha\alpha}$ vanish while the off-diagonals vary according to[+]

$$\eta^{r2}_{\alpha\alpha'} = Y^{+}_{\alpha\alpha'} \exp(i\omega' t) + Y^{-}_{\alpha\alpha'} \exp(-i\omega' t) \qquad [B.19]$$

where $\omega'=\omega_1'-\omega_2'$ and where the $Y^{+}_{\alpha\alpha'} = (Y^{-}_{\alpha\alpha'})^{*}$ are time-independent. With these assumptions and using [B.18], one obtains yet another set of simultaneous linear equations in the elements $\eta^{r2}_{\alpha\alpha'}$, upon performing the differentiation called for in [B.18] using [B.19]. Not all these elements must be solved for, however, since the signal in this representation picks out only a few off-diagonals (as before):

$$S \propto tr\,(\rho I_+) \exp(-i\omega_1' t) = tr\,(\rho^{r2} I_+^{r2}) \exp(-i\omega_1' t)$$

$$= tr\,(\rho^{r2} I_+) \exp(-i\omega' t) \; . \qquad [B.20]$$

The signal is therefore proportional to only some of the off-diagonals of ρ^{r2}; these elements consist of a time-independent contribution from the matrix χ^{r2} and two oscillating contributions (at $\pm\omega'$) from $\eta^{r2}(t)$. After demodulation, according to [B.20], the net signal then consists of a stationary signal (from η^{r2}) upon which is superimposed signals oscillating at the frequencies $\omega_1'-\omega_2'$ and $2(\omega_1'-\omega_2')$ (from η^{r2} and χ^{r2}). For the usual experimental arrangement in double resonance, the

[+]not valid if the observing field is strong enough to produce saturation effects. This case has been discussed in the literature (89,107).

signal of interest[+] is the stationary part which is extracted by means of a narrow-pass band filter; for the steady-state calculations one merely picks out the appropriate terms in $\eta^{r2}_{\alpha\alpha'}$, (ie. one performs, effectively, a Fourier analysis of the signal; cf. reference (99)). The method developed in this thesis could not proceed so directly since the net signal consists of a set of points as a function of time and since the frequency ω_1' is time-dependent. The actual procedure employed is in fact closely related to the filter used in a conventional double resonance spectrometer.

Once again the indirect method may be used to evaluate the double resonance transition frequencies and intensities (cf. reference (77)), but at the expense of a suitable description of the interactions causing relaxation. The steady-state approximations required for the direct method also restrict the calculated line shapes to the slow passage limit, and in addition the equations [B.16] and [B.19] may not always represent valid approximations.

3. The First Echo of the Carr-Purcell Pulse Sequence.

In the ensuing discussion, the procedure for the calculation of the modulation of the first echo envelope in a Carr-Purcell experiment is presented (a similar development exists for the Carr-Purcell-Meiboom-Gill pulse sequence). Although the steady-state approximation

[+] the signal at $\omega_1'-\omega_2'$ is a strong beat deriving from the experimental arrangements; the signal at $2(\omega_1'-\omega_2')$ has been observed with some difficulty (139).

as described for the cw experiments will not be required, it will be shown that very similar approximations are required, with the result that the derived expressions are limited with respect to their range of applicability.

A schematic diagram is shown below for the Carr-Purcell pulse sequence, with the superscripts A, B, etc. on ρ referring to the spin density matrix at various times in the sequence (all equations are given in the rotating frame, but the superscript "r" has been omitted for convenience of notation). At time t=0, for example, ρ^A is assumed to be the equilibrium spin density matrix:

$$\rho^A \simeq 1/Z \ (\mathbb{1} - C I_z) \qquad [B.21]$$

using the results of equation [3.12].

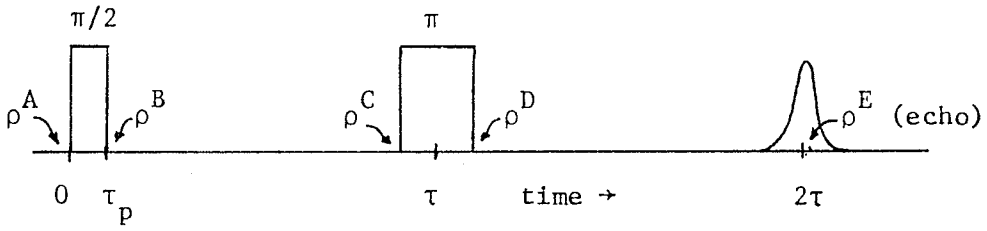

Exactly at time t=0, a nonselective $\pi/2$ pulse is applied to this system; it is assumed that the amplitude and duration of the pulse satisfy equations [3.41] and [3.42]; ie. during the pulse only the Hamiltonian describing the pulsing field is important and relaxation effects are negligible (a partial steady-state approximation) Now, since H_p^r is time-independent in the rotating frame, a formal solution obtains for ρ immediately after the pulse (cf. Slichter (7)):

$$\rho^B = \exp(-iH_p^r\tau_p) \ \rho^A \exp(iH_p^r\tau_p) \qquad [B.22]$$

where $H_p^r \simeq \omega_p I_x$ is the pulse Hamiltonian and τ_p is the pulse duration time (the former expression for H_p^r is a simplification of [3.18a], involving the assumption of homonuclear systems). This last equation may be rewritten, using [B.21] and some commutation rules, in the form

$$\rho^B = 1/Z - C(-I_y \, \mathrm{Sin}\omega_p\tau_p + I_z \, \mathrm{Cos}\omega_p\tau_p)$$

$$= 1/Z + C \, I_y \qquad [B.23]$$

assuming that C<<1 and, in the last step, that $\omega_p\tau_p=\pi/2$. Thus the effect of this pulse is to produce small off-diagonal terms in the spin density matrix, and one predicts that the out-of-phase mode of the signal is nonzero while the in-phase mode is everywhere zero (for an AB system of spin-1/2 nuclei, an application of [B.2] yields $S \propto 4iC$; this signal is not detectable experimentally since the receiver coil is "saturated" by the pulse (8)).

In order to solve for ρ^C, the spin density matrix between the pulses, it is necessary to solve the equation of motion

$$d\rho^C/dt = i \, [\rho^C, \, H_o^r + H_c^r] + (\partial\rho/\partial t)_{relax} \qquad [B.24]$$

where the Hamiltonians are the usual high-resolution NMR Hamiltonians and with the initial condition that $\rho^C(t=\tau_p \simeq 0) = \rho^B$. Ignoring the effects of relaxation for the moment, this last equation is similar to the situation leading to [B.22]; ie. the Hamiltonian is time-independent, and therefore a formal solution for ρ^C is, simply,

$$\rho^C \simeq \exp\,[-i(H_o^r+H_c^r)\tau] \; \rho^B \; \exp[i(H_o^r+H_c^r)\tau] \qquad [B.25]$$

setting $t=\tau+\tau_p \simeq \tau$ so that ρ^C is now the spin density matrix just <u>before</u> the second pulse. It is apparent that inclusion of relaxation terms

will make a similar analytical solution much more difficult to realize, and the usual procedure (reference (24), for example) is to add a dissipative term, such as the phenomenological relaxation model discussed in Chapter II. If all the nuclei have the same spin-spin relaxation time, for example, then all the off-diagonal elements of ρ^C are modified to the form $\rho^C \cdot \exp(-t/T_2)$ and one predicts a free induction decay signal (for $\tau_p < t < \tau$) which decays at the rate $1/T_2$ (ignoring the effects of inhomogeneity). Another more convenient method for the inclusion of relaxation effects is to add a similar term to the final expression for the signal, as shown below.

A second pulse is applied at time $t=\tau$; it has the same amplitude as the preceding pulse but the pulse duration time is twice as long (but still much less than τ or the relaxation times). This pulse is therefore a π pulse, and using the same procedure as for the first pulse, one obtains

$$\rho^D \simeq \exp(-i\pi I_x)\ \rho^C \exp(i\pi I_x) \ . \qquad [B.26]$$

Finally, τ seconds later, at time $t=2\tau$, ρ^E is given by

$$\rho^E \simeq \exp[-i(H_o^r+H_c^r)\tau]\ \rho^D \exp[i(H_o^r+H_c^r)\tau] \ . \qquad [B.27]$$

The signal amplitude at time $t=2\tau+3\tau_p \simeq 2\tau$ is therefore given by

$$|S(t=2\tau)| \propto |\mathrm{tr}\ (\rho^E I_+)\ \exp(-2\tau/T_2)| \qquad [B.28]$$

where relaxation effects have been included in a phenomenological manner (note that the trace involves only the off-diagonal elements of ρ^C so that only a spin-spin relaxation time is required).

The evaluation of this trace is relatively straight-forward but

exceedingly tedious, and the result, for an AB system of spin-1/2 nuclei is (4,23,50)

$$|S(2\tau)| = \left|(\delta^2/R^2)\mathrm{Cos}J\tau + (J^2/R^2)\mathrm{Cos}R\tau\mathrm{Cos}J\tau + (J/R)\mathrm{Sin}R\tau\mathrm{Sin}J\tau\right| \exp(-2\tau/T_2) \qquad [B.29]$$

where $R=(\delta^2+J^2)^{1/2}$ and $\delta=\omega_1-\omega_2$. An important point to note here is that, although the trace in [B.27] is dependent on the magnitude of the static magnetic field (in the Larmor frequencies ω_i), the final result for the signal in [B.29] does not carry this dependence. This indicates that the effects of inhomogeneity of the static magnetic field are thwarted when one employs this pulse sequence (or the Carr-Purcell-Meiboom-Gill modified pulse sequence) and when only the signal at time $t=2\tau$ is calculated.

Similar applications of the above procedure may be followed for more complex spin systems or for different pulse sequences, although the extraction of a simple expression for the signal quickly becomes a formidable task. Hence the procedure is effectively limited to only a few special cases; furthermore the above restrictions limit the calculations to nonselective pulse sequences for which the effects of inhomogeneity are negligible (or are nullified at some time in the experiment), and for which the effects of relaxation may be described by a phenomenological model.

C. Selective Pulse Experiments.

1. Definition.

From the viewpoint of experimental requirements, the most accessible type of selective pulse experiment is that involving a heteronuclear spin system. Consider, for example, an AX system of spin-1/2 nuclei where $|J| << |\omega_A - \omega_X|$ and where the frequency ω of the pulsing rf field is near ω_A but far from ω_X. The Hamiltonian for this system in the rotating frame is given by the expression

$$\begin{aligned} H_s^r &= (\omega_A-\omega) I_{Az} + (\omega_X-\omega) I_{Xz} + J I_{Az} I_{Xz} + \omega_1 I_{Ax} + \omega_2 I_{Xx} \\ &\simeq (\omega_X-\omega) I_{Xz} + \omega_1 I_{Ax} + \omega_2 I_{Xx} \end{aligned} \qquad [C.1]$$

where $\omega_1 = \gamma_A H_1$ and $\omega_2 = \gamma_X H_1$. In the last step, it is assumed that (during a pulse) $\omega_1, \omega_2 >> |\omega_A - \omega|, J$ so that their corresponding terms may be neglected. If the system is initially in thermal equilibrium, then the effect of a pulse of duration τ_p on the equilibrium spin density matrix is given by the equation

$$\rho^r = T \rho^o T^{-1} \qquad [C.2]$$

where $$T = \exp[-i(\omega_1 I_{Ax} + \omega_2 I_{Xx} + (\omega_X-\omega) I_{Xz})\tau_p] \qquad [C.3]$$

(cf. Appendix B, section 3), and where it is assumed that

$$\tau_p << T_1, T_2 \qquad [C.4]$$

so that the effects due to relaxation may be ignored. Suppose further that the pulse amplitude and durations are adjusted so that

$$\gamma_A H_1 \tau_p = \omega_1 \tau_p = \pi/2 \ . \qquad [C.5]$$

Thus the experimental conditions are in fact very similar to those

described for a nonselective pulse experiment, except that there one also has that ω_1, ω_2 >> $|\omega_X-\omega|$ and $\omega_1 \simeq \omega_2$.

From equation [3.12] for the equilibrium spin density matrix, and from the identity (cf. Abragam (4), page 517)

$$T = \exp(-i\omega_1 I_{Ax})\exp[-ia\tau_p(\mathrm{Cos}\phi I_{Xz} + \mathrm{Sin}\phi I_{Xx})]$$

$$= \exp(-i\omega_1 I_{Ax})\exp(-i\phi I_{Xy})\exp(-ia\tau_p I_{Xz})\exp(i\phi I_{Xy}) \quad [C.6]$$

where $$a = [(\omega_X-\omega)^2 + \omega_2{}^2]^{1/2} \quad [C.7]$$

and $$\mathrm{Tan}\phi = \omega_2/(\omega_B-\omega), \quad [C.8]$$

and using the properties of the exponential angular momentum operators (cf. Appendix A), one finds that (cf. reference (111))

$$\rho^r = 1/Z - C[-I_{Ay} - I_{Xy}\mathrm{Sin}\phi\mathrm{Sin}\, a\tau_p + I_{Xx}\mathrm{Sin}\phi\mathrm{Cos}\phi(1-\mathrm{Cos}\, a\tau_p)$$

$$+ I_{Xz}(\mathrm{Cos}\, a\tau_p \mathrm{Sin}^2\phi - \mathrm{Cos}^2\phi)]. \quad [C.9]$$

Thus the effect of the particular pulse defined by [C.5] is to rotate nuclear species A by $\pi/2$ radians, while nuclear species X undergoes a complex rotational and precessional motion. In the case that

$$|\omega_X-\omega| >> |\omega_2| = |\omega_1\gamma_X/\gamma_A| \quad [C.10]$$

then [C.9] simplifies since $\phi \to 0$, and it follows immediately that

$$\rho^r = 1/Z - C(-I_{Ay} + I_{Xz}) \quad [C.11]$$

ie. the pulse is selective in the sense that <u>only</u> the A nuclei are rotated (effectively) by the pulse. This result may also apply to homonuclear systems if [C.10] holds (111); note further that [C.9] reduces to the expected result for a nonselective pulse, where, if

$\omega_1 \simeq \omega_2 \simeq a$ and $a\tau_p \simeq \phi \simeq \pi/2$, then

$$\rho^{r\phi} = +/Z - C\,(-I_{Ay} - I_{Xy}). \qquad [C.12]$$

It appears, then, that the distinction between nonselective and selective pulses is one of degree rather than of kind, since a given set of experimental conditions can correspond to either type of pulse, depending on the parameters of the spin system. Another more direct way of interpreting these results follows by considering the rf pulse envelope as a square wave which contains Fourier components over a frequency range Ω where (8)

$$\Omega = \omega \pm 1/\tau_p . \qquad [C.13]$$

Now one has a nonselective pulse if all transition frequencies lie within the range Ω, and a selective pulse if, for example, the transitions of nuclear species A are within Ω while the transitions of species X lie outside the range Ω. Since the range is obviously a continuous variable, there is a region where a distinction between nonselective and selective pulses is untenable. In a more strict mathematical sense, this means that simplifications like [C.11] or [C.12] must be replaced by [C.9].

One may define yet another type of "selective" pulse by extending the pulse duration time such that the range encompasses only <u>one</u> particular transition frequency (62-63,113). Such experiments have been performed in proton NMR, and it turns out that the required pulse duration times are of the order of a few seconds (compared with microseconds for a usual nonselective pulse experiments), so that

the effective frequency range is of the order of a few radians/second. The following discussion is concerned with a derivation of the exact pulse conditions required for this type of selective pulse.

2. The Pulse Parameters.

The calculations for this problem are very complex, and it is convenient to limit the discussion to an AB system of spin-1/2 nuclei. For this case, suppose that one of the "B" transitions is being selectively pulsed; one then has the Hamiltonian

$$H_s^r = \sum_i (\omega_i-\omega)I_{iz} + J\,\underline{I}_A\cdot\underline{I}_B + \sum_i \omega_1/2(I_{i+}+I_{i-}) \qquad [C.14]$$

where $\omega_1=\gamma_A H_1=\gamma_B H_1$. In this case H_2^r is not readily simplified; furthermore since τ_p is long, relaxation effects are no longer negligible. Ignoring relaxation effects, however, so that a simple closed analytical expression may be obtained, it follows that (cf. Table III)

$$H_s^r = \begin{bmatrix} \Delta+J/4 & q & 0 & 0 \\ q & R/2-J/4 & 0 & 0 \\ 0 & 0 & -R/2+J/4 & 0 \\ 0 & 0 & 0 & -\Delta+J/4 \end{bmatrix} \qquad [C.15]$$

where $q = \omega_1\lambda_{12}/2$ and $\lambda_{12}=\langle 1|I_+|2'\rangle$ is the transition matrix element for the transition $|2'\rangle \rightarrow |1\rangle$ (cf. Table III and [1.10] for example). It is also assumed that [C.15] follows from [C.14] if the pulsing frequency ω is centered at the transition at frequency $\Delta=-R/2+J/2$, and that the pulse duration is so long that any neighbouring transitions are not affected (ie. $\omega_{12}\simeq 0$ but $\omega_{ij} >> \omega_1$ if $i\neq 1$ and $j\neq 2$, where $\omega_{ij} = (H_s^r)_{ii}-(H_s^r)_{jj}$). Now if D is a matrix which diagon-

alizes H_s^r to H_D, with $H_D = D\, H_s^r\, D^{-1}$, then from [C.2],

$$\rho^r = D^{-1} \exp(-iH_D\tau_p)\, D\, \rho^o\, D^{-1} \exp(iH_D\tau_p)\, D \qquad [C.16]$$

where the exponential matrix is now in a more manageable form. Upon expanding this last equation, one obtains, after considerable manipulation:

$$\rho^r = \mathbb{1}/Z - C \begin{bmatrix} w & x & 0 & 0 \\ x^* & y & 0 & 0 \\ 0 & 0 & 0 & 0 \\ 0 & 0 & 0 & -1 \end{bmatrix} \qquad [C.17a]$$

where
$$w = (c^4+s^4) - c^2s^2[\exp(iV\tau_p)+\exp(-iV\tau_p)]$$
$$y = 2c^2s^2 + c^2s^2\,[\exp(iV\tau_p)+\exp(-iV\tau_p)]$$
$$x = x^* = -c^3s[1-\exp(iV\tau_p)] + cs^3[1-\exp(-iV\tau_p)] \qquad [C.17b]$$
and
$$c = \cos\phi,\ s=\sin\phi,\ \tan 2\phi=\lambda_{12}\omega_1/[(H_s^r)_{11}-(H_s^r)_{22}]$$
with
$$V = (H_D)_{11} - (H_D)_{22} \simeq \omega_1\lambda_{12} \quad (\text{as } 2\phi \to \pi/2).$$

One now defines a selective $\pi/2$ pulse (selective to the transition $|r\rangle \to |s\rangle$) by the general expression (cf. reference (113))

$$\omega_1\, \lambda_{rs}\, \tau_p = \gamma_A\, H_1\, \lambda_{rs}\, \tau_p = \pi/2 \qquad [C.18]$$

where λ_{rs} is the transition matrix element of the transition in question. For such a pulse applied to the $|2'\rangle \to |1\rangle$ transition,

$$\rho^r = \mathbb{1}/Z - C \begin{bmatrix} 1/2 & i/2 & 0 & 0 \\ -i/2 & 1/2 & 0 & 0 \\ 0 & 0 & 0 & 0 \\ 0 & 0 & 0 & -1 \end{bmatrix} \qquad [C.19]$$

which is similar to equation [C.11].

Finally, it is constructive to consider the effects of a selective

π pulse on a system of nuclei. It follows that

$$\rho^r = 1/Z - C \begin{bmatrix} 0 & 0 & 0 & 0 \\ 0 & 1 & 0 & 0 \\ 0 & 0 & 0 & 0 \\ 0 & 0 & 0 & -1 \end{bmatrix} \quad \text{(selective)} \quad [C.20]$$

which may be compared with the effect of a nonselective π pulse:

$$\rho^r = 1/Z - C \begin{bmatrix} -1 & 0 & 0 & 0 \\ 0 & 0 & 0 & 0 \\ 0 & 0 & 0 & 0 \\ 0 & 0 & 0 & 1 \end{bmatrix} \quad \text{(nonselective)} \quad [C.21]$$

and with the equilibrium spin density matrix:

$$\rho^o = 1/Z - C \begin{bmatrix} 1 & 0 & 0 & 0 \\ 0 & 0 & 0 & 0 \\ 0 & 0 & 0 & 0 \\ 0 & 0 & 0 & -1 \end{bmatrix}. \quad \text{(equilibrium)} \quad [C.22]$$

It is apparent that a nonselective π pulse inverts all the spin populations while a π pulse which is selective to some transition inverts only the spin populations across the levels connected by that transition. These results exemplify one of the principal differences between pulsed and cw NMR: whereas pulsed NMR can result in inverted populations, cw NMR can only produce population equalizations (saturation). Consequently pulsed NMR is of particular value for the study of the rates of approach of a system to equilibrium, that is for the study of relaxation phenomena. One example of such a study is contained in the recent report by Freeman, Wittekoek and Ernst (113) which is concerned with the relaxation mechanisms prevalent in AB systems of protons.

D. Listings of the Computer Programmes.

The following section contains documented listings of the computer programmes written for the evaluation of all of the calculated results presented in this thesis. There are three versions of the Runge-Kutta-Gill integration routine: one for the pulse simulations (in the rotating frame), and two for the cw simulations, one each in the frame rotating at the frequency of the observing rf field and in the interaction representation. The last two routines are not listed completely; some subroutines which are required may be found in the listing for the first programme (these subroutines, for example the "RUNGE" routine, are almost identical for all the programmes. The major variations lie in the attributes associated with the variable array HAMILT, which may be either REAL*8 or COMPLEX*16, and which is determined by the main programme).

These programmes have been set up so as to minimize the handling of data. Thus, for example, the RKG programme for the simulation of double resonance experiments evaluates the signal and stores the results on disk. Successive programmes then accept this data and "filter" the signal, add on inhomogeneity effects, and, finally, plot the spectrum. The relevant input parameters and requirements are described in the listings of the programmes.

```
      IMPLICIT REAL*8 (A-H,O-Z)
C  THIS PROGRAM CALCULATES THE RESPONSE OF TWO SPIN-1/2 NUCLEI SUBJECTE
C      TO A SEQUENCE OF PULSES IN PULSED NMR EXPERIMENTS.  WRITTEN IN
C      FORTRAN IV BY B.GOODWIN; SEE DETAILS IN J.MAGN.RES. (IN PRESS,
C      1973).  THIS PROGRAMME HAS BEEN MODIFIED TO ACCEPT FOUR TYPES OF
C      RELAXATION MECHANISMS: BLOCH-TYPE (J.MAGN.RES., VOL. 8, P 41
C      (1972)); RANDOM ISOTROPIC EXTERNAL FIELDS (R.HOFFMAN IN ADV. IN
C      MAGN. RES. VOL 4, P 87 (1970)); INTERNAL DIPOLE-DIPOLE (R.FREEMA
C      ET AL IN J.CHEM.PHYS. 52, P 1529 (1970)); AND AN INDEPENDENT
C      MIXTURE OF THE LATTER TWO.
      LOGICAL*1 OFF, ONDISK, NEW, SIGOUT, DIODE
      INTEGER DISK/10/, NDIM, NDIM2, ISTOP, ISTORE, KK, IX, I,
     1        DISK2/12/, SIMPSN, CPMG, IDISK/20/
      REAL*4 SIGNAL(8), TT(16),PULSEM, STOTAL(8)
      REAL*8 RHOEQ(4),V1,V2,TIME,DELT,JAB,DEL,VP1,HP1,TW1,TE2,RN,RR,DD,
     1       TAB
      COMPLEX*16 RHO(10), QRUNGE(10), KRUNGE(10), NORM, DCONJG,
     1           HAMILT(10)
      COMMON /INFO/ RHOEQ,V1,V2,DEL,JAB,TW1,TE2,RN,RR,DD,VP1,HP1,CPMG,
     1              MECH,OFF,ONDISK
      EXTERNAL FXY
C  DEPENDING ON THE INPUT, A VARIETY OF OUTPUT MAY BE OBTAINED.  FOR
C      EXAMPLE IF ISTORE LE ISTOP, THE PROGRAM BECOMES RESTARTABLE SO
C      THAT A PULSE SEQUENCE MAY BE CARRIED ON FROM THE LAST PULSE, OR
C      FOR A CARR-PURCELL SEQUENCE WHERE VARIOUS TAU VALUES ARE DESIRED
C      THE PROGRAM COULD CARRY ON FROM THE PULSE FOLLOWING THE PI/2
C      PULSE, NEGATING THE PROBLEM OF RESTARTING THE ENTIRE PULSE
C      SEQUENCE FROM THE BEGINNING.  ON THE OTHER HAND, IF THE SIGNAL
C      WITH INHOMOGENEITY EFFECTS ARE DESIRED, THIS MAY BE ACCOMPLISHED
C      BY DEFINING THE PARAMETERS SIMPSN, BETA, H, ETC (BELOW).
      NDIM=4
      NDIM2=10
C  INPUT PARAMETERS ARE BROKEN INTO TWO SECTIONS:
C  ********************
C      SECTION (A).
C      IWRITE -EVERY IWRITE ITERATION IS OUTPUT TO DEVICE 6 AND IF
C              REQUESTED, TO DEVICE 10.
C      SIGOUT -IF SIGOUT=T, THE SIGNAL IS OUTPUT TO DEVICE 10; ELSE
C              THERE IS NO OUTPUT TO DEVICE 10.
C      ISTORE -FOR RESTARTABLE CAPABILITIES; ALL DATA REQUIRED IN SECT-
C              ION (B) INCLUDING THE CURRENT VALUE OF THE DENSITY MATRI
C              ARE STORED ON DEVICE 20 AT THE END OF PULSE "ISTORE".
C      ISTOP  -AT THE END OF PULSE "ISTOP", THE CALCULATION TERMINATES.
C      ONDISK -IF DATA HAS BEEN PREVIOUSLY STORED, ONDISK=T; ELSE IF
C              DATA IS TO BE READ IN FROM THE CARD READER, ONDISK=F.
C              THIS APPLIES ONLY TO DATA IN SECTION (B).
C      OFF    -CONDITION OF THE FIRST PULSE; IF THE PULSING FIELD IS ON
C              OFF=F; ELSE OFF=T.  IT IS ASSUMED THAT THE PULSE IS
C              ALTERNATELY ON AND OFF FOR THE DURATIONS GIVEN BELOW, AN
C              THAT THE STRENGTH OF THE PERTURBATION IS EITHER NON-ZERO
```

```
C                (=HP1, BELOW) OR ZERO RESPECTIVELY.
C       CPMG    -AT PULSE "CPMG", THE PERTURBATION IS APPLIED ALONG THE
C                NEGATIVE Y AXIS; OTHERWISE IT IS DIRECTED ALONG THE
C                NEGATIVE X AXIS (AS USUAL). CF. CARR-PURCELL-MEIBOOM-
C                GILL SEQUENCE OF PULSES.  SEE OPTION BELOW FOR CPMG<0.
C       DIODE   - IF DIODE=T, A DIODE DETECTOR IS TO BE SIMULATED; ELSE
C                THE DETECTOR IS PHASE-SENSITIVE AND THE ABSORPTION MODE
C                SIGNAL IS CALCULATED.
C       TPULSE-STEP-SIZE OF THE TIME, REQUIRED FOR THE RUNGE-KUTTA-GILL
C                INTEGRATION ROUTINE, APPLYING WHEN THE PULSE IS ON.
C       TSTAT   -AS ABOVE; APPLYING WHEN THE PULSE IS OFF.  NOTE:  TSTAT
C                IS MUCH GREATER THAN TPULSE FOR NONSELECTIVE PULSES.
C       TT(I)   -UP TO 16 VARIABLES CONTAINING THE PULSE DURATION TIMES,
C                IN SEQUENCE.
      DELW=0.0D00
C   THE FOLLOWING PARAMETERS REFER TO INHOMOGENEITY CALCULATIONS.
C       THE INTEGRATION IS CARRIED OUT USING SIMPSONS RULE; THIS PROGRAM
C       MUST BE SUBMITTED FOR EACH POINT IN THE EXPRESSION FOR THE SIGNAL
C       WITH SIGNAL=1.0/3.0*(S(-N)+4*S(-N+1)+2*(-N+2))+...+4*S(N-1)+S(N))
C       WITH N EVEN AND WHERE S(I)=SIGNAL AT BETA=I*H.  FOR THE FIRST
C       SERIES, TAKE ONLY THOSE POINTS WITH SIMPSN=1 OR 2 (THE FIRST
C       POINT HAS NEW=T,SIMPSN=1,I=-N , THE REST NEW=F, I=N-2, ETC);
C       THE SECOND SERIES TAKE ONLY THOSE POINTS WITH SIMPSN=4.  THE
C       TWO RESULTANT DATA SETS ARE READILY COMBINED IN PROGRAM SIGNL,
C       WHICH ALSO ENABLES A DOUBLING OF THE NUMBER OF POINTS WITH A
C       MINIMUM OF DUPLICATION (THE TWO SERIES ABOVE COULD BE COMBINED IN
C       THIS PROGRAM, BUT DOUBLING OF THE NUMBER OF POINTS WOULD NOT
C       BE FEASIBLE).  TO DOUBLE THE NUMBER OF POINTS IN THE INTEGRAL,
C       CALCULATE THE IN-BETWEEN POINTS S(J) WHERE J=-N+1/2,-N+3/2,...
C       N-1/2 (2N TOTAL; SIMPSN=4) AND COMBINE USING PROGRAM SIGNL
C       THESE RESULTS WITH DATA SET "21" FROM THE PREVIOUS RUN OF
C       PROGRAM SIGNL.   THIS PROCEDURE SAVE DUPLICATION OF RESULTS.
C       SUGGESTED INITIAL VALUES ARE BETA = -3H TO +3H IN STEPS OF H.
C       NEW     -NEW=T FOR NO INHOMOGENEITY CALCULATIONS OR FOR THE FIRST
C                MEMBER OF A SET OF INHOMOGENEITY CALCULATIONS.
C                NOTE THAT IF NEW=F, ONE REQUIRES A DEVICE 12 WHICH
C                CONTAINS THE PREVIOUS INHOMOGENEITY CALCULATION.
C       SIMPSN -EQUAL TO 1,2,OR 4 (SEE ABOVE).
C       INHOM   -EQUAL TO 1 OR 2 FOR A LORENTZIAN OR GAUSSIAN DISTRIBUTION
C                OF INHOMOGENEITY, RESPECTIVELY.  NOTE:  THE WEIGHTS ARE
C                NOT NORMALIZED.
C       BETA    -EQUAL TO I    (ABOVE) IN UNITS OF H.
C       STEP    -DUMMY VARIABLE FOR BOOK-KEEPING PURPOSES.
C       H       -HALF-HEIGHT LINE WIDTH OF THE DISTRIBUTION=2.0*H, IN
C                UNITS OF HERTZ.  SET H=0.0 FOR NO INHOMOGENEITY.
C       VPM,HPM-IF THE FREQUENCY AND/OR POWER OF THE RF PULSE CHANGES IN
C                THE MIDDLE OF A PULSE SEQUENCE, THEIR NEW VALUES MAY BE
C                INPUT HERE.  THESE ARE IMPLEMENTED IF CPMG<0 AND AT
C                PULSE=-CPMG (FOR SELECTIVE PULSES; CF FREEMAN ET. AL.).
C     FORMAT IS (5X,I2,6X,L1,6X,I2,6X,I2,8X,L1,5X,L1,6X,I2,6X,L1,2D10.4,
C                  /8D10.4,/8D10.4,/4X,L1,8X,I1,7X,I1,8X,5D10.4)
C       SAMPLE DATA:
```

```
CRIT=01,SIGO=F,STOR=99,STOP=05,ONDISK=F,OFF=T,CPMG=99,DIOD=T1.0000D-06
                                                              1.0000d-03
C00001794  .050      .00003588 .100
C
CEW=T,SIMPSN=2,INHOM=1,B,S,H= +0.000D+000.8000D+000.1774D-00(HERTZ)
   99 READ (5,100,END=166) IWRITE,SIGOUT,ISTORE,ISTOP,ONDISK,OFF,CPMG,
     1     DIODE,TPULSE,TSTAT,(TT(I),I=1,16),NEW,SIMPSN,INHOM,BETA,STEP,
     2     H,VPM,HPM
  100 FORMAT (5X,I2,6X,L1,6X,I2,6X,I2,8X,L1,5X,L1,6X,I2,6X,L1,2D10.4,/
     1        8D10.4,/8D10.4,/4X,L1,8X,I1,7X,I1,8X,5D10.4)
      TEST=TPULSE/2.0D00
      IF (CPMG.LT.0) CPMG=900+CPMG
      IF (IWRITE.LT.1) IWRITE=1
C  CHECK FOR LOCATION OF FOLLOWING INPUT.
      IF (ONDISK) GO TO 103
C ********************
C      SECTION (B), INPUT FROM CARDS IS AS FOLLOWS:
C      V1      -LARMOR FREQUENCY OF NUCLEUS 1, IN HERTZ.
C      DEL     -CHEMICAL SHIFT BETWEEN NUCLEI 1 AND 2, IN HERTZ.
C               V2 = V1 + DEL.
C      JAB     -COUPLING CONSTANT BETWEEN NUCLEI 1 AND 2, IN HERTZ.
C      HP1     -STRENGTH OF THE PULSING FIELD, WHEN ON.
C      VP1     -FREQUENCY (FIXED) OF THE PULSING FIELD.
C      TIME    -TIME AT THE START OF THE FIRST PULSE (USUALLY=0.0).
C      TW1     -SPIN-LATTICE RELAXATION TIME (IN SECONDS) FOR MECHANISM
C               (1), OR WS FOR (2) AND (4) (STRENGTH OF EXTERNAL FIELDS,
C               IN HERTZ).
C      TE2     -SPIN-SPIN RELAXATION TIME (IN SECONDS) FOR MECHANISM (1)
C               OR EPSILON FOR (2) AND (4) (RATIO OF SPECTRAL DENSITIES).
C      RN      -NETA FOR (2) OR (4) (ASSYMETRY PARAMETER).
C      RR      -CORRELATION PARAMETER FOR (2) OR (4).
C      DD      -K**2*TC (OR 2/3/TD) FOR (3) OR (4) (DIPOLE-DIPOLE TERM
C               IN RADIANS/SECOND).
C      MECH    -TYPE OF RELAXATION MECHANISM DESIRED:
C               MECH=1 GIVES BLOCK TYPE OF EXPONENTIAL DECAY.
C               MECH=2 GIVES RANDOM FLUCTUATING ISOTROPIC FIELDS.
C               MECH=3 GIVES INTERNAL DIPOLE-DIPOLE.
C               MECH=4 GIVES AN INDEPENDENT MIXTURE OF (2) AND (3).
C  NOTE:  MECHANISMS (2-4) ASSUME THE CONDITION OF EXTREME NARROWING.
C      FORMAT IS (6D10.4,/5D10.4,6X,I1)
C      SAMPLE DATA:
C   2.1500D 073.9700D 003.8700D 006.4816D-040.0000D 00
C   0.0960D 001.0000D 000.0000D 001.0000D 000.0000D 00,MECH=2
  101 READ (5,102,END=166) V1,DEL,JAB,HP1,VP1,TIME,TW1,TE2,RN,RR,DD,
     1                     MECH
  102 FORMAT (6D10.4,/5D10.4,6X,I1)
      TMECH=MECH
      GO TO 105
  103 READ (IDISK,104,END=162) V1,DEL,JAB,HP1,VP1,TIME,TW1,TE2,RN,RR,DD,
     1                  TMECH,(RHOEQ(I),I=1,NDIM),(RHO(I),I=1,NDIM2)
  104 FORMAT (4D20.13)
```

```
      MECH=TMECH
C  CORRECT FOR FREQUENCY SHIFT DUE TO INHOMOGENEITY.  ASSUME DEL FIXED.
  105 FOO=BETA*H
      IF (INHOM.EQ.2) FOO=FOO*2.0D00/1.664D00
C  CORRECT FOR DESCREPANCIES IN DEFINITION OF H FOR GAUSSIAN DIST'N.
      VP1=VP1+V1
      V1=V1+FOO
      V2=V1+DEL
C  SET UP WEIGHTING FACTOR FOR INHOMOGENEITY.
      GO TO (1051,1052), INHOM
C  THE FACTOR OF 3 APPEARS IN THE EXPRESSION FOR SIMPSON'S RULE.
 1051 WEIGHT=1.0D00/(1.0D00+BETA*BETA)/3.0D00
C  LORENTZIAN.
      GO TO 1053
 1052 WEIGHT=DEXP(-BETA*BETA)/3.0D00
C  GAUSSIAN.
 1053 WEIGHT=WEIGHT*SIMPSN
  107 IF (DABS(H).LT.1.0D-49) WEIGHT=1.0D00
      IF (CPMG.LT.2) CPMG=-99
C  INITIALIZE SOME OF THE MATRICES.
      CALL EQBLIM (NDIM, NDIM2, TIME, RHO, HAMILT)
      IF (OFF) GO TO 109
  108 DELT=TPULSE
      PULSEM=1.0E50
      GO TO 110
  109 DELT=TSTAT
      PULSEM=0.0
  110 WRITE (6,111) V1,DEL,JAB,HP1,VP1,TIME,TPULSE,TSTAT,TW1,TE2,RN,RR,
     1    DD,MECH,(RHOEQ(I),I=1,NDIM),(RHO(I),I=1,NDIM2),ISTORE,ISTOP,
     2       IWRITE,SIGOUT,CPMG,DIODE,ONDISK,OFF
  111 FORMAT (1H1,//1H ,10X,'PULSED NMR OF AN AB SYSTEM',//1H ,15X,
     1'INITIAL CONDITIONS:',/1H ,15X,'V1  =',D20.13,/1H ,15X,'DEL =',
     2D20.13,/1H ,15X,'JAB =',D20.13,/1H ,15X,'HP1 =',D20.13,/1H ,15X,
     3'VP1 =',D20.13,/1H ,15X,'TIME=',D20.13,/1H ,15X,'DELT=',D20.13,
     4' /',D20.13,/1H ,15X,'TW1 =',D15.7,', TE2=',D15.7,/1H ,15X,'RN  ='
     5,D15.7,', RR  =',D15.7,/1H ,15X,'DD  =',D15.7,'; MECHANISM=',I2,/
     6/1H  15X,'EQUILIBRIUM DENSITY MATRIX:',/1H ,14X,4D20.13,//1H ,15X,
     7'DENSITY MATRIX:',2(/1H ,15X,10D10.4),//1H ,15X,'ISTORE=',I2,'; IS
     8TOP=',I2,'; IWRITE=',I2,'; SIGOUT=',L1,'; CPMG=',I2,'; DIODE=',
     9L1,/1H ,15X,'ONDISK=',L1,'; OFF=',L1)
      WRITE (6,1111) (TT(I),I=1,16),INHOM,BETA,WEIGHT,H,STEP,SIMPSN,NEW
 1111 FORMAT (/1H ,15X,'PULSE DURATIONS',2(/1H ,14X,8D12.5),//1H ,15X,
     1'INHOMOGENEITY PARAMETERS:',/1H ,15X,'DISTRIBUTION TYPE=',I2,
     2/1H ,15X,'BETA=',D15.7,'; WEIGHT=',D15.7,/1H ,15X,'H =',D15.7,
     3'; STEP=',D15.7,/1H ,15X,'SIMPSN=',I2,'; NEW=',L1,'.')
      WRITE (6,112) OFF,TIME,DELT
  112 FORMAT (//1H ,15X,'***OFF =',1X,L1,' AT TIME=',F15.7,'; DELT=',
     1          D15.7)
      T1=TW1
      T2=TE2
```

```
      DDD=DD
C  PLAY AROUND WITH THE RELAXATION PARAMETERS.
      IF (MECH.GT.1) GO TO 1122
 1121 TW1=1.0D00/TW1
      TE2=1.0D00/TE2
      GO TO 1123
 1122 TW1=TW1*6.28319D00/3.0D00
      DD=DD*0.10D00
 1123 DO 113 I=1,NDIM2
  113 QRUNGE(I)=(0.0D00,0.0D00)
      KK=1
      ICOUNT=IWRITE
      ITAB=1
      TAB=TIME+TT(1)
      DELT=DELT*IWRITE
      IF (.NOT.NEW) READ (DISK2,114,END=160) (STOTAL(I),I=1,5)
  114 FORMAT (5E16.8)
      IF (SIGOUT) WRITE (DISK,114) TIME,DELW,DELT,H,PULSEM
      DELT=DELT/IWRITE
C  ENTER THE INTEGRATION ROUTINE.
      GO TO 116
  115 TIME=TIME+DELT
  116 IF ((TIME+DELT-TAB).LT.TEST) GO TO 138
C  CHECK FOR END OF THIS PULSE.
  117 IF (ITAB.NE.ISTORE) GO TO 120
C  STORE DATA FOR RESTARTING THE PROGRAM.
  118 V1=V1-FOO
      VP1=VP1-V1
      REWIND IDISK
      WRITE (IDISK,104) V1,DEL,JAB,HP1,VP1,TIME,T1,T2,RN,RR,DDD,
     1                  TMECH,(RHOEQ(I),I=1,NDIM),(RHO(I),I=1,NDIM2)
      END FILE IDISK
      REWIND IDISK
      VP1=VP1+V1
      V1=V1+FOO
      WRITE (6,119) TIME
  119 FORMAT (1H ,25X,'DATA TO DEVICE 20 AT TIME=',D15.7)
  120 IF (ITAB.EQ.ISTOP) GO TO 164
  121 ITAB=ITAB+1
      TAB=TIME+TT(ITAB)
      IF ((900-CPMG).NE.ITAB) GO TO 1213
 1211 IF (DABS(VPM).GT.1.0D-49) VP1=VPM+V1-FOO
      IF (DABS(HPM).GT.1.0D-49) HP1=HPM
      WRITE (6,1212) VP1,HP1,TIME
C  NEW PULSEING FREQUENCY AND/OR POWER LEVEL?
      HAMILT(1)=3.14159D00*(V1+V2-VP1-VP1+JAB*0.50D00)
 1212 FORMAT (1H ,15X,'NEW FREQUENCY/POWER =',2D23.15,' AT TIME=',
     1 D15.7)
      HAMILT(10)=3.14159D00*(VP1+VP1-V1-V2+JAB*0.50D00)
 1213 IF (DIODE) GO TO 123
```

```
  122 SIGNAL(KK)=(RHO(2)+RHO(4)+RHO(8)+RHO(9))*(0.0D00,+1.0D00)*WEIGHT
      GO TO 124
  123 SIGNAL(KK)=CDABS(RHO(2)+RHO(4)+RHO(8)+RHO(9))*WEIGHT
  124 IF (NEW) GO TO 128
C  READ IN PREVIOUS INHOMOGENEOUS SIGNAL AND ADD TOGETHER.
  125 READ (DISK2,126,END=160) (STOTAL(I),I=1,8)
  126 FORMAT (8E10.4)
      DO 127 I=1,KK
  127 SIGNAL(I)=SIGNAL(I)+STOTAL(I)
  128 IF (KK.LT.8) GO TO 130
  129 WRITE (6,133) TIME,ITAB,(SIGNAL(I),I=1,8)
      IF (SIGOUT) WRITE (DISK,126) (SIGNAL(I),I=1,8)
      IF (.NOT.NEW) READ (DISK2,126,END=160) (STOTAL(I),I=1,8)
      KK=0
  130 I=KK+1
C  EIGHT SIGNALS ARE WRITTEN OUT AT ONE TIME; AT THE END OF A PULSE
C       THE REMAINDER OF A LINE OR A FULL LINE IS LOADED WITH 1.0E50 IN
C       ORDER TO FACILITATE PLOTTING (STEP-SIZE CHANGES).
      DO 131 KK=I,8
  131 SIGNAL(KK)=1.0D+50
  132 WRITE (6,133) TIME,ITAB,(SIGNAL(I),I=1,8)
  133 FORMAT  (/1H ,10X,F12.7,I3,3X,8E12.4)
      IF (SIGOUT) WRITE (DISK,126) (SIGNAL(I),I=1,8)
C  PULSE HAS GONE ON OR OFF.
      KK=1
      ICOUNT=-1
      OFF=.NOT.OFF
      IF (OFF) GO TO 135
  134 DELT=TPULSE
      PULSEM=1.0E50
      GO TO 136
  135 DELT=TSTAT
      PULSEM=0.0
  136 WRITE (6,112) OFF,TIME,DELT
      DELT=DELT*IWRITE
      IF (SIGOUT) WRITE (DISK,114) TIME,DELW,DELT,H,PULSEM
      DELT=DELT/IWRITE
      IF (.NOT.NEW) READ (DISK2,114,END=160) (STOTAL(I),I=1,5)
C  CHECK FOR START OF NEW PULSE DIRECTION.
      IF (CPMG.EQ.ITAB) CPMG=-99
  137 CALL DGEN (NDIM, NDIM2, TIME, HAMILT)
C  GENERATE THE HAMILTONIAN (CHANGES WHEN THE PULSE CHANGES).
  138 NORM=(0.0D00,0.0D00)
C  NORMALIZE THE SOLUTION BY USING THE FACT THAT TR(RHO)=(1,0).  NOTE:
C       SINCE THE EQUATIONS ARE OFTEN "STIFF", DIVERGENCE MAY BE READILY
C       DETECTED BY THE DEVIATION OF THE VARIABLE NORM FROM (1,0).
      IX=0
      DO 139 I=1,NDIM
      IX=IX+I
  139 NORM=NORM+RHO(IX)
```

```
      NORM=1.0D00/NORM
      DO 140 I=1,NDIM2
  140 RHO(I)=RHO(I)*NORM
  141 ICOUNT=ICOUNT+1
      IF (ICOUNT.LT.IWRITE) GO TO 150
  142 ICOUNT=0
      IF (DIODE) GO TO 144
  143 SIGNAL(KK)=(RHO(2)+RHO(4)+RHO(8)+RHO(9))*(0.0D00,+1.0D00)*WEIGHT
      GO TO 145
  144 SIGNAL(KK)=CDABS(RHO(2)+RHO(4)+RHO(8)+RHO(9))*WEIGHT
  145 KK=KK+1
      IF (KK.LT.9) GO TO 150
  146 IF (NEW) GO TO 149
  147 READ (DISK2,126,END=160) (STOTAL(I),I=1,8)
      DO 148 I=1,8
  148 SIGNAL(I)=SIGNAL(I)+STOTAL(I)
  149 WRITE (6,133) TIME,ITAB,(SIGNAL(I),I=1,8)
      IF (SIGOUT) WRITE (DISK,126) (SIGNAL(I),I=1,8)
      KK=1
  150 CALL RUNGE (NDIM,NDIM2,TIME,DELT,RHO,FXY,QRUNGE,KRUNGE,HAMILT)
C  CALCULATE THE DENSITY MATRIX AT TIME+DELT AND GO BACK TO THE START
      GO TO 115
  160 WRITE (6,161)
  161 FORMAT (1H ,15X,'***END OF DATA ON DEVICE 12.')
      GO TO 166
  162 WRITE (6,163)
  163 FORMAT (1H ,15X,'***END OF DATA ON DEVICE 20.')
      GO TO 166
  164 KK=KK-1
      WRITE (6,133) TIME,ITAB,(SIGNAL(I),I=1,KK)
      IF (SIGOUT) WRITE (DISK,126) (SIGNAL(I),I=1,KK)
      WRITE (6,165)
  165 FORMAT (///1H ,15X,'END OF THIS SEQUENCE.')
      GO TO 99
  166 WRITE (6,167)
  167 FORMAT (///1H ,15X,'END OF JOB.')
      STOP
      END
```

```
      SUBROUTINE EQBLIM (NDIM, NDIM2, TIME, RHO, HAMILT)
      IMPLICIT REAL*8 (A-H,O-Z)
      LOGICAL*1 OFF, ONDISK
      INTEGER NDIM,NDIM2,CPMG
      REAL*8 DELT
      REAL*8 RHOEQ(4), V1, V2, VP1, HP1, K1, K2, DEL, JAB
      COMPLEX*16 RHO(NDIM2), HAMILT(NDIM2)
      COMMON /INFO/ RHOEQ,V1,V2,DEL,JAB,TW1,TE2,RN,RR,DD,VP1,HP1,CPMG,
     1              MECH,OFF,ONDISK
C  SUBROUTINE EQBLIM PERFORMS THE FOLLOWING CALCULATIONS:
C       1.) GENERATES THE HAMILTONIAN IN THE ROTATING FRAME.
C       2.) EVALUATES THE BOLTZMANN FACTORS (RHOEQ) IF NECESSARY.
C       3.) INITIALIZES THE DENSITY MATRIX TO THAT OF A SYSTEM IN
C       THERMAL EQUILIBRIUM, IF NECESSAY.
C  TIME-INDEPENDENT ELEMENTS OF THE HAMILTONIAN.
      HAMILT(1)=3.14159D00*(V1+V2-VP1-VP1+JAB*0.50D00)
      HAMILT(3)=3.14159D00*(V1-V2-JAB*0.50D00)
      HAMILT(5)=3.14159D00*JAB
      HAMILT(6)=3.14159D00*(V2-V1-JAB*0.50D00)
      HAMILT(7)=(0.0D00,0.0D00)
      HAMILT(10)=3.14159D00*(VP1+VP1-V1-V2+JAB*0.50D00)
      CALL DGEN (NDIM, NDIM2, TIME, HAMILT)
C  TIME-DEPENDENT ELEMENTS CALCULATED IN SUBROUTINE DGEN.
      IF (ONDISK) RETURN
C  BOLTZMANN FACTORS.
      RHOEQ(1)=DEXP(-(V1+V2)*0.50D00*6.6238D-27/(1.38053D-16*298.0D00))
      TEMP    =DEXP(+(JAB  )*0.25D00*6.6238D-27/(1.38053D-16*298.0D00))
      RHOEQ(2)=DEXP(-(V1-V2)*0.50D00*6.6238D-27/(1.38053D-16*298.0D00))
      RHOEQ(3)=1.0D00/RHOEQ(2)
      RHOEQ(4)=1.0D00/RHOEQ(1)
      RHOEQ(1)=RHOEQ(1)*TEMP
      RHOEQ(4)=RHOEQ(4)*TEMP
      RHOEQ(2)=RHOEQ(2)*1.0D00/TEMP
      RHOEQ(3)=RHOEQ(3)*1.0D00/TEMP
      TEMP=RHOEQ(1)+RHOEQ(2)+RHOEQ(3)+RHOEQ(4)
C  INITIALIZE DENSITY MATRIX.
      DO 200 I=1,NDIM2
  200 RHO(I)=(0.0D00,0.0D00)
      DO 201 I=1,NDIM
      RHOEQ(I)=RHOEQ(I)/TEMP
      IX=(I*I+I)/2
  201 RHO(IX)=RHOEQ(I)
      RETURN
      END
```

```
      SUBROUTINE RUNGE (NDIM,NDIM2,TIME,DELT,Y,FXY,Q,K,V)
      IMPLICIT REAL*8 (A-H,O-Z)
      INTEGER NDIM,NDIM2
      REAL*8 TIME, DELT, A/.2928932188134 52D00/, B/.1707106781186 55D01/
      COMPLEX*16 Q(NDIM2), K(NDIM2), Y(NDIM2), V(NDIM2), TEMP
      EXTERNAL FXY, DGEN
C  RUNGE-KUTTA-GILL ROUTINE FOR THE SOLUTION OF A SYSTEM OF FIRST ORDER
C       DIFFERENTIAL EQUATIONS Y' = F(X,Y).  F IS CALCULATED IN THE
C       SUBROUTINE FXY USING THE HAMILTONIAN V AND DENSITY MATRIX Y,
C       RETURNING THE RESULT Y' (CALLED K); THE INDEPENDENT VARIABLE IS
C       TIME.
      CALL FXY (NDIM,NDIM2,Y,K,V)
      DO 500 I=1,NDIM2
      TEMP=DELT*K(I)
      Y(I)=Y(I)+0.50D00*(TEMP-2.0D00*Q(I))
  500 Q(I)=Q(I)+3.0D00*(0.50D00*(TEMP-2.0D00*Q(I)))-0.50D00*TEMP
      CALL FXY (NDIM,NDIM2,Y,K,V)
      DO 501 I=1,NDIM2
      TEMP=DELT*K(I)
      Y(I)=Y(I)+A*(TEMP-Q(I))
  501 Q(I)=Q(I)+3.0D00*(A*(TEMP-Q(I)))-A*TEMP
      CALL FXY (NDIM,NDIM2,Y,K,V)
      DO 502 I=1,NDIM2
      TEMP=DELT*K(I)
      Y(I)=Y(I)+B*(TEMP-Q(I))
  502 Q(I)=Q(I)+3.0D00*(B*(TEMP-Q(I)))-B*TEMP
      CALL FXY (NDIM,NDIM2,Y,K,V)
      DO 503 I=1,NDIM2
      TEMP=DELT*K(I)
      Y(I)=Y(I)+(TEMP-2.0D00*Q(I))/6.0D00
  503 Q(I)=Q(I)+3.0D00*((TEMP-2.0D00*Q(I))/6.0D00)-TEMP*0.50D00
      RETURN
      END
```

```
      SUBROUTINE DGEN (NDIM, NDIM2, TIME, HAMILT)
      IMPLICIT REAL*8 (A-H,O-Z)
      LOGICAL*1 OFF, ONDISK
      INTEGER NDIM,NDIM2,CPMG
      REAL*8 DELT
      REAL*8 RHOEQ(4), V1, V2, VP1, HP1, K1, K2, DEL, JAB
      COMPLEX*16 HAMILT(NDIM2), TEMP
      COMMON /INFO/ RHOEQ,V1,V2,DEL,JAB,TW1,TE2,RN,RR,DD,VP1,HP1,CPMG,
     1              MECH,OFF,ONDISK
C  CALCULATES THE ELEMENTS OF THE HAMILTONIAN (IN THE ROTATING FRAME)
C       WHICH ARE ALTERED BY THE END OR START OF A PULSE.
      IF (OFF) GO TO 602
C  IF THE PARAMETER CPMG   0, THE PULSE IS APPLIED ALONG THE NEGATIVE
C       Y AXIS; OTHERWISE IT IS DIRECTED (AS USUAL) ALONG THE NEGATIVE
C       X AXIS.
  600 TEMP=1.0
      IF (CPMG.LT.-98) TEMP=(0.0D00,-1.0D00)
  601 HAMILT(2)=3.141590D00*V2*HP1*TEMP
      HAMILT(4)=3.141590D00*V1*HP1*TEMP
      HAMILT(8)=HAMILT(4)
      HAMILT(9)=HAMILT(2)
      GO TO 603
  602 HAMILT(2)=(0.0D00,0.0D00)
      HAMILT(4)=(0.0D00,0.0D00)
      HAMILT(8)=(0.0D00,0.0D00)
      HAMILT(9)=(0.0D00,0.0D00)
  603 RETURN
      END
```

```
      SUBROUTINE FXY (NDIM,NDIM2,RHO,K,HAMILT)
      IMPLICIT REAL*8 (A-H,O-Z)
      LOGICAL*1 OFF, ONDISK
      INTEGER NDIM,NDIM2,CPMG
      REAL*8 RHOEQ(4), V1, V2, VP1, HP1, K1, K2, DEL, JAB
      COMPLEX*16 RHO(NDIM2), K(NDIM2), HAMILT(NDIM2), DCONJG, F1
      COMMON /INFO/ RHOEQ,V1,V2,DEL,JAB, RW, RE,RN,RR,DD,VP1,HP1,CPMG,
     1              MECH,OFF,ONDISK
C  GENERATE THE TIME-DERIVATIVE OF RHO, EQUAL TO THE COMMUTATOR OF RHO
C      WITH THE HAMILTONIAN PLUS ADDITIONAL RELAXATION TERMS.
      CALL COMMUT  (NDIM,NDIM2,RHO,HAMILT,K)
C       ADD ON THE RELAXATION TERMS.
      GO TO (204,201,202,201), MECH
C       TERMS FOR AN ISOTROPIC RANDOM EXTERNAL FIELD.
  201 FF=RR*(RHO(5)*(2.0D00,0.0D00))
      K(1)=K(1)+RW*RE*(-2.0D00*(RHO(1)-RHOEQ(1))+(1.0D00-RN)*
     1           (RHO(3)-RHOEQ(2))+(1.0D00+RN)*(RHO(6)-RHOEQ(3))+FF)
      K(3)=K(3)+RW*RE*(-2.0D00*(RHO(3)-RHOEQ(2))+(1.0D00-RN)*
     1           (RHO(1)-RHOEQ(1))+(1.0D00+RN)*(RHO(10)-RHOEQ(4))-FF)
      K(6)=K(6)+RW*RE*(-2.0D00*(RHO(6)-RHOEQ(3))+(1.0D00-RN)*
     1           (RHO(10)-RHOEQ(4))+(1.0D00+RN)*(RHO(1)-RHOEQ(1))-FF)
      K(10)=K(10)+RW*RE*(-2.0D00*(RHO(10)-RHOEQ(4))+(1.0D00-RN)*
     1           (RHO(6)-RHOEQ(3))+(1.0D00+RN)*(RHO(3)-RHOEQ(2))+FF)
      FF=2.0D00*RE+1.0D00-RN
      K(2)=K(2)+RW*(-FF*RHO(2)-RR*RE*(RHO(4)-RHO(8))+RE*(1.0D00+RN)*
     1           RHO(9))
      K(9)=K(9)+RW*(-FF*RHO(9)+RR*RE*(RHO(4)-RHO(8))+RE*(1.0D00+RN)*
     1           RHO(2))
      FF=FF+RN+RN
      K(4)=K(4)+RW*(-FF*RHO(4)+RR*RE*(RHO(9)-RHO(2))+RE*(1.0D00+RN)*
     1           RHO(8))
      K(8)=K(8)+RW*(-FF*RHO(8)-RR*RE*(RHO(9)-RHO(2))+RE*(1.0D00+RN)*
     1           RHO(4))
      K(5)=K(5)+RW*(-2.0D00*(RE+1.0D00-RR)*RHO(5)+RE*RR*(RHO(1)+
     1      RHO(10)+RHOEQ(2)+RHOEQ(3)-RHO(3)-RHO(6)-RHOEQ(1)-RHOEQ(4)))
      K(7)=K(7)-RW*2.0D00*RHO(7)*(RE+RR+1.0D00)
      IF (MECH.LT.3) GO TO 208
  202 FF=RHO(5)*(2.0D00,0.0D00)
C       TERMS FOR AN INTRAMOLECULAR DIPOLAR INTERACTION.
C       FOR THE MECHANISM 4, THE STATEMENTS 201-204 INCLUSIVE ARE
C       EXECUTED.
      K(1)=K(1)+DD*(-9.0D00*(RHO(1)-RHOEQ(1))+1.50D00*(RHO(3)-
     1RHOEQ(2)+RHO(6)   -RHOEQ(3)+4.0D00*(RHO(10)-RHOEQ(4))+FF))
      K(10)=K(10)+DD*(-9.0D00*(RHO(10)-RHOEQ(4))+1.50D00*(RHO(3)-
     1RHOEQ(2)+RHO(6)   -RHOEQ(3)+4.0D00*(RHO(01)-RHOEQ(1))+FF))
      F1=1.50D00*(-FF+RHO(1)+RHO(10)-RHOEQ(1)-RHOEQ(4))
      K(3)=K(3)+DD*(-4.0D00*(RHO(3)-RHOEQ(2))+RHO(6)-RHOEQ(3)+F1)
      K(6)=K(6)+DD*(-4.0D00*(RHO(6)-RHOEQ(3))+RHO(3)-RHOEQ(2)+F1)
      F1=(RHO(8)+RHO(9))*1.50D00
      K(2)=K(2)+DD*(-8.50D00*RHO(2)-3.50D00*RHO(4)+F1)
      K(4)=K(4)+DD*(-8.50D00*RHO(4)-3.50D00*RHO(2)+F1)
      F1=(RHO(2)+RHO(4))*1.50D00
      K(8)=K(8)+DD*(-8.50D00*RHO(8)-3.50D00*RHO(9)+F1)
      K(9)=K(9)+DD*(-8.50D00*RHO(9)-3.50D00*RHO(8)+F1)
      K(7)=K(7)-DD*9.0D00*RHO(7)
```

```
      K(5)=K(5)+DD*(-4.0D00*RHO(5)+DCONJG(RHO(5))+1.50D00*(RHO(1)+
     1RHO(10)-RHO(3)-RHO(6)-RHOEQ(1)-RHOEQ(4)+RHOEQ(2)+RHOEQ(3)))
      GO TO 208
  204 J=1
C      BLOCH-TYPE EXPONENTIAL DECAY (PHENOMENOLOGICAL MODEL).
      IX=1
      DO 207 I=1,NDIM2
      IF (I.EQ.IX) GO TO 206
  205 K(I)=K(I)-RE*RHO(I)
      GO TO 207
  206 K(IX)=K(IX)+RW*(RHOEQ(J)-RHO(IX))
      J=J+1
      IX=IX+J
  207 CONTINUE
  208 RETURN
      END
```

```
      SUBROUTINE COMMUT  (NDIM,NDIM2,A,B,R)
      INTEGER NDIM,NDIM2
      COMPLEX*16 A(NDIM2), R(NDIM2), TEMP, DCONJG, B(NDIM2)
C  SUBROUTINE COMMUT COMMUTES THE HERMITIAN MATRICES A  AND B, AND
C       PREMULTIPLIES THE RESULTANT MATRIX BY THE IMAGINARY NUMBER TO
C       YIELD THE HERMITIAN MATRIX R.  THE MATRICES ARE ALL SQUARE AND OF
C       ORDER NDIM; ONLY THE NDIM2 ELEMENTS OF THEIR UPPER TRIANGLE ARE
C       STORED BY COLUMNS (NDIM2=N*(N+1)/2).
      DO 409 K=1,NDIM
      KX=(K*K-K)/2
      DO 408 J=1,K
      IR=J+KX
      TEMP=(0.0D00,0.0D00)
      DO 407 I=1,NDIM
      IF (I.LT.J) GO TO 405
  403 IA=J+(I*I-I)/2
      IF (I.LE.K) GO TO 406
  404 IB=IA-J+K
      TEMP=TEMP+A(IA)*DCONJG(B(IB))-DCONJG(A(IB))*B(IA)
      GO TO 407
  405 IA=I+(J*J-J)/2
      IB=I+KX
      TEMP=TEMP+DCONJG(A(IA))*B(IB)-A(IB)*DCONJG(B(IA))
      GO TO 407
  406 IB=I+KX
      TEMP=TEMP+A(IA)*B(IB)-A(IB)*B(IA)
  407 CONTINUE
  408 R(IR)=TEMP*(0.0D00,1.0D00)
  409 CONTINUE
      RETURN
      END
```

(End of the pulse programme.)

```
      IMPLICIT REAL*8 (A-H,O-Z)
C  THIS PROGRAM CALCULATES DYNAMIC NUCLEAR MAGNETIC SINGLE RESONANCE
C      LINE SHAPES FOR TWO SPIN-1/2 NUCLEI.  WRITTEN IN FORTRAN IV BY
C      B.GOODWIN; SEE DETAILS IN J. MAGN. RES. VOL. 8, P. 41 (1972).
C      THIS PROGRAMME HAS BEEN MODIFIED TO ACCEPT FOUR TYPES OF MECH-
C      ANISMS FOR RELAXATION:  BLOCH-TYPE, RANDOM ISOTROPIC EXTERNAL
C      FIELDS, INTERNAL DIPOLE-DIPOLE, AND A MIXTURE OF THE LATTER TWO.
C      DETAILS OF THE LAST THREE MECHANSIMS MAY BE SEEN IN THE ARTICLES
C      BY R.HOFFMAN IN ADV. IN MAGN. RES. 4, P87 (1970), AND R.FREEMAN
C      ET. AL. IN J. CHEM. PHYS. 52, P 1529 (1970).
C      NOTE:  THE FOLLOWING PROGRAM IS NOMINALLY FOR AN AB SYSTEM; FOR
C      AN AX SYSTEM THE "X" APPROXIMATION WILL RESULT IN REDUCED
C      EXECUTION TIME SINCE THERE WILL BE CONVERGENCE FOR LARGER DELT.
      REAL LINE(8)
      REAL*8 RHOEQ(4),V1,V2,VSTART,VSTOP,DELV,TIME,DELT,JAB,RR,RN,DEL,
     1       VP1,HP1,HAMILT(10),TW1,TE2,DD
      COMPLEX*16 RHO(10), ORUNGE(10), KRUNGE(10), NORM, DCONJG
      COMMON /NO/ RHOEQ, V1,V2,VP1,HP1,DEL,JAB,DELV,VSTART,TW1,TE2,RN,
     1            RR,DD,MECH
C  THE MATRICES RHO, ORUNGE AND KRUNGE ARE HERMITIAN AND HAMILT IS
C      SYMMETRIC; ONLY THE UPPER TRIANGULAR PARTS ARE STORED (BY
C      COLUMNS).  RHO IS THE DENSITY MATRIX, KRUNGE ITS TIME DERIVATIVE,
C      HAMILT THE HAMILTONIAN AND RHOEQ THE EQUILIBRIUM DENSITY MATRIX.
C      ORUNGE IS REQUIRED IN THE RUNGE-KUTTA-GILL INTEGRATION ROUTINE.
      EXTERNAL FXY
C  INPUT PARAMETERS ARE AS FOLLOWS:
C      HP1     -RATIO OF OBSERVING FIELD TO STATIC FIELD.
C      V1      -LARMOR FREQUENCY OF NUCLEUS 1, IN HERTZ.
C      DEL     -CHEMICAL SHIFT BETWEEN NUCLEI 1 AND 2, IN HERTZ.
C               V2 = V1 + DEL.
C      JAB     -COUPLING CONSTANT BETWEEN NUCLEI 1 AND 2, IN HERTZ.
C      IWRITE -FREQUENCY OF OUTPUT (EVERY IWRITE ITERATION IS OUTPUT).
C      MECH    -TYPE OF RELAXATION MECHANSIM DESIRED:
C               MECH=1 GIVES A BLOCK TYPE OF EXPONENTIAL DECAY.
C               MECH=2 GIVES RANDOM FLUCTUATING ISOTROPIC FIELDS.
C               MECH=3 GIVES INTERNAL DIPOLE-DIPOLE.
C               MECH=4 GIVES A MIXTURE OF (2) AND (3).  MECHANISMS (2)
C                  TO (4) ASSUME THE CONDITION OF EXTREME NARROWING.
C      DELT    -STEP SIZE IN RUNGE-KUTTA-GILL INTEGRATION, IN SECONDS.
C      DELV    -RATE OF FREQUENCY SCAN, IN HERTZ/SECOND.
C      VSTART,VSTOP-STARTING AND STOPPING POSITION OF FREQUENCY SCAN
C               RELATIVE TO V1, IN HERTZ.
C      TW1     -SPIN-LATTICE RELAXATION TIME (IN SECONDS) FOR MECHANISM
C               (1), OR WS FOR (2) AND (4) (STRENGTH OF EXTERNAL FIELDS,
C               IN HERTZ).
C      TE2     -SPIN-SPIN RELAXATION TIME (IN SECONDS) FOR MECHANISM (1)
C               OR EPSILON FOR (2) AND (4) (RATIO OF SPECTRAL DENSITIES).
C      RN      -NETA FOR (2) OR (4) (ASSYMETRY PARAMETER).
C      RR      -CORRELATION PARAMETER R FOR (2) OR (4).
C      DD      -K**2*TC (OR 2/3/TD) FOR (3) OR (4) (DIPOLE-DIPOSE TERM
C               IN RADIANS/SECOND).
C
```

```
C       FORMAT IS (4D10.4,2I3,/4D10.4,/5D10.4)
C
C       SAMPLE DATA:
C       1.0000D-0942.577D 060.0000D 001.0000D 00001004
C       0.0500D 000.1000D 00-2.000D 001.0000D 00
C       0.1020D 001.0000D 000.0000D 000.6667D 000.1600D 00
C
      READ (5,100,END=114,ERR=114) HP1,V1,DEL,JAB,IWRITE,MECH,
     1              DELT,DELV,VSTART,VSTOP,TW1,TE2,RN,RR,DD
  100 FORMAT (4D10.4,2I3,/4D10.4,/5D10.4)
      IF (IWRITE.LT.1) IWRITE = 1
      IF (MECH.GT.4.OR.MECH.LT.1) MECH=1
      NDIM=4
      NDIM2=10
C      TIME=0.0 IS ARBITRARY.
      TIME=0.0D00
      NOITER=DABS((VSTART-VSTOP)/DELT/DELV/IWPITE/8)
      V2=V1+DEL
      VSTART=VSTART+V1
      VSTOP=VSTOP+V1
C  OUTPUT IS TO THE PRINTER (DEVICE 6) AND TO A DISK (DEVICE 10).  THE
C       LATTER OUTPUT IS THEN PLOTTED ON A CALCOMP PLOTTER BY ANOTHER
C       PROGRAM.
      WRITE (6,101) HP1,VSTART,DELV,VSTOP,V1,V2,DEL,JAB,
     1              DELT,TW1,TE2,PN,RR,DD,MECH,IWRITE
  101 FORMAT (1H1,//1H ,10X,'TIME-EVOLUTION OF A TWO SPIN-1/2 SYSTEM',
     1//1H ,15X,'HP1=',D23.15,/1H ,15X,'VP1=',D23.15,' /',D15.7,'  /',
     2 D23.15,/1H ,15X,'V1  =',D23.15,/1H ,15X,'V2  =',D23.15,/1H ,15X,
     3 'DEL =',D23.15,/1H ,15X,'JAB =',D23.15,/1H ,15X,'DELT=',D23.15,
     4 /1H ,15X,'TW1 =',D23.15,/1H ,15X,'TE2 =',D23.15,/1H ,15X,'RN  =',
     5 D23.15,/1H ,15X,'RR  =',D23.15,/1H ,15X,'DD  =',D23.15,/1H ,15X,
     6 'RELAXATION MECHANSIM=',I2,/1H ,15X,'IWRITE=',I3,///1H )
C  CONVERT TO RADIANS/SECOND AND INITIALIZE ALL MATRICES.
      IF (MECH.EQ.2.OR.MECH.EQ.4) TW1=TW1*6.28319D00/3.0D00
      IF (MECH.GT.1) GO TO 1012
 1011 TW1=1.0D00/TW1
      TE2=1.0D00/TE2
 1012 DD=DD*0.10D00
      VSTOP=VSTOP-V1
      VSTART=VSTART-V1
      V1=V1*6.28319D00
      V2=V2*6.28319D00
      DEL=DEL*6.28319D00
      DELV=DELV*6.28319D 00
      VSTART=VSTART*6.28319D00
      JAB=JAB*6.28319D00
      CALL INITIL  (NDIM,NDIM2,TIME,RHO,HAMILT)
      DO 102 I=1,NDIM2
  102 ORUNGE(I)=(0.0D00,0.0D00)
      KK=1
```

```
      ICOUNT=IWRITE
      DELT=DELT*IWRITE
      WRITE (10,1021) VSTART, DELV, DELT, RR, VSTOP
 1021 FORMAT (5E16.8)
      DELT=DELT/IWRITE
      ITER=0
C  ENTER THE INTEGRATION LOOP.
      GO TO 104
  103 TIME=TIME+DELT
  104 NORM=(0.0D00,0.0D00)
C  NORMALIZE THE SOLUTION BY USING THE FACT THAT TR(RHO)=(1,0).
C       NOTE:  SINCE THE EQUATIONS ARE OFTEN "STIFF", DIVERGENCE MAY BE
C       READILY DETECTED BY THE DEVIATION OF THE VARIABLE NORM FROM (1,0)
      IX=0
      DO 105 I=1,NDIM
      IX=IX+I
  105 NORM=NORM+RHO(IX)
      DO 106 I=1,NDIM2
  106 RHO(I)=RHO(I)/NORM
      ICOUNT=ICOUNT+1
      IF (ICOUNT.LT.IWRITE) GO TO 113
  107 ICOUNT=0
C  CALCULATE THE ABSORPTION SIGNAL (IN THE ROTATING FRAME).
      LINE(KK)=(RHO(2)+RHO(4)+RHO(8)+RHO(9))*(0.0D00,1.0D00)
      KK=KK+1
      IF (KK.LT.9) GO TO 113
C  WRITE 8 CALCULATED SIGNALS AT A TIME.
  108 WRITE (10,109) (LINE(KK),KK=1,8)
  109 FORMAT (8E10.4)
      VPP=VP1/6.28319D00
      WRITE (6,110) TIME,VPP,(LINE(KK),KK=1,8)
  110 FORMAT (/1H ,F8.2,F15.7,8D12.3)
      KK=1
      ITER=ITER+1
      IF (ITER.GT.NOITER) GO TO 116
  113 CALL RUNGE (NDIM,NDIM2,TIME,DELT,RHO,FXY,ORUNGE,KRUNGE,HAMILT)
      GO TO 103
  114 WRITE (6,115)
  115 FORMAT (//1H ,15X,'INPUT WRONG')
  116 WRITE (6,117)
  117 FORMAT (//1H ,15X,'END OF JOB')
      END FILE 10
      STOP
      END
```

```
      SUBROUTINE INITIL  (NDIM,NDIM2,TIME,RHO,HAMILT)
      IMPLICIT REAL*8 (A-H,O-Z)
      INTEGER NDIM,NDIM2
      REAL*8 RHOEQ(4),V1,V2,VP1,HP1,DEL,JAB,DELV,VSTART,RN,RR,DD,TW1,TE2
      REAL*8 HAMILT(NDIM2)
      COMPLEX*16 RHO(NDIM2)
      COMMON /NO/ RHOEQ, V1,V2,VP1,HP1,DEL,JAB,DELV,VSTART,TW1,TE2,RN,
     1            RR,DD,MECH
C  SUBROUTINE INITIL PERFORMS THE FOLLOWING CALCULATIONS:
C      1.) GENERATES THE HAMILTONIAN AT FREQUENCY VSTART IN THE
C      ROTATING FRAME.
C      2.) EVALUATES THE BOLTZMANN FACTORS (STORED IN RHOEQ) ASSUMING
C      THAT THE SPIN PRODUCT VECTORS ARE EIGENVECTORS OF THE STATIC
C      HAMILTONIAN.
C      3.) INITIALIZES THE DENSITY MATRIX TO THAT OF A SYSTEM IN
C      THERMAL EQUILIBRIUM.
      JAB=+JAB*0.250D00
C  CALCULATE TIME-INDEPENDENT TERMS.
      HAMILT(2)=0.50D00*V2*HP1
      HAMILT(3)=-0.50D00*DEL-JAB
      HAMILT(4)=0.50D00*V1*HP1
      HAMILT(5)=JAB+JAB
      HAMILT(6)=-HAMILT(3)-JAB-JAB
      HAMILT(7)=0.0D00
      HAMILT(8)=HAMILT(4)
      HAMILT(9)=HAMILT(2)
      DEL=DEL*0.50D00
C  CALCULATE TIME-DEPENDENT TERMS.
      CALL DGEN (NDIM,NDIM2,TIME,HAMILT)
C  CALCULATE BOLTZMANN FACTORS.
      RHOEQ(1)=DEXP(-(V1+V2)*0.50D00*1.0544D-27/(1.38053D-16*298.0D00))
      TEMP    =DEXP(+(JAB)  *1.00D00*1.0544D-27/(1.38053D-16*298.0D00))
      RHOEQ(2)=DEXP(-(V1-V2)*0.50D00*1.0544D-27/(1.38053D-16*298.0D00))
      RHOEQ(3)=1.0D00/RHOEQ(2)
      RHOEQ(4)=1.0D00/RHOEQ(1)
      RHOEQ(1)=RHOEQ(1)*TEMP
      RHOEQ(4)=RHOEQ(4)*TEMP
      RHOEQ(2)=RHOEQ(2)*1.0D00/TEMP
      RHOEQ(3)=RHOEQ(3)*1.0D00/TEMP
      TEMP=RHOEQ(1)+RHOEQ(2)+RHOEQ(3)+RHOEQ(4)
C  INITIALIZE DENSITY MATRIX.
      DO 200 I=1,NDIM2
  200 RHO(I)=(0.0D00,0.0D00)
      DO 201 I=1,NDIM
      RHOEQ(I)=RHOEQ(I)/TEMP
      IX=(I*I+I)/2
  201 RHO(IX)=RHOEQ(I)
      WRITE (6,202) (I,RHOEQ(I),I=1,NDIM)
  202 FORMAT (1H ,15X,'INITIAL POPULATIONS:',4(/1H ,15X,I2,2X,D23.15),
     1 ////1H ,4X,'TIME',6X,'FREQUENCY',45X,'SIGNAL')
      RETURN
      END
```

```
      SUBROUTINE DGEN (NDIM,NDIM2,TIME,HAMILT)
      IMPLICIT REAL*8 (A-H,O-Z)
      INTEGER NDIM,NDIM2
      REAL*8 RHOEQ(4),V1,V2,VP1,HP1,DEL,JAB,DELV,VSTART,RN,RR,DD,TW1,TE2
      REAL*8 HAMILT(NDIM2)
      COMMON /NO/ RHOEQ, V1,V2,VP1,HP1,DEL,JAB,DELV,VSTART,TW1,TE2,
     1            RR,DD,MECH
C  CALCULATE THE NEW POSITION OF THE FREQUENCY AND UPDATE THE PERTINENT
C       ELEMENTS OF THE HAMILTONIAN IN THE ROTATING FRAME.
      VP1=VSTART+DELV*TIME
      HAMILT(1)=DEL-VP1+JAB
      HAMILT(10)=-DEL+VP1+JAB
      RETURN
      END
```

NOTE: for subroutines "RUNGE", "FXY" and "COMMUT" see the listing for the pulse programme. Those subroutines differ only in that, for this programme, the array "HAMILT" has the attributes REAL*8. Subroutine "COMMUT" may also be simplified, therefore, since the variable "B" (corresponding to HAMILT) is not a complex array, and the statements with "DCONJG(B(IB))" may be written just as "B(IB))".

```
      IMPLICIT REAL*8 (A-H,O-Z)
C  THIS PROGRAM CALCULATES DYNAMIC NUCLEAR MAGNETIC DOUBLE RESONANCE
C     LINE SHAPES FOR TWO SPIN-1/2 NUCLEI.  WRITTEN IN FORTRAN IV BY
C     B.GOODWIN; SEE DETAILS IN J. MAGN. RES. VOL. 8, P. 41 (1972).
C      THIS PROGRAMME HAS BEEN MODIFIED TO ACCEPT FOUR TYPES OF MECH-
C      ANISMS FOR RELAXATION:  BLOCH, RANDOM ISOTROPIC EXTERNAL FIELDS,
C      INTERNAL DIPOLE-DIPOLE, AND A MIXTURE OF THE LATTER TWO.
C      SEE DETAILS IN J.MAGN.RES. 8, P 41 (1972); R.HOFFMAN IN
C      ADV. IN MAGN. RES. 4, P 87 (1970); AND R.FREEMAN ET. AL.
C      IN J.CHEM.PHYS. 52, P 1529 (1970).
      REAL LINE(8)
      REAL*8 RHOEQ(4),V1,V2,VSTART,VSTOP,DELV,TIME,DELT,JAB,DEL,
     1       VP1,VP2,HP1,HP2, DCOS, DSIN, XX
      COMPLEX*16 RHO(10), QRUNGE(10), KRUNGE(10), NORM, HAMILT(10),
     1           EXPCD, DCONJG
C  THE MATRICES RHO, QRUNGE, KRUNGE AND HAMILT(10) ARE HERMITIAN AND
C     ONLY THE UPPER TRIANGULAR PARTS ARE STORED (BY COLUMNS).  RHO
C     IS THE DENSITY MATRIX, KRUNGE ITS TIME DERIVATIVE, HAMILT THE
C     HAMILTONIAN AND RHOEQ THE EQUILIBRIUM DENSITY MATRIX.  QRUNGE IS
C     REQUIRED IN THE RUNGE-KUTTA-GILL INTEGRATION PROCEDURE.
      COMMON /NO/ RHOEQ,V1,V2,VP1,VP2,HP1,HP2,DEL,JAB,DELV,VSTART,
     1            TW1,TE2,RN,RR,DD,MECH
      EXTERNAL FXY
      EXPCD(XX)=DCOS(XX)+DSIN(XX)*(0.0D00,1.0D00)
C  INPUT PARAMETERS ARE AS FOLLOWS:
C     HP1      -RATIO OF OBSERVING FIELD TO STATIC FIELD.
C     HP2      -RATIO OF PERTURBING FIELD TO STATIC FIELD.
C     VP2      -FREQUENCY OF PERTURBING FIELD RELATIVE TO V1, IN HERTZ.
C     V1       -LARMOR FREQUENCY OF NUCLEUS 1, IN HERTZ.
C     DEL      -CHEMICAL SHIFT BETWEEN NUCLEUS 1 AND 2, IN HERTZ.  V2=
C               V1+DEL.
C     JAB      -COUPLING CONSTANT BETWEEN NUCLEUS 1 AND 2, IN HERTZ.
C     IWRITE   -FREQUENCY OF OUTPUT (EVERY IWRITE ITERATION IS OUTPUT).
C     MECH     -TYPE OF RELAXATION MECHANISM DESIRED:
C               MECH=1 GIVES A BLOCH TYPE OF EXPONENTIAL DECAY.
C               MECH=2 GIVES RANDOM FLUCTUATING ISOTROPIC FIELDS.
C               MECH=3 GIVES INTERNAL DIPOLE-DIPOLE.
C               MECH=4 GIVES MIXTURE OF 2 AND 3.  BOTH MECHANSIMS 2 AN
C                   3 ASSUME THE CONDITION OF EXTREME NARROWING.
C     DELT     -STEP SIZE IN RUNGE-KUTTA-GILL INTEGRATION, IN SECONDS.
C     DELV     -RATE OF FREQUENCY SCAN, IN HERTZ/SECOND.
C     VSTART, VSTOP-STARTING AND STOPPING POSITION OF FREQUENCY SCAN
C               RELATIVE TO V1, IN HERTZ.
C     TW1      -SPIN-LATTICE RELAXATION TIME FOR MECHANISM 1 (SECONDS),
C               OR WS FOR 2 AND 4 (STRENGTH OF EXTERNAL FLUCTUATING
C               FIELDS, IN HERTZ).
C     TE2      -SPIN-SPIN RELAXATION TIME FOR MECHANISM 1 (SECONDS),
C               OR EPSILON FOR 2 AND 4 (RATIO OF SPECTRAL DENSITIES).
C     RN       -NETA FOR 2 OR 4 (ASSYMETRY PARAMETER).
C     RR       -CORRELATION PARAMETER R FOR 2 OR 4.
C     DD       -K**2*TC (OR 2/3/TD) FOR 3 OR 4 (DIPOLE-DIPOLE TERM,
```

```
C               IN RADIANS/SECOND).
C
C      FORMAT IS (6D10.4,2I3,/4D10.4,/5D10.4)
C      SAMPLE DATA:
C      1.0000D-091.0000D-088.0000D+004.2577D+078.0000D+002.0000D+00003002
C      0.0300D 000.1000D 00-3.000D 003.0000D 00
C      0.2040D 001.0000D 000.0000D 001.0000D 000.0000D 00
       READ(5,100,END=113 ,ERR=113) HP1,HP2,VP2,V1,DEL,JAB,IWRITE,MECH,
      1            DELT,DELV,VSTART,VSTOP,TW1,TE2,RN,RR,DD
  100  FORMAT (6D10.4,2I3,/4D10.4,/5D10.4)
       IF (MECH.GT.4.OR.MECH.LT.1) MECH=1
       NDIM=4
       NDIM2 = 10
C   TIME=0.0 IS ARBITRARY
       TIME = 0.0
       IF (IWRITE.LT.1) IWRITE = 1
       V2=V1+DEL
       NOITER=DABS((VSTART-VSTOP)/DELT/DELV/IWRITE/8)
       VSTART=VSTART+V1
       VSTOP=VSTOP+V1
       VP2=VP2+V1
C   OUTPUT IS TO THE PRINTER (DEVICE 6) AND TO A DISK (DEVICE 10).  THE
C      LATTER OUTPUT IS THEN "FILTERED" AND THEN PLOTTED (OR PLOTTED
C      DIRECTLY FOR SINGLE RESONANCE) BY ANOTHER PROGRAM.
       WRITE (6,101) HP1,HP2,VP2,VSTART,DELV,VSTOP,V1,V2,DEL,JAB,TIME,
      1              DELT,TW1,TE2,RN,RR,DD,NDIM,NDIM2,IWRITE,MECH
  101  FORMAT (1H1,//1H ,10X,'TIME-EVOLUTION OF A TWO-SPIN NMR. SYSTEM'
     1//1H ,15X,'HP1 =',D23.15,/1H ,15X,'HP2 =',D23.15,/1H ,15X,'VP2='
     2 D23.15,/1H ,15X,'VP1 =',D18.10,' /',F9.5,' / ',D17.10,/1H ,15X,
     3 'V1  =',D23.15,/1H ,15X,'V2  =',D23.15,/1H ,15X,'DEL =',D23.15,/
     4 1H ,15X,'JAB =',D23.15,/1H ,15X,'TIME=',D23.15,/1H ,15X,'DELT=',
     5 D23.15,/1H ,15X,'TW1 =',D23.15,/1H ,15X,'TE2 =',D23.15,/1H ,15X,
     6 'RN  =',D23.15,/1H ,15X,'RR  =',D23.15,/1H ,15X,'DD  =',D23.15,
     7 /1H ,15X,3I2,5X,'MECHANISM=',I2,'.',///1H )
C   CONVERT TO RADIANS/SECOND AND INITIALIZE MATRICES.
       IF (MECH.EQ.2.OR.MECH.EQ.4) TW1=TW1*6.28319D00/3.0D00
       IF (MECH.GT.1) GO TO 1012
 1011  TW1=1.0D00/TW1
       TE2=1.0D00/TE2
 1012  DD=DD*0.10D00
       VSTOP=VSTOP-V1
       V1=V1*6.28319D00
       V2=V2*6.28319D00
       DEL=DEL*6.28319D00
       VP2=VP2*6.28319D00
       VSTART=VSTART*6.28319D00
       DELV=DELV*3.14159D00
       JAB=JAB*6.28319D00
       CALL INITIL  (NDIM,NDIM2,TIME,RHO,HAMILT)
       DO 102 I=1,NDIM2
  102  QRUNGE(I)=(0.0D00,0.0D00)
```

```
            KK=1
            ICOUNT=IWRITE
            VSTART=VSTART-V1
            DELV=DELV+DELV
            VP2=VP2-V1
            DELT=DELT*IWRITE
            WRITE (10,1021) VSTART, DELV, DELT, VP2,VSTOP
         1021 FORMAT (5E16.8)
            DELT=DELT/IWRITE
            VSTART=VSTART+V1
            DELV=DELV/2.0D00
            VP2=VP2+V1
            ITER = 0
      C  ENTER THE INTEGRATION LOOP.
            GO TO 104
           103 TIME=TIME+DELT
      C  NORMALIZE THE SOLUTION BY USING THE FACT THAT TR(RHO)=(1,0).
      C     NOTE:  SINCE THE EQUATIONS ARE OFTEN "STIFF", DIVERGENCE MAY BE
      C     READILY DETECTED BY THE DEVIATION OF THE VARIABLE NORM FROM (1,0).
           104 NORM=(0.0D00,0.0D00)
            IX=0
            DO 105 I=1,NDIM
            IX=IX+I
           105 NORM=NORM+RHO(IX)
            DO 106 I=1,NDIM2
           106 RHO(I)=RHO(I)/NORM
            ICOUNT=ICOUNT+1
            IF (ICOUNT.LT.IWRITE) GO TO 112
           107 ICOUNT=0
      C  CALCULATE THE ABSORPTION SIGNAL.
      C     LINE(KK)=(DCONJG(RHO(2)+RHO(9))*(EXPCD((VP1-V2)*TIME))+
      ****  LINE(KK)=(
           2          DCONJG(RHO(4)+RHO(8))*(EXPCD((VP1-V1)*TIME))
           4       )  * (0.0D00,-1.0D00)
            KK=KK+1
            IF (KK.LT.9) GO TO 112
      C  WRITE 8 CALCULATED SIGNALS AT A TIME.
           108 WRITE (10,109) (LINE(KK),KK=1,8)
           109 FORMAT (8E10.4)
            VPP=(VSTART-V1+DELV*TIME*2.0D00)/6.28319D00
            WRITE (6,110) TIME,VPP,(LINE(KK),KK=1,8)
           110 FORMAT (/1H ,F8.2,F15.7,8D12.3)
            KK=1
            ITER = ITER + 1
      C  CHECK FOR TERMINATION OF THE JOB.
           111 IF (ITER.GT.NOITER) GO TO 115
      C  ENTER INTEGRATION ROUTINE AND EVALUATE RHO AT (TIME+DELT).
           112 CALL RUNGE (NDIM,NDIM2,TIME,DELT,RHO,FXY,QRUNGE,KRUNGE,HAMILT)
            GO TO 103
      C  DIAGNOSTIC MESSAGE AND EXIT.
           113 WRITE (6,114)
```

```
114 FORMAT (///1H ,15X,'INPUT WRONG')
115 WRITE (6,116)
116 FORMAT (///1H ,15X,'END OF JOB.')
    END FILE 10
    STOP
    END
```

```
      SUBROUTINE DGEN (NDIM,NDIM2,TIME,HAMILT)
      IMPLICIT REAL*8 (A-H,O-Z)
      INTEGER NDIM,NDIM2
      REAL*8 RHOEQ(4),V1,V2,VP1,VP2,HP1,HP2,DEL,JAB,DELV,VSTART,RN,RR,DI
      REAL*8 XX, DCOS, DSIN
      COMPLEX*16 HAMILT(NDIM2), EXPCD
      COMMON /NO/ RHOEQ,V1,V2,VP1,VP2,HP1,HP2,DEL,JAB,DELV,VSTART,
     1           TW1,TE2,RN,RR,DD,MECH
      EXPCD(XX)=DCOS(XX)+DSIN(XX)*(0.0D00,1.0D00)
C     CALCULATE THE NEW POSITION OF THE FREQUENCY AND UPDATE THE PERTINENT
C     ELEMENTS OF THE HAMILTONIAN IN THE INTERACTION REPRESENTATION.
      VP1=VSTART+DELV*TIME
***   C     HAMILT(2)=+0.50D00*V2*(HP1*EXPCD((VP1-V2)*TIME)
      HAMILT(2)=+0.50D00*V2*(
     1                +HP2*EXPCD((VP2-V2)*TIME))
      HAMILT(4)=+0.50D00*V1*(HP1*EXPCD((VP1-V1)*TIME)
***   C    1                +HP2*EXPCD((VP2-V1)*TIME))
     1 )
***   C     HAMILT(5)=JAB*EXPCD( DEL*TIME)
      HAMILT(5)=(0.0D 00,0.0D 00)
      HAMILT(8)=HAMILT(4)
      HAMILT(9)=HAMILT(2)
      RETURN
      END
```

NOTE: this programme, as written, is for an AX system with the corresponding AX approximation (including the extension). If an AB system is to be simulated, the statements preceded by "****" should be employed instead of the statements immediately below them. For example, in the above subroutine "DGEN", the statement "C HAMILT(2)=+0.50D00*V2*(HP1* ..." should replace the statement "HAMILT(2)=0.50D00*V2*(". The given statements are for the simulation of the double resonance of an AX system for which the perturbing rf frequency is near the X Larmor frequency while the A nuclei are being observed. For the listings of subroutines "RUNGE", "FXY" and "COMMUT" see the listing for the pulse programme.

```
      INTEGER OLD12/10/,OLD4/11/,NPLOT/20/,NEXT/21/
      REAL S12(8),S4(8),STOTAL(8),H,STEP
C  THIS PROGRAM ADDS TOGETHER DATA SETS ON DEVICES 10 AND 11
C       TO DOUBLE THE NUMBER OF POINTS APPROXIMATING THE INTEG-
C       RATION OVER THE STATIC FIELD INHOMOGENEITY (USING SIMPSON'S
C       RULE; POINTS CALCULATED USING PROGRAM PULSE).  DEVICE
C       10 CONTAINS THE N+1 POINTS S12=1/3*(S(-N)+2S(-N+1)+2S(-N+2)
C       +...+2S(N-1)+S(N)) AND DEVICE 11 THE N POINTS
C       S4=4/3(S(-N+1/2)+S(-N+3/2)+...+S(N-1/2)).  OUTPUT IS TO
C       DEVICES 20 AND 21.  DEVICE 20 CONTAINS THE AVERAGED SIGNAL
C       (=STEP*(S12+S4)) WHICH MAY BE PLOTTED, AND DEVICE 21 CONTAINS
C       A DATA SET SIMILAR TO THAT ON DEVICE 10 (=S12+S4/2) FOR THE
C       NEXT DOUBLING OF POINTS.
C       INPUT PARAMETER IS THE STEP-SIZE(OF BETA) IN THE INTEGRATION,
C       USING F10.4 FORMAT.
   99 READ (5,100,END=140) STEP
  100 FORMAT (F10.4)
C       READ IN DATA FROM DISKS 10 AND 11.
      READ (OLD12,101,END=138,ERR=136) VSTART,DELV,DELT,H,VSTOP
      READ (OLD4 ,101,END=138,ERR=136) VSTART,DELV,DELT,H,VSTOP
  101 FORMAT (5E16.8)
      WRITE (6,102) VSTART,DELT,DELV,VSTOP,H,STEP
  102 FORMAT (1H1,///1H ,15X,'SIGNAL AVERAGING OVER INHOMOGENEITY',/
     1 /1H ,15X,'TIME=',E12.4,' /',E12.4,' (',E12.4,' ) /',/1H ,15X,
     2'PULSE=',F4.0,/1H ,15X,'HALF-WIDTH OF INHOMOGENEITY=',E12.4,
     3' HZ.',/1H ,15X,'STEP-SIZE=',E12.4,///1H ,60X,'SIGNAL')
C       SET UP DISKS 20 AND 21.
      WRITE (NEXT,101) VSTART,DELV,DELT,H,VSTOP
      WRITE (NPLOT,101) VSTART,DELV,DELT,H,VSTOP
  103 READ (OLD12,104,END=138,ERR=136) (S12(I),I=1,8)
      READ (OLD4 ,104,END=138,ERR=136) (S4(I) ,I=1,8)
  104 FORMAT (8E10.4)
      DO 105 I=1,8
  105 STOTAL(I)=S12(I)+S4(I)*0.500E00
      WRITE (NEXT,104) (STOTAL(I),I=1,8)
      DO 106 I=1,8
  106 STOTAL(I)=(S12(I)+S4(I))*STEP
      WRITE (NPLOT,104) (STOTAL(I),I=1,8)
      WRITE (6,107) (STOTAL(I),I=1,8)
  107 FORMAT (1H ,15X,8E12.4)
      IF (S12(8).LT.1.0E+45) GO TO 103
C       END OF THIS PULSE; LOOK FOR NEW PARAMETERS.
  108 READ (OLD12,101,END=138,ERR=136) VSTART,DELV,DELT,H,VSTOP
      READ (OLD4, 101,END=138,ERR=136) VSTART,DELV,DELT,H,VSTOP
      WRITE (NEXT, 101) VSTART,DELV,DELT,H,VSTOP
      WRITE (NPLOT,101) VSTART,DELV,DELT,H,VSTOP
      WRITE (6,109) VSTART,DELT,VSTOP
  109 FORMAT (///1H ,15X,'TIME=',E12.4,' /',E12.4,' /',/1H ,15X,
     1 'PULSE=',F4.0,///1H ,60X,'SIGNAL')
      GO TO 103
  136 WRITE (6,137)
```

```
137 FORMAT (///1H ,15X,'***READ ERROR FROM DISK.')
138 WRITE (6,139)
139 FORMAT (/1H ,15X,'***END OF FILE.')
140 END FILE NEXT
    END FILE NPLOT
    WRITE (6,141)
141 FORMAT (1H ,15X,'***END OF JOB.')
    STOP
    END
```

```
      REAL ST(2500), CW(800)
      LOGICAL*1 ABSN
      INTEGER DISK/10/,ONDISK/20/
C  THIS PROGRAM CALCULATES THE FOURIER TRANSFORM OF A FREE INDUCTION
C       DECAY SIGNAL.  WRITTEN IN FORTRAN IV BY B.GOODWIN.  INPUT
C       FROM DEVICE 10 IS THE CALCULATED FREE INDUCTION DECAY SIGNAL AS
C       CALCULATED BY THE PULSE PROGRAM.  INPUT FROM CARDS IS
C       VSTART    -START OF THE FOURIER TRANSFORM, RELATIVE TO THE
C                  FREQUENCY OF THE PULSING FIELD, IN HERTZ.
C       DELV      -DESIRED STEP-SIZE OF FREQUENCY, IN HERTZ.
C       VSTOP     -STOPPING FREQUENCY, IN HERTZ.
C       TSTOP     -THE SIGNAL AFTER TIME TSTOP IS IGNORED.
C       NSKIP     -THE FIRST NSKIP PULSES ARE IGNORED AND THE FOURIER
C                  TRANSFORM STARTS AT THE BEGINNING OF THE NEXT PULSE.
C       ABSN      -IF ABSN=T, THE ABSORPTION MODE IS CALCULATED; ELSE THE
C                  DISPERSION MODE IS CALCULATED.
C  OUTPUT IS TO DEVICE 20; OUTPUT IS A HIGH-RESOLUTION TYPE SUITABLE FOR
C       SUBSEQUENT PLOTTING.
   99 READ (5,100,END=140) VSTART,DELV,VSTOP,TSTOP,NSKIP,ABSN
  100 FORMAT (4D10.4,7X,I2,6X,L1)
      J=1
  101 IF (J.GT.NSKIP) GO TO 106
C  SKIP THE FIRST NSKIP PULSES
      READ (DISK,102,END=136,ERR=136) TIME,DELW1,DELT,H,PULSEM
  102 FORMAT (5E16.8)
      J=J+1
  103 READ (DISK,104,END=136,ERR=136) (ST(I),I=1,8)
  104 FORMAT (8E10.4)
       IF (ST(8).LT.1.0E+49) GO TO 103
  105 GO TO 101
  106 READ (DISK,102,END=136,ERR=136) TIME,DELW1,DELT,H,PULSEM
C  INPUT DATA FOR THIS FID.
      NOTS=(TSTOP-TIME)/DELT
      NOTS=NOTS/8*8
      IF (NOTS.GT.2500) NOTS=2500
  108 WRITE (6,109) NSKIP,TIME,VSTART,DELV,VSTOP,TSTOP,DELW1,DELT,H,NOTS
     1                , ABSN
  109 FORMAT (1H1,//1H ,15X,'DESCRETE FOURIER TRANSFORM',/1H ,15X,
     1'TRANSFORM STARTS AT END OF PULSE',I2,'; TIME=',E15.7,/1H ,15X,
     2'FREQUENCY RANGE=',E12.4,' /',E12.4,' /',E12.4,/1H ,15X,
     3'IGNORE DATA AFTER TIME=',E15.7,/1H ,15X,'STEP-SIZE=(',E15.7,')',
     4 E15.7,/1H ,15X,'H =',E15.7,/1H ,15X,'NUMBER OF POINTS=',I3,/
     5 1H ,15X,'ABSN MODE?: ',L1,///1H ,15X,'PULSE SIGNAL IS:')
C  CONVERT TO RADIANS/SEC.
      DELW=DELV*6.28319
      WSTART=VSTART*6.28319
      WSTOP=VSTOP*6.28319
      PULSEM=1.0
      NOTS=NOTS+1
C  PICK UP THE FIRST POINT OF THE FID.
```

```
      DO 1091 I=1,8
 1091 IF (ST(I).LT.1.0E45) ST(1)=ST(I)
      WRITE (ONDISK,102) WSTART,DELW,PULSEM,H,VSTOP
      READ (DISK,104,END=138,ERR=136) (ST(I),I=2,NOTS)
 1101 WRITE (6,110) (ST(I),I=1,NOTS,2)
  110 FORMAT (1H ,15X,8E10.4)
C  START THE TRANSFORM.
      W=WSTART-DELW
      L=(WSTOP-WSTART)/DELW
      NOTS1=NOTS-1
  112 DO 114 J=1,L
      W=W+DELW
      TIME=0.0
      TEMPC=0.0
      DO 113 I=1,NOTS1
      IF (ABSN) GO TO 1122
 1121 TEMPC=TEMPC+ST(I)*SIN(W*TIME)
      GO TO 113
 1122 TEMPC=TEMPC+ST(I)*COS(W*TIME)
  113 TIME=TIME+DELT
C  THIS DOES ALL THE WORK.
  114 CW(J)=TEMPC*DELT
      WRITE (6,119)
  119 FORMAT (///1H ,15X,'FOURIER TRANSFORM IS:')
      V=VSTART
C  OUTPUT TO PRINTER AND TO DEVICE 20.
      K=L/8
      DO 122 J=1,K
      I=8*J-7
      II=I+7
      WRITE (6,121) V,(CW(L),L=I,II)
  121 FORMAT (1H ,15X,F8.3,3X,8E12.4)
  122 V=V+8*DELV
      K=K*8
      WRITE (ONDISK,104) (CW(J),J=1,K)
      END FILE ONDISK
      DISK=DISK+1
      ONDISK=ONDISK+1
      GO TO 99
  136 WRITE (6,137)
  137 FORMAT (1H ,15X,'***READ ERROR OR END OF FILE; STOPPING.')
      GO TO 140
  138 NOTS=I-1
      NOTS=NOTS/8*8
      WRITE (6,139) NOTS
  139 FORMAT (1H ,15X,'***END OF FILE; TRYING WITH NOTS=',I4)
      GO TO 1101
  140 WRITE (6,141)
  141 FORMAT (//1H ,15X,'END OF JOB.')
      STOP
      END
```

```
      REAL S(2500),SAV(8),WEIGHT(59)
C  THIS PROGRAMME INTEGRATES HIGH-RESOLUTION NMR SIGNALS OVER INHOMO-
C      GENEITY DISTRIBUTIONS (INTEGRATION BY TRAPEZOIDAL FORMULAE).  THE
C      TYPES OF DISTRIBUTIONS ARE LORENTZIAN, GAUSSIAN AND RECTANGULAR,
C      AND INPUT DATA FROM DEVICE 10 IS THE NMR LINE SHAPE CALCULATED
C      FOR THE "CENTRAL" OR MOST COMMON ENSEMBLE, WHICH DERIVES FROM
C      OTHER PROGRAMS IN THE SERIES (DRABR, SRABR, ETC.).  WRITTEN IN
C      FORTRAN IV BY B.GOODWIN; SEE DETAILS IN J.MAGN RES. (IN PRESS).
C      NOTE:  FOR DOUBLE RESONANCE SPECTRA THE FILTERING SHOULD BE
C      CARRIED OUT BEFORE INTEGRATION OVER INHOMOGENEITY.
      INTEGER SOLD/09/, ISAVE/19/,TYPE
C  INPUT PARAMETERS ARE AS FOLLOWS:
C      NOINT  -NUMBER OF POINTS TO BE USED IN ESTIMATING THE INTEGRAL;
C              SINCE THE INTEGRAL EXTENDS TO INFINITY, ENOUGH POINTS
C              MUST BE INCLUDED SO THAT THE WEIGHTING FACTORS BECOME
C              VERY SMALL AT THE FINITE LIMITS CHOSEN.  MAXIMUM NUMBER
C              OF POINTS IS 59 FOR THIS PROGRAMME.
C      NOSKIP -EVERY "NOSKIP" POINT IN THE DATA SET CONTAINING THE
C              SIGNAL IS TO BE CONSIDERED, ALL OTHERS ARE OMITTED.  THIS
C              IS USED IN CONJECTION WITH NOINT TO OBTAIN FINITE LIMITS.
C      TYPE   -TYPE OF DISTRIBUTION:
C              TYPE=1 - LORENTZIAN; HHLW = 2*H.
C              TYPE=2 - GAUSSIAN; HHLW = 2*H.
C              TYPE=3 - RECTANGULAR; HHLW=2*H.
C              (HHLW = HALF-HEIGHT LINE-WIDTH).
C      H      -RELATED TO THE WIDTH OF THE DISTRIBUTION (SEE ABOVE).
C              UNITS ARE GAUSS (SEE BELOW).
C      GAMMA  -GYROMAGNETIC RATIO  OF NUCLEUS 1, IN /SEC./GAUSS.
C              BY SETTING GAMMA=1.0E00, H MAY BE EXPRESSED IN HERTZ.
   99 READ (5,100,END=140) NOINT,NOSKIP,TYPE,H,GAMMA
  100 FORMAT (3(7X,I2),/2D10.4)
      IF (TYPE.GT.3.OR.TYPE.LT.1) TYPE=1
      IF (ABS(GAMMA).LT.1.0E-49) GAMMA=2.67519E04
      SOLD=SOLD+1
      ISAVE=ISAVE+1
C  USE AN ODD NUMBER OF POINTS.
      NOINT=NOINT/2*2+1
C  READ IN THE DATA SET; ASSUME HERE THAT ONLY 2500 POINTS EXIST.
      READ (SOLD,101) WSTART,DW,DT,BETA,VSTOP
  101 FORMAT (5E16.8)
      NOPTS=(VSTOP*6.28319-WSTART)/DW/DT-8
      IF (NOPTS.GT.2500) NOPTS=2500
      READ (SOLD,103,END=138) (S(I),I=1,NOPTS)
  103 FORMAT (8E10.4)
  104 IF (NOSKIP.LT.2) GO TO 107
C  GET RID OF THE EXTRA POINTS.
  105 K=NOPTS
      NOPTS=NOPTS/NOSKIP
      DW=DW*NOSKIP
      J=0
      DO 106 I=1,K,NOSKIP
      J=J+1
```

```
  106 S(J)=S(I)
  107 WRITE (6,108) TYPE,H,NOINT,NOPTS,GAMMA,NOSKIP,WSTART,DW,DT,VSTOP
  108 FORMAT (///1H ,10X,'INTEGRATION OVER INHOMOGENEITY',/1H ,15X,
     1'TYPE OF DISTRIBUTION=',I2,/1H ,15X,'H=',E12.4,/1H ,15X,'NUMBER OF
     2 POINTS=',I3,/1H ,15X,'NUMBER OF DATA POINTS=',I5,/1H ,15X,'GAMMA=
     3',E12.4,/1H ,15X,'NOSKIP=',I3,/1H ,15X,'FREQUENCIES =',E12.4,
     4 E12.4,' (',E12.4,' ) /',E12.4,///1H ,21X,'BETA',14X,
     5 'WEIGHT')
      NOINT=NOINT-1
      IF (TYPE.EQ.2) H=2.0E00*H/1.664E00
      IF (ABS(GAMMA-1.0E00).LT.1.0E-07) H=H*6.28319E00
      DWS=DW*DT
      BETA=ABS(DWS/H/GAMMA)
      WS=WSTART+DWS*(NOINT/2+1)
      WRITE (ISAVE,101) WS,DW,DT,H,VSTOP
      K=NOINT/2+1
C  CALCULATE WEIGHTS; NOTE THAT EACH POINT IS DWS HZ APPART.
      SUM=0.0E00
      DO  113 I=1,K
      TEMP=BETA*(K-I)
      GO TO (109,110,111), TYPE
  109 WEIGHT(I)=1.0E00/(1.0E00+TEMP*TEMP)
      GO TO 112
  110 WEIGHT(I)=EXP(-TEMP*TEMP)
      GO TO 112
  111 WEIGHT(I)=1.0E00
      IF (TEMP.GT.1.0E00) WEIGHT(I)=0.0E00
  112 SUM=SUM+2.0E00*(WEIGHT(I))
  113 CONTINUE
C       NORMALIZE DISTRIBUTION
      SUM=(SUM-WEIGHT(1)-WEIGHT(K))*BETA
      DO 1141 I=1,K
      TEMP=BETA*(K-I)
      WEIGHT(I)=WEIGHT(I)/SUM
      WEIGHT(NOINT-I+2)=WEIGHT(I)
      WRITE (6,114) TEMP, WEIGHT(I)
  114 FORMAT (1H ,16X,'+/- ',E10.4,5X,E12.4)
 1141 CONTINUE
      K=0
C  CALCULATE INHOMOGENEOUS SIGNAL FOR EIGHT POINTS AT A TIME.
  115 DO 117 I=1,8
      TEMP=0.0E00
      K=K+1
      L=K+NOINT
      M=0
      DO 116 J=K,L
      M=M+1
  116 TEMP=TEMP+S(J)*WEIGHT(M)
  117 SAV(I)=(TEMP-0.50*(S(K)+S(L))*WEIGHT(1))*BETA
      VPP=(WS+K*DWS)/6.28319
      WRITE (6,118) VPP, (SAV(I),I=1,8)
```

```
  118 FORMAT (1H ,5X,9E12.4)
      WRITE (ISAVE,103)  (SAV(I),I=1,8)
C  FINISHED?
      IF (K+NOINT.LT.NOPTS) GO TO 115
  119 GO TO 99
  138 WRITE (6,139)
  139 FORMAT (1H ,15X,'***END OF DATA ON DEVICE 10; TRYING TO GO ON.')
      NOPTS=I-8
      IF (NOPTS.GT.0) GO TO 104
  140 WRITE (6,141)
  141 FORMAT (1H ,5X,'END OF JOB')
      STOP
      END
```

```
      REAL*4 ST(5000), SF(5000)
C  THIS PROGRAM 'FILTERS' THE DISK OUTPUT (OF DATA SETS ON DEVICES 10
C       THROUGH 19) OF CALCULATED DOUBLE RESONANCE SIGNALS FROM THE
C       PROGRAM DRAB OR DRABR.  WRITTEN IN FORTRAN IV BY B.GOODWIN.
C       OUTPUT IS TO DISK (DEVICES 20 THROUGH 29) IN THE SAME FORM AS
C       THE INPUT.  THE METHOD IS RELATED TO A FOURIER TRANSFORM OF THE
C       SIGNAL FOR THE RESPONSE AT THE OBSERVING FREQUENCY; THE FILTERING
C       IS DONE BY AVERAGING THE SIGNAL FOR EACH POINT OVER A PERIOD
C       1.0/(W2P-W1P)  WHERE W2P AND W1P ARE RESPECTIVELY THE PERTURBING
C       AND OBSERVING FREQUENCIES (W1P IS A FUNCTION OF TIME, AND AS A
C       RESULT THE FOURIER TRANSFORM BECOMES MORE COMPLICATED).  THE
C       INPUT MUST CONSEQUENTLY BE SUCH THAT THERE IS AT LEAST ONE POINT
C       EVERY PERIOD OF THE OSCILLATION; UP TO 5000 POINTS CAN BE
C       FILTERED USING THE PRESENT PROGRAM. (NOTE: FOR AN AX SYSTEM THE
C       NONSECULAR TERMS IN THE HAMILTONIAN AND THE SIGNAL MAY BE OMITTED
C       WITH THE RESULT THAT NO FILTERING NEED BE DONE.)
      EQUIVALENCE (ST(1),SF(1))
      INTEGER DISC1/09/, DISC2/19/, COMM(4)
C  INPUT PARAMETERS ARE AS FOLLOWS:
C       W1       LARMOUR FREQUENCY OF NUCLEUS 1, THE FREQUENCY ORIGON OF
C                SUBSEQUENT FREQUENCIES (WSTART, W2, ETC.), IN HERTZ.
C       IFT     -THE NUMBER OF TIMES THE FILTERING IS TO BE DONE; DUE TO
C                THE DESCRETE NATURE OF THE DATA MORE THAN ONE FILTERING
C                MAY BE REQUIRED.
C       COMM    -COMMENT OR TITLE OF THIS JOB.
   99 READ (5,100,END=136) W1,IFT,COMM
  100 FORMAT (D20.12,7X,I2,4A4)
      WRITE (6,101) COMM, W1, IFT
  101 FORMAT (///1H ,15X,'FILTERING OF THE DOUBLE RESONANCE SIGNAL OF:',
     1/1H ,18X,4A4,/1H ,18X,'FREQUENCY ORIGIN=',D20.12,/1H ,18X,'NUMBER
     2OF FILTERS =',I3,'.')
      IC=0
  102 DISC1=DISC1+1
      DISC2=DISC2+1
C  READ IN THE SIGNAL.
      READ (DISC1,103,END=130) WSTART,DELW,DELT,W2,WSTOP
  103 FORMAT (5E16.8)
C  CONVERT TO RADIANS/SECOND.
      W1=W1*6.28319D00
      WSTOP=WSTOP*6.28319D00
      W2=W2+W1
  104 NDIM=(WSTOP-WSTART)/DELW/DELT
      IF (NDIM.GT.5000) NDIM=5000
  105 FORMAT (1H ,10X,5E16.8,I4)
      WRITE (6,105) W2,WSTART,WSTOP,DELT,DELW,NDIM
      IF (IC.GT.0) GO TO 108
  106 READ (DISC1,107,END=130) (ST(I),I=1,NDIM)
  107 FORMAT (8E10.4)
  108 WSTART=WSTART-W2+W1
C  BIT OF HOCKUS-POCKUS.
```

```
      W=WSTOP-W2+W1
      T0=DABS(12.56638D00/W)
      TIME=NDIM*DELT-T0+DELT
      IST=TIME/DELT+0.50D00
      ISF=NDIM+1
  109 TIME=TIME-DELT
      IST=IST-1
      W=WSTART+DELW*TIME
C  CALCULATE NUMBER OF POINTS/PERIOD AT THIS FREQUENCY (W1P=W).
      N=DABS(6.28319D00/W/DELT+0.50D00)
      IF (N.LT.1) N=1
C  FILTER THE SIGNAL AT ST(IST) BY AVERAGING THE POINTS FROM ST(NLOW)
C       TO ST(NUP), AND STORE THE RESULT IN SF(ISF).  THE ARRAYS ST AND
C       SF ARE EQUIVALENCED BUT ISF AND IST ARE ARRANGED TO PROTECT THE
C       POSSIBLE PREMATURE DESTRUCTION OF DATA.
      NLOW=IST-N/2
      IF (NLOW.LT.1) GO TO 112
  110 ISF=ISF-1
      NUP=IST+N/2.0D00-0.4999999D00
      SUM=0.0D00
C  THESE STATEMENTS DO ALL THE WORK.
      DO 111 I=NLOW,NUP
  111 SUM=SUM+ST(I)
      SF(ISF)=SUM/N
      GO TO 109
  112 WSTART=WSTART+W2
      WSTOP=WSTOP-DELW*T0
      WSTART=WSTART-W1+DELW*T0
      IC=IC+1
C  FILTER AGAIN?
      IF (IFT.GT.IC)  GO TO 104
  113 W2=W2-W1
      WSTOP=WSTOP/6.28319D00
C  WRITE OUT FILTERED DATA AND GO ON TO THE NEXT SET.  NOTE THE FACT
C       THAT WSTART AND WSTOP ARE CLOSER TOGETHER:  SOME POINTS HAVE BEEN
C       LOST AT THE BEGINNING AND END OF THE DATA SET.
      WRITE (DISC2,114) WSTART, DELW, DELT, W2, WSTOP
  114 FORMAT (5E16.8)
      I=NDIM-ISF
      WRITE (6,105) W2,WSTART,WSTOP,DELT,DELW,I
      WRITE (DISC2,115) (SF(I),I=ISF,NDIM)
  115 FORMAT (8E10.4)
      END FILE DISC2
      WRITE (6,116) DISC1, DISC2
  116 FORMAT (1H ,10X,'DATA HAS BEEN SUCCESSFULLY FILTERED FROM DISK',
     1 I3,' TO DISK',I3,'.')
      GO TO 99
  130 WRITE (6,131)
  131 FORMAT (//1H ,10X,'***DATA ON DISK MISSING?')
  136 WRITE (6,137)
  137 FORMAT (//1H ,15X,'END OF JOB')
      STOP
      END
```

```
      REAL YY(8)
C  THIS PROGRAM PLOTS OUTPUT FROM UP TO 10 DATA SETS ON DISK (DEVICES
C       NUMBERED 10 THROUGH 20); THE OUTPUT BEING PLOTTED BEING THE
C       CALCULATED SIGNAL OF EITHER HIGH-RESOLUTION (AS A FUNCTION OF
C       FREQUENCY) OR PULSED (AS A FUNCTION OF TIME) NMR.  WRITTEN IN
C       FORTRAN IV BY B.GOODWIN.  THIS PROGRAM REQUIRES THE STANDARD
C       ROUTINES PLOTS, PLOT, NUMBER AND SYMBOL WHICH ARE AVAILABLE
C       WITH THE CALCOMP PLOTTER FOR AN IBM 360/65 SYSTEM.
      INTEGER TITLE(5), INDATA/5/, ONPRTR/6/, DISC/10/
      INTEGER IBUF (3000)
      CALL PLOTS (IBUF,3000,9)
C  INPUT PARAMETERS (EXCLUDING DISK INPUT) ARE AS FOLLOWS:
C       TITLE  -IDENTIFICATION OF PLOT.
C       YMULT  -VERTICAL SCALING FACTOR; USE WITH YSTART, YSTOP AND
C               YSCALE TO EXPAND THE VERTICAL AXIS.
C       IR     -FREQUENCY OF OUTPUT TO LINE PRINTER; EVERY IR*8 POINT
C               IS OUTPUT.
C       XSTART, XSTOP -STARTING AND STOPPING VALUES OF THE X-AXIS.
C       XSCALE -SCALING FACTOR OF THE X-AXIS, IN #UNITS/CM.
C       YSTART, YSTOP -STARTING AND STOPPING VALUES OF THE Y-AXIS.
C       YSCALE -SCALING FACTOR OF THE Y-AXIS, IN #UNITS/CM.
C       IX,IY  -FOR IX(IY)=0, NO X-AXIS(Y-AXIS) IS DRAWN.
C               FOR IX(IY) > 100 AN AXIS IS DRAWN BUT NOT LABELLED.
C               FOR IX(IY) < 100 BUT > 0 AN AXIS IS DRAWN WITH A 'TICK'
C                   EVERY CM., AND WITH A LARGER 'TICK' AND A LABEL OF
C                   THE CURRENT X (Y) VALUE WRITTEN OUT EVERY IX(IY) CM.
C       NO     -NUMBER OF DATA SETS TO BE PLOTTED ON THE AXES DEFINED
C               ABOVE.  IF NO<2, NEW AXES ARE DRAWN FOR THE NEX DATA SET.
C       FORMAT IS (5A4,F10.4,2I2,/3F10.4,I3,7X,3F10.4,I3)
   99 READ (INDATA, 102, END=140) TITLE, YMULT, IR,NO
  102 FORMAT (5A4,F10.4,2I2)
      IF (IR.LT.1) IR=20
      IF (YMULT.LE.1.0E-49) YMULT=1.0
      READ (INDATA, 103, END=138) XSTART, XSTOP, XSCALE, IX, YSTART,
     1 YSTOP, YSCALE, IY
  103 FORMAT (3F10.4,I3,7X,3F10.4,I3)
      IF (XSTART.EQ.XSTOP.OR.YSTART.EQ.YSTOP) GO TO 138
  104 IF (XSCALE.LE.0.0) XSCALE=ABS(XSTOP-XSTART)/10.0
      IF (YSCALE.LE.0.0) YSCALE=(YSTOP-YSTART)/10.
      ISX=1
      IF (XSTOP.LT.XSTART) ISX=-1
C  CALCOMP PLOTS IN INCHES; CONVERT FROM CENTIMETERS.
      XSCAL2=1.0/(XSCALE*2.54)*ISX
      YSCAL2=1.0/(YSCALE*2.54)
      XLENGT=ABS((XSTOP-XSTART)*XSCAL2)
      YLENGT=ABS((YSTOP-YSTART)*YSCAL2)
      YMAX=ABS(YSTART)
      IF (YSTOP.GT.YMAX) YMAX=YSTOP
      YMAX=YMAX/YMULT
C  SET UP PEN POSITION.
```

```
  105 CALL PLOT (2.0,-5.0,-3)
      CALL PLOT (0.0, 1.0, -3)
      TEMP1=0.0
      IF (YSTART.LE.0.0.AND.YSTOP.GT.0.0) TEMP1=-YSTART*YSCAL2
      IF (IX.LT.0) GO TO 110
  106 I=IX
      IF (IX.GT.100) I=0
      X=XSTART-XSCALE*ISX
      CALL PLOT (0.0,TEMP1,3)
  107 X=X+XSCALE*ISX
      TEMP=(X-XSTART)*XSCAL2
      CALL PLOT (TEMP, TEMP1, 2)
      CALL PLOT (TEMP,TEMP1-0.05,2)
      I=I+1
      IF (I.LT.IX) GO TO 109
  108 I=0
      CALL PLOT (TEMP, TEMP1-0.10, 2)
      CALL NUMBER (TEMP-0.3,TEMP1-.31,0.14,X,0.0,2)
  109 CALL PLOT (TEMP, TEMP1, 3)
      IF (X*ISX.LT.XSTOP*ISX) GO TO 107
  110 TEMP1=0.0
      IF (IY.LT.0) GO TO 115
  111 I=IY
      IF (IY.GT.100) I=0
      Y=YSTART-YSCALE
      CALL PLOT (TEMP1, 0.0, 3)
  112 Y=Y+YSCALE
      TEMP=(Y-YSTART)*YSCAL2
      CALL PLOT (TEMP1,TEMP,2)
      CALL PLOT (TEMP1-0.05,TEMP,2)
      I=I+1
      IF (I.LT.IY) GO TO 114
  113 I=0
      CALL PLOT (TEMP1-0.10, TEMP, 2)
      CALL NUMBER (TEMP1-0.3,TEMP-0.3,0.14,Y,90.0,2)
  114 CALL PLOT (TEMP1,TEMP,3)
      IF (Y.LT.YSTOP) GO TO 112
  115 WRITE (ONPRTR, 116) TITLE, XSTART, XSTOP, XSCALE, IX, YSTART,
     1                    YSTOP, YSCALE, IY, XLENGT, YLENGT, YMULT, IR
  116 FORMAT (1H1,10X,'INPUT PARAMETERS',//1H ,15X,'TITLE: ',5A4,
     1 /1H ,15X,'X-START =',F10.4,/1H ,15X,'X-STOP  =',F10.4,/1H ,15X,
     2 'X-SCALE =',F10.4,/1H ,15X,'IX =',I4,/1H ,15X,'Y-START =',F10.4,/
     31H ,15X,'Y-STOP  =',F10.4,/1H ,15X,'Y-SCALE =',F10.4,/1H ,15X,'IY
     4 =',I4,/1H ,15X,'X-LENGTH=',F10.4,/1H ,15X,'Y-LENGTH=',F10.4,/1H ,
     515X,'Y-MULT  =',E10.3,/1H ,15X,'IR =',I3,///1H )
      TEMP=(YSTOP-YSTART)*YSCAL2+0.5
      CALL SYMBOL (1.0,TEMP,0.14,TITLE,0.0,20)
      CALL NUMBER (1.0,TEMP-0.25,0.14,YMULT,0.0,1)
C  READ THE FIRST RECORD ON DISK.  WA IS THE STARTING POSITION (RAD./
C       SEC.), DELW THE FREQUENCY SWEEP RATE (RAD./SEC./SEC.), DELT THE
```

```
C       STEP SIZE (SEC.) W2P IS A DUMMY VARIABLE AND PULSE > 1.0E49
C       DENOTES A PULSED NMR PLOT.  THIS RECORD IS REPEATED FOR EACH NEW
C       PULSE.
  117 READ (DISC,118,END=136) WA,DELW,DELT,W2P,PULSE
  118 FORMAT (5E16.8)
      IF (ABS(DELW).GT.1.0E-49) GO TO 1191
C  DELW=0.0 FOR PULSED NMR.
  119 XXSTEP=DELT
      GO TO 1192
C  CALCULATE STEP SIZE AND RECONVERT TO HERTZ.
 1191 XXSTEP=DELW*DELT/6.28319
      WA=WA/6.28319
 1192 WRITE (ONPRTR,120) WA,DELW,DELT,XXSTEP,W2P,PULSE
  120 FORMAT (1H ,15X,'START=',E11.4,' / (',E12.4,',',E12.4,')',E13.4,
     1' /',/1H ,15X,'W2P  =',E12.4,/1H ,15X,'PULSE=',F4.1)
C  READ IN SIGNAL IN BATCHES OF EIGHT.
      READ (DISC,121,END=136) (YY(JJ),JJ=1,8)
  121 FORMAT (8E10.4)
C  CHECK FOR END OF THIS PULSE (A NULL PULSE).
      IF (YY(1).GT.1.0E49) GO TO 117
 1210 XX=WA-XXSTEP
      TEMP2=(XX-XSTART+XXSTEP)*XSCAL2
      TEMP1=(YY(01)*YMULT-YSTART)*YSCAL2
      TEMP=1.0
C  THE PULSE PLOTS HAVE A "1" WRITTEN IMMEDIATELY BELOW THE START OR
C       STOP OF A PULSE.
      IF (PULSE.GT.1.0E49) CALL NUMBER (TEMP2,TEMP1-.25,.07,TEMP,0.0,0)
C  MOVE PEN TO FIRST POINT.
      CALL PLOT (TEMP2,TEMP1,3)
      KKK=1
      GO TO 1212
C  READ IN REST OF SIGNAL IN BATCHES OF EIGHT.
 1211 READ (DISC,121,END=136) (YY(JJ),JJ=1,8)
      KKK=KKK+1
 1212 DO 1216 JJ=1,8
C  CHECK FOR END OF THIS PULSE.
      IF (YY(JJ).GT.1.0E49) GO TO 117
 1213 XX=XX+XXSTEP
 1214 IF (ABS(YY(JJ)).GT.YMAX) GO TO 1216
C  SCALE AND PLOT SIGNAL.
 1215 TEMP2=(XX-XSTART)*XSCAL2
      TEMP1=(YY(JJ)*YMULT-YSTART)*YSCAL2
 1216 CALL PLOT (TEMP2,TEMP1,2)
C  OUTPUT TO PRINTER.
      IF (KKK/IR*IR.EQ.KKK) WRITE (ONPRTR,122) XX,YY(8)
  122 FORMAT (1H ,19X,F10.4,6X,E15.7)
      GO TO 1211
C  GO TO NEXT DISK AND NEXT PLOT.
  136 DISC=DISC+1
      NO=NO-1
      IF (NO.GT.0) GO TO 117
```

```
137 CALL PLOT ((XSTOP-XSTART)*XSCAL2+1.0,0.0,-3)
    GO TO 99
138 WRITE (ONPRTR, 139)
139 FORMAT (////1H ,15X,'INPUT BUNGLED.')
140 WRITE (ONPRTR, 141)
141 FORMAT (1H ,///,1H ,15X,'END OF JOB')
    CALL PLOT (2.0,0.0,999)
    CALL EXIT
    END
```

BIBLIOGRAPHY

1. J.A.Pople, W.G.Schneider and J.H.Bernstein, "High Resolution Nuclear Magnetic Resonance", McGraw-Hill, New York, 1959.
2. P.L.Corio, "Structure of High-Resolution NMR Spectra", Academic Press, New York, 1967.
3. J.W.Emsley, J.Feeney and L.H.Sutcliffe, "High-Resolution Nuclear Magnetic Resonance Spectroscopy", Vol. 1, Permagon Press, Oxford, 1965.
4. A.Abragam, "The Principles of Nuclear Magnetism", Oxford University Press, 1961.
5. A.Carrington and A.D.McLachlan, "Introduction to Magnetic Resonance", Harper and Row, New York, 1967.
6. E.D.Becker, "High-Resolution NMR", Academic Press, New York, 1969.
7. C.P.Slichter, "Principles of Magnetic Resonance", Harper and Row, New York, 1963.
8. T.C.Farrar and E.D.Becker, "Pulse and Fourier Transform NMR", Academic Press, New York, 1971.
9. B.A.Jacobsohn and R.K.Wangsness, Phys. Rev. 73, 942 (1948).
10. C.A.Reilly, J. Chem. Phys. 25, 604 (1956).
11. R.Freeman and W.A.Anderson, J. Chem. Phys. 37, 2053 (1962).
12. S.Castellano and A.A.Bothner-By, J. Chem. Phys. 41, 3863 (1964).
13. J.D.Swalen, in "Progress in Nuclear Magnetic Resonance Spectroscopy" (J.W.Emsley, J.Feeney and L.H.Sutcliffe, eds.), Vol. 1 p. 205, Permagon Press, Oxford, 1966.
14. C.S.Johnson Jr., in "Advances in Magnetic Resonance" (J.S.Waugh,

ed.), Vol. 1 p. 33, Permagon Press, Oxford, 1965.

15. L.W.Reeves, in "Advances in Physical Organic Chemistry (V.Gould, ed.), Vol. 3, Academic Press, New York, 1965.

16. G.Binsch, in "Topics in Stereochemistry" (E.L.Eliel and N.L Allinger, eds.), Vol. 3, Wiley & Sons, New York, 1968.

17. R.A.Hoffman, in "Advances in Magnetic Resonance" (J.S.Waugh, ed.), Vol. 4 p. 87, Permagon Press, Oxford, 1970.

18. B.D.Nageswara Rao, in "Advances in Magnetic Resonance" (J.S. Waugh, ed.), Vol. 4 p. 271, Permagon Press, Oxford, 1970.

19. H.Y.Carr and E.M.Purcell, Phys. Rev. 94, 630 (1954).

20. S.Meiboom and D.Gill, Rev. Sci. Inst. 29, 688 (1958).

21. D.E.Woessner, J. Chem. Phys. 35, 41 (1961).

22. A.Allerhand, J. Chem. Phys. 50, 5429 (1969).

23. J.G.Powles and A.Hartland, Proc. Phys. Soc. (London) 77, 273 (1961).

24. A.Allerhand, J. Chem. Phys. 44, 1 (1966).

25. F.bloch, Phys. Rev. 70, 460 (1946).

26. F.Bloch, W.W.Hansen and M.E.Packard, Phys. Rev. 70, 474 (1946).

27. N.Bloembergen, E.M.Purcell and R.V.Pound, Phys. Rev. 73, 679 (1948).

28. H.C.Torrey, Phys. Rev. 76, 1059 (1949).

29. E.L.Hahn, Phys. Rev. 80, 580 (1950); 77, 297 (1949).

30. R.K.Wangsness and F.Bloch, Phys. Rev. 89, 728 (1953).

31. E.Strick, R.Bradford, C.Clay and A.Craft, Phys. Rev. 83, 363 (1951).

32. T.P.Das and A.K.Saha, Phys. Rev. 93, 749 (1954).

33. T.P.Das and D.K.Roy, Phys. Rev. 98, 525 (1955).

34. H.L.Bloom, Phys. Rev. 98, 1105 (1955).

35. R.R.Ernst, Rev. Sci. Inst. 36, 1689 (1965).

36. R.R.Ernst and W.A.Anderson, Rev. Sci. Inst. 36, 1696 (1965).

37. R.R.Ernst and W.A.Anderson, Rev. Sci. Inst. 37, 93 (1966).

38. E.A.Allan, M.G.Hogben, L.W.Reeves and K.N.Shaw, Pure and Applied Chemistry 32, 9 (1972).

39. L.W.Reeves and K.N.Shaw, Can. J. Chem. 48, 3641 (1970).

40. W.A.Anderson, Phys. Rev. 102, 151 (1956).

41. S.Alexander, Rev. Sci. Inst. 32, 1066 (1961).

42. E.E.Jones and H.Sternlicht, J. Magn. Resonance 6, 167 (1972).

43. H.S.Gutowsky, D.W.McCall and C.P.Slichter, J. Chem. Phys. 21, 279 (1953).

44. H.S.Gutowsky and C.H.Holm, J. Chem. Phys. 25, 1228 (1956).

45. H.M.McConnell, J. Chem. Phys. 28, 43 (1958).

46. Z.Luz and S.Meiboom, J. Chem. Phys. 39, 366 (1963).

47. J.G.Powles and J.H.Strange, Mol. Phys. 8, 169 (1964).

48. S.Forsén and R.A.Hoffman, J. Chem. Phys. 39, 2892 (1963).

49. A.Allerhand and H.S.Gutowsky, J. Chem. Phys. 41, 2115 (1964).

50. A.Allerhand and H.S.Gutowsky, J. Chem. Phys. 42, 1587 (1965).

51. A.Allerhand, F.Chen and H.S.Gutowsky, J. Chem. Phys. 42, 3040 (1965).

52. M.Bloom, L.W.Reeves and E.J.Wells, J. Chem. Phys. 42, 1615 (1965).

53. H.S.Gutowsky, R.L.Vold and E.J.Wells, J. Chem. Phys. 43, 4107 (1965).

54. C.S.Johnson Jr. and M.Saunders, J. Chem. Phys. 43, 4170 (1965).

55. A.Allerhand and E.Thiele, J. Chem. Phys. 45, 902 (1966).

56. R.A.Hoffman and S.Forsén, J. Chem. Phys. 45, 2049 (1966).

57. A.Allerhand, H.S.Gutowsky, J.Jonas and R.A.Meizner, J. Amer. Chem. Soc. 88, 3185 (1966).

58. P.T.Inglefield, E.Krakower, L.W.Reeves and R.Steward, Mol. Phys. 15, 65 (1968).

59. J.P.Carver and R.E.Richards, J. Magn. Resonance 6, 89 (1972).

60. I.I.Rabi, N.F.Ramsey and J.Schwinger, Rev. Mod. Phys. 26, 967 (1954).

61. R.Freeman and H.D.W.Hill, J. Chem. Phys. 54, 3367 (1971).

62. W.A.Anderson, R.Freeman and H.Hill, Pure and Applied Chemistry 32, 27 (1972).

62a. R.V.Vold, J.S.Waugh, M.P.Klein and D.E.Phelps, J. Chem. Phys. 48, 3831 (1968).

63. R.Freeman and S.Wittekoek, J. Magn. Resonance 1, 238 (1969).

64. C.N.Banwell and H.Primas, Mol. Phys. 6, 225 (1963).

65. G.Binsch, Mol. Phys. 15, 469 (1968).

66. G.Binsch, J.Amer. Chem. Soc. 91, 1304 (1969).

67. J.M.Anderson, J. Magn. Resonance 1, 89 (1969).

68. J.M.Anderson and A.C.-F.Lee, J. Magn. Resonance 3, 427 (1971).

69. S.N.Cohen and M.T.Emerson, J. Magn. Resonance 4, 54 (1971).

70. J.M.Anderson, J. Magn. Resonance 4, 184 (1971).

71. B.Gestblom, O.Hartmann and J.M.Anderson, J. Magn. Resonance 5, 174 (1971).

72. J.B.Rowbotham and T.Schaefer, Can. J. Chem. 50, 2344 (1972).

73. W.A.Anderson, Phys. Rev. 102, 151 (1956).

74. W.A.Anderson and R.Freeman, J. Chem. Phys. 37, 85 (1962).

75. R.Freeman and W.A.Anderson, J. Chem. Phys. 37, 2053 (1962).

76. R.Freeman and D.H.Whiffen, Proc. Phys. Soc. (London) 79, 794 (1962).

77. J.D.Baldeschwieler and E.W.Randall, Chem. Rev. 63, 81 (1963).

78. R.Freeman, R.R.Ernst and W.A.Anderson, J. Chem. Phys. 46, 1125 (1967).

79. W.A.Anderson, Phys. Rev. 104, 850 (1956).

80. E.L.Hahn and D.E.Maxwell, Phys. Rev. 84, 1246 (1951); 88, 1070 (1952).

81. E.B.McNeil, C.P.Slichter and H.S.Gutowsky, Phys. Rev. 84, 1245 (1951).

82. J.G.Powles, Rep. Prog. Phys. (London) 22, 433 (1959).

83. J.G.Powles and J.H.Strange, Disc. Faraday Soc. 34, 30 (1962).

84. R.Freeman and H.D.W.Hill, J. Chem. Phys. 54, 301 (1971).

85. F.Bloch, Phys. Rev. 102, 104 (1956).

86. F.Bloch, Phys. Rev. 105, 1206 (1957).

87. A.G.Redfield, I.B.M. J. Res. Dev. 1, 19 (1957); in "Advances in Magnetic Resonance" (J.S.Waugh, ed.), Vol. 1 p. 1, Permagon Press, Oxford, 1965.

88. J.D.Baldschwieler, J. Chem. Phys. 40, 459 (1964).

89. M.Barfield and J.D.Baldschwieler, J. Chem. Phys. 41, 2633 (1964).

90. M.Shimzu and H.Shimizu, J. Chem. Phys. 41, 2329 (1964).

91. J.H.Noggle, J. Chem. Phys. 43, 3304 (1965).

92. R.R.Ernst, J. Chem. Phys. 45, 3845 (1966).

93. R.H.Wakefield and J.D.Memory, J. Chem. Phys. 48, 2174 (1968).

94. V.Sinivee, Mol. Phys. 17, 41 (1969); and references cited therein.

95. B.Gestblom and O.Hartmann, J. Magn. Resonance 4, 322 (1971).

96. S.Yatsiv, Phys. Rev. 113, 1522 (1959).

97. J.Kaplan, J. Chem. Phys. 28, 278 (1958); 29, 492 (1959).

98. S.Alexander, J. Chem. Phys. 37, 967 (1962); 38, 1787 (1963).

99. R.M.Lynden-Bell, in "Progress in NMR Spectroscopy" (J.W.Emsley, J.Feeney and L.H.Sutcliffe, eds.), Vol. 2 p. 163, Permagon Press, Oxford, 1966.

100. C.S.Johnson Jr., J. Chem. Phys. 41, 3277 (1964); J. Magn. Resonance 1, 98 (1969).

101. S.L.Gordon and J.D.Baldeschwieler, J. Chem. Phys. 41, 571 (a964); 43, 76 (1965).

102. R.K.Harris and K.M.Worvill, Chem. Phys. Lett. 14, 598 (1972); J. Magn. Resonance 9, 383 and 394 (1973).

103. B.Gestblom and O.Hartmann, J. Magn. Resonance 8, 230 (1972).

104. B.D.Nageswara Rao, Phys. Rev. 137, A467 (1965).

105. A.Kumar, N.R.Krishna and B.D.Nageswara Rao, Mol. Phys. 18, 11 (1970).

106. N.R.Krishna and B.D.Nageswara Rao, Mol. Phys. 20, 981 (1971); 22, 937 (1971); 23, 1013 (1972).

107. A.Kumar and S.L.Gordon, J. Chem. Phys. 54, 3207 (1971).

108. A.Allerhand and H.S.Gutowsky, J. Chem. Phys. 42, 4203 (1965).

109. R.L.Vold and H.S.Gutowsky, J. Chem. Phys. 47, 2495 (1967).

110. T.Tokuhiro and G.Fraenkel, J. Chem. Phys. 49, 3998 (1968).

111. T.Tokuhiro and G.Fraenkel, J. Chem. Phys. 55, 2797 (1971).

112. E.S.Gore and H.S.Gutowsky, J. Chem. Phys. 48, 3260 (1968).

113. R.Freeman, S.Wittekoek and R.R.Ernst, J. Chem. Phys. 52, 1529

(1970).

114. B.W.Goodwin and R.Wallace, J. Magn. Resonance 8, 41 (1972).

115. B.W.Goodwin and R.Wallace, J. Magn. Resonance 9, 280 (1973).

116. B.W.Goodwin and R.Wallace, J. Magn. Resonance, in press.

117. U.Fano, Rev. Mod. Phys. 29, 74 (1957).

118. D.Ter Harr, Rep. Prog. in Phys. 24, 304 (1961).

119. A.Kumar and B.D.Nageswara Rao, J. Magn. Resonance 8, 1 (1972).

120. A.W.Overhauser, Phys. Rev. 92, 411 (1953).

121. F.Bloch and A.Siegert, Phys. Rev. 57, 522 (1940).

122. A.R.Edmonds, "Angular Momentum in Quantum Mechanics", Princeton University Press, 1960.

123. P.A.M.Dirac, "The Principles of Quantum Mechanics" (Chapter IV), Oxford University Press, 1958.

124. I.J.Lowe and R.E.Norberg, Phys. Rev. 107, 46 (1957).

125. R.Freeman and H.D.W.Hill, J. Chem. Phys. 54, 301 (1971).

126. S.L.Gordon and J.D.Baldeschwieler, J. Chem. Phys. 41, 571 (1964); 43, 76 (1965).

127. R.A.Hoffman and S.Forsén, J. Chem. Phys. 45, 2049 (1966).

128. J.A.Ferretti and R.Freeman, J. Chem. Phys. 44, 2054 (1966).

129. E.Lippmaa and S.Rodmar, J. Chem. Phys. 50, 2764 (1969).

130. P.Henrici, "Discrete Variable Methods in Ordinary Differential Equations", Wiley & Sons, New York, 1962.

131. W.E.Milne, "Numerical Solutions of Differential Equations", Wiley & Sons, New York, 1953.

132. C.-E. Fröberg, "Introduction to Numerical Analysis", Addison-

Wesley, Reading Mass., 1969.

133. R.G.Stanton, "Numerical Methods for Science and Engineering", Prentice-Hall, New Jersey, 1961.

134. S.Gill, Proc. Cambridge Phil. Soc. 47, 96 (1951).

135. M.J.Romanelli, in "Mathematical Methods for Digital Computers" (A.Ralston and H.S.Wilf, eds.), Wiley, New York, 1967.

136. A.I.A.Karim, The Computer Journal 9, 308 (1966-67).

137. J.D.Lawson, S.I.A.M. Num. Analysis 4, 372 (1967).

138. T.M.Apostol, "Calculus", Vol. I, Blaisdell Pub. Co., New York, 1962.

139. L.R.Anders and J.D.Baldeschwieler, J. Chem. Phys. 43, 2147 (1962).

140. J.S.Leigh, Rev. Sci. Inst. 39, 1594 (1968).

141. R.R.Ernst, J. Chem. Phys. 45, 3845 (1966).

142. I.Solomon and N.Bloembergen, J. Chem. Phys. 25, 261 (1956).

143. A.L.Bloom and J.N.Schoolery, Phys. Rev. 97, 1261 (1965).

144. V.F.Bystrov, J. Magn. Resonance 2, 267 (1970).

145. B.Gestblom and O. Hartmann, J. Magn. Resonance 4, 322 (1971).

146. O. Hartmann and B. Gestblom, Acta. Chem. Scand. 26, 1817 (1972).